


5-2011

Protein-lipid Interactions: Influence of Anchoring Groups and Buried Arginine on the Properties of Membrane-spanning Peptides

Vitaly V. Vostrikov

University of Arkansas, Fayetteville

Follow this and additional works at: <http://scholarworks.uark.edu/etd>

 Part of the [Biochemistry Commons](#), [Biophysics Commons](#), and the [Physical Chemistry Commons](#)

Recommended Citation

Vostrikov, Vitaly V., "Protein-lipid Interactions: Influence of Anchoring Groups and Buried Arginine on the Properties of Membrane-spanning Peptides" (2011). *Theses and Dissertations*. 77.
<http://scholarworks.uark.edu/etd/77>

This Dissertation is brought to you for free and open access by ScholarWorks@UARK. It has been accepted for inclusion in Theses and Dissertations by an authorized administrator of ScholarWorks@UARK. For more information, please contact scholar@uark.edu, ccmiddle@uark.edu.

**PROTEIN-LIPID INTERACTIONS:
INFLUENCE OF ANCHORING GROUPS AND BURIED ARGININE
ON THE PROPERTIES OF MEMBRANE-SPANNING PEPTIDES**

PROTEIN-LIPID INTERACTIONS:
INFLUENCE OF ANCHORING GROUPS AND BURIED ARGININE
ON THE PROPERTIES OF MEMBRANE-SPANNING PEPTIDES

A dissertation submitted in partial fulfillment
of the requirements for the degree of
Doctor of Philosophy in Chemistry

By

Vitaly V. Vostrikov
Moscow State Academy of Fine Chemical Technology
Bachelor of Science in Chemical Technology and Biotechnology, 2004
Moscow State Academy of Fine Chemical Technology
Master of Science in Molecular and Cellular Biotechnology, 2006

May 2011
University of Arkansas

ABSTRACT

Designed transmembrane peptides were employed for investigations of protein-lipid interactions by means of oriented solid-state deuterium NMR spectroscopy using isotope-enriched alanine residues. Using the model GWALP23 sequence (GGALW(LA)₆LWLAGA) as a host peptide having single interfacial tryptophan anchor residues, the effects of different guest mutations were explored. Replacements of glycine residues 2 and 22 to positively charged lysine or arginine on both termini had little influence on the peptide average orientation. Conversely, glycine to tryptophan substitutions had profound effects, manifested in the increased dynamics and altered tilt direction of the peptide. While the charged residues at the peptide termini did not cause significant changes relative to the GWALP23 sequence, leucine to arginine mutations close to the peptide center led to dramatic consequences. Thus GWALP23-R14 retained a transmembrane topology, with the orientation and dynamics largely governed by the arginine residue, while GWALP23-R12 adopted multistate behavior in DOPC, with both transmembrane and interfacial states being populated. Coarse-grained molecular dynamics simulations, performed by collaborators, yielded substantial agreement concerning the interactions among arginine, tryptophan and lipid bilayers. Further insights into the multistate behavior of GWALP23-R12 were acquired by altering the host sequence to the isomeric GW^{3,21}ALP23, which offers a longer separation between the tryptophan anchor residues. Both the L12R and L14R mutants of this modified sequence retained transmembrane topology, suggesting that the unique arrangement of tryptophan and arginine residues in GWALP23-R12 is responsible for its multistate character. In addition to serving as a host sequence, GWALP23 itself was modified for an

investigation of hydrophobic matching, by shifting the tryptophan residues outward toward the termini (GW^{3,21}ALP23) or inward toward the center (GW^{7,17}ALP23), leading to peptide isomers with identical amino acid composition, but different effective hydrophobic (inter-Trp) lengths. In addition to altered tilt angles, tryptophan side chain reorientation was investigated and was found to provide additional response to hydrophobic mismatch conditions. In selected cases the ²H NMR data were analyzed in conjunction with restraints from separated local-field ¹⁵N solid-state NMR spectra. The combined analysis of the ²H and ¹⁵N NMR data provided multiple constraints and proved advantageous for explicit modeling of the peptide dynamics.

This dissertation is approved for
Recommendation to the
Graduate Council

Dissertation Director:

Dr. Roger E. Koeppe II

Dissertation Committee:

Dr. Francis S. Millett

Dr. Thallapuram Krishnaswamy S. Kumar

Dr. James F. Hinton

DISSERTATION DUPLICATION RELEASE

I hereby authorize the University of Arkansas Libraries to duplicate this dissertation when needed for research and/or scholarship.

Agreed _____

Vitaly V. Vostrikov

Refused _____

Vitaly V. Vostrikov

ACKNOWLEDGMENTS

There are many people I would like to acknowledge. Without their support few of this would have been possible. First and foremost, I would like to thank my advisor Dr. Roger Koeppel for his guidance and advice throughout the years. On countless occasions our conversations provided the inspiration and motivation for my work. My sincere gratitude goes to the members of the Koeppel lab. Nick Gleason, for helping out, maintaining high integrity of the lab and tolerating the practical jokes (Nick, if you are reading this, check your latest MS form). Anne Froyd-Rankenbergh, who has been immensely helpful by providing common sense when I was overcomplicating simple and oversimplifying complex. I have enjoyed many productive conversations and feel/am honored to call her a friend. Few if any NMR experiments in this thesis/that I have done would have been possible without Dr. James Hinton. His expertise, willingness to help and sense of humor (“Chemists are...”) made working with him a lot of fun. Marv Leister has been instrumental in maintaining the NMR spectrometers, consequently we had little if any downtime (I just hope that in the future an empirical rule “unresolvable hardware issues arise on Friday evenings” will no longer hold). Over the time that I worked at the Koeppel lab, I was involved in numerous fruitful collaborations. I am very grateful to Dr. Stanley Opella and Dr. Christopher Grant for performing SLF experiments on our samples, as well as providing an opportunity to get some hands on experience (not to mention that it was nice finally meeting a Formula-1 fan in the USA). I would like to offer my “most enthusiastic contrafibularities” to Dr. Mark Sansom and Dr. Benjamin Hall, whose MD work significantly contributed to our understanding. Finally, I would like to thank my

former Russian advisors Dr. Galina Sorokoumova and Dr. Alla Selishcheva for introducing me to the exciting world of biomembranes.

TABLE OF CONTENTS

ABSTRACT	ii
DISSERTATION DUPLICATION RELEASE	v
ACKNOWLEDGMENTS	vi
TABLE OF CONTENTS.....	viii
LIST OF THE ORIGINAL PAPERS	xi
INTRODUCTION	1
CHAPTER 1 On the Combined Analysis of ^2H and $^{15}\text{N}/^1\text{H}$ Solid-State NMR Data for Determination of Transmembrane Peptide Orientation and Dynamics	6
1.1 Abstract	6
1.2 Introduction	7
1.3 Materials and Methods	10
1.4 Results	16
1.5 Discussion	25
1.6 Acknowledgments.....	29
1.7 References	30
1.8 Tables	33
1.9 Figures	37
1.10 Supporting Information	47
CHAPTER 2 Charged or Aromatic Anchor Residue Dependence of Transmembrane Peptide Tilt.....	56
2.1 Abstract	56
2.2 Introduction	57
2.3 Experimental Procedures.....	61
2.4 Results	65
2.5 Discussion	70
2.6 Acknowledgments.....	76

2.7 References	77
2.8 Tables	81
2.9 Figures	83
2.10 Supplemental Data	90
CHAPTER 3 Response of GWALP Transmembrane Peptides to Lipid Bilayer	
Hydrophobic Mismatch	101
3.1 Abstract	101
3.2 Introduction	102
3.3 Materials and Methods	105
3.4 Results	109
3.5 Discussion	117
3.6 Acknowledgments	122
3.7 References	123
3.8 Tables	127
3.9 Figures	132
3.10 Supporting Information	143
CHAPTER 4 Changes in Transmembrane Helix Alignment by Arginine Residues	
Revealed by Solid-State NMR Experiments and Coarse-Grained MD Simulations	153
4.1 Abstract	153
4.2 Introduction	154
4.3 Results	156
4.4 Discussion	163
4.5 Materials and Methods	167
4.6 Acknowledgments	169
4.7 References	171
4.8 Tables	175
4.9 Figures	177
4.10 Supporting Information	187

4.11 Copyright Clearance Form	193
CHAPTER 5 “Rescue” of a Central Arginine in a Transmembrane Peptide by Changing the Placement of Anchor Residues	198
5.1 Abstract	198
5.2 Introduction	199
5.3 Materials and Methods	202
5.4 Results	206
5.5 Discussion	215
5.6 Acknowledgments	221
5.7 References	222
5.8 Tables	225
5.9 Figures	228
5.10 Supporting Information	238
CONCLUSIONS.....	245

LIST OF THE ORIGINAL PAPERS

Chapter 2: Vostrikov, V.V., A.E. Daily, D.V. Greathouse, and R.E. Koeppe 2nd, 2010.

Charged or aromatic anchor residue dependence of transmembrane peptide tilt. *J Biol Chem* 285: 31723-31730.

Chapter 4: Vostrikov, V.V., B.A. Hall, D.V. Greathouse, R.E. Koeppe 2nd, and M.S.P.

Sansom, 2010. Changes in transmembrane helix alignment by arginine residues revealed by solid-state NMR experiments and coarse-grained MD simulations. *J Am Chem Soc* 132: 5803-5811.

INTRODUCTION

Biological membranes represent complex, highly heterogeneous combinations of lipids and proteins of different types. Interaction of membrane-spanning proteins with lipid bilayers is a complicated process, driven by numerous factors, which are still incompletely understood. Investigating systems of such complexity requires systematic approaches, which in turn call for the use of less intricate model systems. Usually, the complex biological lipid bilayer membrane environment is substituted with individual synthetic lipids having a particular hydrocarbon chain length. Due to the large size of membrane proteins, smaller membrane-spanning α -helical peptides may typically be used for particular experiments. To minimize the interactions between transmembrane helices, single-span peptides, such as model WALP sequence (GWW(LA)_nLWWA), have been employed to good advantage for systematic experiments (de Planque et al., 1999; Killian et al., 1996; van der Wel et al., 2002). The overall theme of this dissertation is the development of “next generation” model transmembrane peptides that go “beyond WALP” and development of experimental methods which will enhance understanding of peptide/lipid interactions as well as peptide and/or lipid response to hydrophobic mismatch conditions.

The response of the original WALP peptides to hydrophobic mismatch turned out to be fairly small, as shown by solid-state ²H NMR (Strandberg et al.; van der Wel et al.). Molecular dynamics simulations disagreed with experiments in predicting greater lipid dependence and consistently larger tilt angles with respect to the lipid bilayer normal (Kandasamy and Larson, 2006; Kim and Im, 2010; Ozdirekcan et al., 2007). To address

this apparent discrepancy, we have employed independent experimental methods, using oriented, hydrated peptide/lipid bilayer samples and based on solid-state ^2H NMR spectroscopy and ^{15}N separated local field NMR spectroscopy. Using a wide variety of new peptides, encompassing a wide range of the tilt angles and different regimes for the peptide dynamics, we have investigated the sensitivity and accuracy of different solid-state NMR restraints, as well as different approaches to treat the whole-body dynamics. The results, described in [Chapter 1](#), identify cases where the transmembrane peptide orientation and dynamics can be extracted from a single type of NMR restraint, and then move on to more complex scenarios that are found to require additional constraints that derive from multiple experimental NMR methods.

Among the different peptides discussed in Chapter 1, the GWALP23 sequence (GGALW⁵(LA)₆LW¹⁹LAGA) turned out to be sensitive to lipid bilayer acyl-chain composition and thickness, unlike the original WALP prototypes. Capitalizing on this aspect, we have adopted the GWALP23 peptide as a new primary reference standard for probing a variety of biophysical properties. In [Chapter 2](#) we describe the application of the GWALP23 sequence to the investigation of different anchoring amino acids by employing XWALP23 sequences. These peptides were derived from GWALP23, by substituting both G2 and G22 with X = K or R or W. The behavior of positively charged X residues K or R was similar to the parent case when X = G; however, the case where X = W was very different. The WWALP23 peptide displayed extensive dynamics while adopting fairly small apparent tilt angles, with a preferred tilt direction nearly opposite from the rest of the XWALP23 series. The results with the XWALP23 peptides illustrate

directly the role of interfacial tryptophan residues as primary determinants of peptide orientation and dynamics.

Hydrophobic matching, defined as the difference between peptide hydrophobic length and lipid bilayer hydrophobic thickness (de Planque and Killian, 2003; Harzer and Bechinger, 2000; Killian et al., 1996), is an important concept in the arena of protein-lipid interactions. The GWALP23 sequence—with its single but not overly dominant tryptophan anchor residues that flank a hydrophobic helical core—is ideally suited for the investigation of hydrophobic mismatch conditions. The effective hydrophobic length of GWALP23 can be altered by shifting the tryptophan residues toward the center of the peptide to give $\text{GW}^{7,17}\text{ALP23}$ ($\text{GG}(\text{AL})_2\text{W}^7(\text{LA})_4\text{LW}^{17}(\text{LA})_2\text{GA}$), or toward the termini to give $\text{GW}^{3,21}\text{ALP23}$ ($\text{GGW}^3(\text{LA})_8\text{LW}^{21}\text{GA}$). Chapter 3 deals with the behavior of these peptides when incorporated in lipid bilayers of various thickness. Further investigations were performed using ^2H labels in the Trp indole rings of the $\text{GW}^{x,y}\text{ALP23}$ peptides. In addition to the changes of peptide tilt angles, we observed alterations of tryptophan side chain orientations, further highlighting the role of Trp residues at a membrane-water interface.

Multiple recent computational studies investigated the possibility of placing a charged amino acid in the hydrophobic region of a lipid bilayer (Li et al., 2008; MacCallum et al., 2008), which is particularly interesting in scope of voltage gated ion channels (Jiang et al., 2003). In Chapter 4, an experimental approach to this problem is reported. Using once again GWALP23, this time as a carrier for a single arginine residue, we have created two sequence isomers by mutating either Leu^{12} or Leu^{14} to Arg. The behavior of these two

isomeric peptides was dramatically different: while GWALP23-R14 adopted a stable and well-defined transmembrane orientation, GWALP23-R12 exhibited multiple states.

Coarse-grained molecular dynamics simulations of these peptides replicated the NMR results remarkably well and provided further insights into their interactions with the lipid bilayer, namely peptide translational displacement and bilayer deformation.

In order to find an explanation for such different behavior of GWALP23-R14 and -R12 peptides, we have switched the host peptide from GW^{5,19}ALP23 to GW^{3,21}ALP23, described in Chapter 3. This rearrangement of the tryptophan residues allowed for testing of whether the multistate behavior of GWALP23-R12 results solely from a central arginine location, or whether it is mediated by the anchoring Trp residues. [Chapter 5](#) describes the behavior of GW^{3,21}ALP23-R12 and -R14 peptides incorporated in lipid bilayer membranes. Strikingly, both of these peptides adopt a unique transmembrane orientation, indicating that a single uncompensated arginine can be introduced at the center of the membrane-spanning peptide sequence in selected cases.

Overall, the experiments to be described define an attractive new host transmembrane peptide framework for posing specific questions in the realm of protein/lipid interactions. The specific applications will illustrate the utility of the parent peptide framework for defining not only the preferred orientations of membrane-spanning peptides but also the peptide dynamics and the detailed responses to a wide variety of single-site mutations. Importantly, the GWALP23 framework will be suitable for many additional future applications, not limited to the particular examples described here.

- de Planque, M.R., and J.A. Killian, 2003. Protein-lipid interactions studied with designed transmembrane peptides: role of hydrophobic matching and interfacial anchoring. *Mol Membr Biol* 20: 271-284.
- de Planque, M.R., J.A. Kruijtzter, R.M. Liskamp, D. Marsh, D.V. Greathouse, R.E. Koeppe 2nd, B. de Kruijff, and J.A. Killian, 1999. Different membrane anchoring positions of tryptophan and lysine in synthetic transmembrane α -helical peptides. *J Biol Chem* 274: 20839-20846.
- Harzer, U., and B. Bechinger, 2000. Alignment of lysine-anchored membrane peptides under conditions of hydrophobic mismatch: a CD, ^{15}N and ^{31}P solid-state NMR spectroscopy investigation. *Biochemistry* 39: 13106-13114.
- Jiang, Y., V. Ruta, J. Chen, A. Lee, and R. MacKinnon, 2003. The principle of gating charge movement in a voltage-dependent K^+ channel. *Nature* 423: 42-48.
- Kandasamy, S.K., and R.G. Larson, 2006. Molecular dynamics simulations of model trans-membrane peptides in lipid bilayers: a systematic investigation of hydrophobic mismatch. *Biophys J* 90: 2326-2343.
- Killian, J.A., I. Salemink, M.R. de Planque, G. Lindblom, R.E. Koeppe 2nd, and D.V. Greathouse, 1996. Induction of nonbilayer structures in diacylphosphatidylcholine model membranes by transmembrane α -helical peptides: importance of hydrophobic mismatch and proposed role of tryptophans. *Biochemistry* 35: 1037-1045.
- Kim, T., and W. Im, 2010. Revisiting hydrophobic mismatch with free energy simulation studies of transmembrane helix tilt and rotation. *Biophys J* 99: 175-183.
- Li, L., I. Vorobyov, A.D. MacKerell, Jr., and T.W. Allen, 2008. Is arginine charged in a membrane? *Biophys J* 94: L11-L13.
- MacCallum, J.L., W.F. Bennett, and D.P. Tieleman, 2008. Distribution of amino acids in a lipid bilayer from computer simulations. *Biophys J* 94: 3393-3404.
- Ozdirekcan, S., C. Etchebest, J.A. Killian, and P.F.J. Fuchs, 2007. On the orientation of a designed transmembrane peptide: toward the right tilt angle? *J Am Chem Soc* 129: 15174-15181.
- Strandberg, E., S. Ozdirekcan, D.T. Rijkers, P.C. van der Wel, R.E. Koeppe 2nd, R.M. Liskamp, and J.A. Killian, 2004. Tilt angles of transmembrane model peptides in oriented and non-oriented lipid bilayers as determined by ^2H solid-state NMR. *Biophys J* 86: 3709-3721.
- van der Wel, P.C., E. Strandberg, J.A. Killian, and R.E. Koeppe 2nd, 2002. Geometry and intrinsic tilt of a tryptophan-anchored transmembrane α -helix determined by ^2H NMR. *Biophys J* 83: 1479-1488.

CHAPTER 1

On the Combined Analysis of ^2H and $^{15}\text{N}/^1\text{H}$ Solid-State NMR Data for Determination of Transmembrane Peptide Orientation and Dynamics

1.1 Abstract

Knowledge of transmembrane α -helix dynamics is important for interpretation of solid-state NMR observables. While precession of tilted peptides about the bilayer normal is commonly observed, additional dynamic features, such as anisotropic contributions from distributions of helix tilt or helix rotation, have the potential to influence the analysis. Previously, we compared independent analysis of ^2H -alanine (“GALA”) and $^{15}\text{N}/^1\text{H}$ -backbone data sets (“PISEMA”) as constraints for determining helix tilt. Here we report combined analysis of ^2H quadrupolar splittings together with $^{15}\text{N}/^1\text{H}$ dipolar couplings, using two methods to treat the dynamics, for the systematic evaluation of several membrane-spanning peptides based on the GWALP sequence (acetyl-GGALW(LA)₆LWLAGA-amide), which tilt by 2° - 30° in lipid bilayer membranes.

By comparing individual and combined analyses of specifically ^2H or ^{15}N labeled peptides incorporated in mechanically or magnetically aligned lipid bilayers of differing thickness, we investigated the influence of data set size/identity, and of explicitly modeled dynamics, on the average apparent orientations of the peptides. We conclude that the peptides with small (less than $\sim 10^\circ$) apparent tilt values can be fitted by extensive collections of solutions, which can be narrowed by incorporating additional ^{15}N as well as ^2H restraints. Conversely, peptides that exhibit larger tilt angles have a narrower range of distributions of tilt and rotation that are consistent with the experimental data. The

resulting smaller range can then be fitted using smaller sets of experimental constraints, or even with ^2H or ^{15}N data alone. Importantly, for the peptides that tilt significantly more than 10° from the bilayer normal, the contribution from rigid body dynamics can be approximated by a simple scaling factor (principal order parameter), and the concomitant apparent peptide orientation remains reasonably accurate.

1.2 Introduction

Solid-state NMR provides a powerful means for deducing the structure and behavior of transmembrane helical domains of proteins in the native lipid environment (Bechinger et al., 2011). The ability to probe the structure in atomic detail makes NMR a method of choice for investigation of protein-lipid interactions. Solid-state NMR of oriented lipid-bilayer systems offers a way to obtain the average orientation of membrane-spanning helical segments in the form of the magnitude (τ) and direction (ρ) of the helix tilt. Different NMR observables, nevertheless, have different sensitivities to the orientation of an α -helix, due to different respective directions of the interaction axes, different sensitivities, and different physical basis for each particular nuclear interaction with an external magnetic field. The reorientation of an isotope-labeled group over the NMR acquisition time poses another potential issue due to the inherent averaging of instantaneous signals. While the fast precession of individual transmembrane helices around the lipid bilayer (Lee and Im; van der Wel et al.) normal does not influence the NMR signals, oscillations around the average tilt and rotation angles will produce more drastic effects (Esteban-Martin et al., 2009; Strandberg et al., 2009).

The contributions of molecular oscillations to the NMR observables often are taken into account by multiplying the values for a hypothetical case of no molecular motion by a scaling factor (principal order parameter, S_{zz}) between 0 and 1. The limit $S_{zz} = 0$ corresponds to isotropic motion of the helix, while the limit $S_{zz} = 1$ corresponds to completely immobilized peptide. Such a scaling factor can be applied as an additional fitting parameter, although a fixed value of 0.8 has been extensively assumed (Doherty et al., 2010; Page et al., 2008; Park et al., 2006). An alternative way of describing the whole-body dynamics is to model explicit motions in the form of specific fluctuations in the tilt magnitude τ and tilt direction ρ (Bertelsen et al., 2011; Holt et al., 2010; Strandberg et al., 2009). In this treatment, the theoretical rigid-case NMR observables are multiplied by a normalized two-dimensional probability distribution generated for every possible (τ, ρ) combination. The sum of the elements of each resulting matrix yields a predicted motionally averaged value for each particular NMR signal.

Among the conventional methods employed to deduce the transmembrane peptide orientation in lipid bilayers, separated local field (SLF) PISEMA or SAMMY experiments (Marassi and Opella, 2000; Nevzorov and Opella, 2003; Wang et al., 2000; Wu et al., 1994) and deuterium quadrupolar splitting measurements (Jones et al.; van der Wel et al.; Whiles et al.) have been used extensively. In the SLF method, the ^{15}N chemical shifts (CS) correlated with ^1H - ^{15}N dipolar couplings (DC) result in characteristic spectra for the peptide backbone of a tilted α -helix, which are sometimes referred to as “PISA wheels.” The CS and DC principal interaction axes – namely, the σ_{33} CS tensor component and the NH bond, respectively – are aligned close to the

peptide's helix axis (Figure 1A). These observables therefore undergo slight changes at small tilt angles ($<10^\circ$) and more dramatic changes at larger tilt angles. The proximity of the interaction axes to the helix axis dictates that the CS and DC values typically undergo monotonic changes without changing sign or passing through the isotropic limit. The trends in CS and DC can be visualized on helical wave curves for the individual restraints (Figure 1, B). In practice the curves imply that a rough estimate of the tilt angle can be obtained with 2-3 ^{15}N -labeled sites.

Deuterium NMR spectra of the methyl groups in Ala- d_4 residues in conjunction with GALA analysis offers a highly sensitive metric of the transmembrane peptide behavior (Strandberg et al., 2004; van der Wel et al., 2002). The $\text{C}_\alpha\text{-C}_\beta$ bond geometry dictates that the methyl quadrupolar splittings (QS) pass through the isotropic nodes twice for transmembrane helices and four times for a helix in the interfacial orientation. Such degeneracy of the QS helical curves combined with the inability to measure the sign of the QS interaction typically leads to a requirement of four or more data points for the orientation analysis.

The aforementioned restraints in principle can be used individually, or combined together. Several examples of a combined orientational analysis have been reported for the antimicrobial peptide distinctin (Resende et al., 2009) (CS and QS), the peptaibol alamethicin (Bertelsen et al., 2011) (CS, DC and QS) and the model peptide WALP23 (Holt et al., 2010) (QS, ^{13}C - ^{15}N DC as well as ^{13}C and ^{15}N CS anisotropies). Each of these studies was performed with only a few labeled sites, making it difficult to compare

the predictive value of the different types of individual restraints for molecular orientation and dynamics.

In this paper we perform a systematic analysis of several transmembrane peptides, based on the GWALP23 sequence (Vostrikov et al., 2008) in lipid bilayer membranes.

GWALP23, acetyl-GGALW(LA)₆LWLAGA-amide, with single Trp interfacial anchor residues, has proven to show particularly systematic behavior in a series of lipid bilayer membranes (Vostrikov et al.). The peptides chosen for this investigation represent a variety of cases, covering different dynamic and orientation ranges (Table 1). Extensive isotope labeling (employing 5-11 restraints of an individual kind, and up to 29 total restraints) made it possible to experimentally compare the sensitivities of different individual restraints toward the dynamic averaging. We compare the semi-static (variable S_{zz}) or explicit Gaussian (τ , ρ distributions) methods for treating the peptide dynamics and identify those cases where the methods converge to similar results or diverge to significantly different results. The goal of this work is to provide a framework for the orientation analysis of solid-state NMR data of oriented lipid/protein systems while identifying potential pitfalls.

1.3 Materials and Methods

Peptides were synthesized on the model 433A peptide synthesizer (Applied Biosystems by Life Technologies, Foster City, CA) using the established methods for GWALP23 and related sequences. Protected amino acids were from NovaBiochem (San Diego, CA) and the isotope enriched amino acids from Cambridge Isotope Laboratories (Andover, MA).

Peptide purification was accomplished by means of reversed phase HPLC utilizing previously published gradient conditions (Vostrikov et al., 2010a; Vostrikov et al., 2010b).

Mechanically aligned samples for the NMR spectroscopy were prepared with 80 μmol lipid (Avanti, Alabaster, AL) and 1.3 ($\text{GW}^{3,21}\text{ALP23-R14}$) or 2 μmol of peptide (peptide/lipid ratio being 1/60 or 1/40 respectively). The peptide/lipid mixture in 95:5 methanol:water was deposited on the glass slides (Marienfeld, Lauda-Konigshofen, Germany), dried extensively and hydrated to 45% w/w with ^2H -depleted water (Cambridge).

Magnetically aligned samples for NMR spectroscopy were prepared with 61 μmol DMPC, 19 μmol DHPC ($q = 3.2$) and 0.75 μmol of peptide (peptide/lipid ratio of 1/80). Peptide in trifluoroethanol and DHPC in chloroform were mixed and dried *in vacuo* for 48 hours as well as the appropriate amount of DMPC (in a separate vial). DMPC and DHPC/peptide were hydrated with 100 μl and 75 μl of ^2H -depleted water at 45 $^\circ\text{C}$ for three hours with intermittent vortexing. Mixture of DHPC/peptide was transferred to DMPC and the solution was cycled between 45 $^\circ\text{C}$ and 4 $^\circ\text{C}$ three times (15 min equilibration time for each temperature), gently vortexing the sample at the end of each cycle. The solution was transferred to a bicelle tube (New Era Enterprises, Vineland, NJ) after a 4 $^\circ\text{C}$ cycle using a pre-chilled pipette, as the sample had low viscosity at this temperature. For the samples with ^{15}N labels ether analogues of DMPC and DHPC were used. For the majority of the peptides we observe very close signals between the bicelles

and glass slides at $\beta=90^\circ$ macroscopic orientation. To minimize potential discrepancies, we have used identical alignment methods between ^2H and ^{15}N sets for a given peptide.

Solid-state NMR experiments were performed using Bruker Avance spectrometers (Billerica, MA), operating at proton frequency of 300 MHz (^2H) or 500 MHz (^{15}N). Deuterium NMR utilized quadrupolar echo pulse sequence with full phase cycling (Davis et al., 1976). Recycle delay was 90 ms, 90° pulse time of 3.2-4.5 μs (depending on the probe) and echo delay times of 80-110 μs . Separated local field experiments were accomplished with SAMMY pulse sequence (Nevzorov and Opella, 2003) using 7.5 s recycle delay, 5 μs pulse duration and 1 ms cross-polarization contact time.

For data analysis purposes a poly-alanine α -helix was generated, using Swiss-PdbViewer 4.0 (Guex and Peitsch, 1997). Backbone (Θ , Ψ , Ω) angles were set to (-65, -40, 180) (Page et al., 2008). The coordinates of C_β , H_α and H atoms were translated to ensure the identical local geometry throughout the sequence, with the $\varepsilon_{//}$ and ε_{\perp} angles (van der Wel et al., 2002) being 59.4 and -43.0 (C_α - C_β vector), 122.0 and 55.0 (C_α - H_α) and 14.0 and 131.0 (N-H). The helix was positioned such that the C_α carbon of residue 1 was placed on the positive direction of the X-axis, having Y coordinate of zero, providing the initial orientation identical to the one described by van der Wel *et al.* (van der Wel et al., 2002) NMR observables were calculated according to:

$$QS = QCC \cdot S_{zz} \left(\frac{1}{2} [3 \cos^2 \theta - 1] \right) \left(\frac{1}{2} [3 \cos^2 \beta - 1] \right) \quad \text{Eq. 1}$$

$$DC = DCC \cdot S_{zz} \left(\frac{1}{2} [3 \cos^2 \theta - 1] \right) \left(\frac{1}{2} [3 \cos^2 \beta - 1] \right) \quad \text{Eq. 2}$$

$$CS = (CS_{static} - CS_{iso}) \cdot S_{zz} \cdot \frac{1}{2} (3 \cos^2 \beta - 1) + CS_{iso} \quad \text{Eq. 3}$$

In equations 1 and 2 QCC and DCC refer to quadrupolar and dipolar coupling constants (168 kHz and 10.22 kHz respectively; note that there is a further 1/3 reduction of QCC to 56 kHz in the case of the methyl group), θ is the angle between the applied magnetic field and the bond vector in question, β corresponds to the macroscopic orientation of the aligned bilayers relative to the applied magnetic field ($\beta = 0^\circ$ for the aligned glass slides and $\beta = 90^\circ$ for bicelles). In equation 3 CS_{static} corresponds to the chemical shift observed at the rigid limit. The reference frame for the ^{15}N chemical shift was constructed according to Bertram *et al.* (Bertram et al., 2000) and its derivation is described in the Supporting Information. Isotropic chemical shift, CS_{iso} in equation 3, was calculated according to:

$$CS_{iso} = \frac{\sigma_{11} + \sigma_{22} + \sigma_{33}}{3} \quad \text{Eq. 4}$$

The chemical shift tensor components were set to 64 ppm (σ_{11}), 77 ppm (σ_{22}) and 224 ppm (σ_{33}). For the case of WWALP23 we found minor improvements to the root mean squared deviation (RMSD) value if σ_{22} was lowered to 72 ppm, the fit results being identical to the case where 77 ppm was used. For calculation purposes ^{15}N CS was converted from ppm to frequency scale according to:

$$\nu = \sigma \cdot \omega_H \frac{\gamma_N}{\gamma_H} \quad \text{Eq. 5}$$

Where σ is CS in ppm, ω_H is the proton Larmor frequency and γ_N and γ_H are gyromagnetic ratios of ^{15}N and ^1H respectively.

Semi-static analysis was performed in the fashion similar to GALA analysis (van der Wel et al., 2002) by rotating the poly-Ala structure by angles $\rho = 0-359^\circ$ and $\tau = 0-90^\circ$, and scaling the obtained rigid-case values with an order parameter $S_{zz} = 0-1$ according to the equations 1-3. Global minimum was defined as the combination of S_{zz} , τ and ρ with the lowest RMSD:

$$RMSD = \sqrt{\frac{\sum_{N_{QS}} (\Delta\Delta v_{QS})^2 + \sum_{N_{NH}} (\Delta\Delta v_{NH})^2 + \sum_{N_{CS}} (\Delta\Delta v_{CS})^2}{N_{QS} + N_{NH} + N_{CS}}} \quad \text{Eq. 6}$$

Where $\Delta\Delta v$ is the difference between the experimental and calculated values of QS, DC or CS and N is the number of the restraints of the given type.

Explicit Gaussian dynamics analysis was performed in a way described by Strandberg *et al.* (Strandberg et al., 2009) Distributions of tilt and rotation around the average values were considered in the following form:

$$P(x) = \exp\left(\frac{-(x-x_0)^2}{2\sigma_x^2}\right)_{x_0=const} \quad \text{Eq. 7}$$

Where x_0 ($x = \tau$ or ρ) is the average value, $x = 0-359^\circ$ and σ_x is standard deviation (note that the full width at half maximum of the Gaussian distribution equals to $\sim 2.4\sigma_x$). The

obtained $P(\tau)$ and $P(\rho)$ for a given set of the average values were multiplied to yield the two-dimensional distribution (Equation 8), which was further normalized so that the sum of the elements resulted in unity (Equation 9):

$$P(\tau, \rho) = \left(\begin{array}{ccc} P(\tau)_o \cdot P(\rho)_o & \dots & P(\tau)_o \cdot P(\rho)_{359} \\ \dots & & \dots \\ P(\tau)_{359} \cdot P(\rho)_o & \dots & P(\tau)_{359} \cdot P(\rho)_{359} \end{array} \right)_{\substack{\tau_0 = \text{const} \\ \rho_0 = \text{const}}} \quad \text{Eq. 8}$$

$$P(\tau, \rho)_{ij} = \frac{P(\tau, \rho)_{ij}}{\sum_{i,j} P(\tau, \rho)_{ij}} \quad \text{Eq. 9}$$

For each of the residues in poly-Ala structure, two-dimensional matrices of the NMR restraints were obtained:

$$\nu(\tau, \rho) = \left(\begin{array}{ccc} \nu(0,0) & \dots & \nu(0,359) \\ \dots & & \dots \\ \nu(359,0) & \dots & \nu(359,359) \end{array} \right) \quad \text{Eq. 10}$$

Where ν is either QS, DC or CS calculated according to the equations 1-3, using a fixed S_{zz} value of 0.88 to account for the internal motion of the peptide (Strandberg et al., 2009). Sample probability distributions (equation 8) and NMR observables (equation 10) are illustrated in Figure S2.

The motionally averaged values of the NMR observables were calculated for a given τ_0 and ρ_0 values:

$$\nu = \left| \sum_{i,j}^{i,j=0-359} P(\tau, \rho)_{ij} \cdot \nu(\tau, \rho)_{ij} \right| \quad \text{Eq. 11}$$

Note that the sign of the calculated NMR observables was discarded after this step, as it cannot be established experimentally. The calculated values from equation 11 were compared with the experimental ones according to the equation 6. The procedure described in the equations 7-11 was then repeated for the σ_τ range of 0-30°, σ_ρ range of 0-200°, τ_0 range of 0-90° and ρ_0 range of 0-359° using 1° increments. Both semi-static and Gaussian analyses were implemented in the in-house program written in C#.

1.4 Results

NMR observables for a transmembrane peptide helix parallel to the bilayer normal (having a zero tilt angle) would be identical for all residues: ~8 kHz (QS), ~8 kHz (DC) and ~202 ppm (CS) at the $\beta=0^\circ$ macroscopic orientation, when the bilayer normal is parallel with the external magnetic field. The corresponding values when $\beta=90^\circ$ (including the case of bicelles samples) are ~4 kHz (QS and DC) and ~82 ppm (CS). Extensive dynamics will have the effect of moving the signals toward their isotropic values: 0 kHz (QS and DC) and ~120 ppm (CS). Intermediate oscillations, which are likely to occur, will cause the reduction of the QS and DC, along with shift of the CS toward the isotropic value, which in severe cases can cause a peptide with a large average tilt angle to appear as if it has a smaller *apparent* tilt angle (Figure S3 of the Supporting Information). Below we discuss three categories, which we class according to the

maximum observable QS value when $\beta = 0^\circ$. (Corresponding ranges of DC and CS can be deduced from Figure 1B.)

Case 1: $QS_{max} < 25$ kHz (intermediate motion). Both GWALP23 and KWALP23 exhibit similar signals in DMPC bicelles, with the QS values of the latter being slightly larger (Figure 2, AB). The SAMMY spectra of both peptides are well dispersed, and can be easily assigned through the use of difference spectra (Vostrikov et al., 2008). The PISA wheel of GWALP23 is somewhat more crowded and marginally smaller than the one of KWALP23. Despite the lower resolution, the eleven peaks can still be assigned by using KWALP23 spectrum as a guide (both peptides have similar rotation angles (Vostrikov et al., 2010a)) and a high-field spectrum of GWALP23 (Figure S4). We also note that the ^2H spectra are virtually identical between DMPC/DHPC bicelles and DMPC glass slides at $\beta = 90^\circ$ orientation, indicating that the data between the two alignment methods can be used interchangeably. The observed values of QS, DC and CS are reported in Table 2.

We begin the analysis using an alanine subset of GWALP23 (residues 7, 9, 11, 13, 15 and 17) in order to have the same number of restraints of different kind, with the similar position on helical wheel projection (these positions are not strictly identical, due to the offset between the C_α and N atoms). Furthermore, the variations of the chemical shift tensor components within this subset should be minimal, since all the residues follow the repeating $\text{Leu}_{i-1} - ^{15}\text{N-Ala}_i - \text{Leu}_{i+1}$ pattern (Poon et al., 2004).

The fits of the experimental data using individual restraints are shown in Figure 3. It can be seen that for all data sets there is a large area of the acceptable solutions for the case of

Gaussian analysis (Figure 3, A). These areas though are not identical for the individual restraints: while DC and CS plots look similar, the QS one is different. These changes are especially apparent for the σ_τ in the 10-20° range, as QS is more prohibitive to larger tilt oscillations. The order parameter analysis reports unique minima for the DC and CS restraints, and the two closely spaced ones for QS (Figure 3, B). It is of interest to note that the decrease of S_{zz} has opposite effects on DC and CS. Lower S_{zz} values will bring the theoretical DC values below the experimental ones and consequently the fit with the lowest deviation between the theoretical and experimental sets will correspond to the tilt of zero degrees. Conversely, lower order parameter in the case of CS favors large tilt angles, since the *center* of the PISA wheel reaches the isotropic chemical shift value when the peptide tilt is at the magic angle, while the individual resonances are located both upfield and downfield.

The orientation of the peptide, corresponding to the global minima is similar for each of the restraints type, and for the both ways of treating the dynamics (Figure 3, CD). Nevertheless, the different sensitivities of QS, DC and CS toward the peptide tilt and rotation are immediately apparent. While the analysis using QS alone yields a single well-defined minimum, the acceptable solution area is much larger both for DC and CS. Notably, these sets have larger uncertainty in the average tilt angle, in particular when the dynamics are treated in a semi-static way (Figure 3, D). Additionally, due to a small dispersion between the smallest and the largest dipolar couplings (0.8 kHz at $\beta=90^\circ$, Table 2), DC set does not differentiate well between the different ρ angles. Similarly, CS

fit is less well defined in terms of the rotation angle, due to the fairly flat helical wave curves (Figure 1, B).

Combining the restraints in a pairwise fashion helps localizing the minimum in the case of Gaussian dynamics (Figure S5). It is particularly helpful when QS are combined either with DC or CS, since their acceptable solutions areas do not completely overlap (Figure 3, A). Thus QS restraints provide a penalty against small oscillations in rotation, while DC or CS discriminate against the small oscillations in tilt. Combining DC and CS does not offer additional insights, due to nearly identical dynamics solutions. If the dynamics are treated in a semi-static way, the fit does not change significantly, since all the individual restraints converge to the similar S_{zz} value. In this case combining the different restraints amounts to additional data points along the already well-defined helical wave curve, which can instead be achieved through the individual analysis of QS, DC or CS restraints with more labeled sites.

In terms of the average orientation, the restraints paired with QS signals appear the most beneficial, because of a sharp minimum for the methyl groups (Figure 3, D). Average peptide orientation deduced from DC and CS combination is not defined better in comparison with DC or CS signals alone. Nevertheless, joint DC and CS fit can be particularly useful if the peptide topology is not initially known. In this case CS contribution in the combined fit can eliminate the possibility of an interfacially bound peptide, while DC restraints will impose a penalty against very large (40° - 60°) tilt angles. RMSD contour maps for the paired restraints analysis are provided in Figure S5.

Can the broader minima of ^{15}N -based restraints be narrowed by more extensive sampling? To answer this, we have analyzed the complete 11 ^{15}N labeled sites using DC or CS alone, combined together, or combined with QS, and finally using all three restraint types simultaneously (Table 3). The introduction of additional DC and CS data points did not have a significant effect on the quality of fit for the individual restraints analysis. Due to a good dispersion of six alanine residues on the helical wheel projection, these amino acids are sufficient to define a DC or CS helical wave with good accuracy, and the addition of five more leucine data points does not offer additional insights. Furthermore, in the case of CS the eleven experimental data points appear to have the largest deviation from the idealized case, suggesting that certain variations in the magnitude and/or orientation of the ^{15}N chemical shift tensor are present between Leu and Ala.

The results of the joint analysis of 6 QS, 11 DC and 11 CS restraints are presented in Table 3 and Figure 4. Notably, the average peptide orientation remains identical to the one obtained from the individual restraints, in particular QS. The rotation angle is different by $\sim 25^\circ$ from the fit of DC or CS alone, but this change does not cause a large rise of the RMSD value, which remains remarkably low. This further highlights the lower sensitivity of DC and CS towards the tilt direction angle.

Similar analysis was performed for KWALP23 in DMPC/DHPC bicelles, which was previously shown to exhibit a tilt angle slightly larger than GWALP23 (Vostrikov et al., 2010a). This difference in the tilt angle can be observed in the individual or combined analyses of QS, DC and CS of KWALP23 (Table 3, Figure S6). As in the case of

GWALP23, the ^{15}N NMR observables alone offer less precision in comparison with QS, the latter being a key restraint type in defining the orientation and the dynamics.

While bicelles provide a convenient system for the sample alignment, it suffers from a small range of long-chain lipids that can be employed. Conversely, mechanical alignment of the lipids on the glass slides offers more flexibility for the selection of the lipid matrix. Similar considerations described above also hold for the case of KWALP23 incorporated in DLPC glass slides. Interestingly, one of its ^2H spectra (Figure S7) contains a low intensity signal, arising from a backbone C_αD group, providing an additional restraint similar in sensitivity to the alanine side chain QS. The semi-static and Gaussian analyses of this system for the individual or combined restraints (29 data points total) are provided in Figure S8. Similar to the magnetic alignment case, QS data offers the most well-defined minima..

Case 2: $QS_{max} < 15$ kHz (extensive motion). Single-span peptides having more than two bulky aromatic groups (Trp or Tyr residues) typically exhibit a narrow range of QS values, consistent with a small tilt angle (Gleason et al.; Strandberg et al., 2004; van der Wel et al., 2002). However, this result can also be interpreted in terms of the extensive averaging of the NMR signal, leading to the “masking” of the larger average tilt (Kandasamy and Larson, 2006; Kim and Im, 2010; Ozdirekcan et al., 2007). Among such peptides, WWALP23 with four tryptophan residues has been shown previously to have a small apparent tilt angle in different lipid membranes using QS as a single restraint type (Vostrikov et al., 2010a). Here we complement the QS data set with the DC and CS restraints from five labeled residues (Table 1). While the ^2H spectra do not exhibit any

unusual features in terms of lineshapes or peak widths, the SAMMY spectrum demonstrates a single cross peak for a peptide with the five labels (Figure 5). While a single DC or CS value for multiple labeled sites can be observed for a peptide with a tilt close to zero (see above), the positions of the WWALP23 resonances (3.2 kHz, 88 ppm) does not match the one calculated for $\tau=0^\circ$ (4.1 kHz, 79.3 ppm; red circle in Figure 5B). Instead the WWALP23 signal is located close to the center of PISA wheels of GWALP23 and KWALP23, an observation implying that the close values of DC and CS at different positions in WWALP23 arise largely due to the dynamics.

The analysis of WWALP23 behavior using the individual restraints and the Gaussian dynamics does not produce a definitive answer. The low RMSD values throughout the $[\sigma_\tau, \sigma_\rho]$ space do not make it possible to reliably differentiate between the different solutions (Figure 6A). While a global minimum appears to be present for the QS dynamics plot, the difference between the adjacent contours is only 0.5 kHz, which is below the experimental error. Both DC and QS demonstrate similar dynamics patterns, when the best fit occurs if very large oscillations in tilt and/or rotation are introduced. Semi-static analyses of WWALP23 result in single minima, although the exact S_{zz} values differ by 0.2. Notably, DC and CS data sets lead to the τ value of zero degrees with undefined ρ angle; however, the non-identical QS signals at different alanine positions make it possible to identify that the peptide is actually tilted and allow for establishing the tilt direction (Table 3).

Unlike the GWALP23 case, the combination of QS, DC and CS sets for WWALP23 offers a much better defined dynamics space. Deuterium data, that prohibits very large

and very small σ_ρ , and ^{15}N data that disfavors large σ_τ and (small σ_ρ + small σ_τ) provide a well-defined elongated minimum (Figure 7A). The effects of the combined restraints of semi-static analysis (Figure 7B) are less dramatic, as the fit is still largely defined by QS, while DC and CS have the effect of fine-tuning the S_{zz} value (Table 3).

Despite the better defined range of acceptable dynamics in the case of the Gaussian analysis, some uncertainty is still present for the WWALP23 average orientation, in particular the tilt angle. Due to the elongated solution space, data can be equally well fitted with the large tilt angle (in the absence of tilt oscillations, but with extensive rotation around the peptide helical axis) or with the smaller tilt angle, approaching the one for the semi-static analysis (in the presence of vigorous σ_τ and moderate σ_ρ motion). Since these solutions result in the identical QS, DC and CS curves, it is not possible to differentiate between them (Table 3, Figure 7CD). The semi-static analysis of the combined restraints leads to the unique minimum with a small tilt angle, similar to the earlier observations with WALP19 and WALP23 model peptides (Strandberg et al., 2004; van der Wel et al., 2002). Nevertheless, the tilt magnitude is some 5-7° lower in comparison with the smallest tilt angle obtained with the Gaussian dynamics.

Case 3: $QS_{max} > 35$ kHz (minimal motion). An introduction of the charged residue close to the center of a GWALP23 peptide can be well tolerated in some cases (Vostrikov et al., 2010b). Recently, we have characterized a modified host peptide, $\text{GW}^{3,21}\text{ALP23}$, that allows for two extra alanine labels in its hydrophobic core. The L14R mutation in this modified sequence has similar consequences on the peptide behavior as in the case of GWALP23-R14, namely a $\sim 10^\circ$ increase in the apparent tilt angle accompanied by a

rotation change. For the GW^{3,21}ALP23-R14 peptide we observe some deviations between the ²H data in mechanically aligned glass slides and magnetically aligned bicelles, the latter system yielding a larger tilt angle (the direction of the tilt is identical). Additionally, the overall RMSD for the ²H data set is ~2.3 kHz in bicelles (*vs.* 1.2 kHz in glass slides), but is lowered to ~0.6 kHz when the most C-terminal data point Ala¹⁹ is excluded (eliminating other Ala data points one at a time with Ala¹⁹ present does not lead to RMSD reduction). Due to these considerations, we do not include any of the restraints from Ala¹⁹ in the fit.

The large magnitudes of QS values imply that the tilt angle is fairly big, irrespective of the extent of the dynamics (Figure 8A). The range of the resonances in the 2D SAMMY spectrum is further indicative of the large tilt magnitude (Figure 8B). The large dispersion of the signals also suggests only minor variations around the average values. Indeed, all of the individual restraints result in a smaller range of acceptable σ_τ and σ_ρ values (Figure 9A). The reduction of oscillations around the average ρ angle is particularly prominent when compared with the GWALP23 peptide (Figure 3A). The average orientation of GW^{3,21}ALP23-R14 is similar between the individual restraints and also between the Gaussian and semi-static ways of the dynamics treatment (Table 3). Due to the enhanced amplitude of the DC and CS helical curves, both tilt magnitude and direction from the ¹⁵N restraints have less uncertainty in comparison with the peptides described above (Figure 9CD). Nevertheless, the QS-derived orientation plot still has the best defined solutions.

A combination of the orientational restraints appears to lead to a minor improvement of the Gaussian dynamics, helping marginally to localize the minimum. The main contribution in the dynamics refinement is CS data; nevertheless, CS restraints have the largest deviations from the theoretical curve and therefore the apparent minimum localization should be treated with caution. The average orientation of the peptide is similar between the Gaussian and semi-static dynamics treatment and closely resembles the one based on the QS data exclusively. The addition of DC and CS restraints somewhat alters the shape of the global orientation minimum. While the QS data results in a minimum elongated in the τ_0 direction, both DC and CS are less defined in ρ_0 , making the combined fit more “circular”.

1.5 Discussion

Membrane-spanning proteins cover a variety of motion regimes, which are governed both by protein-protein and protein-lipid interactions. In this paper we have investigated several transmembrane α -helices, undergoing small, medium and large oscillations around the average tilt and rotation angles. Different solid-state NMR restraints were used individually or combined together to deduce the peptide behavior, and two methods to describe the peptide dynamics were compared.

The orientation and dynamics of GW^{3,21}ALP23-R14 peptide are largely governed by the central arginine residue, that must be positioned in a specific way in order to be able to snorkel to the membrane interface (Vostrikov et al.; Vostrikov et al., 2010b). This has an effect of a large tilt magnitude value and small oscillations around it (Table 3). Such

combination of the large tilt and minor dynamics makes it possible to use either of the QS, DC and CS restraints for the data analysis (Figure 9). The results of using the individual restraints are largely similar and the minute variations mostly result from the global minima shapes. The low extent of the dynamics-induced averaging makes it possible to use either the semi-static or Gaussian analyses, the result being nearly identical for the both methods. In addition to the case where the transmembrane segment behavior is dictated by the charged residues (Butterwick and MacKinnon, 2010), similar behavior can be expected from the helical bundles, where the motion is limited by the neighboring protomers (Hu et al., 2007) or in the presence of an interfacially bound domain (Traaseth et al., 2009), which can be expected to impose the restrictions on the membrane-spanning helix.

Such restrictions are absent for the GWALP23 and KWALP23 peptides, leading to their orientation and dynamics being described by the tryptophan residues at the membrane-water interface (Vostrikov et al., 2010a). The intermediate tilt accompanied by the medium oscillations can still be deduced by employing the individual QS, DC or CS NMR data (Table 3). Each of the individual restraints returns similar orientation angles; however, due to the lower dispersion of the ^{15}N -based data, the DC and CS restraints result in broader minima. This leads to a larger ambiguity for the average τ and especially ρ values (Figure 3). This inherently lower sensitivity cannot be reduced by more extensive data sampling, and it would be highly beneficial to include the QS restraints in the analyses if higher sensitivity is desired.

While we do not find specific preferences of the individual restraints to under- or overestimate the tilt magnitudes as was proposed earlier, (Esteban-Martin et al., 2010; Esteban-Martin et al., 2009) we do observe the consistent 4-6° tilt offset between the semi-static and Gaussian ways of treating the dynamics for the XWALP23 peptides (X = G or K). This variation is fairly constant between the individual and the combined restraints analysis, but is reduced with the decreased dynamics of the system (Table 3, KWALP23 in DLPC vs. DMPC). While in many cases the knowledge of the tilt magnitude within the aforementioned offset is sufficient, it highlights the importance of using the identical dynamics treatment in cases where multiple systems are compared in order to avoid the results misinterpretation.

Unlike the other peptides discussed above, WWALP23 has four tryptophan residues: two at the N-terminus and two at the C-terminus. While one Trp on each terminus is sufficient to promote the membrane anchoring of the peptide, multiple Trps appear to compete among themselves for the most favorable interfacial position, leading to the extensive dynamics of the system (Vostrikov et al., 2010a). The collapse of the PISA wheel to a single crosspeak for multiple labeled positions serves as an indicator of vigorous motion (Figure 5, B). Indeed, cases with the small tilt angle and moderate dynamics have been shown to produce resolved resonances (Froyd-Rankenbergh et al.). In the absence of ¹⁵N data, low S_{zz} value (<0.65) in the course of semi-static analysis may serve as an alternative sign of the extensive dynamics. Despite being a sensitive indicator of the dynamics, the ¹⁵N data alone is not capable of distinguishing the small tilt angles in the

presence of extensive signal averaging: a task that can be accomplished by employing the QS restraints (Table 3).

The explicit Gaussian dynamics analysis of the combined QS, DC and CS restraints leads to a family of solutions with the average tilt angle of $10\text{-}22^\circ$ (Figure 7). Conversely, the semi-static analysis of WWALP23 behavior leads to a unique solution with a fairly small average tilt angle of $4\text{-}6^\circ$. While the different solutions have identical RMSD values which do not allow distinguishing between them, it is reasonable to assume that the tilt magnitude from the semi-static analysis corresponds to the lower limit of the tilt angle, which can be some $10\text{-}15^\circ$ larger.

Irrespective of the motion model used, the helical wave plots for QS, DC and CS restraints retain nearly identical shapes for the peptides of transmembrane topology. The comparison of RMSD values between the semi-static and Gaussian methods for the identical systems indicates that the differences do not exceed 0.15 kHz, and typically are much lower (Table 3). While the Gaussian approach may provide unique helical wave plots for the interfacially bound helices (Strandberg et al., 2009), this does not appear to be the case for the transmembrane ones.

Several arguments can be brought in favor of the semi-static or Gaussian analyses. Thus the semi-static approach is essentially model-free, as the total molecular motion effect is accounted for in a single scaling factor. Conversely, the Gaussian method provides additional insights into the nature of the motion, but forces to assume a particular model. While the molecular dynamics simulations of the XWALP23 transmembrane helices demonstrated the overall Gaussian profiles of both τ and ρ angles, (Vostrikov et al.,

2010b) the ρ angle patterns for other peptides have been more complex (Monticelli et al., 2010; Ozdirekcan et al., 2007).

An additional benefit of employing the semi-static analysis is the minimum number of free parameters, each of them having the distinct effects on the helical wave curves, which allows deducing the peptide behavior from less data sampling. Gaussian approach introduces an additional free parameter due to decomposition of S_{zz} into σ_τ and σ_ρ components, which calls for additional data points. While the latter is less of a problem with model Ala-rich GWALP23 analogues, it can pose difficulties for the investigation of biological systems. In certain cases QS of backbone deuterons can yield additional restraints similar in sensitivity to the QS of Ala methyl groups (Thomas et al., 2009; Vostrikov et al.; Vostrikov et al., 2010b). When using the $C_\alpha D$ QS data, it is advisable to scale down their contribution by a factor of three, due to the very large resonance span of the signals and increased line widths. Within this scope, the variable S_{zz} approach appears to be more robust, while the Gaussian method should be applied in cases where the highly anisotropic motion of the transmembrane segment is expected.

1.6 Acknowledgments

This work was supported in part by grants from the US National Science Foundation (MCB-0841227 and the Arkansas Biosciences Institute. The NMR facility was supported by NIH grant RR31154.

1.7 References

- Bertelsen, K., B. Vad, E.H. Nielsen, S.K. Hansen, T. Skrydstrup, D.E. Otzen, T. Vosegaard, and N.C. Nielsen, 2011. Long-term-stable ether-lipid vs conventional ester-lipid bicelles in oriented solid-state NMR: altered structural information in studies of antimicrobial peptides. *J Phys Chem B* 115: 1767-1774.
- Bertram, R., J.R. Quine, M.S. Chapman, and T.A. Cross, 2000. Atomic refinement using orientational restraints from solid-state NMR. *J Magn Res* 147: 9-16.
- Butterwick, J.A., and R. MacKinnon, 2010. Solution structure and phospholipid interactions of the isolated voltage-sensor domain from KvAP. *J Mol Biol* 403: 591-606.
- Davis, J.H., K.R. Jeffrey, M. Bloom, M.I. Valic, and T.P. Higgs, 1976. Quadrupolar echo deuterium magnetic resonance spectroscopy in ordered hydrocarbon chains. *Chem Phys Lett* 42: 390-394.
- Doherty, T., Y. Su, and M. Hong, 2010. High-resolution orientation and depth of insertion of the voltage-sensing S4 helix of a potassium channel in lipid bilayers. *J Mol Biol* 401: 642-652.
- Esteban-Martin, S., E. Strandberg, J. Salgado, and A.S. Ulrich, 2010. Solid state NMR analysis of peptides in membranes: Influence of dynamics and labeling scheme. *Biochim Biophys Acta* 1798: 252-257.
- Esteban-Martin, S., E. Strandberg, G. Fuertes, A.S. Ulrich, and J. Salgado, 2009. Influence of whole-body dynamics on ^{15}N PISEMA NMR spectra of membrane proteins: a theoretical analysis. *Biophys J* 96: 3233-3241.
- Froyd-Rankenbergh, J.M., D.V. Greathouse, and R.E. Koeppe 2nd, Half-anchored WALP peptides: Effect of anchor position on peptide orientation *in press*.
- Gleason, N.J., V.V. Vostrikov, D.V. Greathouse, C.V. Grant, S.J. Opella, and R.E. Koeppe 2nd, Tyrosine as an anchor replacing a single tryptophan in GWALP peptides *in press*.
- Guex, N., and M.C. Peitsch, 1997. SWISS-MODEL and the Swiss-PdbViewer: an environment for comparative protein modeling. *Electrophoresis* 18: 2714-2723.
- Holt, A., L. Rougier, V. Reat, F. Jolibois, O. Saurel, J. Czaplicki, J.A. Killian, and A. Milon, 2010. Order parameters of a transmembrane helix in a fluid bilayer: case study of a WALP peptide. *Biophys J* 98: 1864-1872.
- Hu, J., T. Asbury, S. Achuthan, C. Li, R. Bertram, J.R. Quine, R. Fu, and T.A. Cross, 2007. Backbone structure of the amantadine-blocked trans-membrane domain M2 proton channel from Influenza A virus. *Biophys J* 92: 4335-4343.

- Jones, D.H., K.R. Barber, E.W. VanDerLoo, and C.W. Grant, 1998. Epidermal growth factor receptor transmembrane domain: ^2H NMR implications for orientation and motion in a bilayer environment. *Biochemistry* 37: 16780-16787.
- Kandasamy, S.K., and R.G. Larson, 2006. Molecular dynamics simulations of model trans-membrane peptides in lipid bilayers: a systematic investigation of hydrophobic mismatch. *Biophys J* 90: 2326-2343.
- Kim, T., and W. Im, 2010. Revisiting hydrophobic mismatch with free energy simulation studies of transmembrane helix tilt and rotation. *Biophys J* 99: 175-183.
- Lee, J., and W. Im, 2008. Transmembrane helix tilting: insights from calculating the potential of mean force. *Phys Rev Lett* 100: 018103.
- Marassi, F.M., and S.J. Opella, 2000. A solid-state NMR index of helical membrane protein structure and topology. *J Magn Res* 144: 150-155.
- Monticelli, L., D.P. Tieleman, and P.F. Fuchs, 2010. Interpretation of ^2H -NMR Experiments on the Orientation of the Transmembrane Helix WALP23 by Computer Simulations. *Biophys J* 99: 1455-1464.
- Nevzorov, A.A., and S.J. Opella, 2003. A "magic sandwich" pulse sequence with reduced offset dependence for high-resolution separated local field spectroscopy. *J Magn Res* 164: 182-186.
- Ozdirekcan, S., C. Etchebest, J.A. Killian, and P.F.J. Fuchs, 2007. On the orientation of a designed transmembrane peptide: toward the right tilt angle? *J Am Chem Soc* 129: 15174-15181.
- Page, R.C., S. Kim, and T.A. Cross, 2008. Transmembrane helix uniformity examined by spectral mapping of torsion angles. *Structure* 16: 787-797.
- Park, S.H., A.A. De Angelis, A.A. Nevzorov, C.H. Wu, and S.J. Opella, 2006. Three-dimensional structure of the transmembrane domain of Vpu from HIV-1 in aligned phospholipid bicelles. *Biophys J* 91: 3032-3042.
- Poon, A., J. Birn, and A. Ramamoorthy, 2004. How does an amide-N chemical shift tensor vary in peptides? *J Phys Chem B* 108: 16577-16585.
- Resende, J.M., C.M. Moraes, V.H. Munhoz, C. Aisenbrey, R.M. Verly, P. Bertani, A. Cesar, D. Pilo-Veloso, and B. Bechinger, 2009. Membrane structure and conformational changes of the antibiotic heterodimeric peptide distinctin by solid-state NMR spectroscopy. *Proc Natl Acad Sci U S A* 106: 16639-16644.
- Strandberg, E., S. Esteban-Martin, J. Salgado, and A.S. Ulrich, 2009. Orientation and dynamics of peptides in membranes calculated from ^2H -NMR data. *Biophys J* 96: 3223-3232.

- Strandberg, E., S. Ozdirekcan, D.T. Rijkers, P.C. van der Wel, R.E. Koeppe 2nd, R.M. Liskamp, and J.A. Killian, 2004. Tilt angles of transmembrane model peptides in oriented and non-oriented lipid bilayers as determined by ^2H solid-state NMR. *Biophys J* 86: 3709-3721.
- Thomas, R., V.V. Vostrikov, D.V. Greathouse, and R.E. Koeppe 2nd, 2009. Influence of proline upon the folding and geometry of the WALP19 transmembrane peptide. *Biochemistry* 48: 11883-11891.
- Traaseth, N.J., L. Shi, R. Verardi, D.G. Mullen, G. Barany, and G. Veglia, 2009. Structure and topology of monomeric phospholamban in lipid membranes determined by a hybrid solution and solid-state NMR approach. *Proc Natl Acad Sci U S A* 106: 10165-10170.
- van der Wel, P.C., E. Strandberg, J.A. Killian, and R.E. Koeppe 2nd, 2002. Geometry and intrinsic tilt of a tryptophan-anchored transmembrane α -helix determined by ^2H NMR. *Biophys J* 83: 1479-1488.
- Vostrikov, V.V., B.A. Hall, M.S.P. Sansom, and R.E. Koeppe 2nd, "Rescue" of a central arginine in a transmembrane peptide by changing the placement of anchor residues *in press*.
- Vostrikov, V.V., A.E. Daily, D.V. Greathouse, and R.E. Koeppe 2nd, 2010a. Charged or aromatic anchor residue dependence of transmembrane peptide tilt. *J Biol Chem* 285: 31723-31730.
- Vostrikov, V.V., C.V. Grant, A.E. Daily, S.J. Opella, and R.E. Koeppe 2nd, 2008. Comparison of "Polarization Inversion with Spin Exchange at Magic Angle" and "Geometric Analysis of Labeled Alanines" methods for transmembrane helix alignment. *J Am Chem Soc* 130: 12584-12585.
- Vostrikov, V.V., B.A. Hall, D.V. Greathouse, R.E. Koeppe 2nd, and M.S.P. Sansom, 2010b. Changes in transmembrane helix alignment by arginine residues revealed by solid-state NMR experiments and coarse-grained MD simulations. *J Am Chem Soc* 132: 5803-5811.
- Wang, J., J. Denny, C. Tian, S. Kim, Y. Mo, F. Kovacs, Z. Song, K. Nishimura, Z. Gan, R. Fu, J.R. Quine, and T.A. Cross, 2000. Imaging membrane protein helical wheels. *J Magn Res* 144: 162-167.
- Whiles, J.A., R. Brasseur, K.J. Glover, G. Melacini, E.A. Komives, and R.R. Vold, 2001. Orientation and effects of mastoparan X on phospholipid bicelles. *Biophys J* 80: 280-293.
- Wu, C.H., A. Ramamoorthy, and S.J. Opella, 1994. High-resolution heteronuclear dipolar solid-state NMR spectroscopy. *J Magn Reson Ser A* 109: 270-272.

1.8 Tables

Table 1. Peptide sequences for GWALP23 and derivatives.

Peptide	Sequence
GWALP23	GGAL <u>WLALALALALALAL</u> WLAGA
KWALP23	GKAL <u>WLALALALALALAL</u> WLAKA
WWALP23	<u>GWAL</u> WLALALALALALAL <u>WLAWA</u>
GW ^{3,21} ALP23-R14	GG <u>WLALALALALAL</u> <u>ARALALAL</u> WGA

Deuterium labeled alanine residues were incorporated in each position between the innermost Trp. ¹⁵N labeled Leu and Ala are underlined.

Table 2. Alanine C β D $_3$ quadrupolar splitting (QS, kHz) and Ala/Leu ^{15}N - ^1H dipolar couplings (DC, kHz) and ^{15}N chemical shifts (CS, ppm) for transmembrane peptides. Data corresponds to $\beta=90^\circ$ (bicelles) or $\beta=0^\circ$ (glass slides), for interconversion between the two refer to equations 1-3.

	GWALP23			KWALP23			KWALP23		
	DMPC ^a			DMPC			DLPC		
	QC	DC	CS	QC ^b	DC	CS	QC	DC	CS
5									
6									
7	10.0	2.6	85.7	11.4	2.5	86.4	28.6	5.6	193.5
8		3.7	86.0		3.6	82.0		8.2	193.0
9	5.1	3.4	99.3	5.9	3.5	99.5	22.2	7.9	175.5
10		2.3	89.6		2.3	91.9		5.5	175.5
11	10.1	3.1	84.3	10.3	2.8	83.8	26.2	6.6	200.5
12		3.9	89.7		3.9	86.6		8.7	186.5
13	4.0	3.0	100.7	4.3	3.1	101.4	13.7	7.4	173.5
14		2.4	87.3		2.3	87.8		5.1	182.5
15	8.5	3.4	85.0	8.3	3.2	83.0	20.2	7.5	201.5
16		3.8	94.0		3.8	92.2		8.5	177.0
17	0.4	2.8	97.0	1.2	2.7	99.5	5.0 ^c	6.3	175.0
18									
19									

Entries left blank were not measured.

a. DMPC refers to DMPC/DHPC q=3.2 bicelles; DLPC refers to glass slides.

b. Data from (Vostrikov et al. 2010a).

c. Backbone C α D signal is 87 kHz.

Continued on next page

Table 2 continued

	WWALP23			GW ^{3,21} ALP23-R14		
	DMPC			DMPC		
	QC	DC	QC	DC	QC	DC
5				18.5		
6						
7	0.6			15.6		
8						
9	6.1			13.3	2.5	115.8
10					0.9	98.2
11	1.0			13.3	2.3	87.1
12					3.5	103.6
13	5.7	3.2	88.0	2.0	1.8	117.4
14		3.2	88.0			
15	1.1	3.2	88.0	4.0	2.6	92.6
16		3.2	88.0		2.7	115.2
17	4.3	3.2	88.0	12.0	0.8	112.5
18					1.1	91.5
19				6.2 ^d	3.2 ^d	100.1 ^d

d. Data points not included in the fit.

Table 3. Peptide dynamics and orientation analysis based on the data from Table 2, using either individual restraints, or combined ones (identical weighing has been used between different restraint types).

	Gaussian					Semi-static			
	τ_0 deg	ρ_0 deg	σ_τ deg	σ_ρ deg	RMSD kHz	τ deg	ρ deg	S_{zz}	RMSD kHz
GWALP23, DMPC/DHPC bicelles									
QS	18	314	16	54	0.41	11	315	0.75	0.49
DC	23	305	5	51	0.20	17	305	0.77	0.21
CS	22	289	5	55	0.78	15	290	0.76	0.80
QS + DC	18	314	16	54	0.42	12	314	0.71	0.45
QS + CS	18	312	15	54	1.09	12	312	0.72	1.11
DC + CS	23	291	0	58	0.60	15	292	0.76	0.62
QS + DC + CS	18	311	15	54	0.72	12	312	0.72	0.90
KWALP23, DMPC/DHPC bicelles									
QS	20	307	14	56	0.83	12	308	0.76	0.91
DC	22	316	12	38	0.14	18	316	0.76	0.14
CS	22	305	0	45	0.89	17	306	0.79	0.91
QS + DC + CS	19	307	13	53	0.93	13	307	0.74	0.95
KWALP23, DLPC glass slides									
QS	21	302	12	33	0.63	18	302	0.78	0.64
DC	18	317	1	22	0.19	17	317	0.86	0.19
CS	14	303	17	10	0.52	13	304	0.76	0.54
QS + DC + CS	18	303	10	23	0.72	17	303	0.81	0.73
QS ^a + DC + CS	21	300	3	37	0.95	18	300	0.83	1.10
WWALP23, DMPC/DHPC bicelles									
QS	- ^b					6	129	0.62	0.35
DC	- ^b					0	- ^b	0.68	0.01
CS	- ^b					0	- ^b	0.83	0.05
QS + DC + CS	22	135	0	140	0.52	4	134	0.71	0.56
	21	133	7	130	0.53				
	17	134	14	115	0.52				
	10	133	21	70	0.56				
GW^{3,21}ALP23-R14, DMPC/DHPC bicelles									
QS	31	267	14	26	0.58	28	267	0.75	0.58
DC	36	298	0	28	0.41	34	298	0.80	0.41
CS	36	280	0	36	1.31	33	280	0.76	1.36
QS + DC + CS	34	267	15	30	1.28	30	267	0.71	1.32

a. Including C_α D signal.

b. Cannot be uniquely defined.

1.9 Figures

Figure 1. Geometry of the orientation constraints. **A:** Primary interaction axes for Ala side chain, backbone NH bond and nitrogen chemical shift (left to right); **B:** Quadrupolar, dipolar and chemical shift helical wave plots for different tilt angles, indicated in the rightmost panel. Here and elsewhere the ranges are 0-55 kHz (QS), 0-10 kHz (DC), 120-220 ppm (CS).

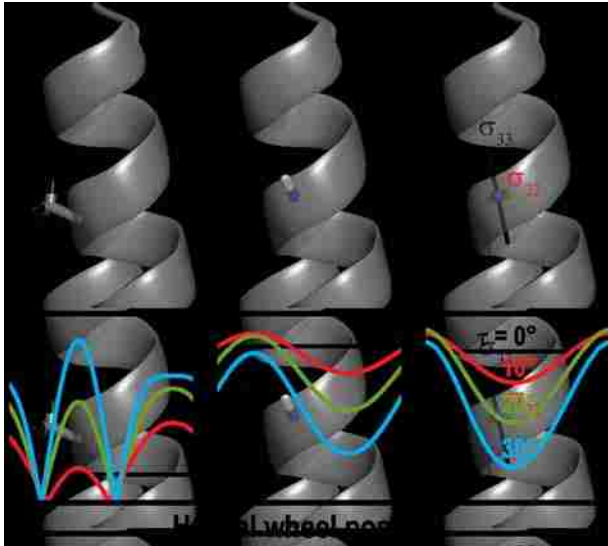


Figure 2. Deuterium and ^{15}N spectra of GWALP23 and KWALP23 in DMPC/DHPC bicelles. **A:** ^2H spectra of GWALP23; **B:** ^2H spectra of KWALP23; **C:** SLF spectrum of GWALP23; **D:** SLF spectrum of KWALP23. Spectral assignments are indicated next to the corresponding resonances.

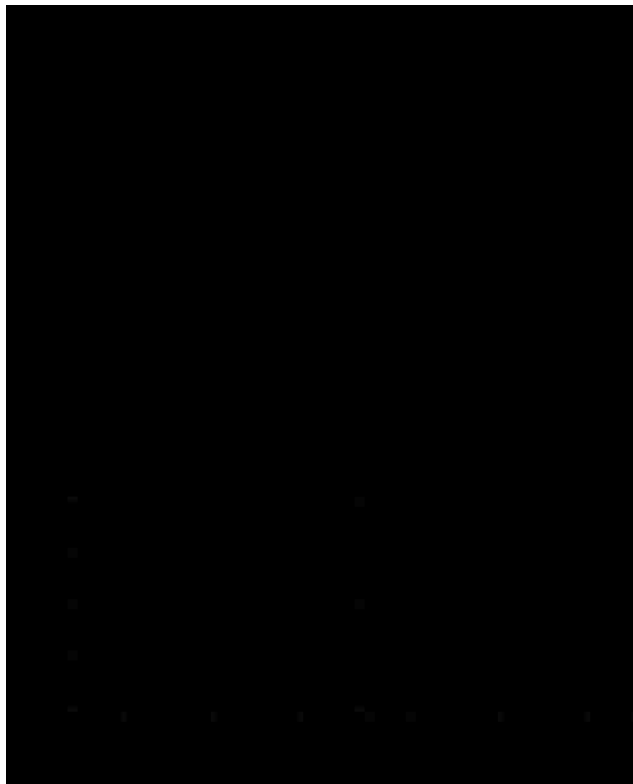


Figure 3. RMSD contour plots of orientation and dynamics of GWALP23 in DMPC/DHPC bicelles, using one type of restraints from 6 Ala residues. Restraints are QS, DC and CS (left to right). **A**: Gaussian distributions of tilt and rotation; **B**: Semi-static dynamics using an order parameter; **C**: Average tilt and rotation from the Gaussian analysis; **D**: Average tilt and rotation from variable S_{zz} analysis. Here and elsewhere the RMSD contours are plotted from 0 kHz (blue) to the maximum value (red) using 10 contours for the dynamics and 15 contours for the orientation.

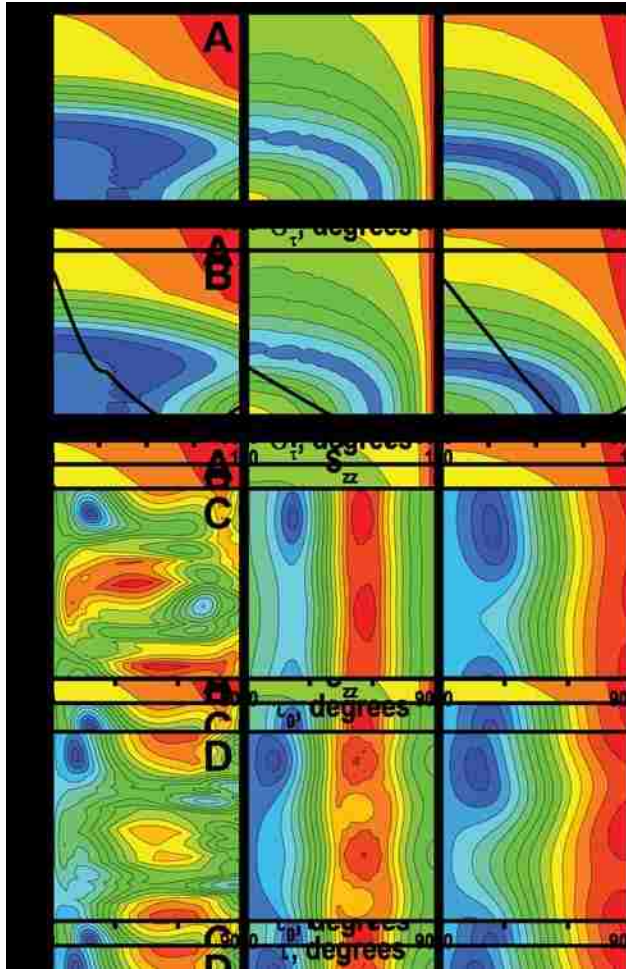


Figure 4. RMSD contour plots of orientation and dynamics of GWALP23 in DMPC/DHPC bicelles, using the combined QS, DC and CS restraints from Table 3. **A**: Gaussian distributions of tilt and rotation; **B**: Semi-static dynamics using an order parameter; **C**: Average tilt and rotation from the Gaussian analysis; **D**: Average tilt and rotation from variable S_{zz} analysis; **E**: Helical wheel plots for QS, DC and CS (left to right). Here and elsewhere filled circles indicate Ala and hollow ones indicate Leu.

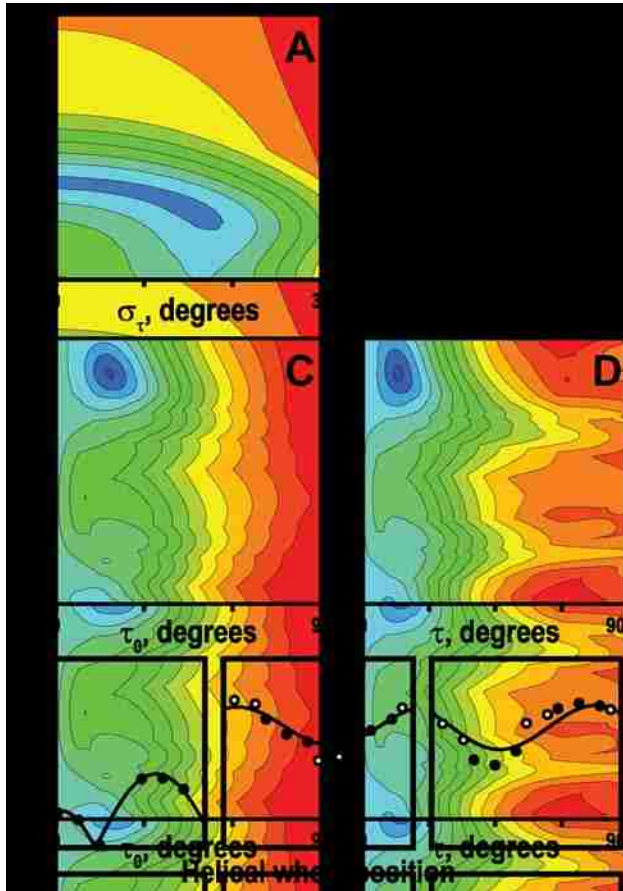


Figure 5. Deuterium and ^{15}N spectra of WWALP23 in DMPC/DHPC bicelles. **A:** ^2H spectra of WWALP23; **B:** SLF spectrum of WWALP23. Red circle in (B) indicates a resonance for a zero tilt angle in the absence of the dynamics.

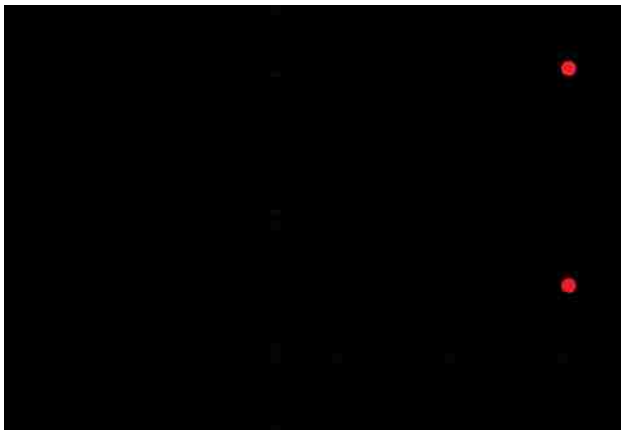


Figure 6. RMSD contour plots of WWALP23 dynamics in DMPC/DHPC bicelles, using one type of restraints: QS, DC or CS (left to right). **A**: Gaussian distributions of tilt and rotation; **B**: Semi-static dynamics using an order parameter.

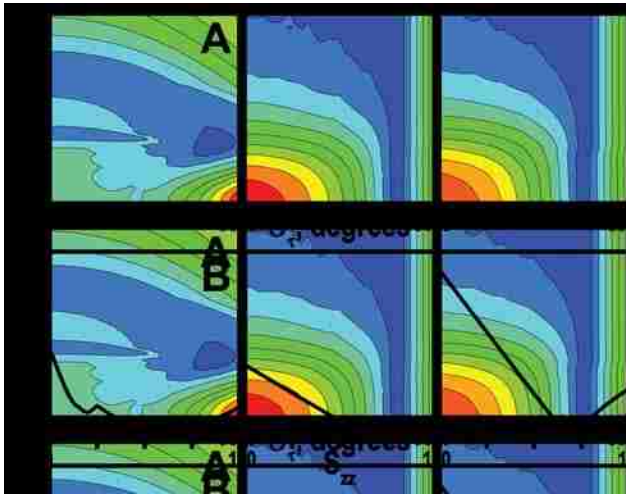


Figure 7. RMSD contour plots of orientation and dynamics of WWALP23 in DMPC/DHPC bicelles, using the combined QS, DC and CS restraints from Table 3. **A**: Gaussian distributions of tilt and rotation; **B**: Semi-static dynamics using an order parameter; **C**: Average tilt and rotation from the Gaussian analysis at point (c) in panel A; **D**: Average tilt and rotation from the Gaussian analysis at point (d) in panel A; **E**: Average tilt and rotation from variable S_{zz} analysis; **F**: Helical wheel plots for QS, DC and CS (left to right).

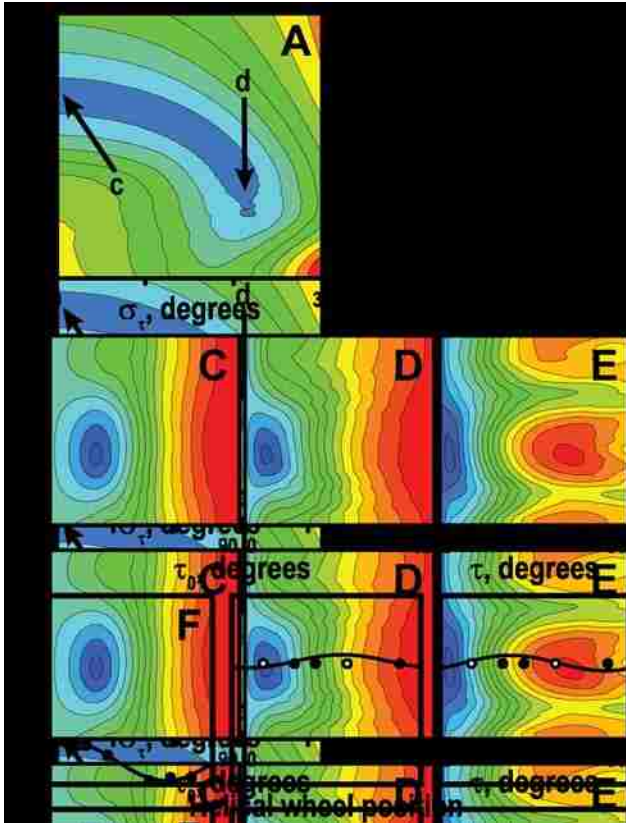


Figure 8. Deuterium and ^{15}N spectra of $\text{GW}^{3,21}$ ALP23-R14 in DMPC/DHPC bicelles. **A:** ^2H spectra of $\text{GW}^{3,21}$ ALP23-R14; **B:** SLF spectra of $\text{GW}^{3,21}$ ALP23-R14.



Figure 9. RMSD contour plots of orientation and dynamics of GW^{3,21}ALP23-R14 in DMPC/DHPC bicelles, using one type of restraints: QS, DC or CS (left to right). **A**: Gaussian distributions of tilt and rotation; **B**: Semi-static dynamics using an order parameter; **C**: Average tilt and rotation from the Gaussian analysis; **D**: Average tilt and rotation from variable S_{zz} analysis.

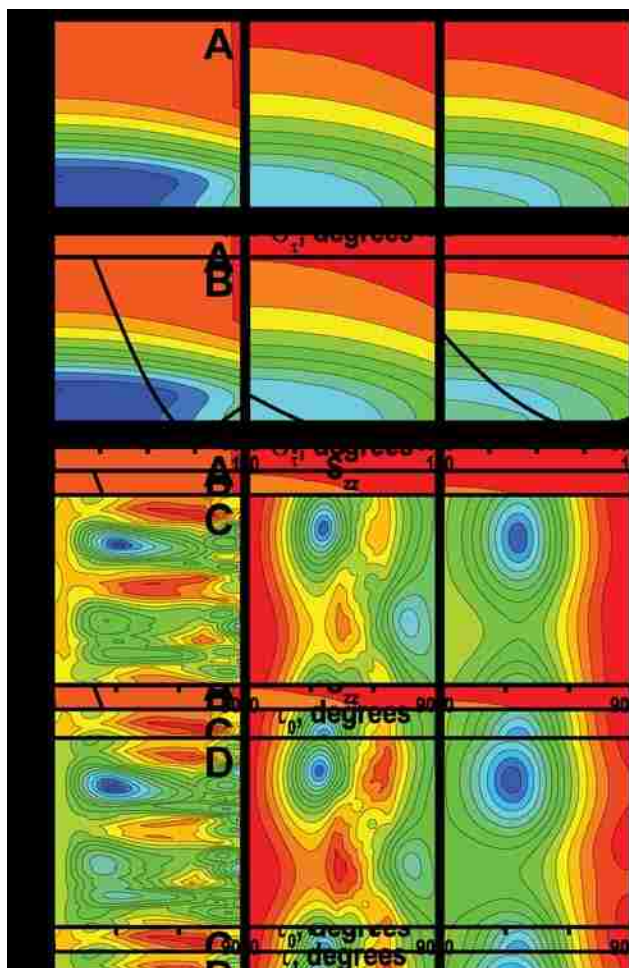
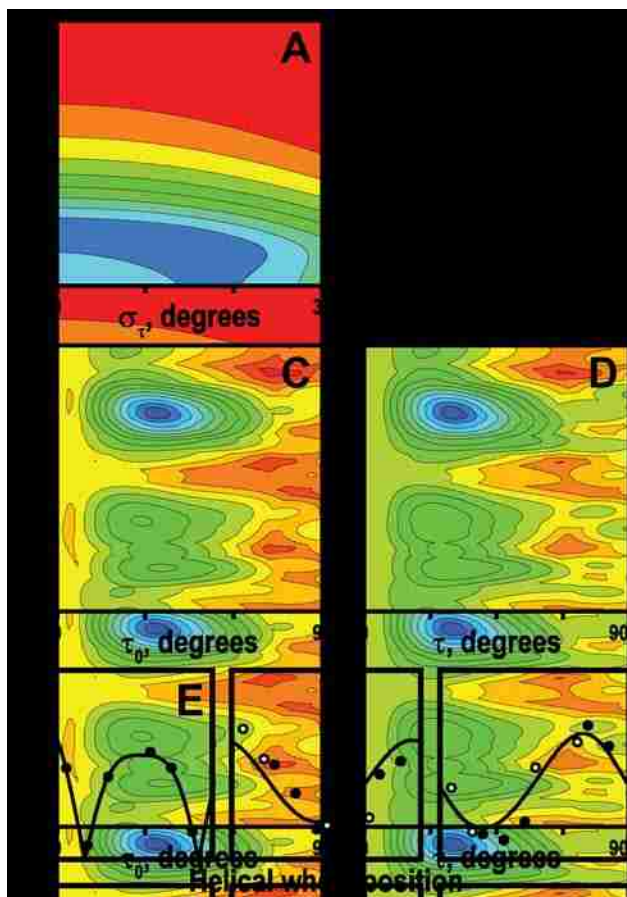


Figure 10. RMSD contour plots of orientation and dynamics of GW^{3,21}ALP23-R14 in DMPC/DHPC bicelles, using the combined QS, DC and CS restraints from Table 3. **A**: Gaussian distributions of tilt and rotation; **B**: Semi-static dynamics using an order parameter; **C**: Average tilt and rotation from the Gaussian analysis; **D**: Average tilt and rotation from variable S_{zz} analysis; **E**: Helical wheel plots for QS, DC and CS (left to right).



1.10 Supporting Information

S1. Definition and derivation of the chemical shift reference frame.

The general equation for the chemical shift is:

$$CS_{static} = \sigma_{11} \cdot \cos^2 \theta_{11} + \sigma_{22} \cdot \cos^2 \theta_{22} + \sigma_{33} \cdot \cos^2 \theta_{33} \quad \text{Eq. S1}$$

Where σ_{ii} are the chemical shift tensor components and θ_{ii} are the angles between the corresponding σ_{ii} and the applied magnetic field. To obtain the latter values, we first define the orthogonal reference frame (Figure S1) for the i -th residue in the peptide plane according to:

$$\begin{aligned} \varepsilon_{11} &= N_i \vec{C}_{i-1} \\ \varepsilon_{22} &= N_i \vec{C}_{i-1} \times N_i \vec{CA}_i \\ \varepsilon_{33} &= N_i \vec{C}_{i-1} \times \left(N_i \vec{C}_{i-1} \times N_i \vec{CA}_i \right) \end{aligned} \quad \text{Eq. S2}$$

In order for the reference frame to be aligned with the chemical shift tensor components, it has to be rotated by the angle $\alpha = 352^\circ$ around the ε_{22} axis, accomplished by the following rotation (note the ε_{ii} have to be re-arranged to form a right-handed set):

$$\sigma_{ii} = \begin{pmatrix} \cos \alpha & \sin \alpha & 0 \\ -\sin \alpha & \cos \alpha & 0 \\ 0 & 0 & 1 \end{pmatrix} \cdot \begin{pmatrix} \varepsilon_{33} \\ \varepsilon_{11} \\ \varepsilon_{22} \end{pmatrix} \quad \text{Eq. S3}$$

The detected components of the interaction with the magnetic field vector $H_0 = (0, 0, 1)$ can be written as series of dot products:

$$\begin{aligned}
 \cos \theta_{11} &= \sigma_{11} \cdot H_0 \\
 \cos \theta_{22} &= \sigma_{22} \cdot H_0 \\
 \cos \theta_{33} &= \sigma_{33} \cdot H_0
 \end{aligned}
 \tag{Eq. S4}$$

Finally, substituting equations S3-4 to equation S1, yields the relationship for the chemical shift:

$$\begin{aligned}
 \sigma_{static} &= \sigma_{11} \cdot (\cos \alpha \cdot \cos \theta_{33} + \sin \alpha \cdot \cos \theta_{22})^2 + \\
 &+ \sigma_{22} \cdot (-\sin \alpha \cdot \cos \theta_{33} + \cos \alpha \cdot \cos \theta_{22})^2 + \sigma_{33} \cdot (\cos \theta_{11})^2
 \end{aligned}
 \tag{Eq. S5}$$

Equation S5 represents the static case, which can be modified to include the sample macroscopic orientation and the order parameter S_{zz} – equation 3 in the main text.

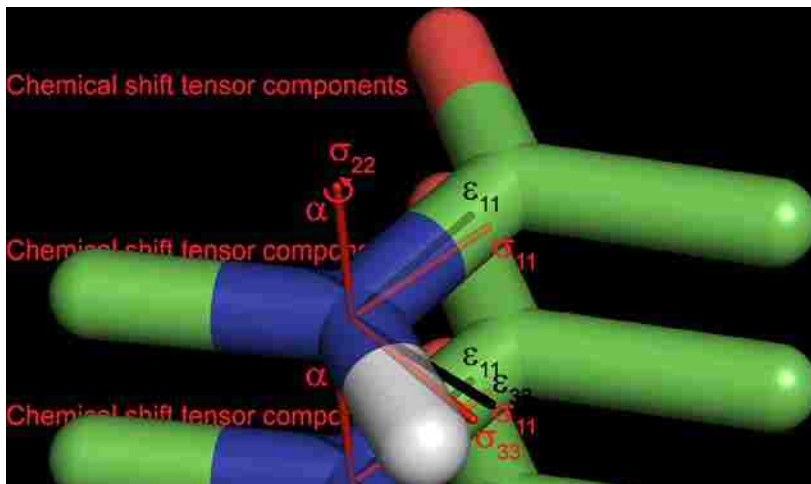


Figure S2. Two-dimensional probability distribution (Eq. 8) and QS values for residue 1 as a function of tilt and rotation (Eq. 10). The range of QS signals is from -37 kHz (blue) to +74 kHz red. Solid line is plotted at 0 kHz contour.

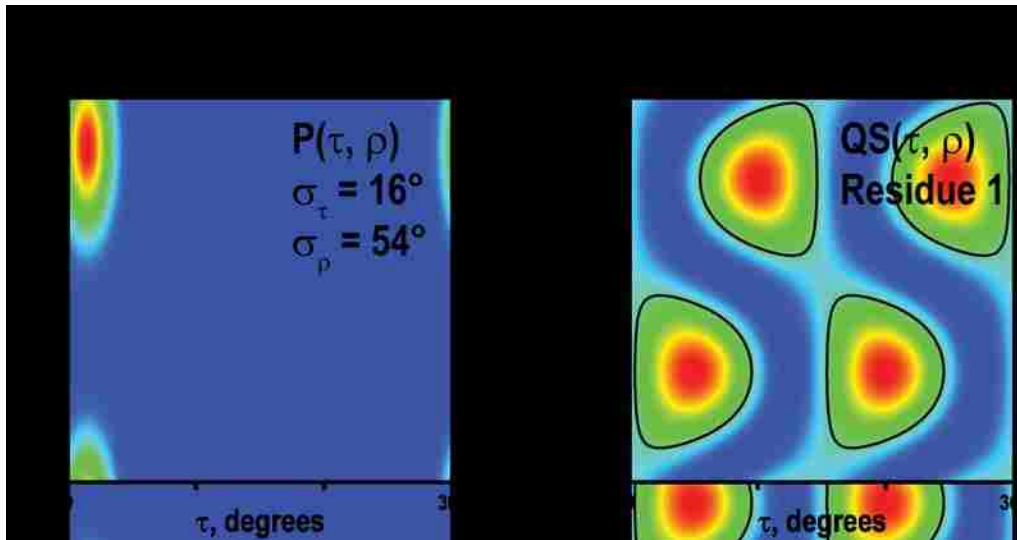


Figure S3. The effect of semi-static (S_{zz}) and Gaussian (σ_τ , σ_ρ) dynamics on QS, DC and CS. The static case (dashed line) represents 20° tilt angle.

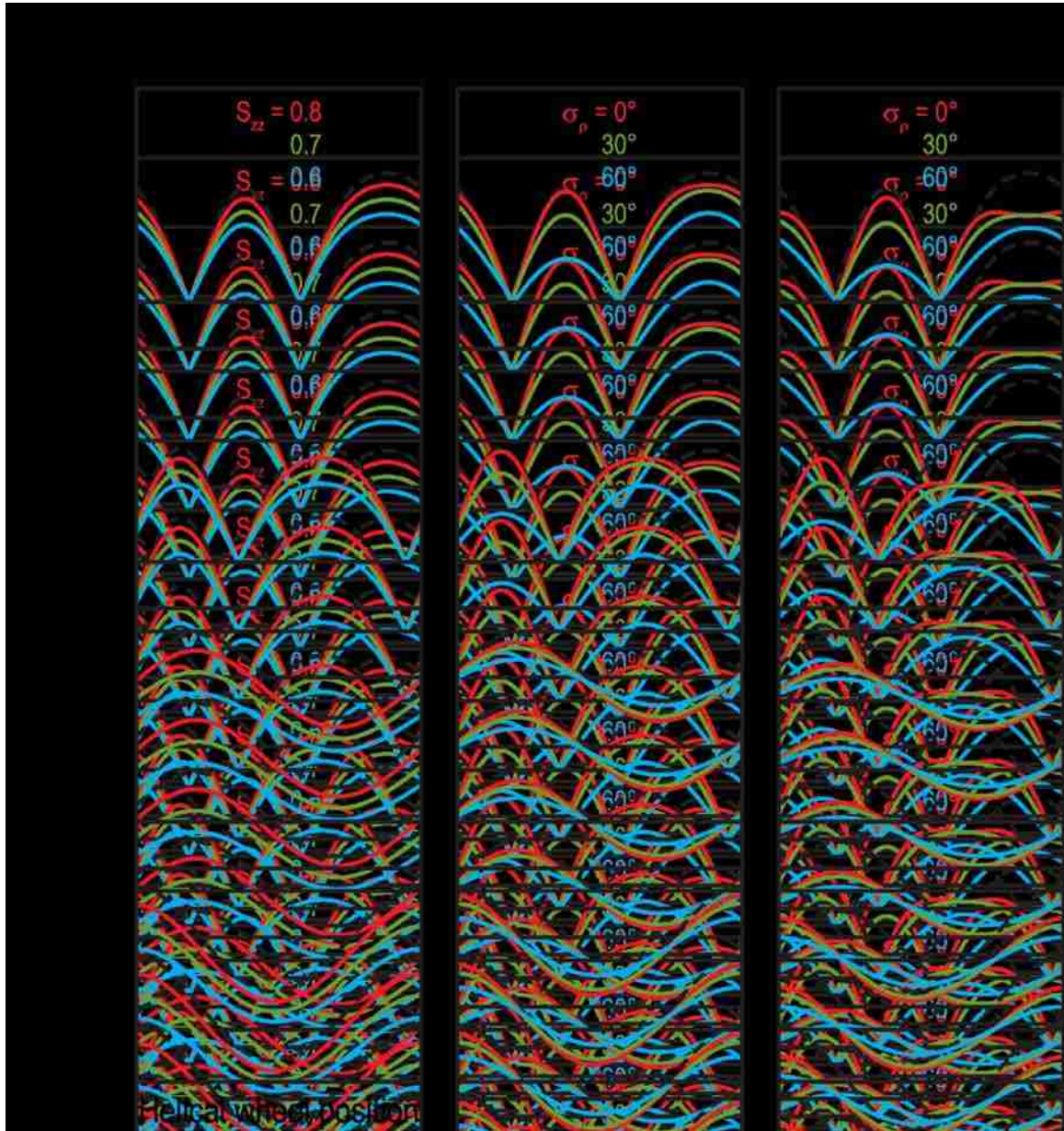


Figure S4. SLF spectrum of GWALP23 at 750 MHz.



Figure S5. Dynamics and orientation of GWALP23 in DMPC/DHPC for paired restraints.

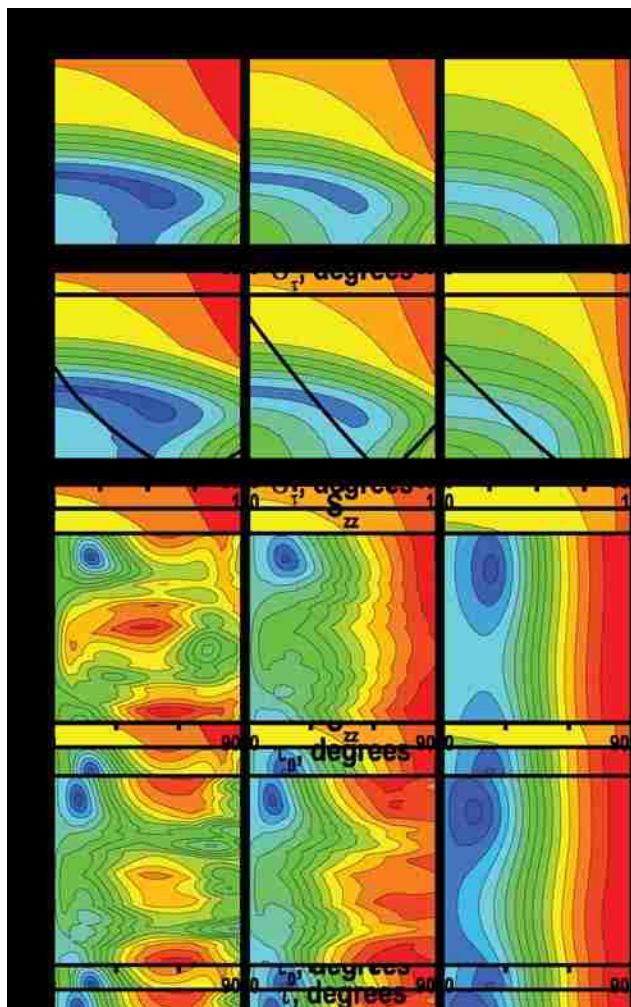


Figure S6. Dynamics and orientation of KWALP23 in DMPC/DHPC for individual and combined restraints.

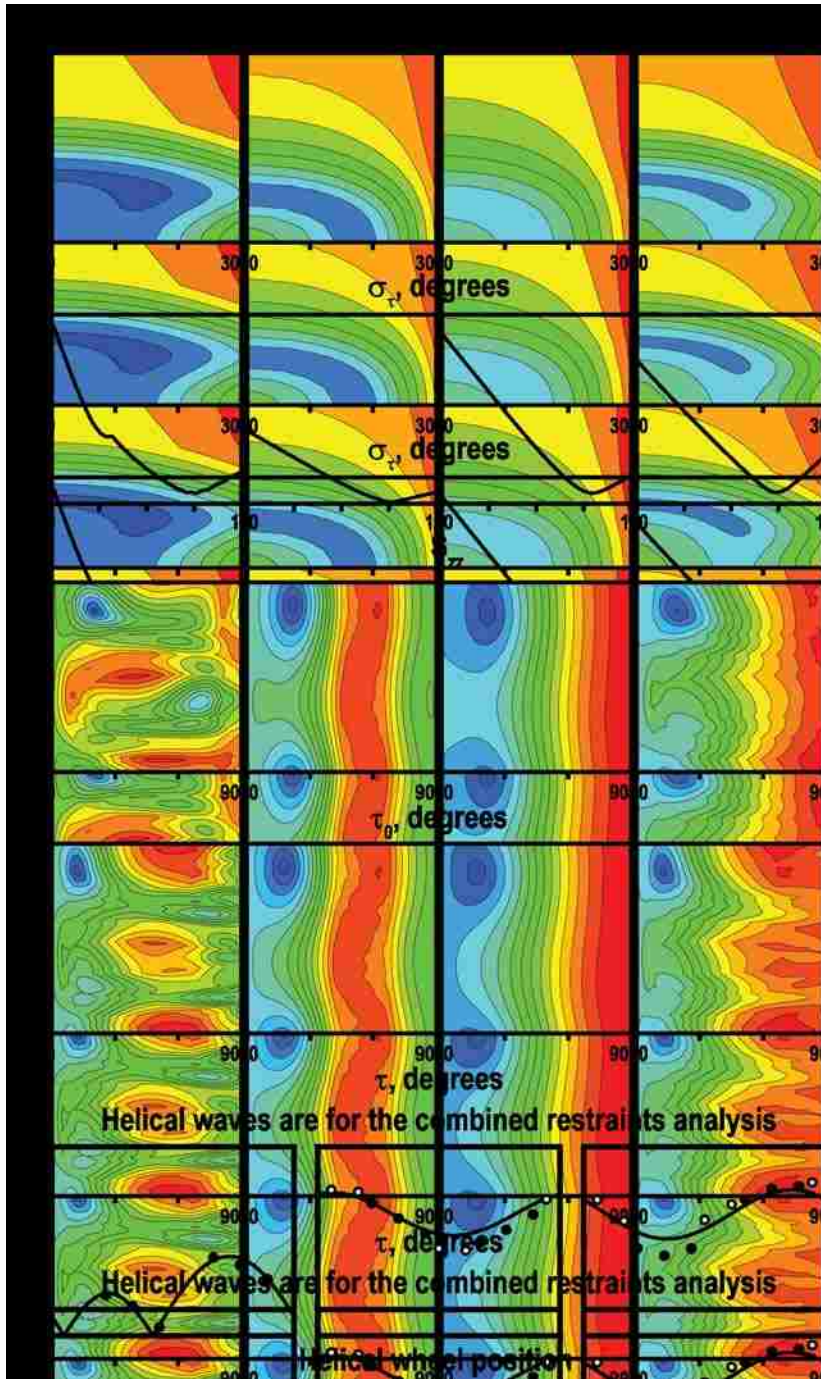
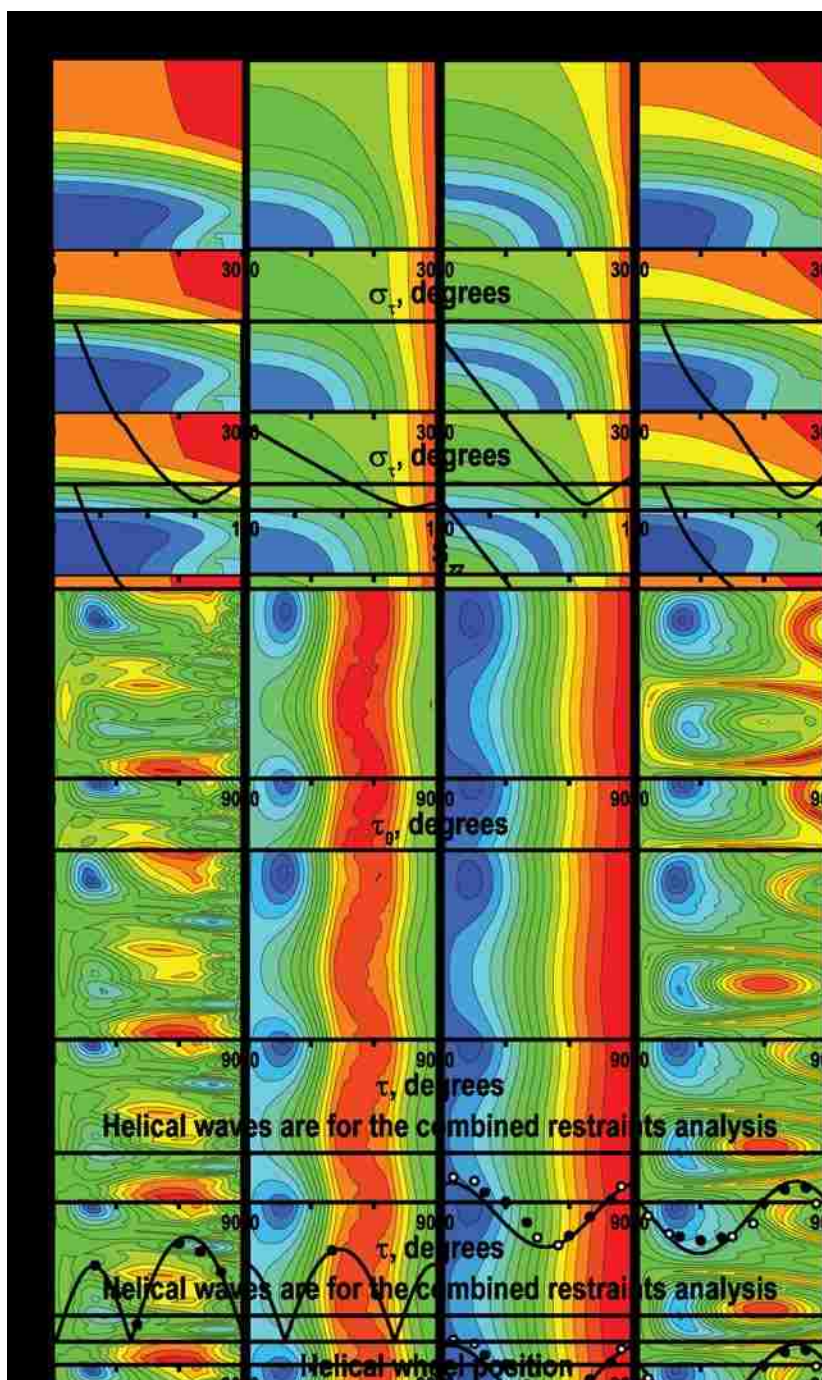


Figure S7. Deuterium and SLF spectra of KWALP23 in DLPC.



Figure S8. Dynamics and orientation of KWALP23 in DLPC for individual and combined restraints. Helical wave plots are for QS side chain, QS backbone (0-180 kHz range), DC and CS (left to right).



CHAPTER 2

Charged or Aromatic Anchor Residue Dependence of Transmembrane Peptide Tilt

This research was originally published in Journal of Biological Chemistry. Vostrikov, V.V., A.E. Daily, D.V. Greathouse, and R.E. Koeppe 2nd. Charged or aromatic anchor residue dependence of transmembrane peptide tilt. *J Biol Chem.* 2010; 285:31723-31730.

© The American Society for Biochemistry and Molecular Biology

2.1 Abstract

The membrane-spanning segments of integral membrane proteins often are flanked by aromatic or charged amino acid residues, which may “anchor” the transmembrane orientation. Single spanning transmembrane peptides such as those of the WALP family, acetyl-GWW(LA)_nLWWA-amide, furthermore adopt a moderate average tilt within lipid bilayer membranes. To understand the anchor residue dependence of the tilt, we introduce Leu-Ala “spacers” between paired anchors and in some cases replace the outer tryptophans. The resulting peptides, acetyl-GX²ALW(LA)₆LWLX²²A-amide, have either Trp, Lys, Arg or Gly in the two “X” positions. The apparent average orientations of the core helical sequences were determined in oriented phosphatidylcholine (PC) bilayer membranes of varying thickness using solid-state ²H NMR spectroscopy. When X is K, R or G, the direction of the tilt is essentially constant in different lipids and presumably is dictated by the tryptophans (W5 and W19) that flank the inner helical core. The Leu-Ala spacers are no longer helical. The magnitude of the apparent helix tilt furthermore scales nicely with the bilayer thickness except when X is W. When X is W, the direction of tilt is less well defined in each PC bilayer and varies up to 70° among DOPC, DMPC and

DLPC bilayer membranes. Indeed the $X = W$ case parallels earlier observations in which WALP-family peptides having multiple Trp anchors show little dependence of the apparent tilt magnitude on bilayer thickness. The results shed new light on the interactions of arginine, lysine, tryptophan and even glycine at lipid bilayer membrane interfaces.

2.2 Introduction

The lipid bilayer environment has a profound influence on the properties of peptides and proteins found within it. It is significant that many membrane-spanning proteins have bands of aromatic and/or positively charged residues at the membrane interface, which could serve as anchors for the protein orientation and promote favorable protein-lipid interactions. This anchoring is a widespread characteristic that is observed for a variety of proteins having both alpha and beta transmembrane folds (Chiang et al., 2005; Gibbons et al., 2006; Page et al., 2009; Stopar et al., 2006; Yau et al., 1998). Furthermore, polar amino acids influence the topology of membrane proteins, as the direction of insertion is driven by the asymmetric positioning of basic residues (Lys and Arg), giving rise to the “positive inside” rule for helical membrane proteins (von Heijne, 1986). Little is known, nevertheless, about the contributions of these residues in defining the orientations of the transmembrane segments within lipid bilayers (Granseth et al., 2005).

Due to the inherent complexity of membrane proteins in the native biological membrane environment, model systems provide meaningful ways to address specific questions about protein/lipid interactions. In particular, model peptides of the “WALP” family, having the general sequence acetyl-GWW(LA)_nLWWA-[ethanol]amide, have yielded

valuable information about peptide orientations, dynamics and lipid phase behavior (Killian et al., 1996; Kovacs et al., 2000; Nomura et al., 2005; White and von Heijne, 2005). An original design of WALP and “KALP” peptides included four anchoring residues: two sequential Trp or Lys residues on each side of a core transmembrane α -helix (de Planque et al., 1998). Comparisons of similar peptides revealed that the lysine-anchored peptides exhibit larger apparent tilt angles than their tryptophan counterparts (Ozdirekcan et al., 2005). Furthermore, the nature of the anchoring residue influences the tilt direction. The detailed factors responsible for the apparent magnitude and direction of tilt are nonetheless still unclear, since it is difficult to draw firm conclusions based upon four identical anchoring residues that are dispersed fairly evenly around a helical wheel projection.

The similar behavior of XALP23 (Leu/Ala core) and XLIP23 (all-Leu core) peptides having the same X residue suggests the importance of the anchor residue identity (Ozdirekcan et al., 2005). Magic angle spinning ^1H NMR experiments with WALP and KALP peptides in DMPC bilayers furthermore indicate anchor-specific perturbations in lipid resonances (de Planque et al., 2003). It was concluded that aromatic residues (such as Trp) are localized primarily to the carbonyl region of phospholipids, while charged residues (Lys, Arg) tend to be positioned farther outside of the membrane, potentially interacting with the lipid phosphate moieties (de Planque et al., 1999) as well as with water. We seek now to address the different influence of aromatic versus charged residues upon the orientations of transmembrane domains, using model peptides as prototype examples.

Phosphorous (^{31}P) NMR spectra of lipid bilayers incorporating WALP or KALP peptides show that the nature of the anchoring group also has a significant influence on the effective hydrophobic length. Both peptide series are capable of inducing isotropic and inverted hexagonal lipid phases—when the peptide length is too short compared to the membrane thickness. The detailed response is different, nevertheless: while KALP16 does not affect the organization of DOPC bilayer vesicles, addition of WALP16 promotes the inverted hexagonal (H_{II}) phase (de Planque et al., 1999). Similar effects have been noted for longer members of the series: Lys-anchored peptides affect lipid phase behavior in a manner that suggests that their effective hydrophobic length is less than that of corresponding Trp-anchored peptides. Interestingly, the arginine-flanked RALP23 has different influence on the lipid phase behavior than comparable lysine and histidine analogues, suggesting that charge delocalization on the Arg guanidium group could play a role (de Planque et al., 2002).

A related study of $\underline{\text{X}}$ ALP23 peptides in lipids prone to the formation of non-bilayer phases indicated that the chemical nature of the anchoring residue plays a smaller role for the phase modulation (Strandberg et al., 2002). The response of mixed phosphatidylethanolamine-phosphatidylglycerol membranes to transmembrane peptides is similar for charged and polar un-ionized $\underline{\text{X}}$ anchors. Somewhat unexpectedly, similar responses have been observed for positively and negatively charged $\underline{\text{X}}$ residues.

To gain further insight into the molecular mechanisms that govern peptide-lipid interactions, several studies have addressed the apparent peptide orientations within lipid bilayers of varying thickness. WALP peptides in particular have been found to exhibit

quite small apparent average tilt angles, with relatively little dependence upon the lipid bilayer thickness, as observed by solid-state ^2H and ^{15}N NMR (van der Wel et al., 2002; Vostrikov et al., 2008). Importantly, the solid-state NMR methods are non-perturbing and allow investigations of the peptide orientations within the actual lipid environment (van der Wel et al., 2002; Vostrikov et al., 2008). The nature of WALP (or KALP) peptides, with four Trp (or Lys) residues occupying four radial locations, remains however less than ideal for assigning the effects of individual anchoring amino acid residues. To better understand the interplay between anchor residue identity and position, therefore, we have designed the “ $\underline{\text{X}}^{2,22}\text{W}^{5,19}\text{ALP23}$ ” series of peptides, bearing the sequence acetyl- $\text{G}\underline{\text{X}}^2\text{ALW(LA)}_6\text{WLA}\underline{\text{X}}^{22}\text{A}$ -[ethanol]amide (Table 1). These sequences share the (Leu-Ala) $_{6,5}$ α -helical core of WALP19, yet the pairs of anchoring amino acids on either side of the core are separated by an additional short Leu-Ala spacer sequence. By keeping the inner anchor identity fixed (W^5 and W^{19}), while varying the outer anchor identity ($\underline{\text{X}}^2$ and $\underline{\text{X}}^{22}$), it becomes possible to examine the effects of different $\underline{\text{X}}$ residues on the peptide average orientation. As a control peptide, having just one obvious anchor on each side of the core helix, we employ the recently introduced GWALP23 sequence (Vostrikov et al., 2008; Vostrikov et al.) in which the $\underline{\text{X}}$ residues are glycine. The model in Figure 1 illustrates the relative positions of the X^2 , W^5 , W^{19} and X^{22} residues.

The design of the $\underline{\text{X}}$ WALP23 peptides enables one to address important questions that have arisen in previous studies. Does the distance between the inner Trp anchors retain primary importance for the peptide behavior, as suggested by ^{31}P NMR studies (de Planque et al., 2003)? Do the outer $\underline{\text{X}}$ anchors make significant contributions to the

apparent average peptide orientation? How do the properties vary with the identity of X? Is the charge on X a significant factor? When X is W, is it possible that the orientation of WWALP23 could be defined by the outer anchor positions? Finally, these peptides may help to promote understanding of a fundamental question: which amino acid residues serve as primary determinants of the transmembrane helix tilt magnitude and direction?

2.3 Experimental Procedures

N-Fmoc protected amino acids, Rink amide resin and Wang resin were purchased from NovaBiochem (San Diego, CA) and Advanced Chemtech (Louisville, KY). Commercial L-alanine, deuterated at C_α and C_β carbons (Ala-d₄), from Cambridge Isotope Laboratories (Andover, MA) was derivatized with an Fmoc protecting group as described previously (Greathouse et al., 1999; ten Kortenaar et al., 1986). DLPC, DMPC and DOPC were purchased from Avanti Polar Lipids (Alabaster, AL). Other reagents were from VWR Chemical (Irving, TX). All chemicals and reagents were of the highest grade available. Water was doubly deionized Milli-Q[®] water.

Peptides were synthesized on a model 433A solid-phase peptide synthesizer (Applied Biosystems; Foster City, CA) using modified FastMoc[®] chemistry, with extended deprotection and coupling times where needed. Two deuterium-labeled alanines at ~60% and 100% isotope abundance levels were incorporated in a single peptide, allowing the NMR signals to be distinguished and assigned based upon the relative intensities (Daily et al., 2008). GWALP23 and WWALP23 were synthesized without protecting groups and were cleaved from Wang resin using 20% ethanolamine in dichloromethane. KWALP23

and RWALP23 were synthesized with protecting groups (*tert*-butyloxycarbonyl [Boc] for Lys and Trp, and pentamethyl-2,3-dihydrobenzofuran-5-sulfonyl [Pbf] for Arg) (Isidro-Llobet et al., 2009) and were simultaneously deprotected and cleaved from Rink amide resin using TFA:phenol:triisopropylsilane:water in a 85:5:5:5 ratio. Crude peptides were purified on a 9.4×250 mm octyl-silica column (5 μm , 80 \AA) using a 96-100% ($\underline{\text{X}} = \text{G}$, W) or 92-96% ($\underline{\text{X}} = \text{K}$, R) methanol gradient over 24 min at a flow rate of 1.7 ml/min (~1100 PSI). Peptides were lyophilized multiple times from acetonitrile:water (1:1) to ensure complete removal of TFA. Purity of the peptides was verified by reversed-phase chromatography (see Fig. S1 in the Supplemental Data). Peptide identity was confirmed by means of MALDI mass-spectrometry (Fig. S2). The absence of TFA in peptide samples was verified by ^{19}F NMR spectroscopy (Fig. S3).

Circular dichroism measurements were performed on peptides incorporated into small unilamellar vesicles of DLPC at 1/40 (mol/mol) peptide/lipid (P/L), obtained by ultrasonic treatment. Spectra were recorded at 22 $^{\circ}\text{C}$ on a Jasco J-710 spectropolarimeter, using a 20 nm/min scan rate, 1.0 mm path length, 1.0 nm band width, and 0.2 nm step resolution. Five scans were averaged to enhance the signal-to-noise ratio.

Solid-state NMR samples were prepared using macroscopically aligned lipid bilayers, as described previously (van der Wel et al., 2002). Briefly, peptide was dissolved in trifluoroethanol, and concentration was determined spectrophotometrically using ϵ_{280} of $5600 \text{ M}^{-1}\text{cm}^{-1}\text{Trp}^{-1}$. Peptide solution was added to 80 μmol of lipid in chloroform to achieve 1/40 P/L molar ratio. Solvent was removed under a stream of nitrogen and sample was dried under vacuum. The peptide-lipid mixed film was redissolved in

methanol:water 95:5 and distributed evenly among 40 glass slides ($4.8 \times 23 \times 0.07$ mm; Marienfeld; Lauda-Königshofen, Germany). Slides were dried under vacuum (< 1.5 Pa) for at least 48 h and hydrated with ^2H -depleted water (Cambridge) to achieve 45% hydration (w/w). Slides were sealed in a glass cuvette using epoxy and left to equilibrate at 40°C for at least 48 h before measurement.

Solid-state NMR spectra were recorded at 50°C using two Bruker (Billerica, MA) Avance spectrometers, each operating at a proton frequency of 300 MHz. Spectra were obtained with the membrane normal either parallel ($\beta=0^\circ$) or perpendicular ($\beta=90^\circ$) to the applied magnetic field. For a peptide with fast averaging around the lipid bilayer normal (but not the peptide axis) the ^2H quadrupolar splittings ($\Delta\nu_q$) observed at $\beta=90^\circ$ have absolute magnitude of $1/2$ those at $\beta=0^\circ$ (Aisenbrey and Bechinger, 2004). Spectra were recorded using a quadrupole echo pulse sequence (Davis et al., 1976), with pulse lengths of 3.2-4.5 μs , echo delays of 110-125 μs and recycle delay of 90 ms. Typically, 700,000 free induction decays were accumulated. Prior to Fourier transformation, an exponential weighting function resulting in a 100 Hz line broadening was applied. Proton-decoupled ^{31}P NMR spectra were obtained with the Bruker “zgpg” pulse program, using recycle delay of 5 s and pulse length of 6 μs . In ^{31}P NMR spectra of aligned bilayers, peaks at $\beta=0^\circ$ and $\beta=90^\circ$ correspond to the $\sigma_{//}$ and σ_{\perp} edges of a powder pattern (see Fig. S4).

Deuterium NMR signals from $\text{C}\alpha\text{-D}_3$ groups of Ala- d_4 residues in XWALP23 peptides were analyzed according to Geometric Analysis of Labeled Alanines (GALA) method, implemented in Microsoft Excel (Thomas et al., 2009; van der Wel et al., 2002). The

analysis is based on a relationship between the alanine C_βD₃ quadrupolar splitting ($\Delta\nu_q$) and the angle θ between the alanine C_α-C_β bond vector and the applied magnetic field:

$$\Delta\nu_q = \frac{3}{2} S_{zz} \frac{e^2 q Q}{h} \left[\frac{1}{2} (3 \cos^2 \theta - 1) \right] \cdot \left[\frac{1}{2} (3 \cos^2 \beta - 1) \right] \cdot \left\langle \frac{1}{2} (3 \cos^2 \gamma - 1) \right\rangle$$

The angle θ can be further expressed analytically in terms of peptide geometry and orientation, namely tilt magnitude (τ) and tilt direction (ρ , relative to C_α of Gly¹), as well as the angle $\varepsilon_{//}$ between the helix axis and C_α-C_β bond vector of a given alanine residue. Angle β represents the macroscopic sample orientation (defined above, with respect to H₀), and angle γ is the tetrahedral bond angle within a methyl group. Based upon earlier experience (van der Wel et al.; Vostrikov et al.), the value of $\varepsilon_{//}$ was set to 59.4°. The variables τ and ρ , and a global order parameter S_{zz} , were treated as free parameters in order to minimize the RMSD between the observed $\Delta\nu_q$ values and those calculated using Equation 1 (Strandberg et al., 2004; van der Wel et al., 2002). This analysis incorporates dynamics in manner similar to “model 3” of Strandberg et al. (Strandberg et al.). Further considerations were given to anisotropic molecular motions and to combined analyses of ¹⁵N-¹H dipolar couplings and ²H quadrupolar splittings (see Discussion). Due to the symmetry considerations, GALA analysis returns four combinations of [τ , ρ] values. Here we report the [τ , ρ] data in a [90°, 360°] space, as in previous studies on WALP peptides (Daily et al., 2008; Strandberg et al., 2004; van der Wel et al., 2002; Vostrikov et al., 2008).

2.4 Results

The hydrophobic core of XWALP23, composed of alternating Leu-Ala residues, is expected to adopt an α -helical conformation. To check the secondary structures, we recorded CD spectra for the peptides having variable X residues and incorporated into hydrated DLPC bilayer membranes. All such peptides exhibited mean residue ellipticity profiles typical of an α -helix, characterized by minima at 208 and 222 nm and by the ratio $\epsilon_{222}/\epsilon_{208}$ between 0.74 and 0.86 (Fig. 2). When X is G, K or R, the CD spectra exhibit high degree of overlap, while there is a change of $\sim 10\%$ in ellipticity in the 205-225 nm region when X is W. The spectral difference when X is W may be indicative of a different extent of helix formation at the peptide termini, but could also be caused by UV absorption by the side chains of the extra Trp residues (Chakrabarty et al., 1993; Stromstedt et al., 2009).

Having confirmed the overall α -helical character of the XWALP23 peptides, we next introduced Ala- d_4 close to the center of the sequence, in positions 11 and 13. Deuterium NMR spectra of these peptides in lipid bilayers of varying thickness are illustrated in Fig. 3. If the peptides were not tilted in the membrane, the signals from all of the alanine $C_{\beta}D_3$ groups would show the same quadrupolar splittings (van der Wel et al., 2002); however, two pairs of peaks are readily identified in each spectrum in Fig. 3. The pattern displayed by variations in the magnitudes of the alanine $C_{\beta}D_3$ quadrupolar splittings is related to the apparent tilt angle τ , defined between the membrane normal and the peptide's helix axis (van der Wel et al., 2002). It can be seen that the particular Ala¹¹ and Ala¹³ $\Delta\nu_q$

magnitudes undergo changes for different \underline{X} residue identities, being smallest for $\underline{X} = \text{W}$, intermediate for $\underline{X} = \text{G}$ and highest for $\underline{X} = \text{K}$ or R . There also exists a definite trend among the host lipids, with the largest $\Delta\nu_q$ values being observed in DLPC bilayer membranes, which suggests that the peptides may be more tilted when shorter lipids compose the bilayer.

For a detailed study of the orientations of the \underline{X} WALP23 peptides in lipid bilayers, we incorporated Ala- d_4 residues throughout the hydrophobic core (residues 7, 9, 11, 13, 15 and 17) of each peptide, labeling two positions in each synthetic peptide. All of the respective ^2H NMR spectra are presented as Supplemental Data (Figures S5, S6, S7, S8), and the observed quadrupolar splitting magnitudes are reported in Table 2. Errors in the observed values were estimated from duplicate samples and also by performing the experiments at β angles of both 0° and 90° for the sample orientation, since $\Delta\nu_q$ for a given peptide-lipid system follows a $\frac{1}{2}(3\cos^2\beta - 1)$ relationship. The standard deviation was found generally to be within ± 0.5 kHz, although larger deviations up to ± 1.2 kHz were observed for a few cases where the peaks are relatively broad and exhibit large $|\Delta\nu_q|$ values.

For the KWALP23 peptide, we have revised a previous incorrect assignment of a $\Delta\nu_q$ value. Due to peak overlap, the $\Delta\nu_q$ for Ala 9 in KWALP23, incorporated in DLPC, was interpreted as 13.6 kHz (Daily et al.), while the actual value is 22.2 kHz (Table 2 and Fig S7). We were able to clarify the situation using singly labeled peptides. With this newly revised assignment, the earlier suggestion of a kink (Daily et al.) disappears from the

GALA analysis of KWALP23 (see discussion). Also for GWALP23, small revisions to the Δv_q values (Table 2) and to the fitted value of S_{zz} led to a moderately larger apparent magnitude for the tilt angle τ in DLPC than previously reported (19).

The observed quadrupolar splittings were subjected to GALA analysis, at first incorporating dynamics by means of a straightforward isotropic variable S_{zz} parameter, according to Equation 1. The quality of the fits was assessed by RMSD values, which typically are close to 1 kHz, or lower. Because overly high or low values of $\epsilon_{//}$ are characteristic of poor fits (van der Wel et al.), the values of $\epsilon_{//}$ representing the alanine side chain geometry was kept at 59.4° . The τ , ρ , S_{zz} and corresponding RMSD values are provided as Table S1, while the theoretical Δv_q curves corresponding to the best-fit τ , ρ and S_{zz} values are presented in Fig. 4, overlaid with the experimental data. The nearly constant phase of the sine wave amplitude curves, except when \underline{X} is W (Fig. 4), illustrates that the screw rotation ρ is essentially constant when \underline{X} is K, R or G. Furthermore, the magnitude of the apparent tilt τ scales with the lipid bilayer thickness when \underline{X} is K, R or G (see Discussion). While the GALA analysis often is not especially sensitive to S_{zz} (van der Wel et al.), the fits for the \underline{X} WALP23 peptides nevertheless show trends toward lower S_{zz} values (Table S1) when the host bilayer is DLPC, or when the identity of \underline{X} is W in all of the lipid bilayers, suggesting increased molecular motion in these cases. The incorporation of more complex dynamics models did not substantially alter the results or conclusions (see Discussion).

To probe the effect of the peptide/lipid ratio on the peptide orientation, we have examined GWALP23 in DMPC at different values of P/L. When P/L is decreased from 1/20 to 1/40 and then to 1/80, there are small yet consistent increases in the quadrupolar splittings throughout the hydrophobic core (Table 2). These changes lead to only minor effects on the apparent tilt angle τ (namely, a change of $<1^\circ$ when the peptide is diluted from 1/20 to 1/40, and about 1° upon further dilution to 1/80).

The side chains of lysine and arginine have high pK_a values in aqueous solution and are expected to be charged at the peptide-lipid interface. It is considered that the anchoring properties of lysine and arginine arise in part from electrostatic interactions with the phosphate groups of lipid molecules, in addition to the propensity of charged polar groups to be in or near the aqueous phase. To test whether the microenvironment of the XWALP23 peptides with ionizable X residues would influence the average peptide orientation, we prepared oriented samples hydrated with HEPES buffer (pH 7.4) in ^2H -depleted water containing 0.1 M NaCl. Deuterium NMR spectra of KWALP23 and RWALP23 incorporated in DMPC bilayers under these conditions were nearly identical to those where only water (unbuffered) was used for hydration (Fig. S9). The only notable effect is a small decrease in the signal-to-noise ratio for samples containing NaCl, which can be attributed to radio frequency power dissipation (Hautbergue and Golovanov, 2008).

The transmembrane segments of proteins strongly favor secondary structures that maximize hydrogen bonding, to help to satisfy the energetic requirements associated with partitioning the peptide backbone polar carbonyl groups into the lipid acyl chain

environment (Page et al., 2008; White and von Heijne, 2005). Nevertheless, the requirements are less stringent for residues that are located near the lipid head group interfacial regions. With respect to the XWALP23 peptides, it is of interest therefore to know whether the α -helical conformation is retained throughout the peptide, including the Leu-Ala “spacer” segments between the inner and outer “anchor” residues, or whether the helical region might encompass only the core segment between Trp⁵ and Trp¹⁹? To address this question, we synthesized GWALP23 peptides having a single Ala-d₄ label incorporated at either Ala³ or Ala²¹. The $\Delta\nu_q$ values from these peptides theoretically will indicate whether or not the secondary structure remains an essentially unbroken α -helix from Ala³ through Ala²¹.

The ²H NMR spectra of GWALP23 with Ala³ or Ala²¹ labeled are shown in Fig. 5. These residues are located 18 amino acids apart, exactly five helical turns in an ideal α -helix model with 100° increment per amino acid, and could therefore give identical ²H quadrupolar splittings. However, the $\Delta\nu_q$ values exhibited by alanines at these two positions are *very* different, with neither of the signals compatible with the quadrupolar wave plot for the core transmembrane helix of GWALP23 (Fig. 4, panel G). These results reveal that the transmembrane α -helix in GWALP23, and presumably in XWALP23 peptides generally, is terminated at or near the innermost Trp residues, resulting in frayed edges outside of the core helix that is both flanked and defined by W⁵ and W¹⁹. This finding that the core helix terminates within or near each of the Leu-Ala spacers is consistent with an earlier statistical survey, which indicated that approximately two thirds

of the folded transmembrane structures were disordered in the interface region (Granseth et al., 2005).

2.5 Discussion

Time-honored experiments with model systems having multiple tryptophans per peptide terminal have demonstrated well the aggregate anchoring properties of Trp residues for gramicidin channels (O'Connell et al., 1990; Separovic et al.) and WALP peptides (de Planque et al.; Killian et al.) at membrane/water interfaces. The present studies with the XWALP23 series of peptides enable initial assessments of the anchoring properties of individual Trp, Lys and Arg residues near the ends of transmembrane peptide domains and segments. The present results concerning helix tilt furthermore complement earlier findings about interfacial side chain locations, namely that Lys side chains prefer anchoring positions that are about 3-4 Å farther from the lipid bilayer center than those of the Trp side chains (de Planque et al.). Indeed, a noteworthy feature for the XWALP23 design is that the X residue α -carbons should be separated from the W residue α -carbons by about 4 Å along the bilayer normal (depending upon the secondary structure of each Leu-Ala spacer). Remarkably, the properties of XWALP23 peptides having Gly residues in the X² and X²² positions are quite similar to those having Lys or Arg. When X² and X²² are Trp, effectively giving rise to “extra” Trp residues, the direction of peptide tilt becomes less well defined, and the magnitude of tilt loses its tendency to scale with the lipid bilayer thickness. Indeed the peptide properties with “extra” Trp residues are present parallel earlier observations with WALP19 and WALP23 (Holt et al.; Strandberg et al.; van der Wel et al., 2002). These particular issues will be discussed in turn.

To visualize the anchor residue dependence of the apparent tilt, RMSD contour plots were constructed for the $[\tau, \rho]$ coordinates (Fig. 6). When fitted using an isotropic principal order parameter, the global minima for each of the \underline{X} WALP23 peptides are well defined and generally encompass only a small range of apparent τ and ρ values.

Reminiscent of WALP23, the largest allowed ranges for both τ and ρ are observed when \underline{X} is W. Comparing the results in different lipids reveals that the apparent peptide tilt generally increases with decreasing hydrophobic thickness of the lipid bilayer; again the exception occurs when $\underline{X} = W$ (Fig. 6). GWALP23 and the peptides with positively charged K or R outer anchors undergo apparent tilt changes of $\sim 4^\circ$ - 6° as the lipid acyl length increases by two methylene groups in each leaflet. The changes in the apparent tilt are presumably a consequence of hydrophobic (mis)matching, as was predicted for WALP family peptides. It is in this regard notable that the variation of apparent helix tilt angle with lipid bilayer thickness was much smaller for the original WALP series peptides: essentially nil for WALP19 (van der Wel et al.), and a difference of only $\sim 4^\circ$ for WALP23 between DLPC and DOPC (Strandberg et al.). By contrast, for the \underline{X} WALP23 series, the mismatch-induced changes in the apparent peptide tilt can be as large as 16° between DLPC and DOPC (Fig. 6). These changes are likely not due to altered lipid packing or acyl chain order because the influence of WALP family peptides on bilayer properties is noticeably small (de Planque et al., 1998; Morein et al., 2002), even at somewhat higher P/L ratios than implemented here.

It has been noted that the fits to the Ala ^2H quadrupolar splittings of WALP23 in DMPC differ when S_{zz} is decomposed into explicit motion parameters ($\Delta\tau$ and $\Delta\rho$), which are

included in the analysis (Esteban-Martin and Salgado; Esteban-Martin et al.; Holt et al.; Ozdirekcan et al.; Strandberg et al.). We now surmise that this feature may be attributed to having “too many” interfacial indole rings, possibly competing with each other when the “extra” Trp residues are present in the interface region, as observed also in striking fashion with WWALP23 (compare panel *W* with the other panels in Fig. 6). With WALP23, the best combined fits to chemical shift anisotropies (^{13}C and ^{15}N), dipolar couplings (^{13}C - ^{15}N) and quadrupolar splitting (^2H) involve $\Delta\rho$ motions of $\pm \sim 80^\circ$ about the helix axis, in addition to rapid rotational averaging about the bilayer normal (Holt et al.). Such large-amplitude $\Delta\rho$ motions would seem unrealistic when Arg and Lys side chains are present together with Trp (see also (Vostrikov et al., 2010)), yet the question of $\Delta\rho$ motion remains pertinent for GWALP23 itself.

The direction and magnitude of the apparent tilt for GWALP23 as well as KWALP23 have been verified by independent ^{15}N PISEMA experimental methods (Vostrikov et al., 2009; Vostrikov et al., 2008). For both peptides, the GALA and PISEMA methods show excellent agreement when using a semistatic analysis with a (variable) principal order parameter S_{zz} . Furthermore, combined analysis using eleven data points (^2H quadrupolar splitting and ^{15}N - ^1H dipolar couplings) also gives an excellent fit for GWALP23 in DLPC (see Table S2), whether or not a Gaussian approach is employed to treat $\Delta\rho$ and $\Delta\tau$ motions. (As noted, refinements of the Δv_q values (Table 2) and of S_{zz} , indicating increased motion, led to a modest increase in the apparent τ for GWALP23 in DLPC, compared to a previous report (19).) Again we infer that the presence of only one Trp at each terminal of the GWALP23 core helix may limit $\Delta\rho$ motions.

Among these XWALP23 peptides, WWALP23 is the outlier. When outer tryptophans W² and W²² are present, the response of WWALP23 toward changes in the lipid environment again resembles that of the original WALP peptides. Indeed there is considerable overlap of $[\tau, \rho]$ solutions for WWALP23 in the three lipids investigated (Fig. 6, panel W).

Conceivably the important common feature among WALP19, WALP23 and WWALP23 is the presence of multiple – possibly competing – tryptophan anchors on both ends of the transmembrane peptide core helical sequence. The RMSD minima for WWALP23 also are broader compared to the other XWALP23 peptides, which reflects an increasing uncertainty in ρ as the “apparent” τ value diminishes, probably reflecting increased motion, including $\Delta\rho$ motion (Holt et al.). It is of further interest that the variation of ρ with lipid identity appears to be larger for WWALP23 (Fig. 6) than for WALP19 (van der Wel et al.), WALP23 (Strandberg et al.) or the other XWALP23 peptides (Fig. 6).

Although the uncertainty in ρ is indeed quite large for WWALP23 in each of the lipid bilayers, the detailed influence of the short two-residue Leu-Ala spacers between the inner/outer Trps in WWALP23 may merit further investigation. It is in this regard noteworthy that the labels at spacer residues A³ and A²¹ (Fig. 4) indicate that the Leu-Ala spacer sequences in GWALP23 are not helical, although the spacer conformation remains unknown for WWALP23. The CD spectra (Fig. 2) suggest marginally increased helicity for WWALP23 compared to the other XWALP23 peptides, which may or may not pertain to the spacer sequences. (Interestingly, a longer helical segment with more rigid ends would be expected to show greater sensitivity to lipid hydrophobic mismatch, whereas the opposite is observed for WWALP23.)

For the case of KWALP23 in DLPC, the quadrupolar splitting magnitudes are closely similar for the alanine 7, 9 and 11 side chains; namely 28.6, 22.2, 26.2 kHz, respectively (Table 2). Also, in DMPC and DOPC the $\Delta\nu_q$ values for the Ala⁷ and Ala¹¹ side chains remain nearly indistinguishable (Table 2). These similarities cause peak overlap in the NMR spectra for multiply labeled peptides, which in turn led us to assign incorrectly the splittings for Ala⁹ in an earlier study (Daily et al., 2008). With the corrected assignments, the GALA fits for KWALP23 now are excellent (Fig. 6), and we dismiss an earlier suggestion of a kink in the transmembrane helix of KWALP23 (Daily et al., 2008). The similar fits for RWALP23 and KWALP23 (Figs. 4, 6) further make the case that these peptides are not kinked.

Remarkably, considerations of $\Delta\rho$ motion do not in any known case influence conclusions about the mean peptide rotation ρ_0 which defines the direction of tilt. The lack of influence on ρ_0 is true in both molecular dynamics simulations (Esteban-Martin and Salgado; Esteban-Martin et al.; Ozdirekcan et al.) and fits to solid-state NMR data (Esteban-Martin et al.; Holt et al.; Strandberg et al.; Vostrikov et al.). The established definite ρ_0 values are well illustrated using polar plots (Fig. 7) to view the best-fit apparent (τ , ρ) results. Indeed Figure 7 shows the remarkable consistency of the tilt direction ρ for XWALP23 peptides in each of the DLPC, DMPC and DOPC lipid bilayer membranes, and for each X residue identity except W. When X is W, by contrast, the preferred ρ values are altered – and unpredictably varied in the different lipids. At the same time, the apparent τ values for WWALP23 become quite similar, unexpectedly small, and rather insensitive to the bilayer hydrophobic thickness (Fig. 7). To be sure, the

situation for WWALP23 is reminiscent of earlier results for WALP19 (van der Wel et al.) and WALP23 (Strandberg et al.), each of which also contains multiple – and possibly competing – Trp residues near each peptide terminal. In these cases, it appears that the added outer tryptophans may preclude additional tilting, and that the preferred rotation angles and significant $\Delta\rho$ motion may arise from a compromise among the different Trp indole side chains that occupy different radial positions. These complexities may relate also to the now numerous comparisons among experimental observations and computational predictions for WALP23 (Esteban-Martin and Salgado; Esteban-Martin et al., 2009a; Holt et al.; Holt et al.; Ozdirekcan et al., 2007; Strandberg et al.; Strandberg et al.). It is further of note that tryptophans near the N- and C-terminals of transmembrane peptides exhibit different geometric and motional properties (van der Wel et al.).

We observe additionally that the positively charged Lys and Arg residues generally increase the apparent tilt angle by small amounts, compared to the case when X is G (Fig. 6-7), although conspicuously without changing the direction of the tilt of XWALP23 peptides. Furthermore, Arg causes marginally larger tilts than does Lys in equivalent situations (Fig. 7).

We conclude with a return to the anchoring properties of the Trp indole rings. An overview of Figures 6 and 7 highlights the importance of the inner tryptophans W^5 and W^{19} for the direction of the tilt. The tilt direction then can change when a single arginine is inserted between W^5 and W^{19} (Vostrikov et al.), and will change even more dramatically when there exist additional tryptophans more distant from the bilayer center (Fig. 7). The added outer tryptophans seem not only to introduce additional dynamics

(Holt et al.), but also to confuse the issue of the preferred tilt, namely in WWALP23, WALP19 and WALP23. Indeed the extra outer tryptophans not only modify the direction of peptide tilt, but also flatten the dependence of the apparent tilt magnitude upon lipid bilayer thickness. In summary, for those XWALP23 membrane-spanning peptides in which only one Trp anchor is present near each end, the residues W⁵ and W¹⁹ seem to determine the direction of the tilt; the magnitude of the apparent tilt away from the bilayer normal scales with the lipid bilayer thickness; and the identity of residues X² and X²²—whether G, K or R—exerts subtle influence upon the magnitude of the apparent tilt. When additional tryptophans W² and W²² are present, the patterns of peptide behavior and response to lipid environment become not only altered but also less systematic.

2.6 Acknowledgments

This work was supported in part by NSF grant MCB-0841227 and by the Arkansas Biosciences Institute. The NMR facility was supported by NIH grant RR 15569.

2.7 References

- Aisenbrey, C., and B. Bechinger, 2004. Investigations of polypeptide rotational diffusion in aligned membranes by ^2H and ^{15}N solid-state NMR spectroscopy. *J Am Chem Soc* 126: 16676-16683.
- Chakrabartty, A., T. Kortemme, S. Padmanabhan, and R.L. Baldwin, 1993. Aromatic side-chain contribution to far-ultraviolet circular dichroism of helical peptides and its effect on measurement of helix propensities. *Biochemistry* 32: 5560-5565.
- Chiang, C.S., L. Shirinian, and S. Sukharev, 2005. Capping transmembrane helices of MscL with aromatic residues changes channel response to membrane stretch. *Biochemistry* 44: 12589-12597.
- Daily, A.E., D.V. Greathouse, P.C. van der Wel, and R.E. Koeppe 2nd, 2008. Helical distortion in tryptophan- and lysine-anchored membrane-spanning α -helices as a function of hydrophobic mismatch: a solid-state deuterium NMR investigation using the geometric analysis of labeled alanines method. *Biophys J* 94: 480-491.
- Davis, J.H., K.R. Jeffrey, M. Bloom, M.I. Valic, and T.P. Higgs, 1976. Quadrupolar echo deuterium magnetic resonance spectroscopy in ordered hydrocarbon chains. *Chem Phys Lett* 42: 390-394.
- de Planque, M.R., D.V. Greathouse, R.E. Koeppe 2nd, H. Schafer, D. Marsh, and J.A. Killian, 1998. Influence of lipid/peptide hydrophobic mismatch on the thickness of diacylphosphatidylcholine bilayers. A ^2H NMR and ESR study using designed transmembrane α -helical peptides and gramicidin A. *Biochemistry* 37: 9333-9345.
- de Planque, M.R., J.W. Boots, D.T. Rijkers, R.M. Liskamp, D.V. Greathouse, and J.A. Killian, 2002. The effects of hydrophobic mismatch between phosphatidylcholine bilayers and transmembrane alpha-helical peptides depend on the nature of interfacially exposed aromatic and charged residues. *Biochemistry* 41: 8396-8404.
- de Planque, M.R., J.A. Kruijtzter, R.M. Liskamp, D. Marsh, D.V. Greathouse, R.E. Koeppe 2nd, B. de Kruijff, and J.A. Killian, 1999. Different membrane anchoring positions of tryptophan and lysine in synthetic transmembrane α -helical peptides. *J Biol Chem* 274: 20839-20846.
- de Planque, M.R., B.B. Bonev, J.A. Demmers, D.V. Greathouse, R.E. Koeppe 2nd, F. Separovic, A. Watts, and J.A. Killian, 2003. Interfacial anchor properties of tryptophan residues in transmembrane peptides can dominate over hydrophobic matching effects in peptide-lipid interactions. *Biochemistry* 42: 5341-5348.
- Esteban-Martin, S., and J. Salgado, 2007. The dynamic orientation of membrane-bound peptides: bridging simulations and experiments. *Biophys J* 93: 4278-4288.

- Esteban-Martin, S., D. Gimenez, G. Fuertes, and J. Salgado, 2009a. Orientational landscapes of peptides in membranes: prediction of ^2H NMR couplings in a dynamic context. *Biochemistry* 48: 11441-11448.
- Esteban-Martin, S., E. Strandberg, G. Fuertes, A.S. Ulrich, and J. Salgado, 2009b. Influence of whole-body dynamics on ^{15}N PISEMA NMR spectra of membrane proteins: a theoretical analysis. *Biophys J* 96: 3233-3241.
- Gibbons, W.J., Jr., E.S. Karp, N.A. Cellar, R.E. Minto, and G.A. Lorigan, 2006. Solid-state NMR studies of a diverged microsomal amino-proximate $\Delta 12$ desaturase peptide reveal causes of stability in bilayer: tyrosine anchoring and arginine snorkeling. *Biophys J* 90: 1249-1259.
- Granseth, E., G. von Heijne, and A. Elofsson, 2005. A study of the membrane-water interface region of membrane proteins. *J Mol Biol* 346: 377-385.
- Greathouse, D.V., R.E. Koeppe 2nd, L.L. Providence, S. Shobana, and O.S. Andersen, 1999. Design and characterization of gramicidin channels. *Methods Enzymol* 294: 525-550.
- Hautbergue, G.M., and A.P. Golovanov, 2008. Increasing the sensitivity of cryoprobe protein NMR experiments by using the sole low-conductivity arginine glutamate salt. *J Magn Res* 191: 335-339.
- Holt, A., R.B. Koehorst, T. Rutters-Meijneke, M.H. Gelb, D.T. Rijkers, M.A. Hemminga, and J.A. Killian, 2009. Tilt and rotation angles of a transmembrane model peptide as studied by fluorescence spectroscopy. *Biophys J* 97: 2258-2266.
- Holt, A., L. Rougier, V. Reat, F. Jolibois, O. Saurel, J. Czaplicki, J.A. Killian, and A. Milon, 2010. Order parameters of a transmembrane helix in a fluid bilayer: case study of a WALP peptide. *Biophys J* 98: 1864-1872.
- Isidro-Llobet, A., M. Alvarez, and F. Albericio, 2009. Amino acid-protecting groups. *Chem Rev* 109: 2455-2504.
- Killian, J.A., I. Salemink, M.R. de Planque, G. Lindblom, R.E. Koeppe 2nd, and D.V. Greathouse, 1996. Induction of nonbilayer structures in diacylphosphatidylcholine model membranes by transmembrane α -helical peptides: importance of hydrophobic mismatch and proposed role of tryptophans. *Biochemistry* 35: 1037-1045.
- Kovacs, F.A., J.K. Denny, Z. Song, J.R. Quine, and T.A. Cross, 2000. Helix tilt of the M2 transmembrane peptide from influenza A virus: an intrinsic property. *J Mol Biol* 295: 117-125.
- Morein, S., J.A. Killian, and M.M. Sperotto, 2002. Characterization of the thermotropic behavior and lateral organization of lipid-peptide mixtures by a combined

- experimental and theoretical approach: effects of hydrophobic mismatch and role of flanking residues. *Biophys J* 82: 1405-1417.
- Nomura, K., G. Ferrat, T. Nakajima, H. Darbon, T. Iwashita, and G. Corzo, 2005. Induction of morphological changes in model lipid membranes and the mechanism of membrane disruption by a large scorpion-derived pore-forming peptide. *Biophys J* 89: 4067-4080.
- O'Connell, A.M., R.E. Koeppe 2nd, and O.S. Andersen, 1990. Kinetics of gramicidin channel formation in lipid bilayers: transmembrane monomer association. *Science* 250: 1256-1259.
- Ozdirekcan, S., D.T. Rijkers, R.M. Liskamp, and J.A. Killian, 2005. Influence of flanking residues on tilt and rotation angles of transmembrane peptides in lipid bilayers. A solid-state ^2H NMR study. *Biochemistry* 44: 1004-1012.
- Ozdirekcan, S., C. Etchebest, J.A. Killian, and P.F.J. Fuchs, 2007. On the orientation of a designed transmembrane peptide: toward the right tilt angle? *J Am Chem Soc* 129: 15174-15181.
- Page, R.C., S. Kim, and T.A. Cross, 2008. Transmembrane helix uniformity examined by spectral mapping of torsion angles. *Structure* 16: 787-797.
- Page, R.C., S. Lee, J.D. Moore, S.J. Opella, and T.A. Cross, 2009. Backbone structure of a small helical integral membrane protein: A unique structural characterization. *Protein Sci* 18: 134-146.
- Separovic, F., J. Gehrmann, T. Milne, B.A. Cornell, S.Y. Lin, and R. Smith, 1994. Sodium ion binding in the gramicidin A channel. Solid-state NMR studies of the tryptophan residues. *Biophys J* 67: 1495-1500.
- Stopar, D., R.B. Spruijt, and M.A. Hemminga, 2006. Anchoring mechanisms of membrane-associated M13 major coat protein. *Chem Phys Lipids* 141: 83-93.
- Strandberg, E., S. Esteban-Martin, J. Salgado, and A.S. Ulrich, 2009. Orientation and dynamics of peptides in membranes calculated from ^2H -NMR data. *Biophys J* 96: 3223-3232.
- Strandberg, E., S. Morein, D.T. Rijkers, R.M. Liskamp, P.C. van der Wel, and J.A. Killian, 2002. Lipid dependence of membrane anchoring properties and snorkeling behavior of aromatic and charged residues in transmembrane peptides. *Biochemistry* 41: 7190-7198.
- Strandberg, E., S. Ozdirekcan, D.T. Rijkers, P.C. van der Wel, R.E. Koeppe 2nd, R.M. Liskamp, and J.A. Killian, 2004. Tilt angles of transmembrane model peptides in oriented and non-oriented lipid bilayers as determined by ^2H solid-state NMR. *Biophys J* 86: 3709-3721.

- Stromstedt, A.A., M. Pasupuleti, A. Schmidtchen, and M. Malmsten, 2009. Oligotryptophan-tagged antimicrobial peptides and the role of the cationic sequence. *Biochim Biophys Acta* 1788: 1916-1923.
- ten Kortenaar, P.B.W., B.G. Van Dijk, J.M. Peeters, B.J. Raaben, P.J.H.M. Adams, and G.I. Tesser, 1986. Rapid and efficient method for the preparation of Fmoc-amino acids starting from 9-fluorenylmethanol. *Int J Pept Protein Res* 27: 398-400.
- Thomas, R., V.V. Vostrikov, D.V. Greathouse, and R.E. Koeppe 2nd, 2009. Influence of proline upon the folding and geometry of the WALP19 transmembrane peptide. *Biochemistry* 48: 11883-11891.
- van der Wel, P.C., E. Strandberg, J.A. Killian, and R.E. Koeppe 2nd, 2002. Geometry and intrinsic tilt of a tryptophan-anchored transmembrane α -helix determined by ^2H NMR. *Biophys J* 83: 1479-1488.
- van der Wel, P.C., N.D. Reed, D.V. Greathouse, and R.E. Koeppe 2nd, 2007. Orientation and motion of tryptophan interfacial anchors in membrane-spanning peptides. *Biochemistry* 46: 7514-7524.
- von Heijne, G., 1986. The distribution of positively charged residues in bacterial inner membrane proteins correlates with the trans-membrane topology. *EMBO J* 5: 3021-3027.
- Vostrikov, V.V., C.V. Grant, S.J. Opella, and R.E. Koeppe 2nd, 2009. Orientation of single-span transmembrane peptides investigated by independent solid-state NMR methods: GALA and PISEMA. *Biophys J* 96: 454a.
- Vostrikov, V.V., C.V. Grant, A.E. Daily, S.J. Opella, and R.E. Koeppe 2nd, 2008. Comparison of "Polarization Inversion with Spin Exchange at Magic Angle" and "Geometric Analysis of Labeled Alanines" methods for transmembrane helix alignment. *J Am Chem Soc* 130: 12584-12585.
- Vostrikov, V.V., B.A. Hall, D.V. Greathouse, R.E. Koeppe 2nd, and M.S.P. Sansom, 2010. Changes in transmembrane helix alignment by arginine residues revealed by solid-state NMR experiments and coarse-grained MD simulations. *J Am Chem Soc* 132: 5803-5811.
- White, S.H., and G. von Heijne, 2005. Transmembrane helices before, during, and after insertion. *Curr Opin Struct Biol* 15: 378-386.
- Yau, W.M., W.C. Wimley, K. Gawrisch, and S.H. White, 1998. The preference of tryptophan for membrane interfaces. *Biochemistry* 37: 14713-14718.

2.8 Tables

Table 1. Peptide sequences

Peptide	Sequence
WALP23	<u>G</u> <u>W</u> <u>W</u> ³ LALALALALALALALALW ²¹ <u>W</u> <u>A</u>
WALP19	<u>G</u> <u>W</u> <u>W</u> ³ LALALALALALALALW ¹⁷ <u>W</u> <u>A</u>
GWALP23	<u>G</u> <u>G</u> <u>A</u> <u>L</u> <u>W</u> ⁵ LALALALALALALALW ¹⁹ <u>L</u> <u>A</u> <u>G</u> <u>A</u>
WWALP23	<u>G</u> <u>W</u> <u>A</u> <u>L</u> <u>W</u> ⁵ LALALALALALALALW ¹⁹ <u>L</u> <u>A</u> <u>W</u> <u>A</u>
KWALP23	<u>G</u> <u>K</u> <u>A</u> <u>L</u> <u>W</u> ⁵ LALALALALALALALW ¹⁹ <u>L</u> <u>A</u> <u>K</u> <u>A</u>
RWALP23	<u>G</u> <u>R</u> <u>A</u> <u>L</u> <u>W</u> ⁵ LALALALALALALALW ¹⁹ <u>L</u> <u>A</u> <u>R</u> <u>A</u>

Table 2. Alanine C β D $_3$ quadrupolar splitting (kHz) for XWALP23 peptides incorporated in different lipids.

Peptide	Lipid*	Alanine position					
		7	9	11	13	15	17
GWALP23	DLPC	26.4	25.5	26.9	14.6	20.7	3.4
	DMPC [†]	21.9	8.9	20.9	3.8	17.6	2.9
	DMPC [‡]	22.6	12.4	21.7	7.4	19.0	2.4
	DOPC	16.6	1.7	16.7	1.5	15.4	2.6
WWALP23	DLPC	1.2	13.9	4.1	13.8	2.2	10.8
	DMPC	1.9	11.8	1.4	11.8	5.0	7.6
	DOPC	5.4	14.2	1.9	11.4	7.9	2.3
KWALP23	DLPC	28.6	22.2	26.2	13.7	20.2	5.0
	DMPC	24.6	14.7	23.6	8.6	18.5	4.0
	DOPC	19.1	4.9	18.6	2.4	15.3	3.7
RWALP23	DLPC	25.7	28.9	29.0	17.2	22.4	4.0
	DMPC	25.7	16.9	24.8	10.4	19.3	3.0
	DOPC	18.7	4.7	18.3	3.0	16.2	2.4

*The peptide/lipid ratio was 1/40, unless noted otherwise.

[†]Signal from Ala³ is 21.1 kHz. Signal from Ala²¹ is 6.0 kHz.

[‡]Peptide/lipid ratio of 1/80.

2.9 Figures

Figure 1. Ribbon model to represent \underline{X} WALP23 peptides. The side chains of Trp⁵ and Trp¹⁹ (green) are roughly on the same side of the helix and are numbered in the lower view. The C_α atoms of residues \underline{X}^2 and \underline{X}^{22} are shown as blue spheres. The core α -helix is intact between the Trp residues, but may unwind at the ends. The arrow shows the approximate direction of tilt when \underline{X} is G, R or K (see text and Figure 6).

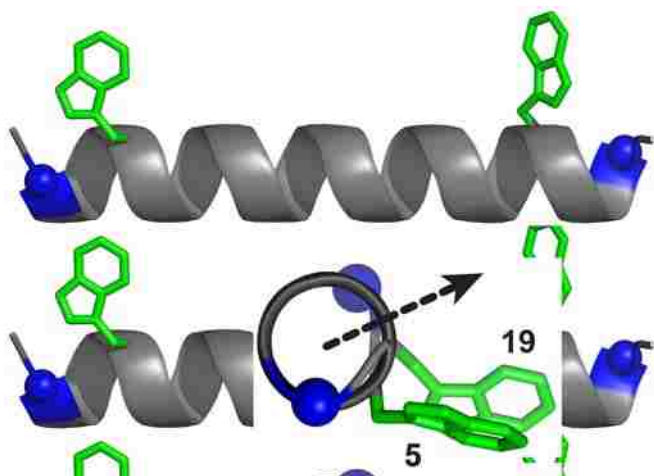


Figure 2. CD spectra of $\underline{X}^{2,22}\text{W}^{5,19}$ ALP23 peptides in DLPC. The color code is gray when \underline{X} is W, or black when \underline{X} is G or K or R.

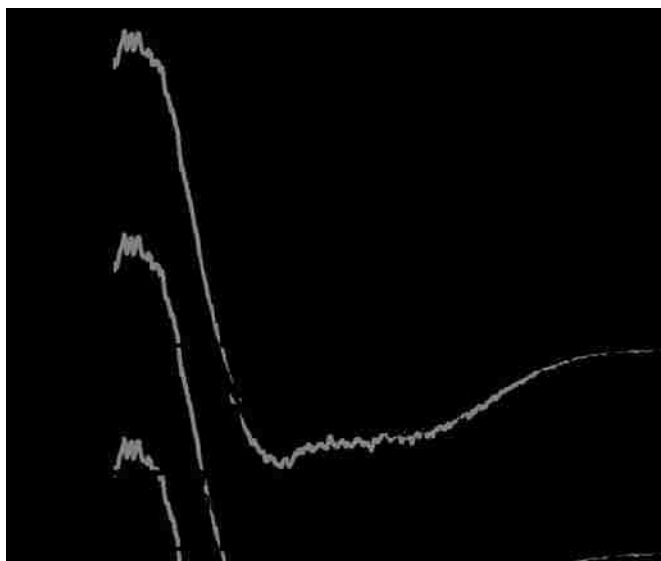


Figure 3. Deuterium NMR spectra for Ala¹³ (full deuteration) and Ala¹¹ (partial deuteration) as a function of X residue identity in X^{2,22}W^{5,19}ALP23 peptides at $\beta=0^\circ$ sample orientation. Peptides are incorporated at 1/40 (P/L) in DLPC, DMPC, or DOPC (left to right). The X residues are G, W, K, or R (top to bottom, as noted).



Figure 4. GALA quadrupolar wave plots for $\underline{X}^{2,22}\text{W}^{5,19}\text{ALP23}$ peptides in DLPC (red triangles), DMPC (green circles) and DOPC (blue squares). The \underline{X} residue identities are noted in each panel (G, W, K, or R). The quadrupolar splittings of Ala³ and Ala²¹ for $\text{G}^{2,22}\text{W}^{5,19}\text{WALP23}$ in DMPC (from Fig. 5) were not used in the fitting, but are shown as filled circles, far off the curve that fits the core α -helix.

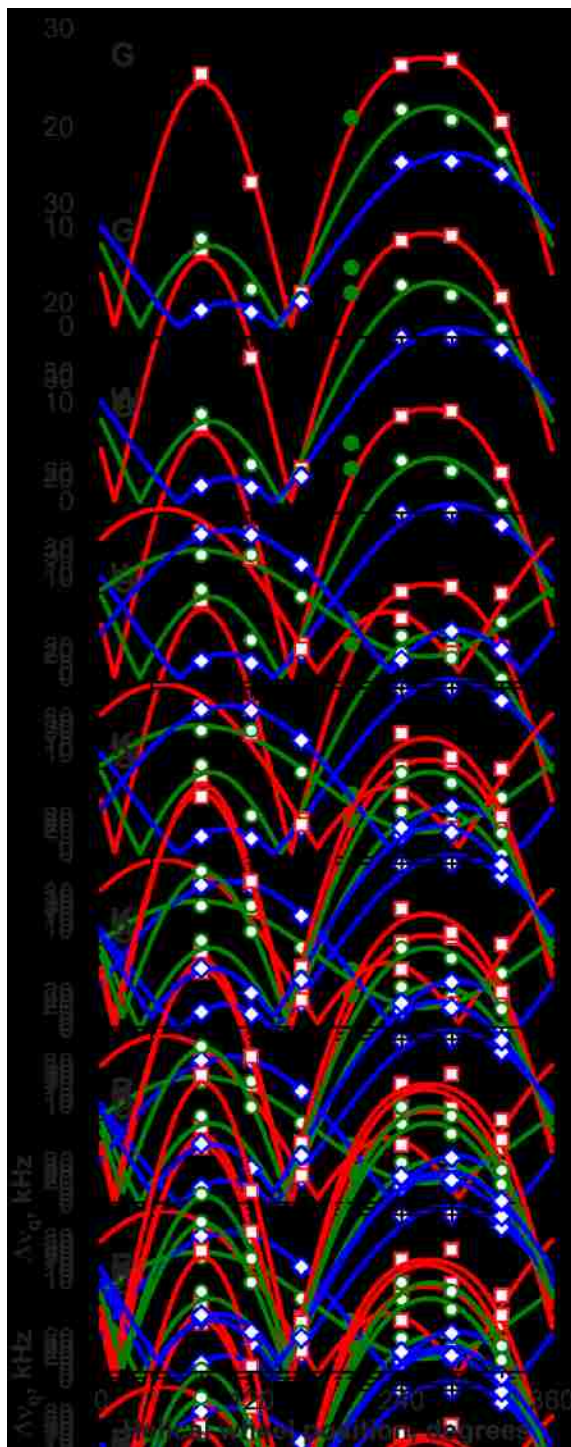


Figure 5. Deuterium NMR spectra of $G^{2,22}W^{5,19}$ ALP23, in DMPC ($\beta=0^\circ$ sample orientation), with Ala- d_4 incorporated outside of the Trp-flanked core sequence. A. Ala- d_4 at position 3. B. Ala- d_4 at position 21.

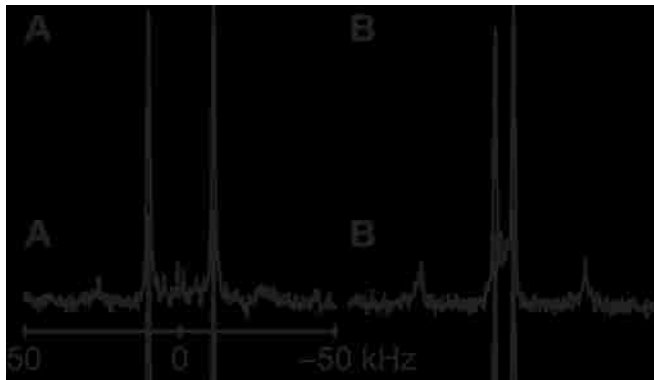


Figure 6. RMSD contour plots for $\underline{X}^{2,22}\text{W}^{5,19}$ ALP23 peptides in DLPC (red), DMPC (green) and DOPC (blue). Residue \underline{X} is G, W, K or R, as noted in the panels. The identities of the bilayer lipids are also indicated by the labels in panel R. Contours are drawn at levels of 1, 2 and 3 kHz.

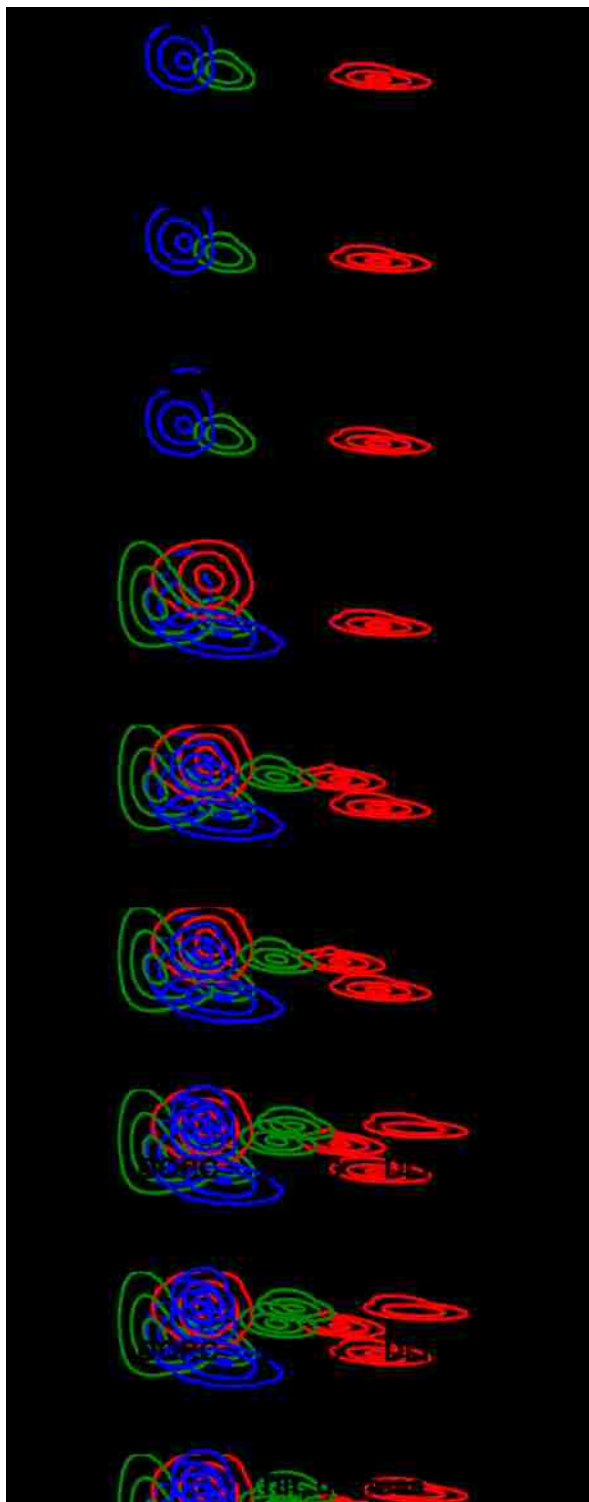
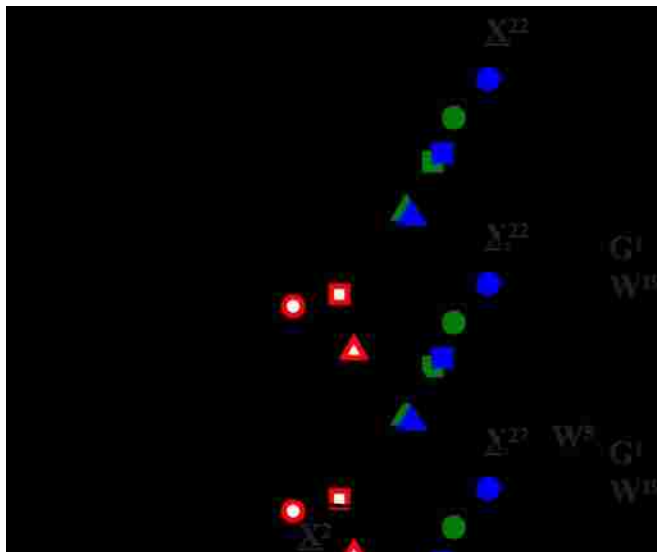


Figure 7. Polar plot of ρ and τ for $\underline{X}^{2,22}\text{W}^{5,19}$ ALP23 peptides in DLPC (circles), DMPC (squares) and DOPC (triangles). Residue \underline{X} is G (black), K (green), R (blue), or W (red, open symbols). Note that ρ values are similar and τ values scale with bilayer thickness, except when \underline{X} is W.



2.10 Supplemental Data

Table S1. GALA fit results for $\underline{X}^{2,22}W^{5,19}$ ALP23 peptides, with $\epsilon_{//}$ fixed at 59.4°. Peptide/lipid ratio was 1/40, unless noted otherwise.

Peptide	Lipid	Fit parameters			
		τ , degrees	ρ , degrees	S_{zz}	RMSD, kHz
GWALP23	DLPC	20.7	305	0.71	0.7
	DMPC	9.0	311	0.89	1.1
	DMPC*	11.7	311	0.86	0.9
	DOPC	6.0	323	0.87	0.6
WWALP23	DLPC	8.0	147	0.61	0.2
	DMPC	3.7	122	0.76	0.5
	DOPC	9.0	93	0.66	0.9
KWALP23	DLPC	18.0	303	0.78	0.7
	DMPC	13.0	306	0.81	0.5
	DOPC	7.3	312	0.86	0.6
RWALP23	DLPC	23.3	305	0.70	1.0
	DMPC	14.3	307	0.80	0.6
	DOPC	7.3	318	0.86	0.7

*Peptide/lipid ratio of 1/80.

Table S2. Combined fit of six ^2H quadrupolar splittings and five ^1H - ^{15}N dipolar couplings to determine the orientation of GWALP23 in hydrated bilayers of DLPC.

Residue	QC (CD_3)		DC (^{15}N - ^1H)	
	Observed (kHz)	Fit (kHz)	Observed (kHz)*	Fit (kHz)
A7	26.4	27.8		
L8				
A9	25.5	23.5		
L10				
A11	26.9	27.8		
L12				
A13	14.6	15.1	7.8	6.5
L14			6.9	5.1
A15	20.7	21.2	8.3	7.8
L16			8.6	8.3
A17	3.4	4.0	7.5	5.4
L18				
Data Set	# data points	(τ , ρ)	S_{zz}	RMSD (kHz)
QC only	6	(20.7°, 305°)	0.71	0.7
QC and DC	11	(18.6°, 304°)	0.78	1.2

QC denotes quadrupolar couplings ($\Delta\nu_q$). DC denotes dipolar couplings.

* Data from Vostrikov et al.

RMSD was calculated according to:

$$RMSD = \sqrt{\frac{\sum_{CD_3} (\Delta\Delta\nu)^2 + \sum_{NH} (\Delta\Delta\nu)^2}{N_{CD_3} + N_{NH}}}$$

where $\Delta\Delta\nu$ is the difference between observed and fit parameter; N is number of data points. A Gaussian fit to the combined data set gave similar results, with (τ_o , ρ_o) of (18°, 306°) and (σ_τ , σ_ρ) of (12°, 10°), and RMSD = 1.1 kHz.

Figure S1. HPLC elution profiles of $X^{2,22}W^{5,19}$ ALP23 peptides. X identities are labeled. Elution time (m:ss) of the main peak is shown for each.



Figure S2. MALDI mass-spectra of $\underline{X}^{2,22}W^{5,19}$ ALP23 peptides, with \underline{X} = G, W, K, or R.

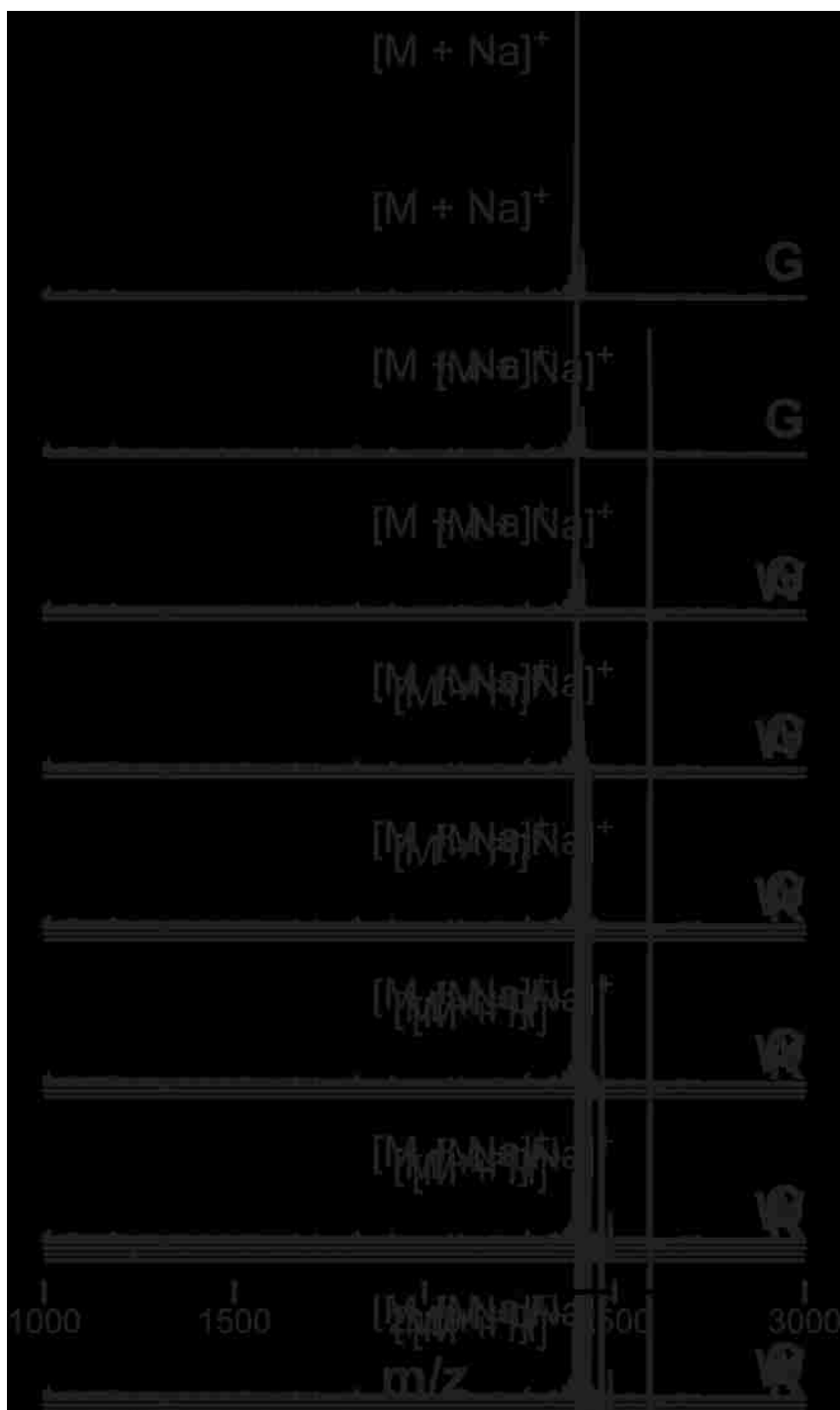


Figure S3. ^{19}F NMR spectra to check for residual trifluoroacetic acid (TFA) in peptide samples. Top to bottom: 0.01% TFA (positive control); solvent only (CD_3OD , negative control); KWALP23 peptide in solvent.

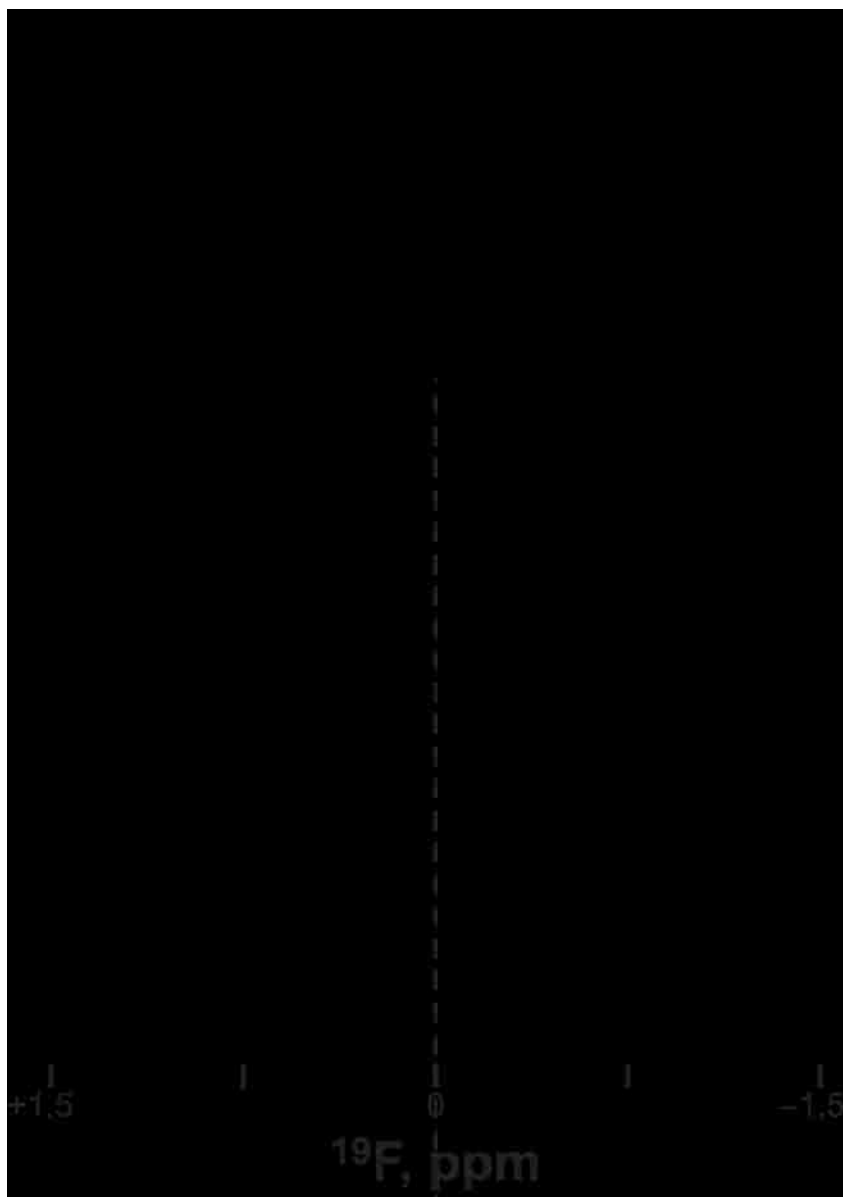


Figure S4. ^{31}P NMR spectra of DOPC with $\text{X}^{2,22}\text{W}^{5,19}$ ALP23 peptides incorporated at 1/40 peptide/lipid ratio.

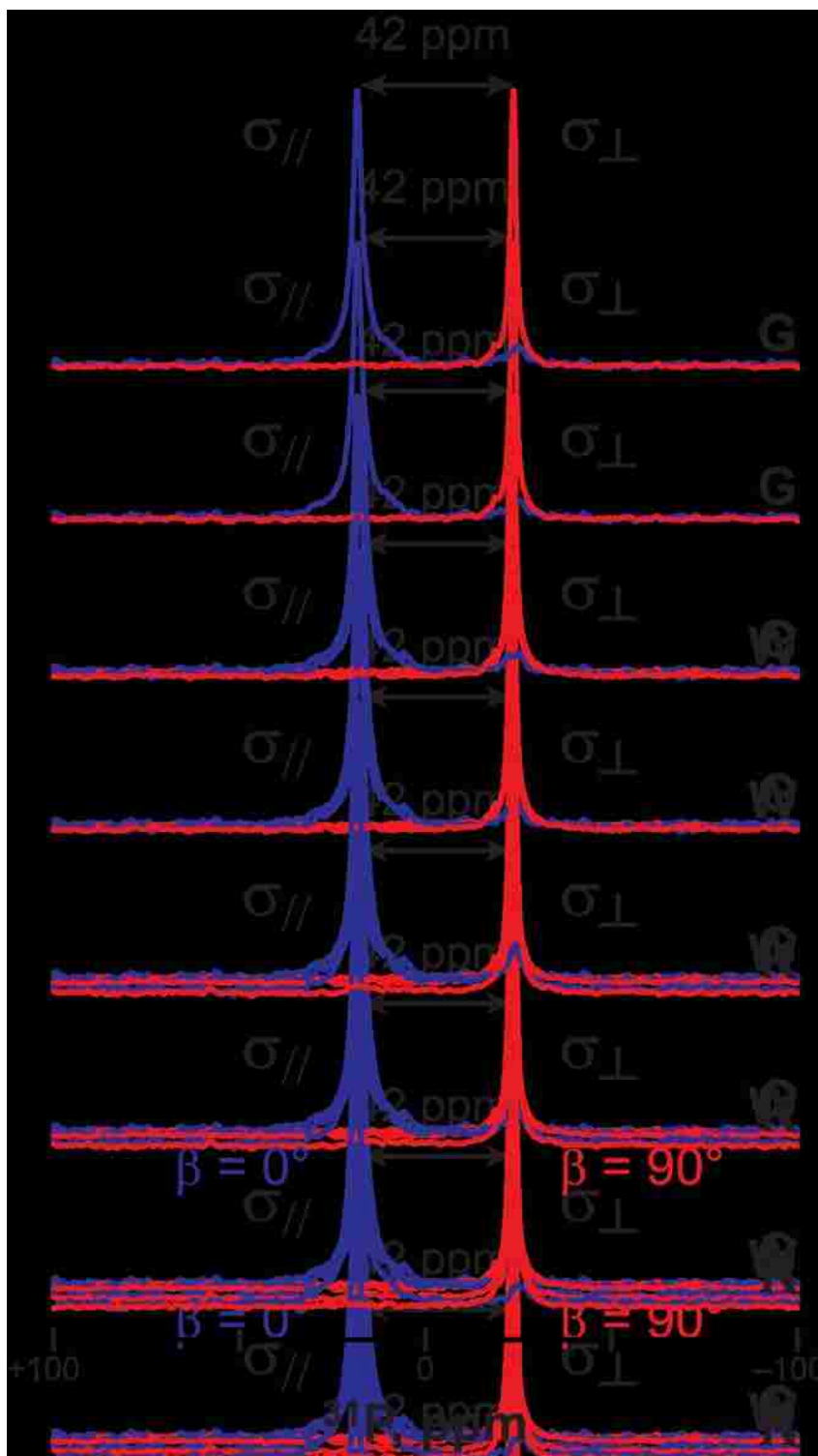


Figure S5. Deuterium NMR spectra for labeled alanines in $G^{2,22}W^{5,19}$ WALP23 in (left to right) DLPC, DMPC, DOPC. The alanine positions and per cent deuteration are shown.

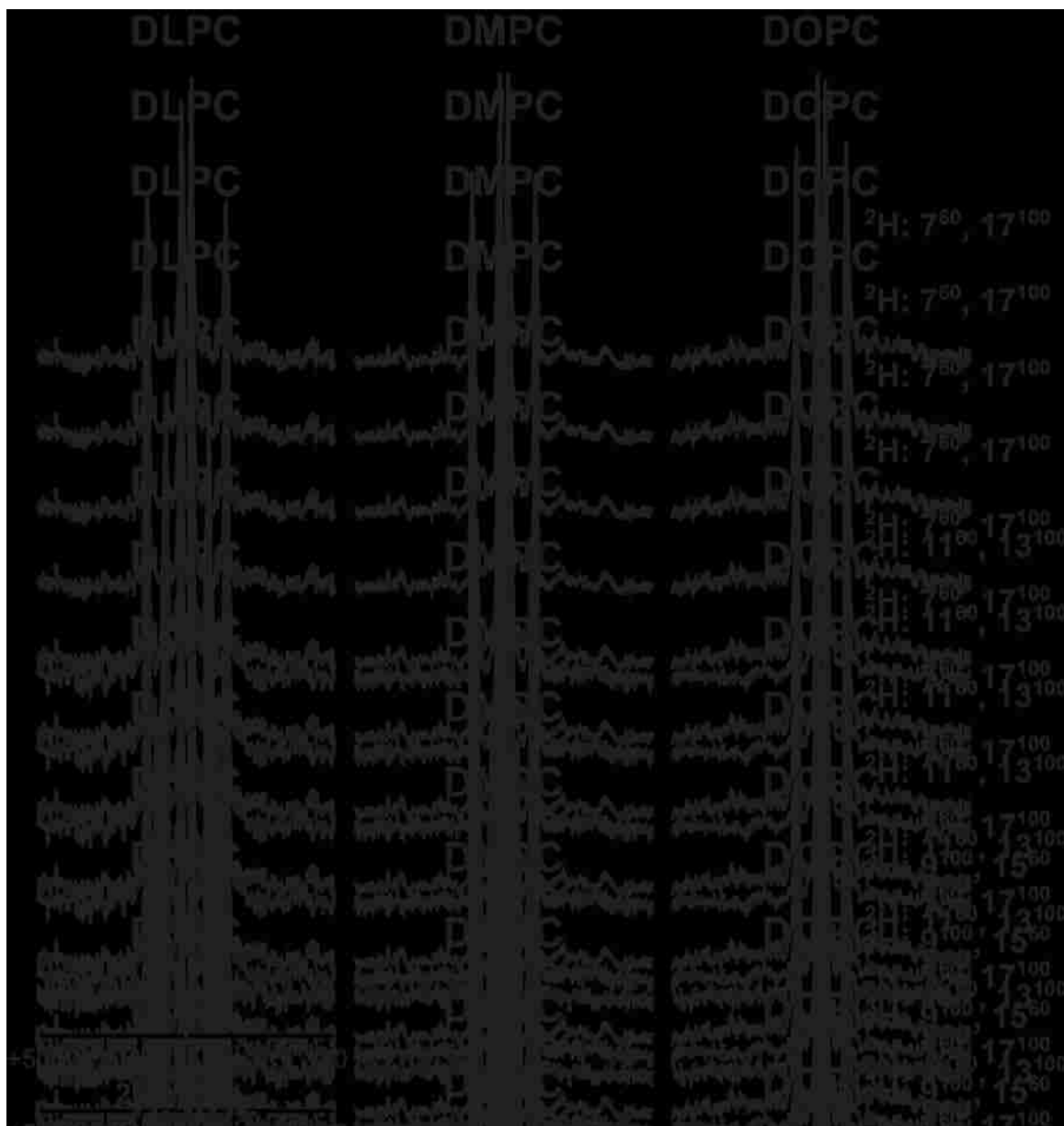


Figure S6. Deuterium NMR spectra for labeled alanines in $W^{2,22}W^{5,19}$ WALP23 in (left to right) DLPC, DMPC, DOPC. The alanine positions and per cent deuteration are shown.

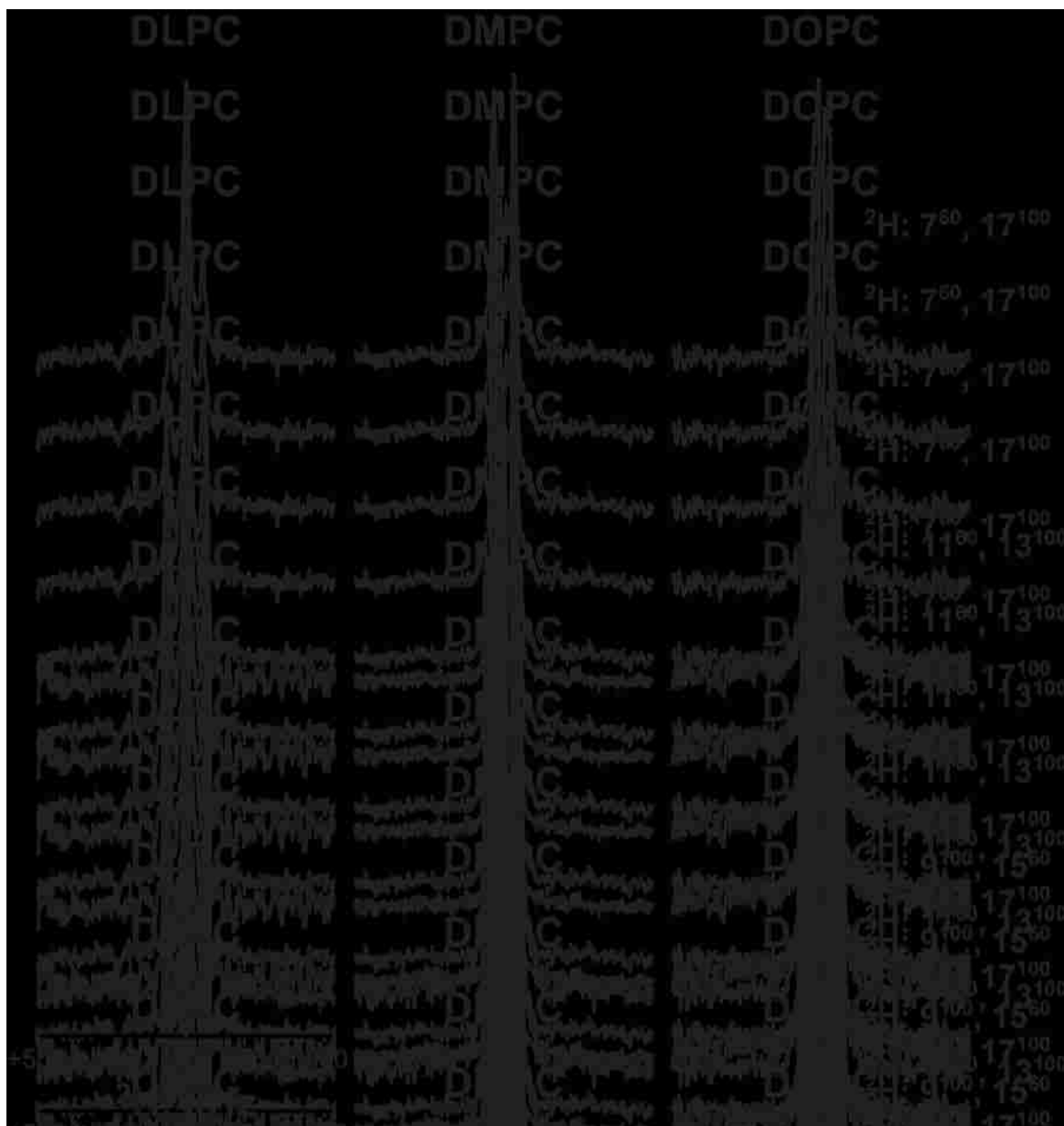


Figure S7. Deuterium NMR spectra for labeled alanines in $K^{2,22}W^{5,19}$ WALP23 in (left to right) DLPC, DMPC, DOPC. The alanine positions and per cent deuteration are shown.

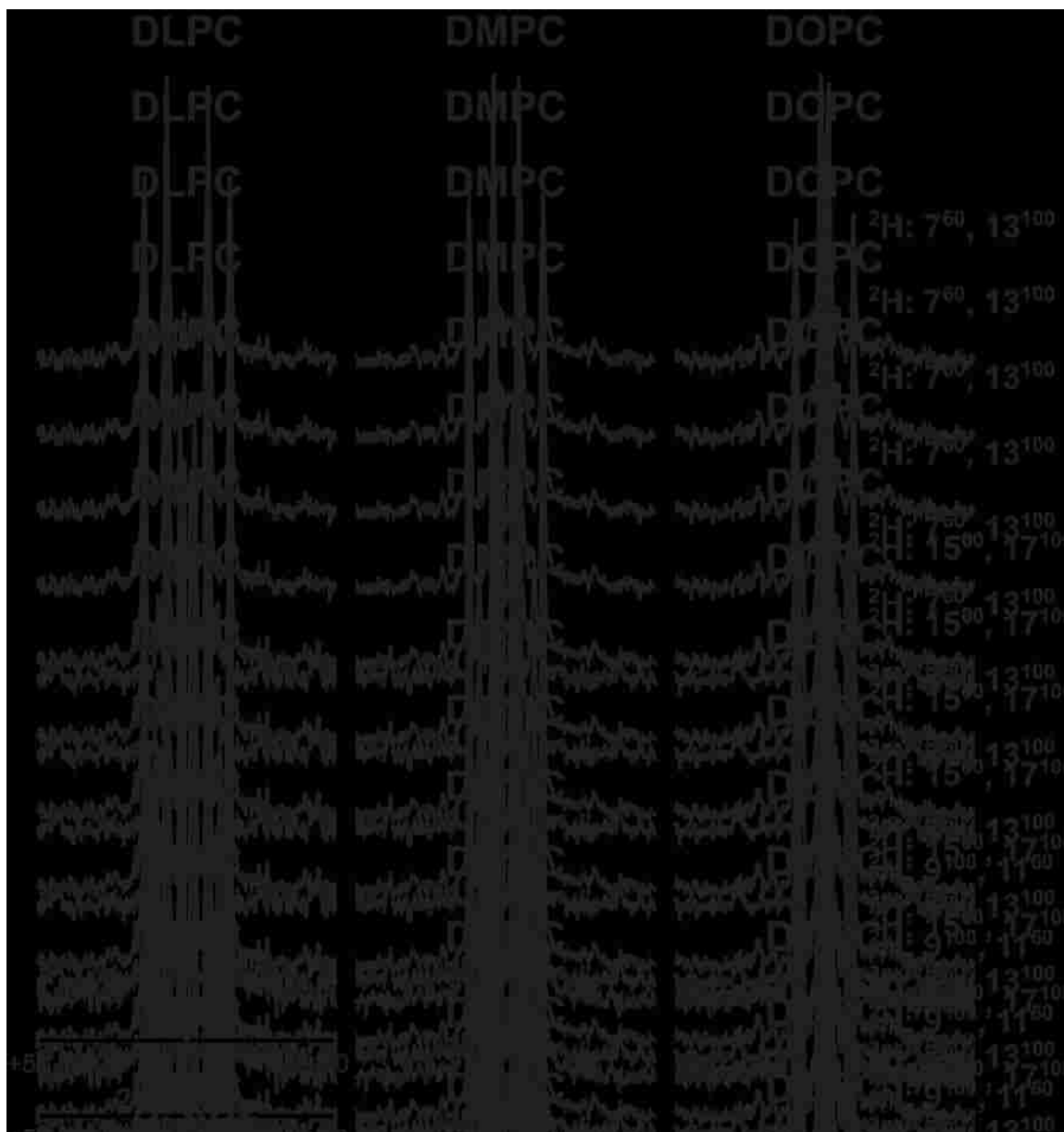


Figure S8. Deuterium NMR spectra for labeled alanines in $R^{2,22}W^{5,19}$ WALP23 in (left to right) DLPC, DMPC, DOPC. The alanine positions and per cent deuteration are shown.

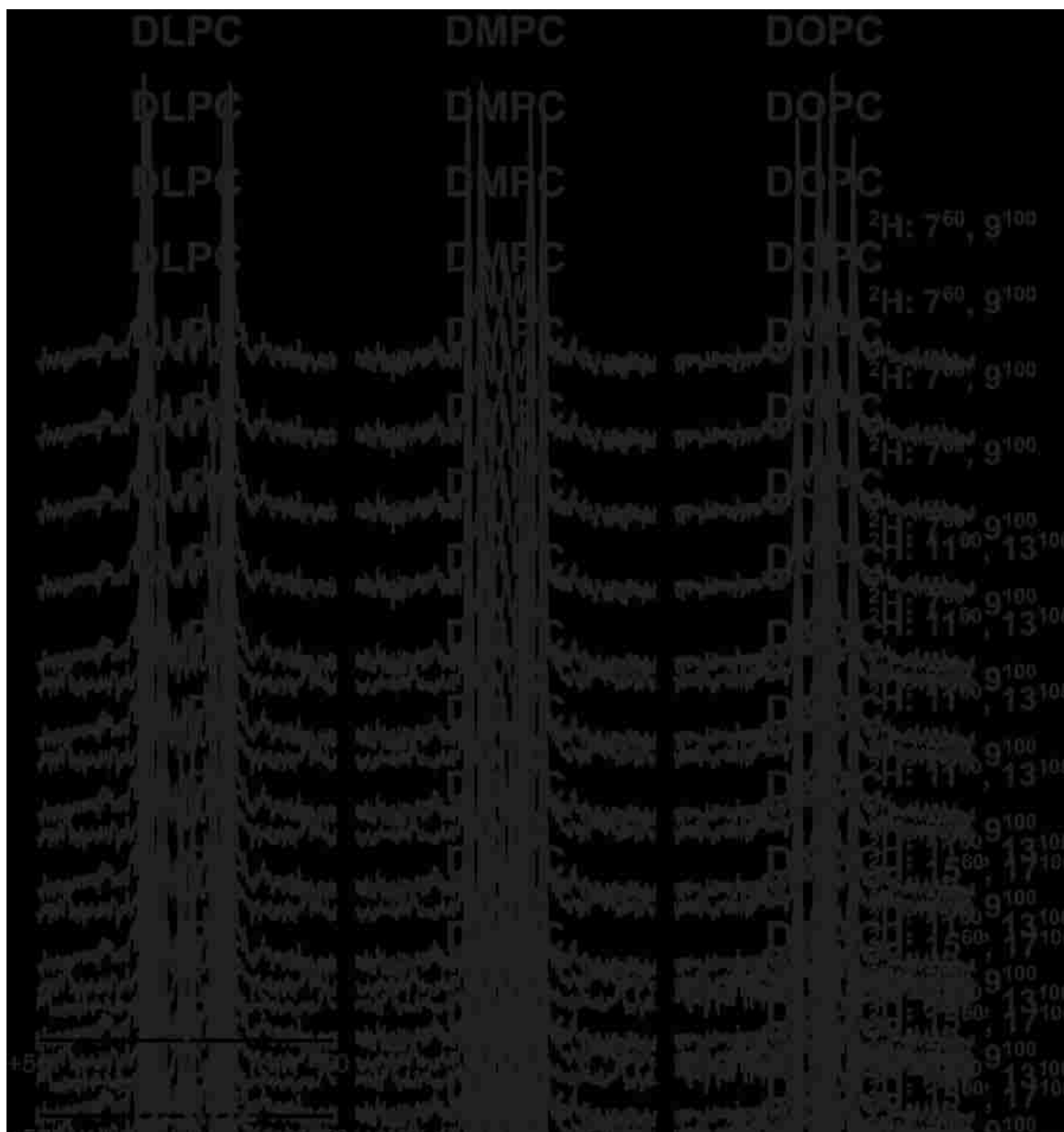
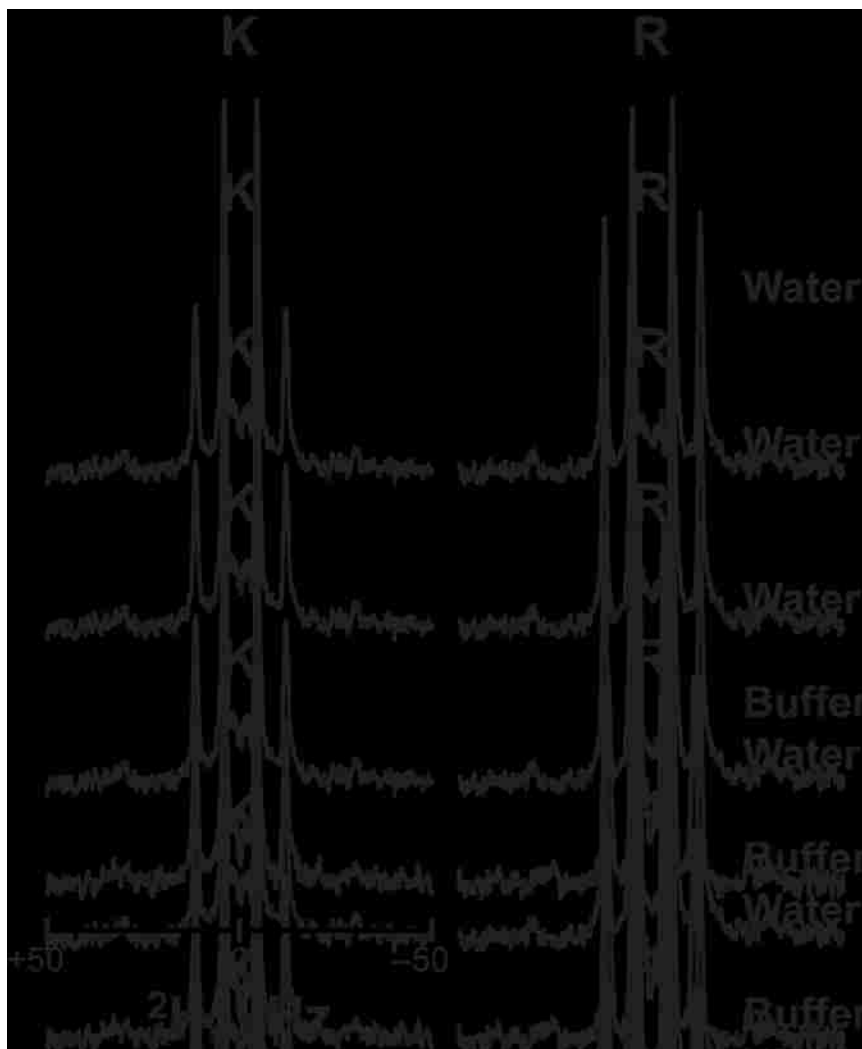


Figure S9. Deuterium NMR spectra of labeled alanines 11 and 13 in: $K^{2,22}W^{5,19}$ ALP23, or $R^{2,22}W^{5,19}$ ALP23, hydrated with 2H -depleted water (top) or HEPES buffer, pH 7.4 with 0.1 M NaCl (bottom).



CHAPTER 3

Response of GWALP Transmembrane Peptides to Lipid Bilayer Hydrophobic Mismatch

3.1 Abstract

Recently we have developed a novel transmembrane peptide, termed GW^{5,19}ALP23 (acetyl-GGALW⁵LALALALALALALW¹⁹LAGA-ethanolamide), which proves to be a well behaved sequence for the systematic investigation of protein-lipid interactions [J Biol Chem, 285:31723]. Its roughly symmetric nature allows for shifting the anchoring Trp residues by one Leu-Ala pair inward (GW^{7,17}ALP23) or outward (GW^{3,21}ALP23), thus providing fine adjustments of the formal hydrophobic length in the range of 15-27 Å (between the tryptophan residues). Importantly, the amino acid composition of the resulting sequences remains identical and the radial separation between tryptophan residues on each side of an α -helix stays similar. These peptides were incorporated into mechanically oriented bilayer membranes composed of phosphatidylcholine lipids with various acyl chain length (~19-27 Å), and the peptide response to hydrophobic (mis)match was evaluated by means of solid-state ²H NMR. All of these sequence isomers adopt transmembrane orientations, even when hydrophobic matching conditions are not readily satisfied. Furthermore, the dynamics for each isomer are less extensive than for peptides that possess additional interfacial Trp residues. Interestingly, there appear to be low and high limits to the peptide tilt angle. We speculate that the interfacial positioning of tryptophan residues dominates over the hydrophobic matching requirement. Additionally we investigate the consequences of hydrophobic matching for the Trp side chain orientations.

3.2 Introduction

The influence of a lipid bilayer membrane on protein organization and function is well documented. For example, the orientation (tilt) angles of virus protein “u” (Park et al., 2006) and of the GABA_A receptor (Kandasamy et al., 2009) have been shown to vary in response to the thickness of the lipid bilayer. The lipid acyl chain identities furthermore influence the assembly of M2 tetramer proton channels (Schick et al., 2010) and alter the functional equilibrium of rhodopsin (Brown, 1994).

A major parameter governing protein-lipid interactions and membrane protein function is the compatibility of the hydrophobic lengths of the membrane lipid acyl chains and the protein transmembrane domains, often referred to as hydrophobic matching. If the protein and lipid hydrophobic lengths are similar, the molecules may be expected to pack favorably into a membrane system with minimal disturbance of their respective conformations or orientations. Conversely, in the case of hydrophobic mismatch, some adaptation may be required to compensate for unfavorable interactions (reviewed in (de Planque and Killian, 2003; Holt and Killian, 2010)). Adaptations may involve molecular orientations or molecular dynamics, or both. Hydrophobic mismatch, defined as the difference between the peptide and lipid hydrophobic lengths, can be either positive or negative.

In order to better understand the protein-lipid interplay with respect to hydrophobic match or mismatch conditions, systematic approaches are essential. It is in this regard useful to consider combinations of synthetic lipids and model peptides, which make it feasible to adjust systematically the lengths of a peptide and the lipid matrix (Davis et al.,

1983; Harzer and Bechinger, 2000; Killian et al., 1996; Krishnakumar and London, 2007). Such model peptide sequences typically have been based on a repeating sequence unit, wherein the addition or removal of an extra hydrophobic block will alter the length of the transmembrane domain with minimal disruption of the other properties. Nevertheless, even such seemingly simple systems pose a number of issues. In addition to the length of the hydrophobic stretch, the identities of the polar or amphiphilic interfacial anchoring amino acid residues are capable of altering the response of the system (Vostrikov et al., 2010a). Furthermore, the geometry of the α -helix dictates that adding or removing core hydrophobic residues inevitably will change also the radial positions of the anchoring residues (Petrache et al.). A further potential issue concerns the overall hydrophobicity of the system in cases where small “blocks” of sequence are added or removed. The sequences with smaller numbers of amino acids thereby may become too polar to insert in a lipid bilayer or too short to form stable helices (Liu et al., 2008), which could lead to oligomerization (Froyd-Rankenbergh et al., 2009).

Recently we improved the design of “WALP” family peptides ($\text{GWW(LA)}_n\text{LWWA}$) (Killian et al., 1996; Strandberg et al., 2004; van der Wel et al., 2002) by replacing two of the tryptophans with glycines (Vostrikov et al.). Unexpectedly, the dependence of the WALP peptide apparent tilt angle on the lipid bilayer thickness is not straightforward. The relatively minor response of the original WALP peptides toward the hydrophobic mismatch conditions was later rationalized in terms of extensive dynamics (Holt et al., 2010; Strandberg et al., 2009). The dynamics can be rationalized in terms of an excess of membrane-anchoring tryptophan residues, dispersed around a helical wheel (Petrache et

al.) and potentially competing among themselves (Ozdirekcan et al., 2005; Vostrikov et al., 2010a).

To circumvent these limitations, we developed $\text{GW}^{5,19}\text{ALP23}$ (GGALW[LA]₆LWLAGA), which proves to be a well behaved transmembrane peptide for the systematic investigation of protein-lipid interactions (Vostrikov et al., 2010a; Vostrikov et al., 2010b). In this study we further exploit its symmetric nature, which allows for shifting the remaining single Trp anchoring residues either inward or outward in pairwise fashion, thereby leading to sequences of the form $\text{GW}^{x,y}\text{ALP23}$, where the “x, y” pairs designate the Trp sequence positions, either “5, 19” (original GWALP23), “3, 21” (outer Trp) or “7, 17” (inner Trp). These sequences allow for fine-tuning the length of the hydrophobic core helix, while maintaining identical amino acid composition, identical hydrophobicity, and similar radial separation between Trp residues on one side of an α -helix (Table 1, Figure 1). The Trp residues on both ends of $\text{GW}^{x,y}\text{ALP23}$ have high propensity to reside at the lipid-water interface (O'Connell et al., 1990; Yau et al., 1998). To maximize the anchoring effect, it is conceivable that the single indole rings may alter their side chain orientations (van der Wel et al.). Here we undertake a comprehensive solid-state NMR study to probe the response of the $\text{GW}^{x,y}\text{ALP23}$ transmembrane peptides to the conditions of hydrophobic mismatch. We employ deuterated Ala and Trp residues to investigate the peptide helix average orientations and dynamics as well as the Trp side chain adjustments. The intent is to provide enhanced understanding of lipid-protein hydrophobic mismatch by providing a better picture of how lipids influence the behavior of membrane-spanning peptides.

3.3 Materials and Methods

All isotope enriched compounds were from Cambridge Isotope Laboratories (Andover, MA). Deuterium labeled alanine (Ala- d_4) and tryptophan (Trp- d_5 ; deuterons on the indole ring) were modified by manual synthesis to introduce an Fmoc group, using an identical protocol for both amino acids (ten Kortenaar et al., 1986). Partial hydrogen/deuterium exchange on the Trp indole side chain was accomplished by incubating commercial Fmoc-Trp (NovaBiochem, San Diego, CA) with deuterated trifluoroacetic acid (TFA- d_1) at 10 °C for 3 hr (Koeppel et al., 2003). This procedure facilitates deuterium incorporation at positions 2 and 5 of the indole ring, which was confirmed by ^1H NMR spectroscopy in DMSO- d_6 , by means of the intensity reduction at position 2 and changes in the multiplet pattern at position 5 (Figure S1 of the Supporting Information). The peptides synthesized with TFA- d_1 treated Trp represent a mixture of $\text{GW}^{x,y}\text{ALP23-Trp-}d_0$, $\text{GW}^{x,y}\text{ALP23-Trp-}d_1$ and $\text{GW}^{x,y}\text{ALP23-Trp-}d_2$. For brevity we further refer to them in the form of $\text{GW}^{x,y}\text{ALP23-Trp-}d_2$.

Peptides were synthesized utilizing a model 433A peptide synthesizer (Applied Biosystems by Life Technologies, Foster City, CA) in a similar manner to GWALP23 (Vostrikov et al., 2010a), using Wang resin and Fmoc-protected amino acids (NovaBiochem). Deuterium-enriched alanines were introduced in pairs at different isotope abundance levels. Deuterium-enriched tryptophans were incorporated in separate peptides one at a time; namely, for each $\text{GW}^{x,y}\text{ALP23}$ sequence, four separate Trp-labeled peptides were synthesized (having full or partial deuteration of the N- or C-terminal Trp). Due to the mild conditions for peptide cleavage from the Wang resin (20%

ethanolamine in dichloromethane), no side chain protecting groups were required (Greathouse et al., 1999). Peptides were purified by reversed-phase HPLC (C8), using the previously established conditions for GWALP23 (Vostrikov et al., 2010a). Confirming HPLC chromatograms and mass spectra are provided in Supporting Information (Figures S2-S3).

Circular dichroism (CD) spectra were obtained for peptides incorporated into small unilamellar vesicles (1/40, peptide/lipid) produced by ultrasonic treatment. Peptide concentrations were determined spectrophotometrically to be in the 100 μ M range. CD spectra were collected using a 1 mm pathlength cell and a Jasco J710 spectropolarimeter (Easton, MD) operated at a 20 nm/min scan rate and 1.0 nm band width. Five spectra were averaged to enhance the signal intensities. Aliquots of the same samples were further diluted 50-fold for steady state fluorescence spectroscopy, using a Perkin Elmer LS-55 fluorescence spectrometer. The excitation wavelength was 284 nm, and emission was recorded between 300 and 500 nm at a rate of 200 nm/min. Ten spectra were acquired and averaged. An asymmetric cuvette was employed, having a 10 mm pathlength for excitation and a 1 mm pathlength for emission.

Samples for solid-state ^2H NMR were prepared by mechanical alignment, as described previously (van der Wel et al., 2002). A mixture of peptide and lipid (Avanti, Alabaster, AL) at 1/40 mol/mol was deposited on glass slides from methanol/water (95/5), dried *in vacuo* (10^{-3} torr) and hydrated with ^2H -depleted water to a 45% level of hydration (w/w). Deuterium NMR spectra were recorded using two Bruker (Billerica, MA) Avance 300 spectrometers operating at a magnetic field of 7.0 T, using a quadrupolar echo pulse

sequence with full phase cycling (Davis et al., 1976). The spectral width was 1,000,000 Hz, recycle delay 90 ms, and pulse durations 3.2 or 4.5 μ s (depending on the spectrometer probe). Approximately 700,000 transients were collected for Ala- d_4 peptides and twice that number for Trp- d_x peptides. Spectra for Ala-labeled peptides were processed by zero filling the time domain to 5120 points, applying 100 Hz exponential apodization and Fourier transformation. The corresponding parameters for the spectra of Trp-labeled peptides were 2048 data points and 300 Hz.

Geometric Analysis of Labeled Alanines (GALA; (van der Wel et al., 2002)) was performed by fitting a generalized order parameter S_{zz} , and the apparent peptide tilt magnitude (τ) and direction (ρ), to a model of a tilted α -helical peptide, with an $\epsilon_{//}$ angle between the alanine C_α - C_β bond vector and peptide helix axis equal to 59.4° (van der Wel et al., 2002). Further, we refer to this S_{zz} value as S_{pept} to avoid confusion with the tryptophan side-chain order parameter (see below). Selected peptide/lipid systems were analyzed also by considering Gaussian distributions of tilt and rotation around average values (τ_0 , ρ_0) with standard deviations (σ_τ , σ_ρ) (Strandberg et al., 2009). In these cases, the order parameter was fixed at 0.88 and a multidimensional grid search was performed by varying σ_ρ between 0° and 200° , σ_τ between 0° and 30° , τ_0 between 0° and 90° , and ρ_0 between 0° and 359° , using 1° increments.

Deuterium NMR data from Trp-labeled peptides were analyzed by rotating the previously refined structure of 3-methyl-indole (Pulay et al., 2005) by two angles, ρ_1 and ρ_2 (defined in Figure S4 of the Supporting Information), and considering the dynamics in the form of an order parameter, S_{zz} (Koeppel et al., 2003; Sun et al., 2008), which

now would incorporate side-chain as well as backbone dynamics. Due to symmetry considerations, such analysis returns eight possible orientations of the indole ring; we report the values for one unique octet with $0^\circ \leq \rho_1 \leq 180^\circ$ and $0^\circ \leq \rho_2 \leq 90^\circ$ (Figure S8). While the fully deuterated Trp side chain has five deuterons, the C-D bond vectors at carbons 4 and 7 are nearly collinear (angle of 179.3° ; (Pulay et al., 2005)), and therefore are generally not resolved.

Indeed, it was assumed that deuterons at positions 4 and 7 are not resolved and produce identical signals, since none of the Trp- d_5 spectra had five distinguishable peaks. Since the spectral assignments are not known, initially $4! = 24$ possible assignment schemes were considered for each Trp. (The number was later reduced in systems where Trp- d_2 data were available). For estimating the root mean squared deviation (RMSD), we treat positions 4 and 7 separately, under the assumption that the corresponding NMR signal represents a superposition of these deuterons. Assignment schemes were selected based on the S_{zz} and RMSD values, as explained in Results.

For the conversion of backbone-independent (ρ_1, ρ_2) angles to Trp side chain (χ_1, χ_2) angles, models of GW^{x,y}ALP23 were constructed using Swiss-PdbViewer 4.0 (Guex and Peitsch, 1997) using (Θ, Ψ, Ω) of $(-65^\circ, -40^\circ, 180^\circ)$ and rotated by angles τ and ρ according to Table 3 (see Results) to yield the coordinates of the tilted peptides. The side chain of a tryptophan residue in question was rotated around the (χ_1, χ_2) angles to yield the indole orientation matching to the previously obtained (ρ_1, ρ_2) angles of 3-methyl-indole. Steric hindrance contours were generated by rotating the Trp side chains through the complete range of (χ_1, χ_2) angles. Steric clash was defined as the distance $< 2 \text{ \AA}$

between any of the non-hydrogen atoms of the indole ring and any non-hydrogen atoms of the peptide backbone.

3.4 Results

Both leucine and alanine are considered to have high α -helix propensity, while tryptophan does not exhibit this property (Monera et al., 1995). A lipid bilayer typically offers a stabilizing environment for the transmembrane helices, which must adopt a secondary structure that maximally satisfies the backbone hydrogen bonding (White and von Heijne, 2008). Nevertheless, in the case of a lipid with a short acyl chain (DLPC), several residues at the peptide termini may protrude into the interfacial and/or aqueous phase, where the deviations from the helical structure can occur more easily. To assess the secondary structure of the $\text{GW}^{\text{x,y}}\text{ALP23}$ peptides we have recorded circular dichroism (CD) spectra of the peptides in DLPC (Figure 2).

All three $\text{GW}^{\text{x,y}}\text{ALP23}$ peptides exhibit the CD spectral signature of an α -helix, with a distinct minimum at 208 nm and a broad shoulder around 222 nm. Furthermore, the mean residue ellipticity values for $\text{GW}^{7,17}\text{ALP23}$ are lower in comparison with the other peptides, suggesting reduced helical structure when the anchoring tryptophans are moved inward. It is widely accepted that due to their amphiphilic character the tryptophan residues prefer the membrane-water interface, which would position the terminal residues 1-6 and 18-23 of $\text{GW}^{7,17}\text{ALP23}$ in more polar regions, where some helix unwinding may be expected (Granseth et al., 2005). The spectral intensities of $\text{GW}^{5,19}\text{ALP23}$ and $\text{GW}^{3,21}\text{ALP23}$ overlap, indicative of similar helicity. Previously we have observed

fraying of the GW^{5,19}ALP23 termini in DMPC (Vostrikov et al., 2010a); within this context the CD data suggest that the GW^{3,21}ALP23 helix may terminate prior to the Trp residues in DLPC.

Earlier studies with the peptides of the WALP family demonstrated a peptide length-dependent formation of non-bilayer phases of phosphatidylcholine membranes at high peptide/lipid ratio: in the case of negative hydrophobic mismatch, the lipid phase underwent transitions from lamellar to isotropic to inverse hexagonal (Killian et al., 1996). To probe this possibility for GW^{x,y}ALP23 peptides, phosphorous NMR spectra of oriented samples were recorded. For all of the peptide-lipid combinations under investigation here, the ³¹P NMR spectra were characteristic of bilayer lipids, with chemical shift anisotropy of ~42 ppm (Figure S5).

To gain insight into the behavior of GW^{x,y}ALP23 peptides in lipid bilayer membranes of various lengths, we introduced deuterium labeled alanine residues into the hydrophobic inter-tryptophan poly-(Leu-Ala) stretch. Previously we have demonstrated that GW^{5,19}ALP23 readily incorporates into lipid bilayers composed of C12-C18 lipids, remains helical and adopts well-defined average orientations (Vostrikov et al., 2010a; Vostrikov et al., 2008). We find that the peptides with shorter or longer Leu-Ala core sequences exhibit similar responses (Figure 3). The Ala methyl ²H quadrupolar splittings ($\Delta\nu_q$) of these peptides are dependent on the macroscopic sample orientation, indicating fast precession of the helix around the lipid bilayer normal (Aisenbrey and Bechinger, 2004). A full set of ²H NMR spectra is provided in Figures S6-S8, and the $\Delta\nu_q$ magnitudes are tabulated in Table 2. From the dependence of $\Delta\nu_q$ on the Ala residue

position, it is apparent that the peptides are tilted in the lipid bilayers. It is notable that a peptide with only nine amino acids between the anchoring Trp residues (GW^{7,17}ALP23) remains capable of adopting a transmembrane orientation. Studies on the translocon-mediated insertion of hydrophobic helices suggest that the free energy of membrane insertion is close to zero in this case (Hessa et al., 2005). Nevertheless, even in the extreme case of negative hydrophobic mismatch, the “short” GW^{7,17}ALP23 still remains tilted in “long” DOPC.

Deuterium NMR $\Delta\nu_q$ magnitudes for the GW^{x,y}ALP23 series were subjected to GALA analysis, using implicit rigid-body dynamics in the form of a principal order parameter (S_{zz} , denoted further as S_{pept}) and peptide average orientation, namely magnitude (τ) and direction (ρ) of tilt as independent variables (van der Wel et al., 2002). The fit quality was assessed by means of the root mean squared deviation (RMSD) between the observed and back-calculated values. A fit is typically considered good when the RMSD value is less than the ²H peak linewidth (usually on the order of 1 kHz). It can be seen in Table 3 that this condition is fulfilled for each peptide-lipid system, with an exception of GW^{3,21}ALP23 in DLPC, where the RMSD approaches 2 kHz. This situation can be understood in terms of partial helix unwinding, as mentioned above. Indeed, the exclusion of the most N-terminal data point (A5) reduces the RMSD to 1.5 kHz, while the exclusion of the most C-terminal point (A19) leads to RMSD of 1.0 kHz (Table 3). Conversely, excluding any individual central data point from A7 to A17 does not improve the fit quality, as the RMSD remains high, in the 1.9-2.1 kHz range when the data for A5 and A19 are present. Interestingly, introducing Arg¹² or Arg¹⁴ in the

GW^{3,21}ALP23 sequence leads to a large tilt and a good fit for the entire helix in DLPC (Vostrikov et al.). When the $\Delta\nu_q$ for A19 is excluded, the average orientation and dynamics of GW^{3,21}ALP23 in DLPC do not differ significantly from the ones obtained using all data points.

Earlier we have demonstrated that the peptide helicity is not completely retained outside of the inter-Trp region in GW^{5,19}ALP23 through ²H labels at alanine positions 3 and 21 (Vostrikov et al., 2010a). While helix fraying near the water exposed termini can be expected, the question as to where the helix distortion begins to occur remains to be answered. To explore this, we have introduced Ala-*d*₄ at positions 5 and 19 in GW^{7,17}ALP23. These amino acids located outside the two Trp residues, but can be expected to be more buried in comparison with A3 and A21 in GW^{5,19}ALP23. Additionally, both A5 and A19 are capable in participating in a more extensive intramolecular hydrogen bonding network due to the presence of $i \pm 4$ residues. The $\Delta\nu_q$ values for these two positions are indicated as filled symbols in Figure 4C. The signals from A5 differ by 5-10 kHz in comparison with the theoretical values, calculated for a central (Leu-Ala)_{4,5} stretch. On the other hand, the values for A19 appear to be closer to the predicted values in DMPC and DOPC, but not in DLPC. Such variation between the lipids as well as possible helix unwinding at A19 in GW^{3,21}ALP23 suggest that A19 is no longer helical in GW^{7,17}ALP23.

As a way of visualizing the quality of GALA analysis, theoretical quadrupolar splittings were calculated and plotted as helical wave plots along with the observed $\Delta\nu_q$ values (Figure 4). Several points of interest emerge from examination of the GALA fits (Table

3, Figure 4). The tilt angles of the peptides fall within a relatively small range of 4-20°, although the theoretical hydrophobic mismatch spans a larger range of ~20 Å (from -12 Å to +8 Å). The average orientations and their uncertainties can also be examined on RMSD contour plots, constructed as a function of the τ and ρ angles (Figure 5). The trend in the tilt angle magnitudes τ is not strictly linear; it rather appears that the tilt magnitudes reach limiting minimum and maximum values. Thus GW^{7,17}ALP23 tilts by only ~4-6° in each of the lipids, while both GW^{5,19}ALP23 and GW^{3,21}ALP23 have 18-21° apparent tilt values in DLPC. In terms of peptide dynamics, GW^{3,21}ALP23 exhibits a tendency toward lower S_{pept} values, suggestive of larger amplitude motions of the long (Leu-Ala)_{8,5} core. Furthermore, the conditions of positive hydrophobic mismatch (“long” peptide, “short” lipid) favor more extensive motions than is the case for negative hydrophobic mismatch.

Tryptophan residues used as membrane-anchoring groups in GW^{x,y}ALP23 peptides are known to reside preferentially at the interfacial region (Hessa et al., 2007; MacCallum et al., 2008; Yau et al., 1998). The region, nevertheless, does not have well-defined borders and spans several angstroms (Wiener and White, 1992). Tryptophan intrinsic fluorescence is a well-known metric of the polarity of the media in the vicinity of Trp, wherein more hydrophobic environments shift the emission maximum (λ_{em}) to lower wavelengths (blue shifts) (Lakowicz, 2006). This property of Trp has been used extensively to probe the hydrophobicity of its immediate environment (Krishnakumar and London, 2007). The GW^{x,y}ALP23 sequences have two Trp residues on each side of an α -helix; therefore steady-state fluorescence may report the average polarity at the peptide termini (subject to considerations of the quantum yield). Despite this limitation, the λ_{em}

values of $GW^{x,y}$ ALP23 in different lipids show a good correlation with the theoretical hydrophobic mismatch (Figure 6). The observed λ_{em} values span a range of 332-344 nm range, indicative of an environment whose polarity is intermediate between those of the aqueous phase and the hydrophobic core of the lipid bilayer, as expected for the interfacial region.

The fluorescence spectra indicate that the average polarity of the environment around the peptide termini changes as a function of hydrophobic mismatch. This observation raises questions of how peptide tilting affects the orientations of the tryptophan side chains. One may speculate that reorientation of the helix axis may alter the indole ring spatial orientations. Alternatively, Trp side chains may have restricted sets of orientations such that the preferential positioning of the Trp indole rings could dictate the peptide tilt. To probe these questions, we have synthesized $GW^{x,y}$ ALP23 peptides with deuterium labels on the indole rings, and have recorded solid-state 2H NMR spectra in different lipid bilayer membranes. Deuterium NMR spectra of partially (d_2) and fully (d_5) labeled indole rings of Trp residues of $GW^{5,19}$ ALP23 are shown in Figure 6. A complete set of spectra for the fully labeled Trps in $GW^{3,21}$ ALP23 and $GW^{7,17}$ ALP23 are included in Figure S9 (see Supporting Information), and spectra for selected partially labeled Trps are shown in Figure S10. Similar to the earlier observations for WALP peptides (van der Wel et al.), the larger quadrupolar splittings are observed at the N-terminus. Indeed, the largest $\Delta\nu_q$ value observed among the N-terminal Trps of the $GW^{x,y}$ ALP23 peptides is 154 kHz, while the corresponding value for the set of C-terminal Trps is only 89 kHz.

Typically 3-4 resonances were observed for the d_5 indole ring and 1-2 for the partially labeled d_2 ring. Quadrupolar splitting magnitudes at $\beta=0^\circ$ and $\beta=90^\circ$ orientations were related by a factor of 1/2, similar to the ones of alanine residues. However, a large span of sometimes quite weak resonances made it hard to observe many of the signals at the $\beta=0^\circ$ orientation. For this reason, the reported data are derived from the spectra from samples oriented at $\beta=90^\circ$. The values observed at $\beta=90^\circ$ were then multiplied by a factor of two to simulate all of the expected values for $\beta=0^\circ$ (Table 4). Partially labeled samples allowed the assignment of signals arising from the deuteron attached to carbon 2 and sometimes carbon 5. The assignments of these two signals were propagated to other samples where possible, using the least change principle. The rest of the resonances were matched by fitting different assignment permutations to a model for the rotated indole ring, and eliminating assignment schemes based on high values of RMSD or unrealistic order parameters. The order parameter reflects the overall motion experienced by a system, and in the case of Trp, it is feasible to deconvolute the S_{zz} value into terms for peptide S_{pept} and side chain S_{sc} motion, such that $S_{zz} = S_{\text{pept}} \times S_{\text{sc}}$ and $S_i \in [0, 1]$. As reported above, the dynamics of $\text{GW}^{x,y}\text{ALP23}$ peptides encompass the S_{pept} range of 0.6-0.9 (Table 3). This range establishes upper limits for the tryptophan S_{zz} . Conversely, the side chain dynamics within the interfacial region are likely to be restricted due to steric hindrance. The value of S_{sc} is therefore likely to be quite high, which would place a lower limit on the Trp S_{zz} value.

Figure 8 shows RMSD as a function of S_{zz} for $\text{GW}^{5,19}\text{ALP23}$. Typically, for each peptide, a unique minimum was observed in such a plot for N-terminal tryptophans,

largely due to the high magnitude of $\Delta\nu_q$ at carbon 5, which could not be fitted by lower values of S_{zz} . The smaller range of quadrupolar splittings exhibited by the C-terminal tryptophans makes it possible to fit alternative ring orientations, manifest by several minima in the (S_{zz} , RMSD) plots. Nevertheless, in some cases, such as W19 in DMPC (Figure 8, B) or W17 in all three lipids, only one global minimum was observed, with an S_{zz} value close to that observed also for the N-terminal Trp. Based on this finding, when the C-terminal Trp has multiple minima, we consider the one closest to the corresponding N-terminal Trp to be the global minimum, even if alternative fits may have slightly lower RMSD (Table 5). The uncertainties of the ρ_1 and ρ_2 angles at the S_{zz} global minimum can be visualized in a similar fashion to the peptide average orientation using RMSD contour plots (Figure 9). It can be seen that the orientations of N- and C-terminal Trp residues are distinct and differ primarily in the ρ_2 angle.

In the case of W17 in GW^{7,17}ALP23, only three pairs of resonances can be identified in the spectra (Figure S9). As the $\Delta\nu_q$ range for the C-terminal tryptophan residues is fairly small, it is conceivable that the missing signal is present, but not resolved due to a spectral overlap. To account for this possibility, in each of the lipids we performed three separate fits of the W17 data by entering one of the quadrupolar splittings twice. Solutions were rejected on the previously described principles; in addition, the best fits among the different lipids were compared, as the C-terminal Trp in GW^{5,19}ALP23 has shown little variation in different bilayer membranes. A possible assignment with the intermediate $\Delta\nu_q$ value involving overlap of deuterons 4/7 and 2 was discarded for reasons of largely different $\rho_{1,2}$ angles ($\sim 70^\circ$ and $\sim 30^\circ$) in comparison with W19.

Conversely, the conditions were readily fulfilled if the outermost quadrupolar splittings resulted from an overlap between deuterons at positions 4/7 and 6, which led to similar orientation angles and S_{zz} for W17 and W19. Furthermore, in ^2H NMR spectra of W17-labeled peptide, the outermost signals typically were strongest. While the intensity alone is hard to interpret in deuterium NMR spectroscopy (due to a number of factors, including radio frequency power profile, contributions from powder pattern, etc.), the consideration of peak intensity nevertheless provides additional confidence in combination with other factors. N-terminal W7 produced four signals in DLPC and DMPC, allowing the assignments, but only two resolved resonances in DOPC, which does not provide sufficient restraints for the analysis.

For GW^{3,21}ALP23, fits for both tryptophans were possible only in DLPC. Broad overlapped peaks of W3 in DMPC and DOPC make it hard to extract or assign $\Delta\nu_q$ values. Uncertainties in peak positions and observation of fewer than four resonances complicate the analysis of W21. While combinations of plausible S_{zz} , ρ_1 , ρ_2 that are similar to the N- or C-terminal Trps in other peptides can be obtained, it is not possible to exclude with confidence alternative assignments and consequently orientations.

3.5 Discussion

In this paper we have investigated the response of model peptides bearing the identical sequence, but different hydrophobic lengths toward the hydrophobic mismatch conditions. The peptides were able to incorporate in the lipid bilayer membrane under positive and negative mismatch conditions. In every case the peptides retained a well-

defined tilt angle, even in the extreme case of negative hydrophobic mismatch, where tilting further reduces the effective hydrophobic length of the peptide. Such an effect has also been observed in umbrella sampling simulations of WALP peptides, and was explained in terms of favorable entropy contribution arising due to peptide precession along the lipid bilayer normal (Kim and Im, 2010).

The analysis of GW^{3,21}ALP23 behavior in lipid bilayers suggests that the longer (Leu-Ala)_{8.5} stretch undergoes more extensive motion relative to its (Leu-Ala)_{6.5} counterpart in GW^{5,19}ALP23 (Table 3). To gain additional insights into the nature of such motion, we have performed explicit dynamics analysis of ²H data of both peptides in DLPC, the system where the tilt angles of the two peptides are similar, but the S_{zz} values are varied. To facilitate direct comparison between the two systems the identical alanine positions for fitting the data were used (residues 7, 9, 11, 13, 15 and 17).

The overall shape of the tilt and rotation distributions (σ_τ and σ_ρ respectively) is similar for both peptides, with moderate oscillations around the average values, the solution area for GW^{5,19}ALP23 being more compact and shifted toward the lower σ_τ range (Figure 10).

The variations around the average ρ angle are close and fairly small for both systems, indicating that each of the peptides (with a single Trp residue at each terminus) does not undergo extensive reorientation around the helical axis (as was proposed for WALP peptides with two Trp at each terminus). Furthermore we note the close correspondence between the average orientation of GW^{x,y}ALP23 between the semi-static (variable order parameter) and explicit (Gaussian distributions of τ and ρ) ways of treating the whole body dynamics. The latter method should be used with caution, as it introduces additional

variables in the analysis procedure, requiring additional sampling of the data. We note that this limitation can be circumvented by combining the ^2H methyl data with the ^{15}N derived restraints, or, in selected cases, backbone deuteron signals (Vostrikov et al.). It is further of note that more extensive treatment of $\text{GW}^{5,19}\text{ALP23}$ in DLPC—using combined ^2H and ^{15}N data with Gaussian dynamics—leads to the same tilt angle as found in a semi-static analysis (Vostrikov et al., 2010a).

Earlier we have established that among different anchoring residues at the lipid bilayer – water interface, tryptophans act as major determinants of the transmembrane peptide orientation (Vostrikov et al., 2010a). The design of $\text{GW}^{x,y}\text{ALP23}$ offers a way to investigate this in further details, due to the similar projections of the N- and C-terminal Trp on the helical wheel. Furthermore, the radial positions of the two Trp in $\text{GW}^{7,17}\text{ALP23}$ resemble closely the ones in $\text{GW}^{3,21}\text{ALP23}$, while both Trp in $\text{GW}^{5,19}\text{ALP23}$ project from a different face of the helix (Figure 1). Indeed, we find that both $\text{GW}^{7,17}\text{ALP23}$ and $\text{GW}^{5,19}\text{ALP23}$ have nearly opposite ρ angles (Table 3), with the peptide tilting approximately in the direction of both Trp. Due to the similar projections of the two tryptophans, it is not yet possible to say whether either of the N- or C-terminal Trp has the main role in the orientation determination, although the advantageous design of the GWALP23 peptide allows testing this in future. The situation is less clear though with $\text{GW}^{3,21}\text{ALP23}$, which does not seem to follow this trend. It is feasible that one of the reasons is the close proximity of W3 and W21 to the peptide termini. The fraying of the termini may include either one or both of the tryptophan residues, which would alter the radial projections and therefore contribute to the change in the rotation angle.

Deuterium labeling of the tryptophan residues allowed for defining the orientation of the indole moieties with respect to the membrane normal in several cases (Table 5). Both N- and C-terminal Trp are tightly clustered, albeit in the different regions of conformational space. To visualize the indole position with respect to the tilted peptide, the $[\rho_1, \rho_2]$ backbone-independent angles of 3-methyl-indole were converted to the Trp side chain $[\chi_1, \chi_2]$ torsion angles (Figure 11). Similar to the backbone-independent analysis, there are eight possible combinations of the $\chi_{1,2}$ torsion angles resulting in the identical orientation of the indole with respect to the applied magnetic field. However, in order to serve as an anchor, Trp side chain has to be positioned so that the $N_\epsilon H$ bond vector points toward the membrane interfacial region. This restricts the number of the $\rho_{1,2}$ (or $\chi_{1,2}$) to four possible combinations (Figure S4) as the $N_\epsilon H$ bond vector of N-terminal Trps has to be directed along the positive direction of the Z-axis, while the one of the C-terminal Trps toward the negative direction. Additionally, in cases where ρ_2 angle is close to zero, the number of possible solutions is further reduced in half due to the symmetry collapse (Figure S4).

The possible side chain angles of the N-terminal Trp fall into two major clusters (Figure 11, ABC), with the indole carbon-carbon “bridge” (between the two ring systems) either co-aligned with the helix axis (negative χ_1 , positive χ_2 cluster), or nearly perpendicular to it (positive χ_1 , negative χ_2 cluster). Interestingly, both possible solutions are located close to the steric hindrance areas, suggesting that the further changes of the Trp orientation are unfavorable, as they would include the re-arrangement of the backbone atoms. On the other hand, the orientation of the C-terminal Trp can be described by four

possible combinations of $\chi_{1,2}$ angles, in each case the “bridge” being perpendicular to the helix axis so that the indole system lies in the membrane plane (Figure 11, DEF). While it appears that the Trps at the C-terminus are located further away from the steric hindrance regions, it should be noted that these areas are likely to change upon the deviations from the α -helical geometry, which were noted for the GW^{x,y}ALP23 peptides (see Results). While deuterium NMR alone does not allow for distinguishing between the four possible solutions, they can be refined in future through the distance measurements data obtained by solution or magic angle spinning NMR.

The GW^{3,21}ALP23 peptide is similar to the WALP sequence in terms of close tryptophan proximity toward the helix termini. It is notable that the Trp steric hindrance areas are less for this peptide, which is particularly manifest for W3 due to the directionality of the C $_{\alpha}$ -C $_{\beta}$ bond vector pointing toward the N-terminus, therefore effectively shifting the side chains closer to the N-terminus. Interestingly, for this particular peptide it was possible to assign the indole quadrupolar splittings only in DLPC, the resonances being broader and less well defined in other lipids. The steric hindrance pattern in the case of WALP peptides can be expected to be more complicated due to the two bulky Trp side chains located next to each other, meaning that the orientation of each indole moiety has to be viewed in the context of the adjacent tryptophan.

3.6 Acknowledgments

We thank James Hinton and Denise Greathouse for helpful discussions. This work was supported in part by NSF grant MCB-0841227 and by the Arkansas Biosciences Institute.

The NMR facility was supported by NIH grant RR31154.

3.7 References

- Aisenbrey, C., and B. Bechinger, 2004. Tilt and rotational pitch angle of membrane-inserted polypeptides from combined ^{15}N and ^2H solid-state NMR spectroscopy. *Biochemistry* 43: 10502-10512.
- Bechinger, B., J.M. Resende, and C. Aisenbrey, 2011. The structural and topological analysis of membrane-associated polypeptides by oriented solid-state NMR spectroscopy: Established concepts and novel developments. *Biophys Chem* 153: 115-125.
- Brown, M.F., 1994. Modulation of rhodopsin function by properties of the membrane bilayer. *Chem Phys Lipids* 73: 159-180.
- Davis, J.H., D.M. Clare, R.S. Hodges, and M. Bloom, 1983. Interaction of a synthetic amphiphilic polypeptide and lipids in a bilayer structure. *Biochemistry* 22: 5298-5305.
- Davis, J.H., K.R. Jeffrey, M. Bloom, M.I. Valic, and T.P. Higgs, 1976. Quadrupolar echo deuteron magnetic resonance spectroscopy in ordered hydrocarbon chains. *Chem Phys Lett* 42: 390-394.
- de Planque, M.R., and J.A. Killian, 2003. Protein-lipid interactions studied with designed transmembrane peptides: role of hydrophobic matching and interfacial anchoring. *Mol Membr Biol* 20: 271-284.
- Froyd-Rankenbergh, J.M., D.V. Greathouse, and R.E. Koeppe 2nd, 2009. Half-anchored WALP peptides: Effect of anchor position on peptide orientation. *Biophys J* 96: 455a-456a.
- Granseth, E., G. von Heijne, and A. Elofsson, 2005. A study of the membrane-water interface region of membrane proteins. *J Mol Biol* 346: 377-385.
- Greathouse, D.V., R.E. Koeppe 2nd, L.L. Providence, S. Shobana, and O.S. Andersen, 1999. Design and characterization of gramicidin channels. *Methods Enzymol* 294: 525-550.
- Guex, N., and M.C. Peitsch, 1997. SWISS-MODEL and the Swiss-PdbViewer: an environment for comparative protein modeling. *Electrophoresis* 18: 2714-2723.
- Harzer, U., and B. Bechinger, 2000. Alignment of lysine-anchored membrane peptides under conditions of hydrophobic mismatch: a CD, ^{15}N and ^{31}P solid-state NMR spectroscopy investigation. *Biochemistry* 39: 13106-13114.
- Hessa, T., H. Kim, K. Bihlmaier, C. Lundin, J. Boekel, H. Andersson, I. Nilsson, S.H. White, and G. von Heijne, 2005. Recognition of transmembrane helices by the endoplasmic reticulum translocon. *Nature* 433: 377-381.

- Hessa, T., N.M. Meindl-Beinker, A. Bernsel, H. Kim, Y. Sato, M. Lerch-Bader, I. Nilsson, S.H. White, and G. von Heijne, 2007. Molecular code for transmembrane-helix recognition by the Sec61 translocon. *Nature* 450: 1026-1030.
- Holt, A., and J.A. Killian, 2010. Orientation and dynamics of transmembrane peptides: the power of simple models. *Eur Biophys J* 39: 609-621.
- Holt, A., L. Rougier, V. Reat, F. Jolibois, O. Saurel, J. Czaplicki, J.A. Killian, and A. Milon, 2010. Order parameters of a transmembrane helix in a fluid bilayer: case study of a WALP peptide. *Biophys J* 98: 1864-1872.
- Kandasamy, S.K., D.K. Lee, R.P. Nanga, J. Xu, J.S. Santos, R.G. Larson, and A. Ramamoorthy, 2009. Solid-state NMR and molecular dynamics simulations reveal the oligomeric ion-channels of TM2-GABA_A stabilized by intermolecular hydrogen bonding. *Biochim Biophys Acta* 1788: 686-695.
- Killian, J.A., I. Salemink, M.R. de Planque, G. Lindblom, R.E. Koeppe 2nd, and D.V. Greathouse, 1996. Induction of nonbilayer structures in diacylphosphatidylcholine model membranes by transmembrane α -helical peptides: importance of hydrophobic mismatch and proposed role of tryptophans. *Biochemistry* 35: 1037-1045.
- Kim, T., and W. Im, 2010. Revisiting hydrophobic mismatch with free energy simulation studies of transmembrane helix tilt and rotation. *Biophys J* 99: 175-183.
- Koeppe 2nd, R.E., H. Sun, P.C. van der Wel, E.M. Scherer, P. Pulay, and D.V. Greathouse, 2003. Combined experimental/theoretical refinement of indole ring geometry using deuterium magnetic resonance and ab initio calculations. *J Am Chem Soc* 125: 12268-12276.
- Krishnakumar, S.S., and E. London, 2007. Effect of sequence hydrophobicity and bilayer width upon the minimum length required for the formation of transmembrane helices in membranes. *J Mol Biol* 374: 671-687.
- Lakowicz, J.R., 2006. *Principles of Fluorescence Spectroscopy*. 3 ed. Springer.
- Liu, J., D. Wang, Q. Zheng, M. Lu, and P.S. Arora, 2008. Atomic structure of a short α -helix stabilized by a main chain hydrogen-bond surrogate. *J Am Chem Soc* 130: 4334-4337.
- MacCallum, J.L., W.F. Bennett, and D.P. Tieleman, 2008. Distribution of amino acids in a lipid bilayer from computer simulations. *Biophys J* 94: 3393-3404.
- Monera, O.D., T.J. Sereda, N.E. Zhou, C.M. Kay, and R.S. Hodges, 1995. Relationship of sidechain hydrophobicity and α -helical propensity on the stability of the single-stranded amphipathic α -helix. *J Pept Sci* 1: 319-329.

- O'Connell, A.M., R.E. Koeppe 2nd, and O.S. Andersen, 1990. Kinetics of gramicidin channel formation in lipid bilayers: transmembrane monomer association. *Science* 250: 1256-1259.
- Ozdirekcan, S., D.T. Rijkers, R.M. Liskamp, and J.A. Killian, 2005. Influence of flanking residues on tilt and rotation angles of transmembrane peptides in lipid bilayers. A solid-state ^2H NMR study. *Biochemistry* 44: 1004-1012.
- Park, S.H., A.A. De Angelis, A.A. Nevzorov, C.H. Wu, and S.J. Opella, 2006. Three-dimensional structure of the transmembrane domain of Vpu from HIV-1 in aligned phospholipid bicelles. *Biophys J* 91: 3032-3042.
- Petrache, H.I., D.M. Zuckerman, J.N. Sachs, J.A. Killian, R.E. Koeppe II, and T.B. Woolf, 2002. Hydrophobic matching mechanism investigated by molecular dynamics simulations. *Langmuir* 18: 1340-1351.
- Pulay, P., E.M. Scherer, P.C. van der Wel, and R.E. Koeppe II, 2005. Importance of tensor asymmetry for the analysis of ^2H NMR spectra from deuterated aromatic rings. *J Am Chem Soc* 127: 17488-17493.
- Schick, S., L. Chen, E. Li, J. Lin, I. Koper, and K. Hristova, 2010. Assembly of the M2 tetramer is strongly modulated by lipid chain length. *Biophys J* 99: 1810-1817.
- Strandberg, E., S. Esteban-Martin, J. Salgado, and A.S. Ulrich, 2009. Orientation and dynamics of peptides in membranes calculated from ^2H -NMR data. *Biophys J* 96: 3223-3232.
- Strandberg, E., S. Ozdirekcan, D.T. Rijkers, P.C. van der Wel, R.E. Koeppe 2nd, R.M. Liskamp, and J.A. Killian, 2004. Tilt angles of transmembrane model peptides in oriented and non-oriented lipid bilayers as determined by ^2H solid-state NMR. *Biophys J* 86: 3709-3721.
- Sun, H., D.V. Greathouse, O.S. Andersen, and R.E. Koeppe 2nd, 2008. The preference of tryptophan for membrane interfaces: insights from N-methylation of tryptophans in gramicidin channels. *J Biol Chem* 283: 22233-22243.
- ten Kortenaar, P.B.W., B.G. Van Dijk, J.M. Peeters, B.J. Raaben, P.J.H.M. Adams, and G.I. Tesser, 1986. Rapid and efficient method for the preparation of Fmoc-amino acids starting from 9-fluorenylmethanol. *Int J Pept Protein Res* 27: 398-400.
- van der Wel, P.C., E. Strandberg, J.A. Killian, and R.E. Koeppe 2nd, 2002. Geometry and intrinsic tilt of a tryptophan-anchored transmembrane α -helix determined by ^2H NMR. *Biophys J* 83: 1479-1488.
- van der Wel, P.C., N.D. Reed, D.V. Greathouse, and R.E. Koeppe 2nd, 2007. Orientation and motion of tryptophan interfacial anchors in membrane-spanning peptides. *Biochemistry* 46: 7514-7524.

- Vostrikov, V.V., B.A. Hall, M.S.P. Sansom, and R.E. Koeppe 2nd, "Rescue" of a central arginine in a transmembrane peptide by changing the placement of anchor residues in press.
- Vostrikov, V.V., A.E. Daily, D.V. Greathouse, and R.E. Koeppe 2nd, 2010a. Charged or aromatic anchor residue dependence of transmembrane peptide tilt. *J Biol Chem* 285: 31723-31730.
- Vostrikov, V.V., C.V. Grant, A.E. Daily, S.J. Opella, and R.E. Koeppe 2nd, 2008. Comparison of "Polarization Inversion with Spin Exchange at Magic Angle" and "Geometric Analysis of Labeled Alanines" methods for transmembrane helix alignment. *J Am Chem Soc* 130: 12584-12585.
- Vostrikov, V.V., B.A. Hall, D.V. Greathouse, R.E. Koeppe 2nd, and M.S.P. Sansom, 2010b. Changes in transmembrane helix alignment by arginine residues revealed by solid-state NMR experiments and coarse-grained MD simulations. *J Am Chem Soc* 132: 5803-5811.
- White, S.H., and G. von Heijne, 2008. How translocons select transmembrane helices. *Annu Rev Biophys* 37: 23-42.
- Wiener, M.C., and S.H. White, 1992. Structure of a fluid dioleoylphosphatidylcholine bilayer determined by joint refinement of x-ray and neutron diffraction data. III. Complete structure. *Biophys J* 61: 434-447.
- Yau, W.M., W.C. Wimley, K. Gawrisch, and S.H. White, 1998. The preference of tryptophan for membrane interfaces. *Biochemistry* 37: 14713-14718.

3.8 Tables

Table 1. Sequences for GW^{x,y}ALP23 peptides.^a

Peptide	Sequence
GW ^{3,21} ALP23	GG <u>W</u> LALALALALALALALAL <u>W</u> GA
GW ^{5,19} ALP23	GGAL <u>W</u> LALALALALALALAL <u>W</u> LAGA
GW ^{7,17} ALP23	GGALAL <u>W</u> LALALALALAL <u>W</u> LALAGA

^aN-terminal Gly residue is acylated. C-terminal Ala residue is blocked with ethanolamide.

Table 2. Alanine C β D $_3$ quadrupolar splittings for GW^{x,y}ALP23 peptides incorporated in DLPC, DMPC or DOPC bilayers.^a

Peptide	Lipid	Alanine position							
		5	7	9	11	13	15	17	19
GW ^{7,17} ALP23	DLPC	8.0	-	6.1	6.1	12.5	0.8	-	7.4
	DMPC	10.9	-	11.2	2.1	13.9	0.8	-	4.1
	DOPC	12.5	-	10.9	3.1	13.4	0.8	-	3.0
GW ^{5,19} ALP23 ^b	DLPC	-	26.4	25.5	26.9	14.6	20.7	3.4	-
	DMPC	-	21.9	8.9	20.9	3.8	17.6	2.9	-
	DOPC	-	16.6	1.7	16.7	1.5	15.4	2.6	-
GW ^{3,21} ALP23	DLPC	19.6	23.8	15.7	18.7	0.9	9.6	11.4	0.8
	DMPC	6.4	17.9	5.2	13.6	6.7	6.7	12.2	0.8
	DOPC	0.8	13.1	2.1	9.3	6.6	6.6	12.3	1.3

^aValues in kHz. Entries left blank were not measured.

^bData from (Vostrikov et al. 2010a).

Table 3. GALA fit results

Peptide (Lipid)				
	S_{pept}	τ , deg	ρ , deg	RMSD, kHz
(DLPC)				
GW ^{7,17} ALP23	0.79	6.7	223	0.1
GW ^{5,19} ALP23 ^a	0.71	20.8	304	0.7
GW ^{3,21} ALP23 ^b	0.63	18.0	281	2.0
(DMPC)				
GW ^{7,17} ALP23	0.82	4.3	182	0.1
GW ^{5,19} ALP23 ^a	0.88	9.1	310	1.1
GW ^{3,21} ALP23	0.75	9.0	268	1.1
(DOPC)				
GW ^{7,17} ALP23	0.83	4.0	186	0.1
GW ^{5,19} ALP23 ^a	0.86	6.1	322	0.6
GW ^{3,21} ALP23	0.80	4.3	257	0.8

^aData from (Vostrikov et al. 2010a).

^bThe RMSD reduces to 1.0 kHz if the A19 data point is omitted and 1.5 kHz if A5 data point is omitted. The corresponding (S_{pept} , τ , ρ) values are (0.60, 19.7, 277) with A19 omitted or (0.68, 15.3, 283) with A5 omitted. Exclusion of both A5 and A19 leads to RMSD = 0.9 kHz, with the corresponding parameters of (0.63, 18.0, 279).

Table 4. Tryptophan side chain CD quadrupolar splitting magnitudes for GW^{x,y}ALP23 peptides incorporated in DLPC, DMPC or DOPC.^a

Peptide	Lipid	$\Delta\nu_q$, kHz							
		N-terminal Trp				C-terminal Trp			
		2	4/7	5	6	2	4/7	5	6
GW ^{7,17} ALP23	DLPC	67	63	154	74	54	63 ^d	4	63 ^d
	DMPC	54 ^b	81	154	85	49 ^a	67 ^d	6 ^b	67 ^d
	DOPC	42 ^c	77 ^c			55	67 ^d	8	67 ^d
GW ^{5,19} ALP23	DLPC	43 ^b	8	105	76	61 ^a	30	6 ^b	85
	DMPC	54 ^b	58	142	85	54 ^a	43	33 ^b	89
	DOPC	39 ^b	86	137 ^b	88	58 ^b	39	8	78
GW ^{3,21} ALP23	DLPC	64 ^b	15	120	51 ^b	53 ^b	36	4	58
	DMPC	64 ^c	42 ^c	145 ^c	50 ^{bc}	40 ^{bc}	27 ^c		59 ^c
	DOPC	62 ^c		141 ^c	52 ^b	27 ^{bc}	19 ^c	7 ^c	51 ^c

^aValues were obtained from the $\beta=90^\circ$ sample orientation and were multiplied by two. Entries left blank were not observed.

^bValue is also observed in a partially deuterated sample.

^cQuadrupolar splittings have not been assigned to labeled sites.

^dSignals not resolved.

Table 5. Tryptophan side chain free rotation fit values for GW^{x,y}ALP23 peptides incorporated in DLPC, DMPC or DOPC.^a

Peptide	Lipid	Fit parameters ^b							
		N-terminal Trp				C-terminal Trp			
		S_{zz}	ρ_1	ρ_2	RMSD	S_{zz}	ρ_1	ρ_2	RMSD
GW ^{7,17} ALP23	DLPC	0.68	137	0	2.8	0.54	165	36	0.3
	DMPC	0.72	140	0	2.2	0.55	162	40	0.3
	DOPC					0.57	165	36	1.7
GW ^{5,19} ALP23	DLPC	0.70	133	30	0.9	0.65	158	44	1.6
	DMPC	0.71	138	15	1.2	0.66	143	59	1.4
	DOPC	0.68	142	4	1.0	0.61	160	42	0.5
GW ^{3,21} ALP23	DLPC	0.54	130	17	0.8	0.50	162	41	3.5
	DMPC								
	DOPC								

^aEntries left blank were not fitted.

^b S_{zz} is a dimensionless entity, ρ angles are in degrees, RMSD is in kHz.

3.9 Figures

Figure 1. Molecular models of GW^{3,21}ALP, GW^{5,19}ALP23 and GW^{7,17}ALP23 (left to right). Black sphere indicates the C_α carbon of Gly¹. Note that the GW^{5,19}ALP23 model is rotated by 180°.

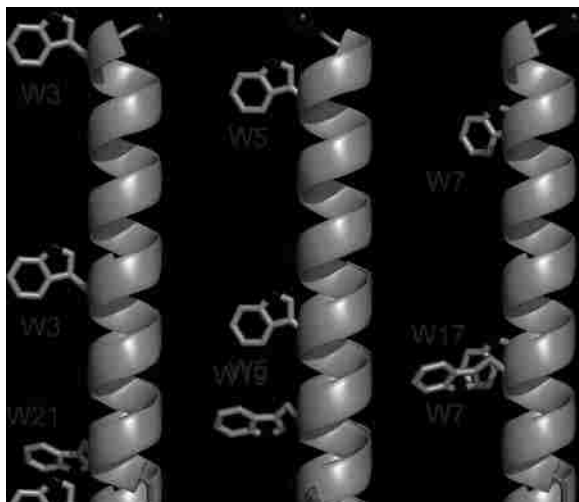


Figure 2. Circular dichroism spectra of GW^{3,21}ALP (black), GW^{5,19}ALP23 (red) and GW^{7,17}ALP23 (blue) in DLPC.

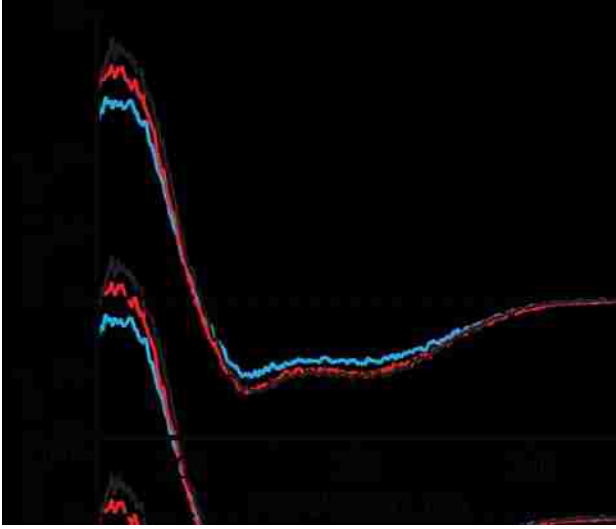


Figure 3. Deuterium NMR spectra of peptides in DMPC. **A-D:** GW^{3,21}ALP23; **E-F:** GW^{7,17}ALP23. Labeled positions are: 5 and 7 (A), 9 and 11 (B, E), 13 and 15 (C, F), 17 and 19 (D). Sample orientation is $\beta=0^\circ$. A complete set of deuterium NMR spectra is provided in Supporting Information.



Figure 4. GALA helical wave plots of peptides in DLPC (red squares), DMPC (green circles) and DOPC (blue diamonds). **A:** $\text{GW}^{3,21}$ ALP23; **B:** $\text{GW}^{5,19}$ ALP23; **C:** $\text{GW}^{7,17}$ ALP23. Deuterium labeled alanine positions are indicated in A.

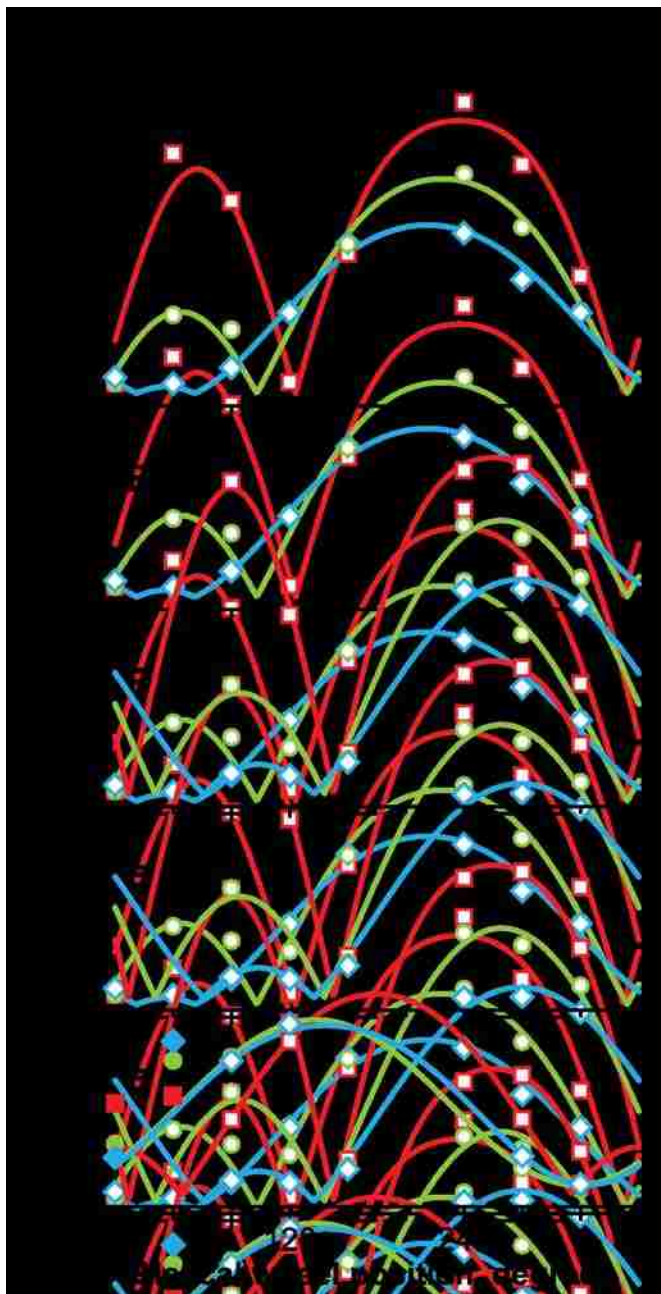


Figure 5. RMSD contour plots of GW^{3,21}ALP23 (black), GW^{5,19}ALP23 (red) and GW^{7,17}ALP23 (blue) in lipids. **A:** DLPC; **B:** DMPC; **C:** DOPC. Contour levels are plotted every 1 kHz; outer contour corresponds to 3 kHz.

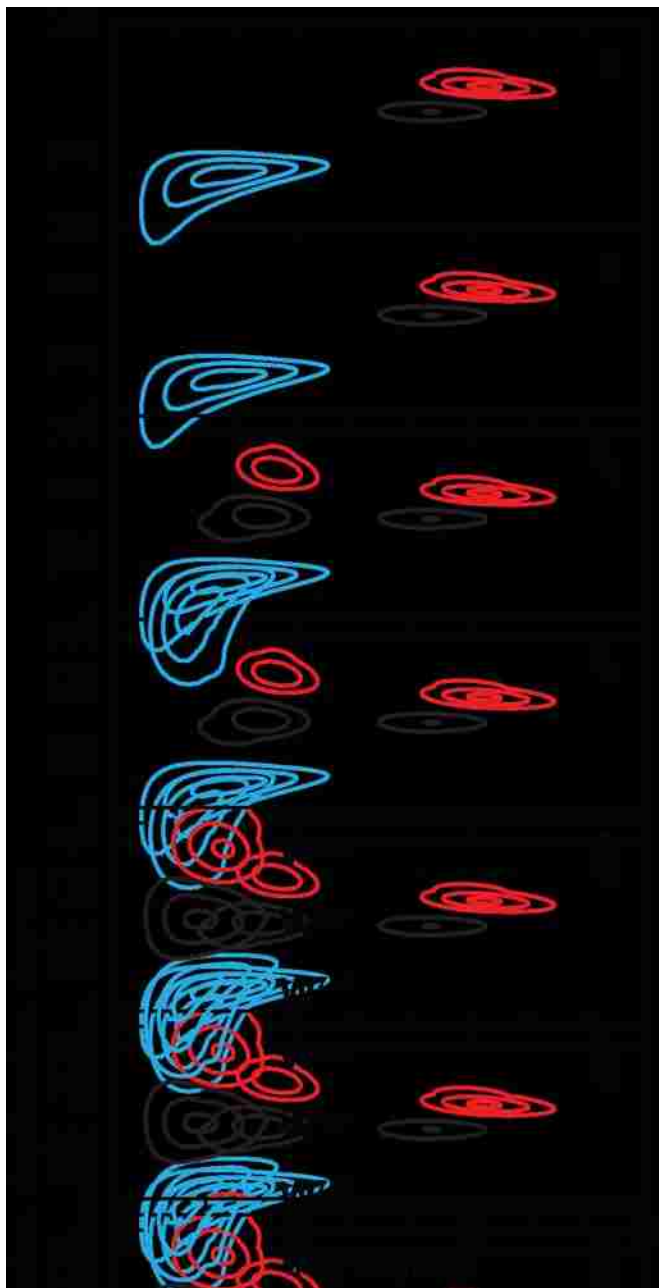


Figure 6. Steady-state fluorescence of $\text{GW}^{x,y}$ ALP23 peptides. **A:** emission spectra of $\text{GW}^{3,21}$ ALP23 (black), $\text{GW}^{5,19}$ ALP23 (red) and $\text{GW}^{7,17}$ ALP23 (blue) in DLPC small unilamellar vesicles; **B:** Tryptophan emission maxima as a function of theoretical hydrophobic mismatch. Peptide hydrophobic length was defined as inter-Trp distance (1.5 Å per amino acid), lipids hydrophobic thickness is from (de Planque et al., 2003).

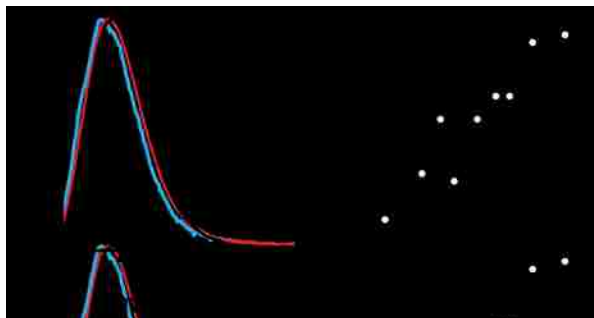


Figure 7. Deuterium NMR spectra of GW^{5,19}ALP23 labeled at Trp side chain in DLPC, DMPC and DOPC (top to bottom). **A:** N-terminal tryptophan, full deuteration; **B:** C-terminal tryptophan, full deuteration; **C:** N-terminal tryptophan, partial deuteration; **D:** C-terminal tryptophan, partial deuteration. Sample orientation is $\beta=90^\circ$.

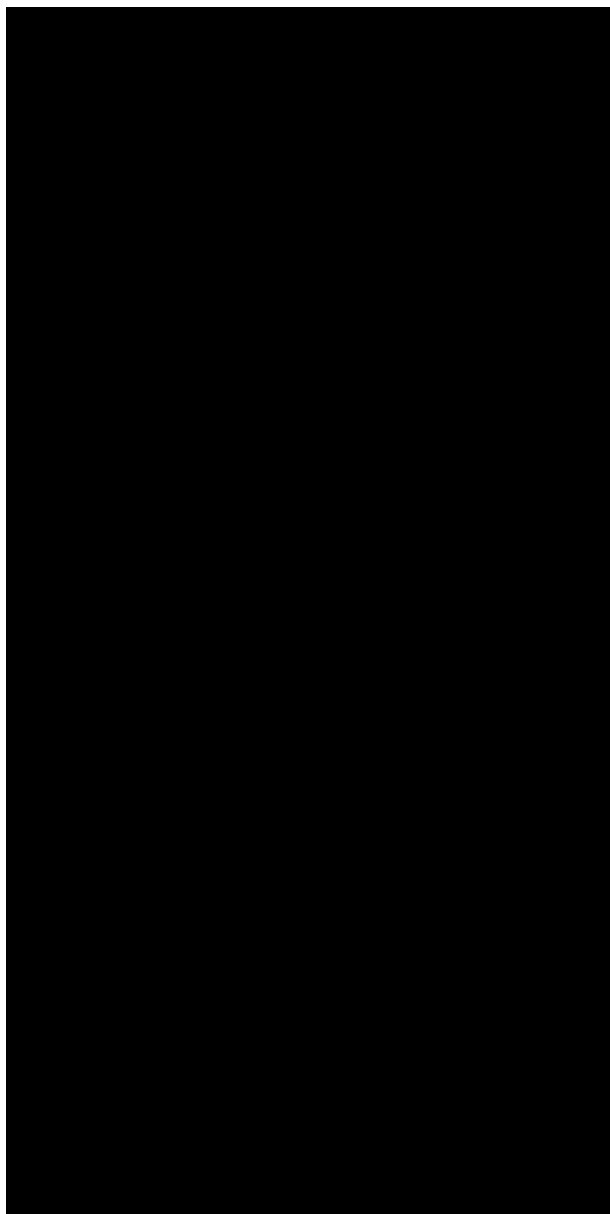


Figure 8. RMSD of fitting the N-terminal (black) and C-terminal (gray) tryptophans of GW^{5,19}ALP23 to the rotated indole model (note the logarithmic scale). **A**: DLPC; **B**: DMPC; **C**: DOPC. Angles ρ_1 , ρ_2 were optimized at each S_{zz} value to achieve lowest possible RMSD. Dashed lines indicate the order parameter of the peptide (Table 3) and correspond to the maximum possible value of the Trp S_{zz} .

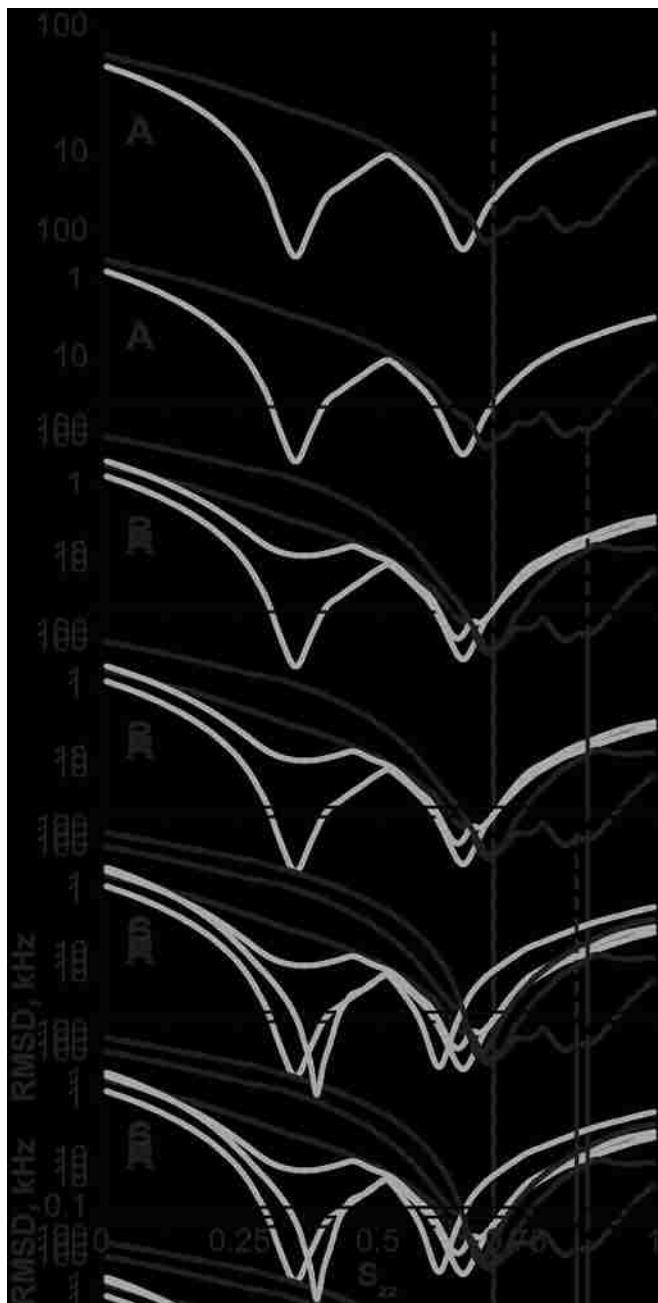


Figure 9. RMSD contour plots of the N-terminal (black) and C-terminal (gray) tryptophans of GW^{5,19}ALP23 as a function of indole ring orientation. **A:** DLPC; **B:** DMPC; **C:** DOPC. Contour levels are plotted every 1 kHz; outer contour corresponds to 5 kHz. Insets show one possible orientation of tryptophan side chains.

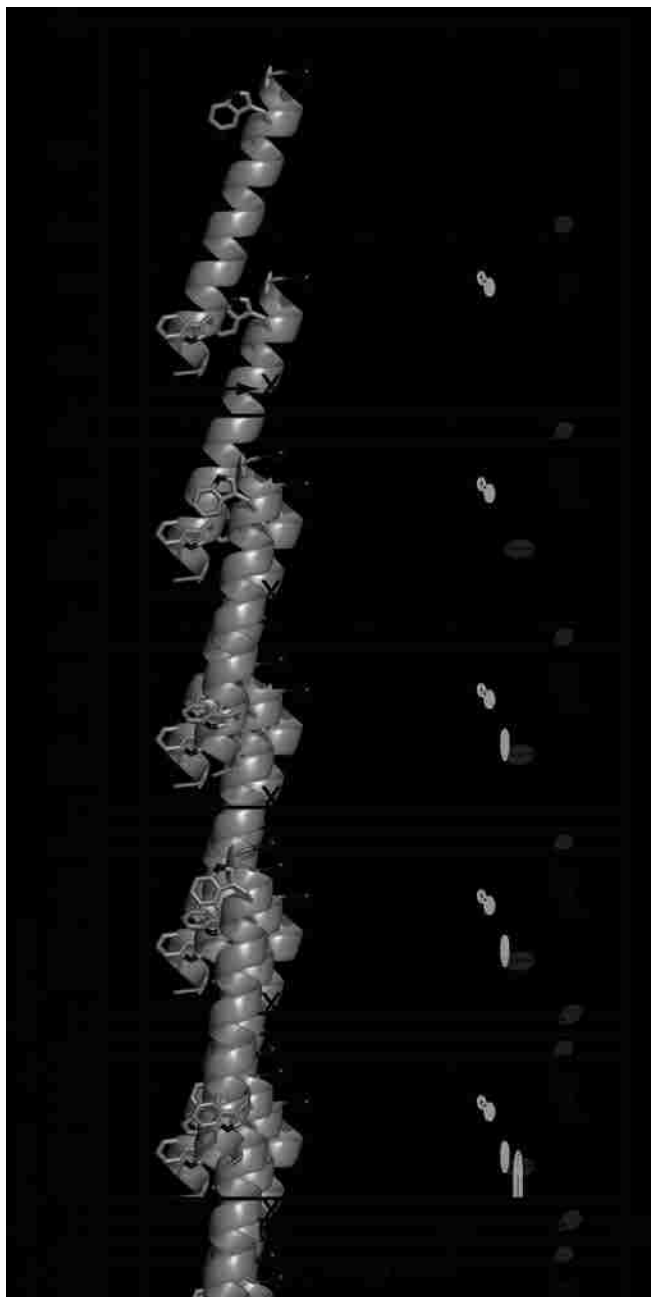


Figure 10. Explicit dynamics analysis of GW^{5,19}ALP23 (A, C) and GW^{3,21}ALP23 in DLPC (B, D), showing the standard deviations of Gaussian distributions (A, B) and their centers (C, D). Six alanine residues were used for the analysis (see text). Dashed lines in A and B indicate the best fit σ_τ and σ_ρ , which were used for generating the plots in C and D respectively. Color scale is identical between A and B (0 to 17 kHz, blue to red) and between C and D (0 to 22 kHz, blue to red). Color increments are at 1 kHz; solid line in C, D is drawn at 3 kHz level. Best fits (τ_0 , σ_τ , ρ_0 , σ_ρ) are (25, 16, 303, 36) for GW^{5,19}ALP23 and (25, 20, 278, 48) for GW^{3,21}ALP23.

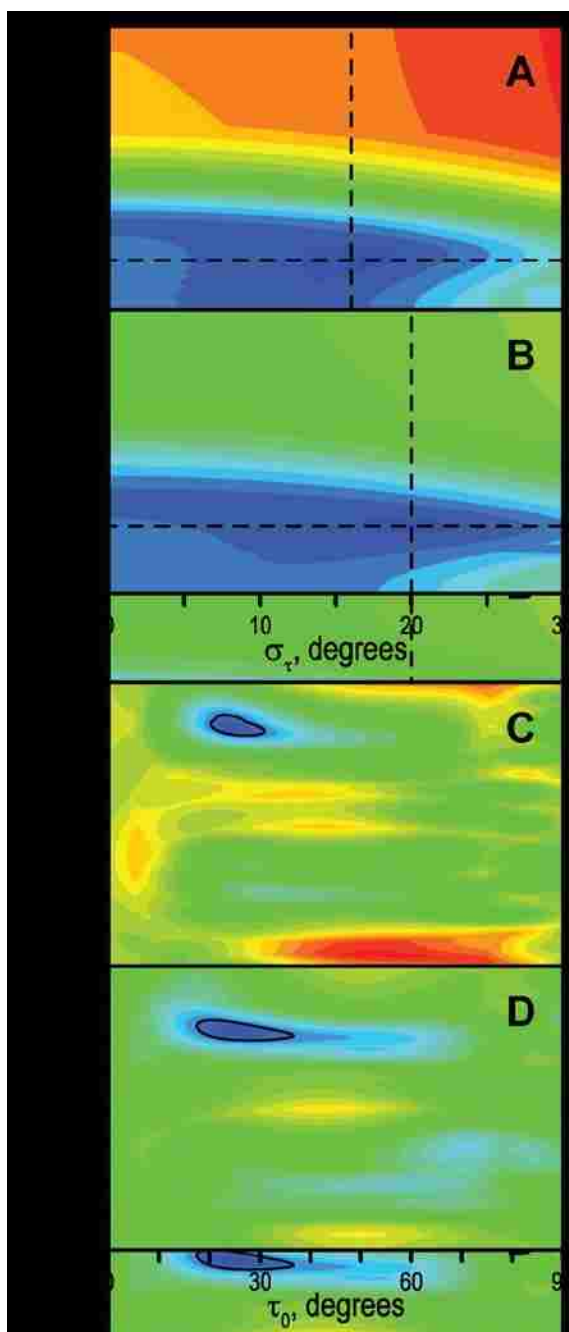
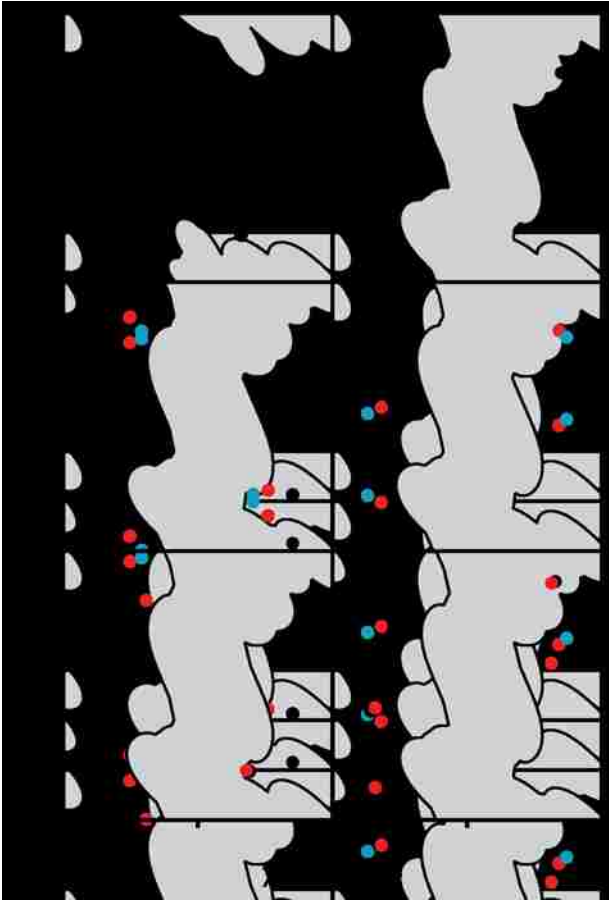


Figure 11. Tryptophan side chain torsion angles. **A:** W3; **B:** W5; **C:** W7; **D:** W21; **E:** W19; **F:** W17. Gray regions indicate steric hindrance area. Lipids are DLPC (black), DMPC (red) and DOPC (blue).



3.10 Supporting Information

Figure S1. Proton NMR spectra of Fmoc-Trp in DMSO- d_6 before and after TFA- d_1 treatment. Protons of the indole ring are indicated with numbers.

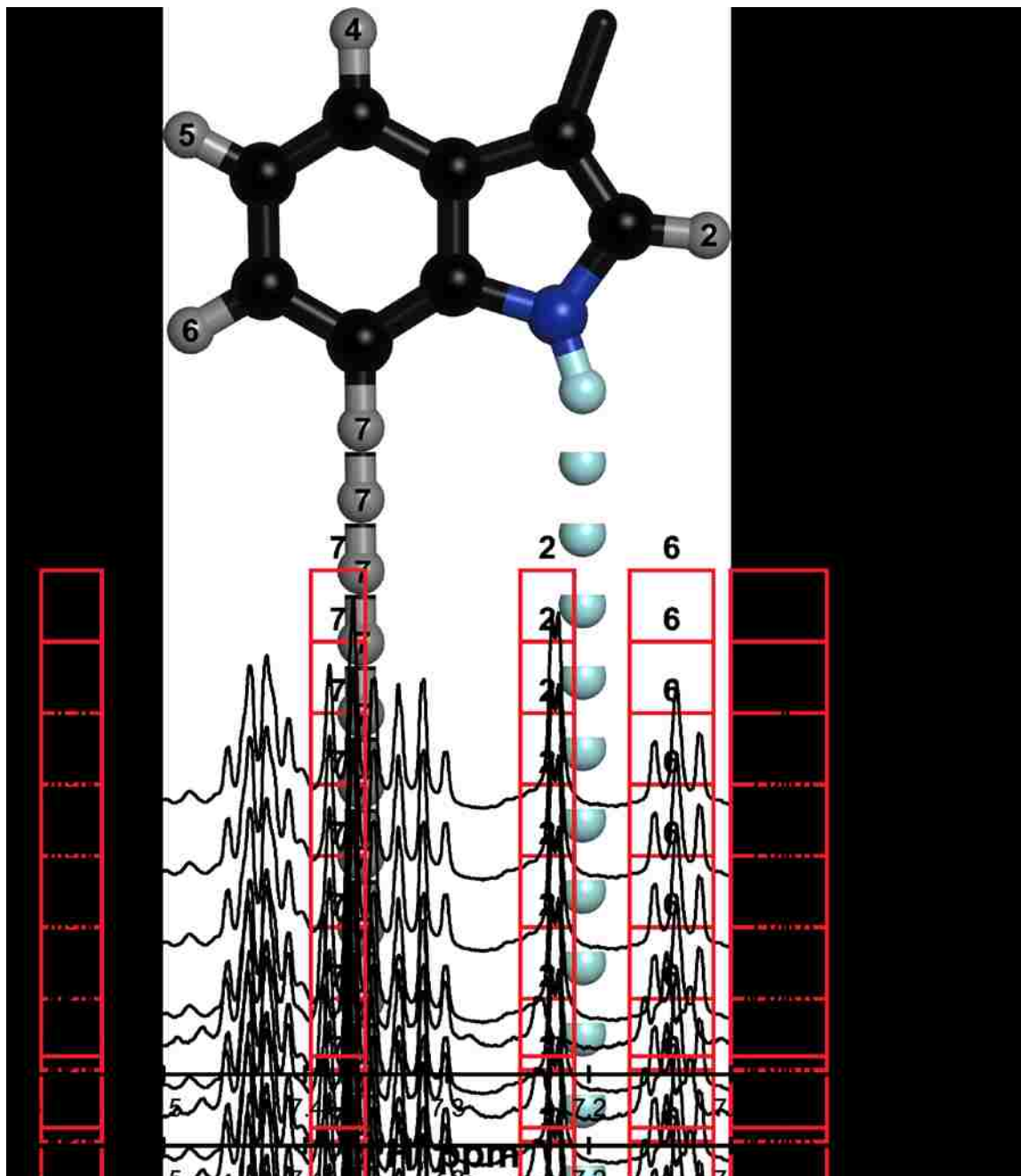


Figure S2. Analytical HPLC of GW^{7,17}ALP23, GW^{5,19}ALP23 and GW^{3,21}ALP.

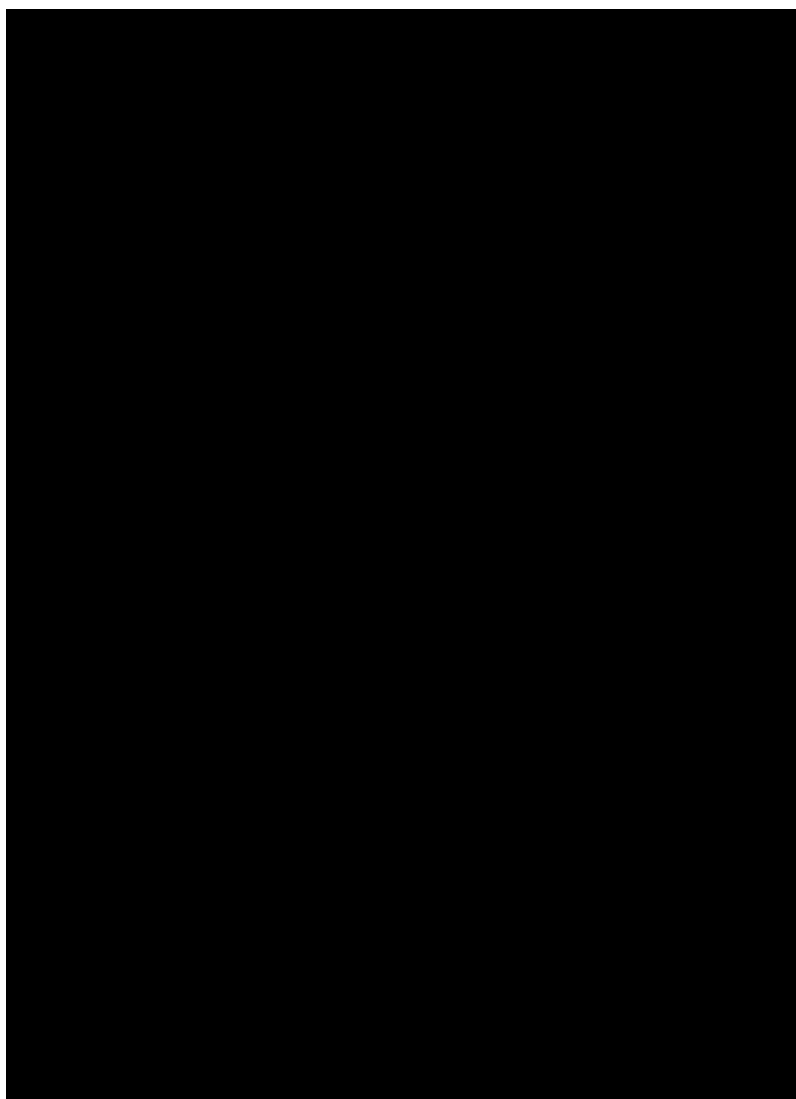


Figure S3. MALDI mass spectra of GWALP23 (no deuterium labels), GWALP23-Trp- d_2 and GWALP23-Trp- d_5 . Note that since GWALP23-Trp- d_2 represents a mixture of three peptides (see Materials and Methods) a change of the intensity pattern is observed.



Figure S4. A complete solution field for N-terminal tryptophan of GW^{5,19}ALP23 in DLPC. Color range is 0-220 kHz, color increments are at 5 kHz, solid lines are drawn every 20 kHz. Dashed lines indicate the 8-fold symmetry of the solution space.

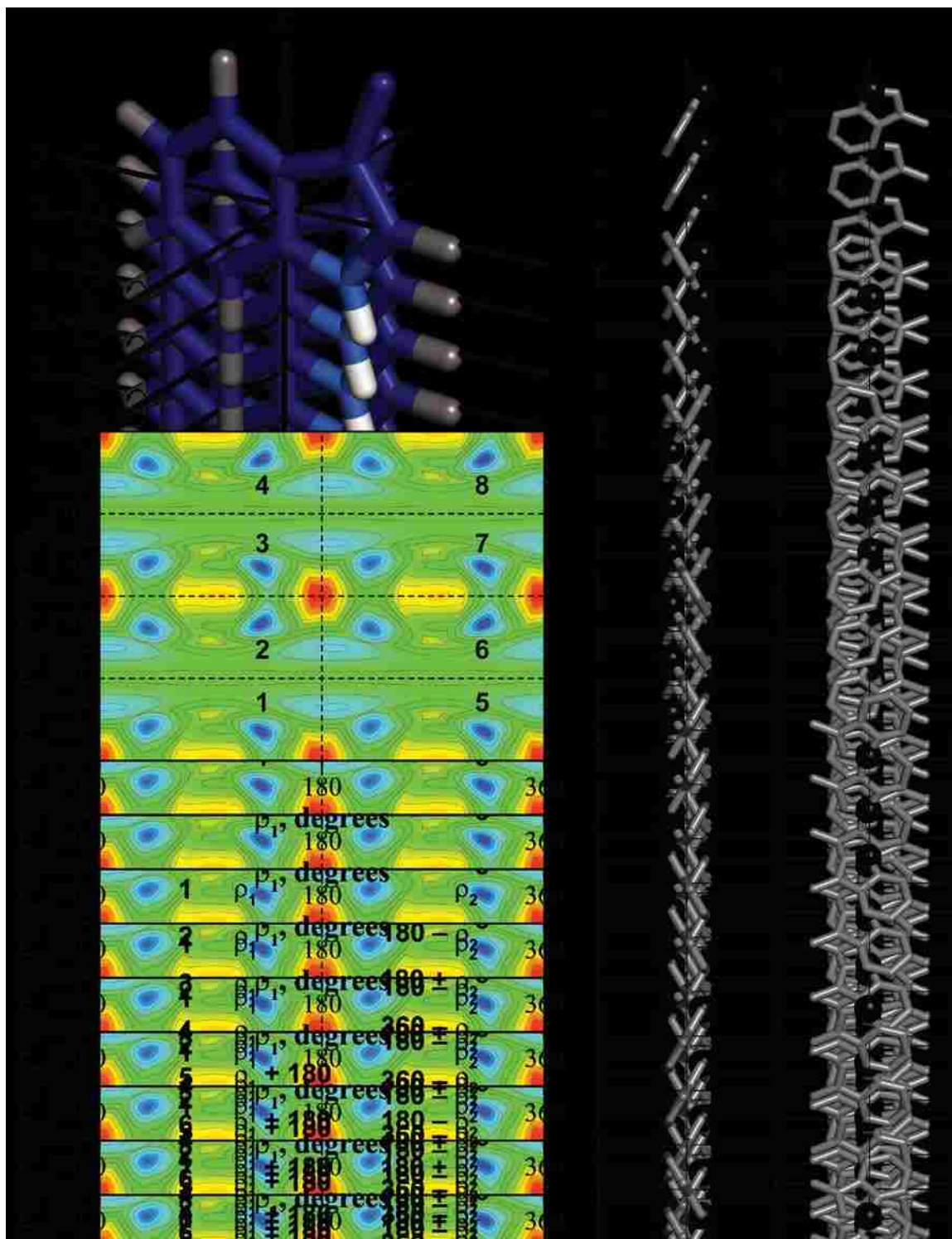


Figure S5. Phosphorus NMR spectra of $\text{GW}^{x,y}\text{ALP23}$ in DOPC.

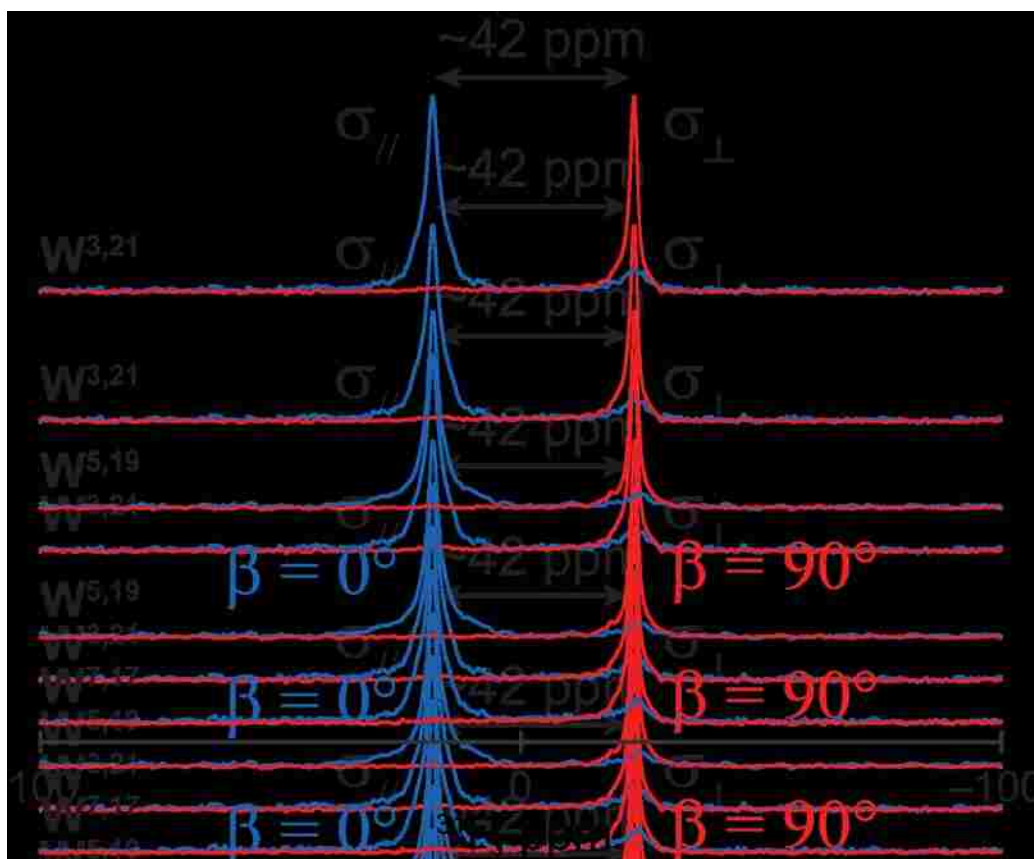


Figure S6. Deuterium NMR spectra of GW^{3,21}ALP23 in DLPC, DMPC and DOPC. Sample orientation is $\beta=0^\circ$.

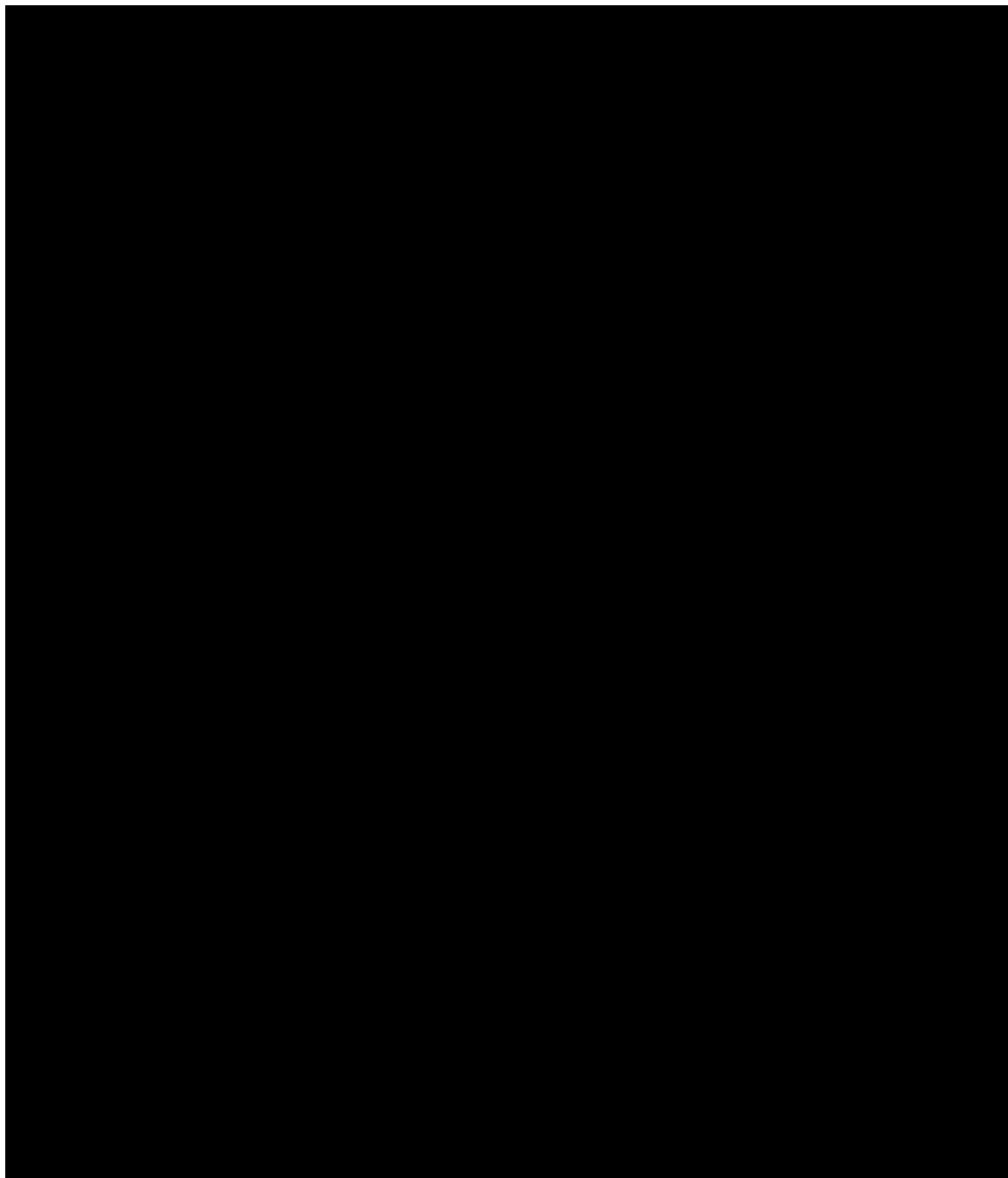


Figure S7. Deuterium NMR spectra of GW^{5,19}ALP23 in DLPC, DMPC and DOPC (Vostrikov et al. 2010a). Sample orientation is $\beta=0^\circ$.

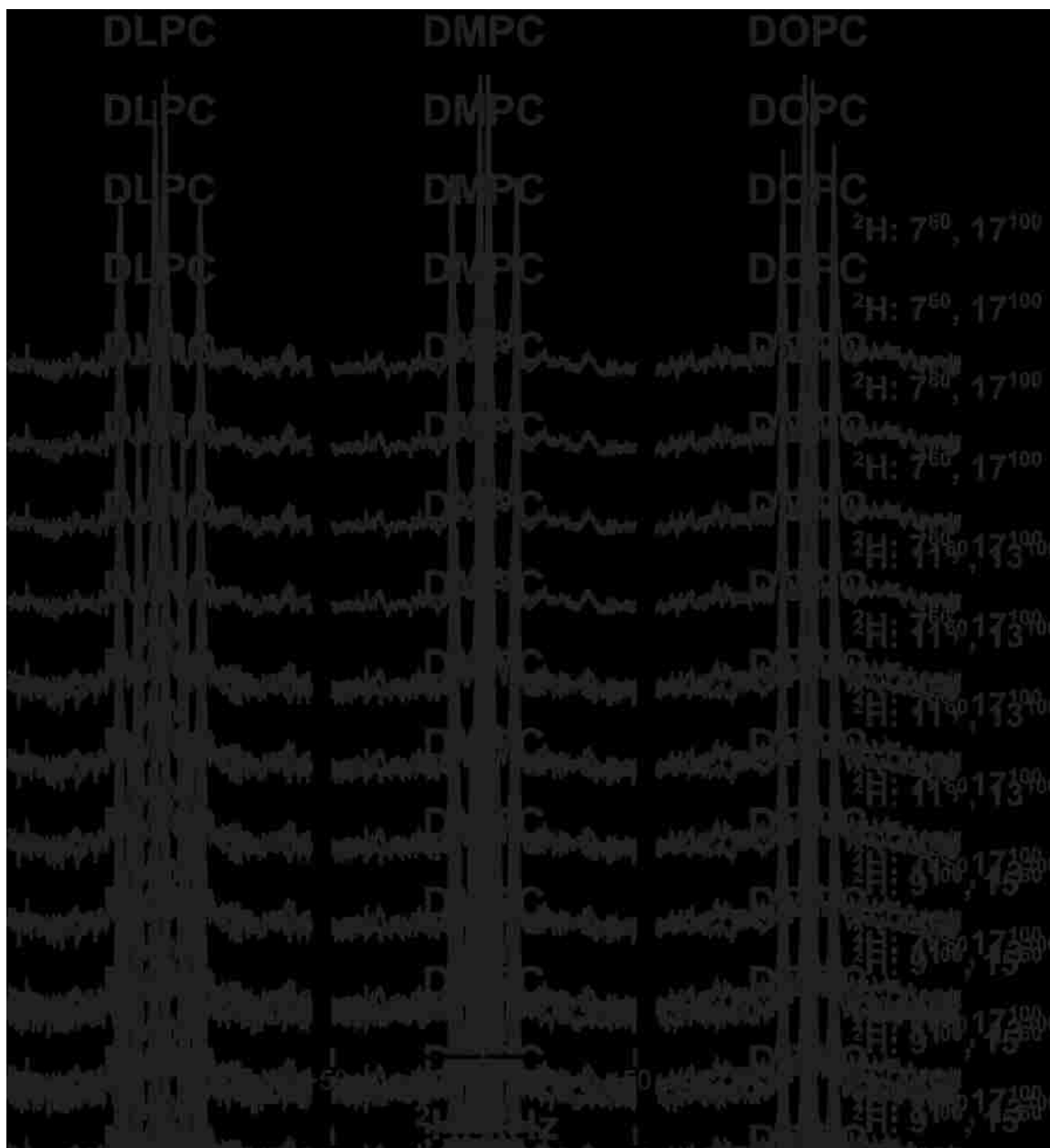


Figure S8. Deuterium NMR spectra of GW^{7,17}ALP23 in DLPC, DMPC and DOPC. Sample orientation is $\beta=0^\circ$.



Figure S9. Deuterium NMR spectra of GW^{x,y}ALP23 labeled at Trp side chain (*d*₅). Sample orientation is $\beta=90^\circ$.



CHAPTER 4

Changes in Transmembrane Helix Alignment by Arginine Residues Revealed by Solid-State NMR Experiments and Coarse-Grained MD Simulations

Reproduced with permission from Vostrikov, V.V., B.A. Hall, D.V. Greathouse, R.E.

Koeppel 2nd, and M.S.P. Sansom. Changes in transmembrane helix alignment by arginine residues revealed by solid-state NMR experiments and coarse-grained MD simulations. *J*

Am Chem Soc. 2010; 132:5803-5811. © 2010 American Chemical Society

4.1 Abstract

Independent experimental and computational approaches show agreement concerning arginine/membrane interactions when a single arginine is introduced at selected positions within the membrane-spanning region of ac-GALW⁵LALALAL¹²AL¹⁴ALALW¹⁹LAGA-ethanolamide, designated GWALP23. Peptide sequence isomers having Arg in position 12 or position 14 display markedly different behaviors, as deduced by both solid-state NMR experiments and coarse-grained molecular dynamics (CG-MD) simulations. With respect to the membrane normal of DOPC or DPPC lipid bilayer membranes, GWALP23-R14 shows one major state whose apparent average tilt is $\sim 10^\circ$ greater than that of GWALP23. The presence of R14 furthermore induces bilayer thinning and peptide displacement to “lift” the charged guanidinium toward the bilayer surface. By contrast, GWALP23-R12 exhibits multiple states that are in slow exchange on the NMR time scale, with CG-MD simulations indicating two distinct positions with different screw rotation angles in the membrane, along with an increased tendency to exit the lipid bilayer.

4.2 Introduction

Membrane proteins play a major role in a range of biological processes, as they represent about 25% of encoded gene products (Wallin and von Heijne, 1998) and ~40% of drug targets (Terstappen and Reggiani, 2001). The structure and function of membrane proteins may be modulated by interactions with their lipid bilayer environment (Lee, 2004). The understanding of how membrane proteins interact with lipid bilayers (Killian and von Heijne, 2000) has been aided by studies of “simple” model transmembrane (TM) α -helices such as the WALP series of peptides. These peptides consist of a variable length poly-alanine/leucine core capped at either end with tryptophan residues that favor the membrane/water interface (de Planque et al., 2003; de Planque and Killian, 2003; de Planque et al., 1999; Killian, 2003; Killian and Nyholm, 2006; Ozdirekcan et al., 2007; Strandberg et al., 2004; van der Wel et al., 2002). WALP peptides have been employed to study a wide range of transmembrane helix behaviors, including hydrophobic mismatch, variation of helix tilt with varying peptide and lipid lengths, and helix dimerization, amongst others. Recently, a novel related peptide was described, GWALP23 (acetyl-GGALW(LA)₆LWLAGA-ethanolamide), (Vostrikov et al., 2008) which differs from the WALP family in having only a single tryptophan residue near each terminus. The defined orientation and dynamics (Vostrikov et al., 2008) of GWALP23 provide exceptional opportunities for investigating the influence of guest residues such as arginine upon the properties and lipid interactions of membrane-spanning peptide helices.

The role and behavior of arginine residues in membrane proteins is the subject of ongoing debate. Arginine residues in TM helices have an important biological role in the voltage

sensor domains of voltage activated channels and enzymes (Swartz, 2008) and have been especially studied in the context of voltage-dependent potassium channels (Bond and Sansom, 2007; Freitas et al., 2005; Hessa et al., 2005; Sands and Sansom, 2007) and cell-penetrating peptides (Schmidt et al.; Su et al.). Due to its high pK_a , the arginine side chain retains a positive charge over a wide range of environmental pH and dielectric constant. The interactions of arginine with lipid bilayers have gained considerable attention, within a context that interactions with the membrane interior are quite different from those at the membrane/solution interface (Dorairaj and Allen, 2007; Johansson and Lindahl, 2009; Li et al., 2008; MacCallum et al., 2008; Roux, 2007).

In this article we present experimental and computational approaches to probe the arginine interaction with lipid bilayer membranes by employing GWALP23 and derivatives. Substitution of leucine (L) with arginine (R) at position 14 or 12 (L14R or L12R) results in peptides having one single Arg placed close to the center of the membrane-spanning segment of GWALP23 (Figure 1). Since the radial separation between the Trp side chains is small, an Arg can be positioned so that it will project either from the same side as both Trp indole rings (R12), or from a different face of the helix (R14). Figure 1 depicts both atomic and coarse-grained (CG) representations of the Arg and Trp side chains projecting from the GWALP23 helical backbone.

To understand the influence of R14 and R12 upon lipid bilayer membrane-incorporated GWALP23, solid-state NMR experiments and molecular dynamics (MD) simulations were undertaken. Circular dichroism spectra will show that the peptides remain helical in the lipid environments. The introduction of ^2H -labeled alanines into the helical sequences

enables the helix orientations with respect to the DOPC bilayer membrane normal to be assessed using the “Geometric Analysis of Labeled Alanines” (GALA) method (van der Wel et al., 2002). In parallel, the application of coarse-grained molecular dynamics (CG-MD) simulations (Bond et al., 2007; Marrink et al., 2004; Nielsen et al., 2004) allowed us to assess the behavior of these peptides in DPPC or DOPC lipid bilayers. CG-MD overcomes the typical time-scale limitations of atomistically detailed simulations of membrane proteins (Lindahl and Sansom, 2008) by combining ~4 non-hydrogen atoms to form a single CG particle. The experiments and simulations give fundamental agreement, with both methods showing markedly different behavior between the R12 and R14 derivatives of GWALP23.

4.3 Results

The ^2H NMR spectra of labeled alanines (Figure 2) reveal obvious differences between bilayer-incorporated samples of the GWALP23-R12 and -R14 peptide sequence isomers. GWALP23-R14 exhibits distinct pairs of signals for the CD_3 methyl side chains of all six core alanines, with spectral quality comparable to that of native GWALP23 (Vostrikov et al., 2008). The pattern of ^2H quadrupolar splittings suggests dynamic averaging about a single predominant state, which is a tilted transmembrane (TM) helix for GWALP23-R14. Conversely, spectra of the R12 variant are characterized by poor signal-to-noise ratio, even though twice as many free induction decays were collected. Multiple low-intensity broad peaks are observed for each labeled Ala in GWALP23-R12, suggesting two or more states for this peptide, in slow exchange with respect to the lipid bilayer

membrane. Tabulated quadrupolar splittings ($\Delta\nu_q$) for the core ^2H -alanines in GWALP23-R12 and -R14 are provided in Table 1.

Given the differences in the ^2H NMR spectra it is important to consider whether the GWALP derivatives remain helical. Indeed, circular dichroism spectra (Figure S1 of the Supporting Information) indicate that GWALP23-R12 and GWALP23-R14 retain the primarily α -helical secondary structure observed for GWALP23 in DOPC. Although the far-UV region (<203 nm) is not accessible due to strong absorption by the DOPC double bond, the features of an α -helix (a minimum at 208 nm and a shoulder at 222 nm) are readily recognized in each of the spectra. The three peptides exhibit similar mean residue ellipticity values, with comparable $\epsilon_{208}/\epsilon_{222}$ ratios. It is significant that the GWALP23-R12 helix does not appreciably unwind when interacting with the DOPC bilayers.

To estimate the charged state of the Arg guanidinium side chain, selected samples were prepared using buffer at either pH 7.4 or pH 4.5, to maintain a constant microenvironment for the arginine. The buffer samples at both pH levels yield spectra of similar quality and identical $\Delta\nu_q$ values to the buffer-free samples prepared with ^2H -depleted water (Figure 3). Because the R14 and R12 side chains undoubtedly both carry a positive charge at pH 4.5, the similar results at pH 7.4 and 4.5 indicate that the guanidinium groups remain charged in all of the samples and experiments reported here. Variations in peptide/lipid ratio from 1/40 to 1/80, or in temperature (30-50 °C), also yielded no significant spectral changes.

Individual signals in the spectra for GWALP23-R14 were assigned and then were analyzed using the GALA method, while incorporating a variable order parameter S_{zz} for the peptide and keeping the $\varepsilon_{//}$ angle fixed at 59.4° (Strandberg et al.; Thomas et al.; van der Wel et al., 2002). The best fit for the tilt of GWALP23-R14 (Table 2; Figure 4) occurs for a relatively high S_{zz} value of 0.94, compared to 0.86 for GWALP23 itself. Introduction of R14 caused the apparent average tilt of the GWALP23 helix axis to increase $\sim 10^\circ$ (relative to the DOPC bilayer normal). Furthermore the direction of the tilt, relative to the G1 reference point, (van der Wel et al., 2002) changed by $\sim 75^\circ$. Despite the presence of Arg near the helix center, the peptide retains predominantly a TM orientation. (One is unable to resolve NMR signals representing minor populations.) The ^2H NMR spectra of GWALP23-R14, in addition to strong $\text{C}_\beta\text{-D}_3$ peaks, furthermore exhibit some weaker signals from backbone $\text{C}_\alpha\text{-D}$ (Figure 2). This observation is noteworthy, since $\text{C}_\alpha\text{-D}$ signals have been observed also when proline is introduced near the center of WALP19, (Thomas et al.) but otherwise not in WALP family peptides, including GWALP23 (Ozdirekcan et al., 2005; Strandberg et al., 2004; Vostrikov et al., 2008). The result could signify that the motional regime of GWALP23-R14 is different from other WALP family peptides that lack Arg or Pro. The $\Delta\nu_q$ values of both the GWALP23-R14 and -R12 alanines, recorded at $\beta=90^\circ$, are half of the corresponding $\Delta\nu_q$ values recorded at $\beta=0^\circ$, indicating that both peptides undergo rapid reorientation (faster than $\sim 4 \times 10^4 \text{ s}^{-1}$) about the DOPC bilayer normal (Luo et al., 2009). The peptide tilt and this “precession” motion (Lee and Im, 2008) together define a cone angle of about 17° for GWALP23-R14 in DOPC.

For the case of GWALP23-R12, multiple peaks are observed in samples with two Ala labels (Figure 2B), or even when only one Ala is labeled (Figure S2 of the Supporting Information). (Control experiments with DOPC alone show that the central pair of very sharp signals—also present in Figure 2A—is from the lipid background (Figure S3). The other peaks from GWALP23-R12 are notably broad and cannot be attributed to natural abundance deuterium in DOPC.) As noted above, CD spectra indicate that the helical secondary structure is largely maintained even with the L12R substitution (Figure S1). With the alanine CD₃ signals being broadened and showing reduced intensity, it is very unlikely that any backbone C_α-D signals for GWALP23-R12 could be observed in these spectra. We therefore attribute the multiple NMR signals to multiple states for the helical backbone that holds the Ala side chains. It is remarkable that some quadrupolar splittings as large as 55 kHz are observed for GWALP23-R12 Ala methyls. For alanine CD₃ groups to exhibit such high $\Delta\nu_q$ values, the helix axis would be nearly perpendicular to the membrane normal, corresponding to an interfacial orientation of the peptide. Multiple signals from each labeled alanine (Figures 2-3; Table 1) imply that several distinct populations of GWALP23-R12 co-exist and exhibit slow exchange. (In principle, GWALP23-R14 also “could” have multiple populations, but they would have to be in fast exchange, since they yield one set of signals.) Together, the experimental data suggest that GWALP23-R12 is present in DOPC as an α -helical peptide which assumes several orientations, at least one of which is a surface bound (interfacially oriented) helix. While slower dynamic averaging is likely responsible not only for distinct populations but also for line broadening, still the dynamics within an individual state are not so slow as to

eliminate the signal averaging that gives rise to the pairs of peaks when samples of GWALP23-R12 are oriented at $\beta=90^\circ$.

To gain further insight into the interactions of these peptides with lipid bilayers, we performed CG-MD simulations. In these simulations, a model helix and randomly positioned lipid (DPPC) molecules and waters were used to self assemble to form a helix/bilayer system. Previous applications of this simulation method (which uses a forcefield derived from the MARTINI (Monticelli et al., 2008) forcefield) for a number of membrane peptides (Bond et al., 2007) and proteins (Scott et al., 2008) have yielded good comparisons with experimental data. For each peptide an ensemble of 100 individual self-assembly simulations, each of duration 100 ns (Figure 5), was performed in order to provide adequate sampling of peptide/bilayer interactions. For each ensemble of simulations, the results were analyzed in terms of three key metrics describing the orientation relative to the lipid bilayer: (i) the displacement of the helix relative to the center of the bilayer; (ii) the tilt of the helix axis relative to the bilayer normal; and (iii) the screw rotation of the helix (about its long axis). The parent GWALP23 helix is seen to adopt a TM orientation (Figure 6), with a mean tilt angle of $\sim 15^\circ$ and its center of mass close to the center of the bilayer (i.e. displacement $\sim 0 \text{ \AA}$). The GWALP23-R14 peptide, in which the Arg side chain is on the opposite side of the α -helix from the two Trp side chains, also adopts mainly (82% of the time) a TM orientation. However, there is a clear increase in the tilt angle of GWALP23-R14 by $\sim 10^\circ$ relative to the parent GWALP23 helix, in good agreement with the NMR experiments. The GWALP23-R14 helix is also displaced by $\sim 5 \text{ \AA}$ towards the leaflet adjacent to the C-terminus of the helix.

Visualization of the simulations indicates furthermore that the R14 side chain snorkels to the interfacial region, adjacent to the C-terminus of the helix. The presence of GWALP23-R14 also creates a local thinning of the bilayer (by 2.5 Å) relative to unmodified GWALP23, as well as increasing contacts of the peptide with water and phosphate particles. There is also a change of $\sim 70^\circ$ in the screw rotation of the GWALP23-R14 helix relative to GWALP23, again in good agreement with NMR data, and a narrowing of the distribution of rotation angles observed. By calculating the absolute rotation angles we are able to confirm close agreement between the rotation angles of the peptides adopted in the CG-MD simulations and the GALA analyses (Table 2), confirming that the CG tryptophans are correctly oriented in the bilayer. There remains a small difference ($\sim 8^\circ$) between the absolute tilt values calculated from the different methods, but this may arise from differences in the algorithms used to calculate these angles in the experimental and simulation systems. In addition, the distributions of rotation and tilt angles closely resemble the distributions observed in contour plots of rotation and tilt from GALA analysis (Figures 4, S4 and S5). HELANAL analysis also reveals that as expected the secondary structure restraints in the coarse grain model prevent any significant difference in bending being observed between GWALP23 and GWALP23-R14, which would agree with CD data indicating that helicity is maintained.

The behavior of GWALP23-R12 in CG-MD simulations is quite different. The helix adopts three different orientations, two TM and one interfacial (labeled INT in Figure 6). In the TM orientations there are two different snorkeling regimes, in which the R12 side chain snorkels either N-terminally or C-terminally. Additionally, for a significant

proportion of the simulation time (35%), the helix adopts an interfacial orientation (Figure 6). This frequency of the INT orientation is significantly higher than for either GWALP23 (~10%) or GWALP23-R14 (~20%). This is unlikely to arise from sampling effects within these simulations, as wider sets of data on the insertion of helical peptides in CG-MD demonstrate expected behaviors for artificial TM and interfacial peptides, and that these behaviors are not altered by extending the simulations (data not shown). Analysis of the screw rotation angle of the helix TM regime also demonstrates a bimodal distribution, occupying two distinct directions each $\sim 50^\circ$ away from the GWALP23 position. Visualization of the simulations reveals quite clearly these three orientations of the GWALP23-R12 helix (Figure 7). The somewhat higher frequency of C terminal snorkeling may be explained by a higher energetic cost for moving the two glycines at the N terminus into the membrane core, as compared to the alanine/glycine residues at the C terminus.

The CG-MD simulations described above were repeated using a CG model of DOPC. The results (Figure 8) were similar in terms of tilt and rotation of the peptides, namely GWALP23-R12 exhibited a shift to an interfacial location. In terms of displacement, R14 again induced a smaller shift towards an interfacial orientation, yet only a single TM peak was seen. Thus, the observation of a shift from a TM orientation (GWALP23, GWALP23-R14) towards an interfacial location (GWALP23-R12) is robust with respect to changes in the lipid bilayer.

The CG models of the three orientations of GWALP23-R12 in a DPPC bilayer (at 323 K) were converted to atomistic (AT) models using a fragment based approach (Stansfeld et

al., 2009). Each system was then simulated for 50 ns using AT-MD. In each case the peptide retained a largely α -helical conformation, and remained stably in its starting orientation. Thus, AT-MD simulations confirm that GWALP23-R12 may adopt multiple conformations relative to a phospholipid bilayer. Examinations of the atomistic GWALP23-R12 simulations also highlight the role for water penetration, as water molecules can be seen to enter the bilayer early in the simulation and then to remain in contact with the arginine side chain throughout the simulation (Figure 9). Examinations of the AT simulations reveal how water molecules and lipid phosphate groups interact closely with the arginine side chain.

4.4 Discussion

We have used a model TM helix (GWALP23) as the hydrophobic “host” for an arginine residue in order to unmask some of the complexities of the interactions of Arg-containing α -helices with lipid bilayers. This is a topic of relevance for the biosynthetic mechanisms and mode of action of voltage-sensor domains which are based upon an Arg-containing S4 helix (Swartz, 2008). Specifically, we have explored the effects on helix orientation within a bilayer of two particular arginine modifications of GWALP23 using both NMR and CG-MD to identify the distinct properties of the individual peptides. GWALP23-R14 is shown to undergo the same changes in helix tilt and rotation relative to GWALP23 in both simulation and experiment, indicating the likely accuracy of the simulation protocol and CG forcefield (Monticelli et al., 2008). The relatively small changes when R14 is introduced most likely reflect a competition of effects from tryptophan and arginine. In unmodified GWALP23, the tryptophans alone determine the helix orientation, with both

Trp side chains lying close to the plane of the membrane interfacial region. The introduction of R14 alters the relative Trp positions by means of helix displacement. At the same time, side-chain snorkeling, in combination with helix displacement and tilt, will permit the R14 guanidinium to interact with the interfacial region, thereby allowing the helix to retain a TM orientation despite introduction of a positively charged side chain near the center of the bilayer-spanning hydrophobic region. The combined helix displacement and side chain snorkeling can be viewed schematically as a positively-charged arginine “cork” making its way toward the bilayer interface (Figure 10).

To estimate the dynamics, (Esteban-Martin and Salgado, 2007; Strandberg et al., 2009) we have employed essentially “model 3” described by Strandberg *et al.*, (Strandberg et al.) which incorporates a variable principal order parameter S_{zz} for the peptide. A value of 0.88 for S_{zz} gives a good fit for both GWALP23 and GWALP23-R14, with RMSD values between 0.6 and 1.0 kHz for both peptides (Table 2). If lower values of S_{zz} are tried, the apparent tilt τ increases slightly (Figure S4), the direction of tilt ρ does not change, and the RMSD increases, indicating poorer fits. While S_{zz} of 0.86 is “best” for GWALP23, the rmsd for GWALP23-R14 falls slightly (to 0.9 kHz) if S_{zz} is increased still more to 0.94. The GALA method, with dynamics, indicates $\Delta\tau$ of about 10° and $\Delta\rho$ of about -75° when R14 is introduced into GWALP23 (Figure 4; Table 2). Additionally, the independent ^{15}N PISEMA and ^2H GALA algorithms, with the latter incorporating S_{zz} , have shown good agreement concerning the tilt of GWALP23 (Vostrikov et al.). The further specific agreement here between NMR and CG-MD methods, concerning the changes in tilt as well as rotation between GWALP23 and GWALP23-R14, despite the

small difference in the absolute tilt values (Table 2), highlights in this case a convergence of independent computational and experimental methods.

It is important to consider the possible limitations of the CG model used, which employs the MARTINI (Monticelli et al., 2008) parameters for lipids and peptides. As has been noted (Vorobyov et al., 2008) CG models such as MARTINI do not fully reproduce the thermodynamics of Arg insertion. Nevertheless, detailed comparison using a MARTINI-derived CG model (Bond et al., 2008) suggested just a ca. 2-fold underestimation of the free energy barrier for burying a single Arg side chain in the bilayer core. Furthermore, comparisons of CG (Bond and Sansom, 2007) and atomistic (Freites et al., 2005) simulations of the S4 helix from Kv channels (which contains multiple Arg side chains) suggest that CG simulations are capable of (qualitatively) reproducing the local bilayer distortions caused by Arg insertion into a bilayer.

Furthermore, CG simulations of the Trp-containing WALP peptide helix (Bond et al., 2008; Bond et al., 2007; Monticelli et al., 2008) suggest that such CG simulations are capable of correctly capturing the interaction of Trp side chains with lipid bilayers. We also are reasonably confident that the observed difference between the R12 and R14 peptides is not simply a kinetic effect, as comparison with a wide range of TM and interfacial membrane peptides (Hall and Sansom, in preparation) indicates that there exists sufficiently good sampling in the current studies to capture such a difference.

The combined results from the NMR and simulations reveal the subtle interplay of Trp and Arg side chains in orienting an α -helix relative to a lipid bilayer (Killian and von Heijne, 2000). Thus the two tryptophan residues of GWALP23 and GWALP23-R14

determine the tilt of the helix relative to the bilayer normal; R14 dictates the rotational preference of the helix due to its tighter interaction with the interfacial region. The R14 snorkeling causes some bilayer deformation as observed in the CG-MD simulations, such that the bilayer is ~ 2.5 Å thinner in the presence of GWALP23-R14. This distortion is accompanied by water particles penetrating into the bilayer, as has been observed also in atomistic simulations (Freites et al., 2005; Li et al., 2008; MacCallum et al., 2008; Monticelli et al., 2004; Sands and Sansom, 2007). It should be noted that the arginine side chain is indicated by the NMR experiments to be protonated (Figure 3), as has been suggested also by a number of calculations (Li et al., 2008; MacCallum et al., 2008).

It is encouraging that the relatively small difference in behavior of GWALP23-R14 relative to unmodified GWALP23 is highly consistent between NMR data and CG-MD simulations. The results suggest that the two methods are capable of reporting correctly on the effects of Arg residues on membrane/helix interactions. In GWALP23-R14 there seems to be cooperation between Trp and Arg to enable maximal access to the headgroup region; furthermore it is likely that W5 and W19 prevent further tilt by anchoring the peptide tips to the headgroup regions.

The behavior of GWALP23-R12 is strikingly different, arising from competition between the tryptophan and arginine side chains for access to the same lipid/water interfacial region. This dynamic competition leads to three different states being significantly populated: two TM orientations and one interfacial orientation. Thus, whether or not an arginine side chain may be accommodated within a hydrophobic TM helix is seen to depend on the sequence context in a non-linear fashion, which in turn reflects a

competition for lipid headgroup and water interactions between the basic and the amphipathic aromatic side chains.

That the GWALP-R12 helix may adopt (meta-stable) TM state(s) in addition to an interfacial state is of interest as it may indicate a potential role for such multi-state behavior in biological as well as synthetic systems, providing thereby a potential orientational “switch” which could respond to changes in the helix/bilayer environment. Such changes may reflect the action of voltage-gated channels and cell-penetrating peptides, amongst others.

In summary, our combined experimental and computational approaches reveal that the introduction of a single arginine residue into a hydrophobic TM helix may result in either (i) a small reorientation of the helix relative to the bilayer interface (R14), or (ii) a dynamic switching between TM and interfacial orientations of the helix (R12). The identification of the charge status of arginine in the membrane through the use of different solution pH values clearly favors models in which the protonated form of the arginine side chain may insert into the membrane by inducing deformation of the bilayer. Further studies may reveal more details, including the role of adjacent TM helices in modulating such behavior in biological membranes (Johansson and Lindahl, 2009).

4.5 Materials and Methods

Protected amino acids and “Rink” amide resin were purchased from NovaBiochem (San Diego, CA). Commercial L-alanine-d₄ from Cambridge Isotope Laboratories (Andover, MA) was modified with an Fmoc group, as described previously (Thomas et al.) and

recrystallized from ethyl acetate:hexane, 80:20. Solid-phase peptide synthesis was performed on 0.1 mmol scale using a Perkin-Elmer / Applied Biosystems 433A synthesizer (Foster City, CA). Two Ala-d₄ residues were incorporated per peptide, at different isotope abundance levels, achieved by mixing appropriate amounts of Fmoc-L-Ala and Fmoc-L-Ala-d₄. Peptides were cleaved from resins using trifluoroacetic acid, resulting in amidated C-termini. Solvents were of the highest available purity. Peptides were purified by reversed-phase HPLC on an octyl-silica column, using a gradient of 92-96% methanol over 24 min. Analytical HPLC results and MALDI-TOF analysis are provided in Figure S6 of the Supporting Information.

Mechanically aligned samples for solid-state NMR spectroscopy (1/60, peptide/lipid) were prepared using DOPC (Avanti Polar Lipids, Alabaster, AL) and deuterium-depleted water (Cambridge; 45% w/w hydration), as described previously.(van der Wel et al., 2002) Deuterium NMR spectra were recorded on a Bruker Avance 300 spectrometer, utilizing a quadrupolar echo pulse sequence(Davis et al., 1976) with 90 ms recycle delay, 3.2 μs pulse length and 115 μs echo delay. Between 750,000 (GWALP23-R14) and 1,500,000 (GWALP23-R12) transients were accumulated. An exponential weighting function with 100 Hz line broadening was applied prior to Fourier transformation. An enhanced GALA analysis (van der Wel et al.) was performed, using essentially model 3 of Strandberg *et al.* (Strandberg et al.) to estimate the dynamics. This model employs a variable order parameter S_{zz} which can be divided (conceptually) into components S^i and S^r (Strandberg et al.). We utilized the helix and alanine geometry described previously

and implemented an interactive grid search programmed in Microsoft Excel (Thomas et al.; van der Wel et al., 2002).

Coarse-grained molecular dynamics (CG-MD) simulations of the peptides in ~128 lipid DPPC bilayer were performed. CG-MD overcomes the typical limitations of atomistically detailed simulations of biomolecules by combining ~ 4 non-hydrogen atoms to form a single CG particle. In the current study we have used the latest version of the MARTINI forcefield with protein parameters, (Marrink et al., 2007; Monticelli et al., 2008) running simulations using Gromacs v3 (Lindahl et al., 2001) on a 56-processor Mac OS X cluster. Long range electrostatics were treated using a cut-off value of 12 Å and $\epsilon = 20$ (additionally, results are robust at $\epsilon = 15$). Temperature and pressure were coupled at 323 K and 1 Bar using the Berendsen (Berendsen et al., 1984) weak coupling algorithm ($\tau_T = 1$ ps and $\tau_P = 10$ ps). The compressibility was 3×10^5 (1/bar). In each simulation the bilayer is allowed to self assemble around the peptide (Figure 5) to reduce potential sources of bias in the simulation. We have performed CG-MD simulations within a high throughput framework which enabled $100 \times 0.1 \mu\text{s}$ simulations to be run (Hall & Sansom, in preparation) for each peptide helix, yielding good sampling of the helix/bilayer interactions.

4.6 Acknowledgments

This work was supported by grants from the US National Science Foundation (MCB-0841227), the Oxford Center for Integrative Systems Biology, the BBSRC and MRC, the Oxford Supercomputing Center, and the Arkansas Biosciences Institute. The NMR

facility was supported by NIH grant RR 15569. Our thanks to Daniel Parton and Chze Ling Wee for useful discussions.

4.7 References

- Berendsen, H.J.C., J.P.M. Postma, W.F. van Gunsteren, A. DiNola, and J.R. Haak, 1984. Molecular dynamics with coupling to an external bath. *J Chem Phys* 81: 3684-3690.
- Bond, P.J., and M.S.P. Sansom, 2007. Bilayer deformation by the Kv channel voltage sensor domain revealed by self-assembly simulations. *Proc Natl Acad Sci U S A* 104: 2631-2636.
- Bond, P.J., C.L. Wee, and M.S. Sansom, 2008. Coarse-grained molecular dynamics simulations of the energetics of helix insertion into a lipid bilayer. *Biochemistry* 47: 11321-11331.
- Bond, P.J., J. Holyoake, A. Ivetac, S. Khalid, and M.S.P. Sansom, 2007. Coarse-grained molecular dynamics simulations of membrane proteins and peptides. *J Struct Biol* 157: 593-605.
- Davis, J.H., K.R. Jeffrey, M. Bloom, M.I. Valic, and T.P. Higgs, 1976. Quadrupolar echo deuterium magnetic resonance spectroscopy in ordered hydrocarbon chains. *Chem Phys Lett* 42: 390-394.
- de Planque, M.R., B.B. Bonev, J.A. Demmers, D.V. Greathouse, Koeppe R.E. 2nd, F. Separovic, A. Watts, and J.A. Killian, 2003. Interfacial anchor properties of tryptophan residues in transmembrane peptides can dominate over hydrophobic matching effects in peptide-lipid interactions. *Biochemistry* 42: 5341-5348.
- de Planque, M.R.R., and J.A. Killian, 2003. Protein-lipid interactions studied with designed transmembrane peptides: Role of hydrophobic matching and interfacial anchoring. *Mol Membr Biol* 20: 271-284.
- de Planque, M.R.R., J.A.W. Kruijtzter, R.M.J. Liskamp, D. Marsh, D.V. Greathouse, Koeppe R.E. 2nd, B. de Kruijff, and J.A. Killian, 1999. Different membrane anchoring positions of tryptophan and lysine in synthetic transmembrane α -helical peptides. *J Biol Chem* 274: 20839-20846.
- Dorairaj, S., and T.W. Allen, 2007. On the thermodynamic stability of a charged arginine side chain in a transmembrane helix. *Proc Natl Acad Sci U S A* 104: 4943-4948.
- Esteban-Martin, S., and J. Salgado, 2007. The dynamic orientation of membrane-bound peptides: Bridging simulations and experiments. *Biophys J* 93: 4278-4288.
- Freites, J.A., D.J. Tobias, G. von Heijne, and S.H. White, 2005. Interface connections of a transmembrane voltage sensor. *Proc Natl Acad Sci U S A* 102: 15059-15064.
- Hessa, T., S.H. White, and G. von Heijne, 2005. Membrane insertion of a potassium-channel voltage sensor. *Science* 307: 1427.

- Johansson, A.C.V., and E. Lindahl, 2009. Protein contents in biological membranes can explain abnormal solvation of charged and polar residues. *Proc Natl Acad Sci U S A* 106: 15684-15689.
- Killian, J.A., 2003. Synthetic peptides as models for intrinsic membrane proteins. *FEBS Lett* 555: 134-138.
- Killian, J.A., and G. von Heijne, 2000. How proteins adapt to a membrane-water interface. *Trends Biochem Sci* 25: 429-434.
- Killian, J.A., and T.K.M. Nyholm, 2006. Peptides in lipid bilayers: the power of simple models. *Curr Opin Struct Biol* 16: 473-479.
- Lee, A.G., 2004. How lipids affect the activities of integral membrane proteins. *Biochim Biophys Acta* 1666: 62-87.
- Lee, J., and W. Im, 2008. Transmembrane helix tilting: Insights from calculating the potential of mean force. *Phys Rev Lett* 100: 018103.
- Li, L., I. Vorobyov, A.D. MacKerell, and T.W. Allen, 2008. Is arginine charged in a membrane? *Biophys J* 94: L11-L13.
- Lindahl, E., and M.S. Sansom, 2008. Membrane proteins: molecular dynamics simulations. *Curr Opin Struct Biol* 18: 425-431.
- Lindahl, E., B. Hess, and D. van der Spoel, 2001. GROMACS 3.0: a package for molecular simulation and trajectory analysis. *J Mol Model* 7: 306-317.
- Luo, W.B., S.D. Cady, and M. Hong, 2009. Immobilization of the influenza A M2 transmembrane peptide in virus envelope-mimetic lipid membranes: A solid-state NMR investigation. *Biochemistry* 48: 6361-6368.
- MacCallum, J.L., W.F.D. Bennett, and D.P. Tieleman, 2008. Distribution of amino acids in a lipid bilayer from computer simulations *Biophys J* 94: 3393-3404.
- Marrink, S.J., A.H. de Vries, and A.E. Mark, 2004. Coarse grained model for semiquantitative lipid simulations. *J Phys Chem B* 108: 750-760.
- Marrink, S.J., J. Risselada, S. Yefimov, D.P. Tieleman, and A.H. de Vries, 2007. The MARTINI forcefield: coarse grained model for biomolecular simulations. *J Phys Chem B* 111: 7812-7824.
- Monticelli, L., K.M. Robertson, J.L. MacCallum, and D.P. Tieleman, 2004. Computer simulation of the KvAP voltage-gated potassium channel: steered molecular dynamics of the voltage sensor. *FEBS Lett* 564: 325-332.
- Monticelli, L., S.K. Kandasamy, X. Periole, R.G. Larson, D.P. Tieleman, and S.J. Marrink, 2008. The MARTINI coarse grained force field: extension to proteins. *J Chem Theory Comput* 4: 819-834.

- Nielsen, S.O., C.F. Lopez, G. Srinivas, and M.L. Klein, 2004. Coarse grain models and the computer simulation of soft materials. *J Phys Condens Matter* 16: R481-R512.
- Ozdirekcan, S., D.T.S. Rijkers, R.M.J. Liskamp, and J.A. Killian, 2005. Influence of flanking residues on tilt and rotation angles of transmembrane peptides in lipid bilayers. A solid-state ^2H NMR study. *Biochemistry* 44: 1004-1012.
- Ozdirekcan, S., C. Etchebest, J.A. Killian, and P.F.J. Fuchs, 2007. On the orientation of a designed transmembrane peptide: Toward the right tilt angle? *J Am Chem Soc* 129: 15174-15181.
- Roux, B., 2007. Lonely arginine seeks friendly environment. *J Gen Physiol* 130: 233-236.
- Sands, Z.A., and M.S.P. Sansom, 2007. How does a voltage-sensor interact with a lipid bilayer? Simulations of a potassium channel domain. *Structure* 15: 235-244.
- Schmidt, N., A. Mishra, G.H. Lai, and G.C. Wong, 2009. Arginine-rich cell-penetrating peptides. *FEBS Lett*: DOI 10.1016/j.febslet.2009.11.046.
- Scott, K.A., P.J. Bond, A. Ivetac, A.P. Chetwynd, S. Khalid, and M.S.P. Sansom, 2008. Coarse-grained MD simulations of membrane protein-bilayer self-assembly. *Structure* 16: 621-630.
- Stansfeld, P.J., R.J. Hopkinson, F.M. Ashcroft, and M.S.P. Sansom, 2009. The PIP_2 binding site in Kir channels: Definition by multi-scale biomolecular simulations. *Biochemistry* 48: 10926-10933.
- Strandberg, E., S. Esteban-Martin, J. Salgado, and A.S. Ulrich, 2009. Orientation and dynamics of peptides in membranes calculated from ^2H -NMR data. *Biophys J* 96: 3223-3232.
- Strandberg, E., S. Özdirekcan, D.T.S. Rijkers, P.C.A. van der Wel, Koeppe R.E. 2nd, R.M.J. Liskamp, and J.A. Killian, 2004. Tilt angles of transmembrane model peptides in oriented and non-oriented lipid bilayers as determined by ^2H solid-state NMR. *Biophys J* 86: 3709-3721.
- Su, Y., T. Doherty, A.J. Waring, P. Ruchala, and M. Hong, 2009. Roles of arginine and lysine residues in the translocation of a cell-penetrating peptide from ^{13}C , ^{31}P , and ^{19}F solid-state NMR. *Biochemistry* 48: 4587-4595.
- Swartz, K.J., 2008. Sensing voltage across lipid membranes. *Nature* 456: 891-897.
- Terstappen, G.C., and A. Reggiani, 2001. *In silico* research in drug discovery. *Trends Pharmacol Sci* 22: 23-26.
- Thomas, R., V.V. Vostrikov, D.V. Greathouse, and Koeppe R.E. 2nd, 2009. Influence of proline upon the folding and geometry of the WALP19 transmembrane peptide. *Biochemistry* 48: 1183-1191.

- van der Wel, P.C.A., E. Strandberg, J.A. Killian, and Koeppe R.E. 2nd, 2002. Geometry and intrinsic tilt of a tryptophan-anchored transmembrane α -helix determined by ^2H NMR. *Biophys J* 83: 1479-1488.
- Vorobyov, I., L. Li, and T.W. Allen, 2008. Assessing atomistic and coarse-grained force fields for protein-lipid interactions: the formidable challenge of an ionizable side chain in a membrane. *J Phys Chem B* 112: 9588-9602.
- Vostrikov, V.V., C.V. Grant, A.E. Daily, S.J. Opella, and Koeppe R.E. 2nd, 2008. Comparison of "Polarization Inversion with Spin Exchange at Magic Angle" and "Geometric Analysis of Labeled Alanines" methods for transmembrane helix alignment. *J Am Chem Soc* 130: 12584-12585.
- Wallin, E., and G. von Heijne, 1998. Genome-wide analysis of integral membrane proteins from eubacterial, archean, and eukaryotic organisms. *Protein Sci* 7: 1029-1038.

4.8 Tables

Table 1. Quadrupolar splittings, $\Delta\nu_q$ in kHz, for ^2H -labeled core alanines of GWALP23-R14 and GWALP23-R12.^a

Ala position	GWALP23-R14	GWALP23-R12 ^b
5	26.6 kHz	3; 22; 32; 55
7	5.5	
9	16.0	2; 14; 22; 39
11	13.1	
13	1.3	2; 12; 21; 31
15	28.0	

^aThe quadrupolar splittings, $\Delta\nu_q$, are measured in kHz. The sample orientation is $\beta = 0^\circ$ in hydrated DOPC bilayer membranes (peptide/lipid ratio 1/60; sample temperature 50 °C).

^bDue to poor signal-to-noise, the values for GWALP23-R12 are approximate. Additionally, since multiple weak signals are observed for each double-labeled sample of GWALP23-R12, it is not possible to complete the individual assignments. Singly labeled samples of GWALP23-R12 (Figure S2 of the Supporting Information) also show multiple peaks; for these cases it still is not possible to correlate the assignments for the different alanines in the different peptide states.

Table 2. Comparison of average tilt and rotation angles of GWALP23 and GWALP23-R14 from GALA fits in DOPC and CG-MD simulations in DPPC and DOPC^a

Peptide	Method	S_{zz}	rmsd ^b	τ	$\Delta\tau^c$	ρ	$\Delta\rho^c$
GWALP23	GALA	0.7	1.7	7.5°		318°	
GWALP23-R14	GALA	0.7	2.1	22.8°	15.3°	247°	-71°
GWALP23	GALA	0.8	0.8	6.5°		321°	
GWALP23-R14	GALA	0.8	1.4	18.6°	12.1°	247°	-74°
GWALP23	GALA	0.88	0.6	5.9°		323°	
GWALP23-R14	GALA	0.88	1.0	16.2°	10.3°	247°	-76°
GWALP23 ^d	CG-MD /DPPC			15°		315°	
GWALP23-R14 ^d	CG-MD /DPPC			25°	10°	245°	-70°
GWALP23 ^d	CG-MD /DOPC			13°		293°	
GWALP23-R14 ^d	CG-MD /DOPC			22°	9°	249°	-44°

^aThe modified GALA analysis was based upon “model 3” of Strandberg *et al.*, (Strandberg *et al.*) with variable order parameter S_{zz} , such that $0 < S_{zz} < 1$. The angle $\epsilon_{//}$ between an alanine C_{α} - C_{β} bond and the helix axis was 59.4° (van der Wel *et al.*).

^bThe rmsd, in kHz, refers to the root mean squared deviation between observed ²H quadrupolar splittings and those predicted by a particular GALA fit.

^cThe values $\Delta\tau$ and $\Delta\rho$ refer to the differences in tilt and rotation, respectively, when comparing GWALP23-R14 and GWALP23 using the same method and same value of S_{zz} .

^dThe absolute rotation values were calculated based on the rotation angles of the backbone particles of all residues in the helix over the course of the simulation, and converted to the common reference used in the NMR calculations (the backbone particle of glycine 1). Tilt values were calculated from fitting a Gaussian distribution to the TM region of the graph.

4.9 Figures

Figure 1. Model structures of (A) GWALP23-R14 and (B) GWALP23-R12. In each case the atomistic side-chain model is shown on a ribbon helix above and the CG model below, with arginine (blue) and tryptophan (green) side chains. Note that the side chain of R14 is on the opposite side of the helix (A) from the tryptophan side chains, whilst the side chain of R12 is on the same side of the helix (B).

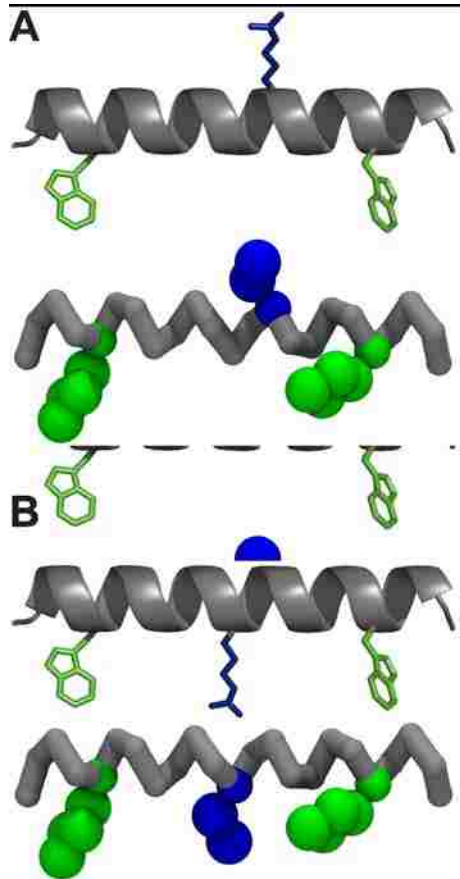


Figure 2. Deuterium NMR spectra of (A) GWALP23-R14 and (B) GWALP23-R12 in hydrated, oriented bilayers of DOPC (peptide/lipid ratio 1/60; $\beta=0^\circ$ sample orientation; temperature 50 °C). The ^2H -labeled alanine residues are (top to bottom): 7 and 9; 11 and 13; 15 and 17.

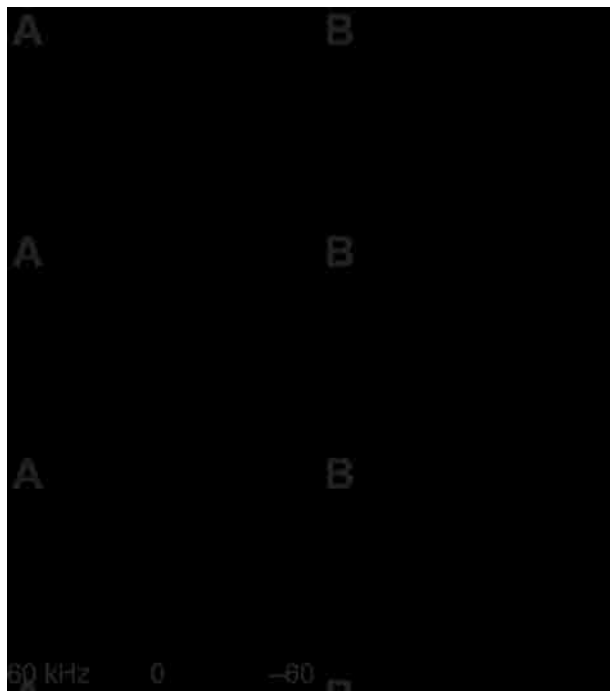


Figure 3. Selected deuterium NMR spectra for two labeled alanines (7 and 9) in GWALP23-R12 (A, B) and GWALP23-R14 (C, D) in DOPC bilayers, hydrated with water, or with buffer at pH 7.4 or pH 4.5 (top to bottom), showing $\beta = 90^\circ$ (A, C) and $\beta = 0^\circ$ (B, D) sample orientations. Samples at pH 7.4 also contain 0.1 M NaCl. The peptide/lipid ratio is 1/60 at a temperature of 50 °C.



Figure 4. GALA analysis of GWALP23-R14 average tilt in DOPC bilayer membranes, with variable S_{zz} and $\epsilon_{//} = 59.4^\circ$. (A) Quadrupolar wave plot with Ala positions indicated. (B) RMSD plot (contoured at 1, 2 and 3 kHz) for tilt τ and rotation ρ of peptides in DOPC: GWALP23 itself (gray); GWALP23-R14 (black). The global minima correspond to (S_{zz}, τ, ρ) of $(0.86, 5.9^\circ, 323^\circ)$ and $(0.94, 16.2^\circ, 247^\circ)$ respectively.

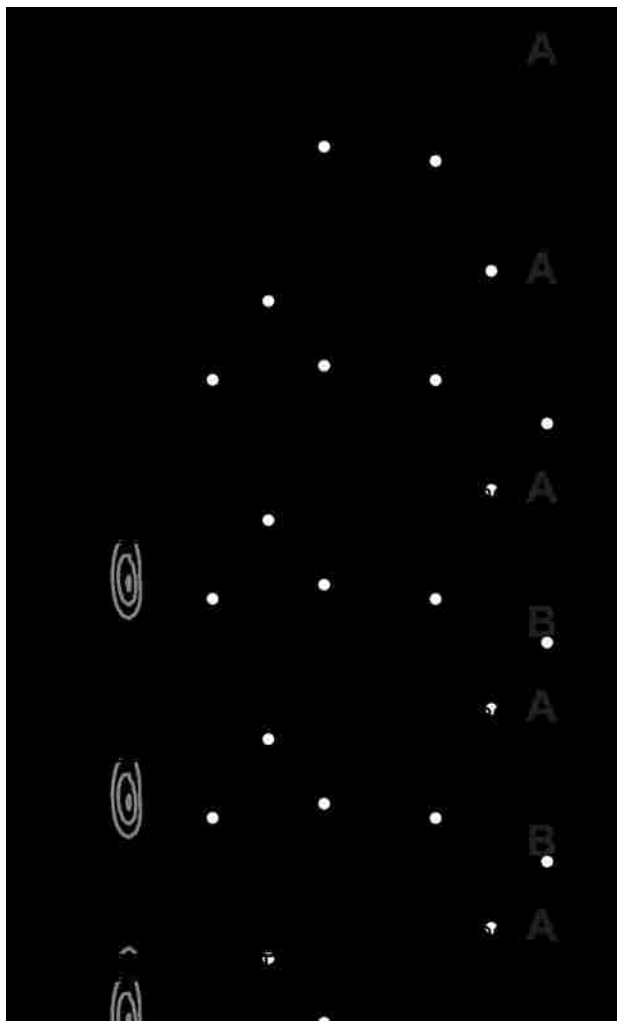


Figure 5. Progress of CG simulation for GWALP23 in a DPPC bilayer. (A) Initial state ($t = 0$ ns) of the simulation system consisting of a GWALP23 α -helix (gray backbone, green Trp side chains) with randomly orientated phospholipids (purple spheres = phosphate particles) and waters (not shown). (B) Final state ($t = 100$ ns) of the system showing the GWALP helix tilted in a TM orientation with the Trp side chains close to the lipid headgroups.

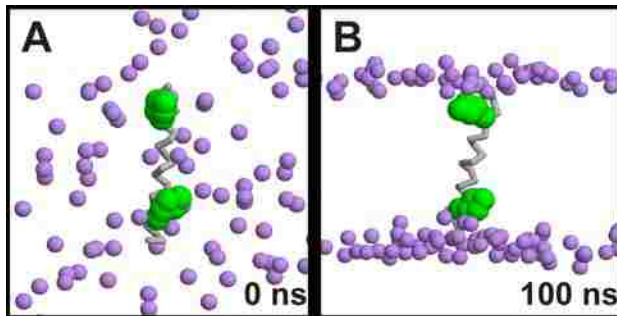


Figure 6. Helix displacement relative to the DPPC bilayer center, tilt relative to the bilayer normal and rotation relative to that of GWALP23 in DPPC. Each curve is derived from analysis of an ensemble of 100×100 ns of CG simulations (analyzing the complete 100 ns simulations in each case). (A) Helix displacement, defined as the difference between the center of mass of the helix backbone and the center of the lipid bilayer. A displacement >10 Å is indicative of an interfacial (INT) orientation. Small negative displacements indicate moving a TM helix towards the C terminal facing leaflet; small positive displacements indicate moving a TM helix towards the N terminal facing leaflet. (B) Helix tilt, defined as the angle between the helix axis and the bilayer normal. A tilt of 90° is indicative of an interfacial location. (C) Helix rotation, referenced to 0° as the tilt direction of GWALP23.

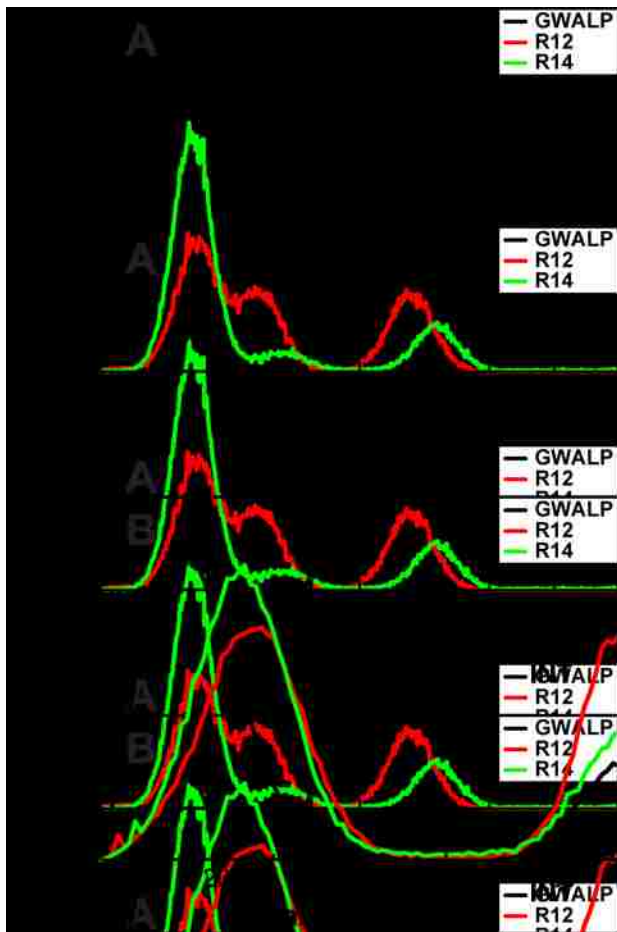


Figure 7. Three orientations of the GWALP-R12 helix seen in CG simulations. The helix may adopt a TM orientation with the R12 side chain (blue) snorkeling towards either the N-terminal (A) or the C-terminal (B) face of the membrane. Alternatively, an interfacial orientation may be adopted (panel C). Trp side chains are green, Arg blue, and the bilayer surface (as defined by the phosphate particles) is a grey mesh.

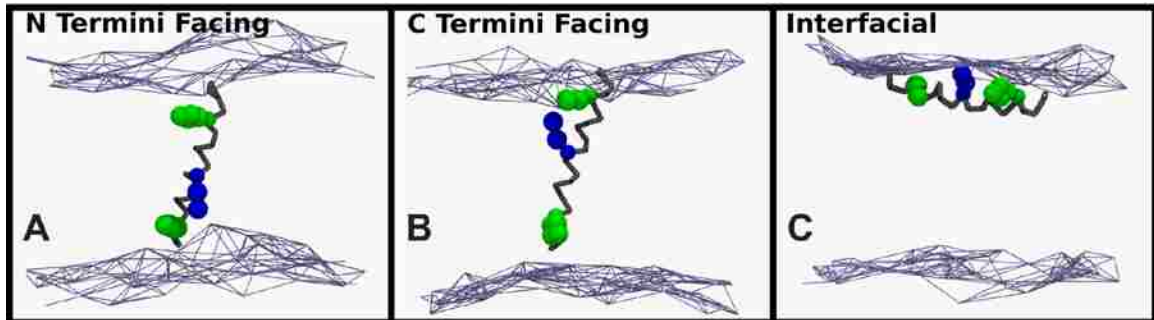


Figure 8. Helix displacement and tilt in DOPC. Each curve is derived from analysis of an ensemble of 100×100 ns of CG simulations. (A) Helix displacement. (B) Helix tilt. (C) Helix rotation. The definition of terms is the same as in Figure 6.

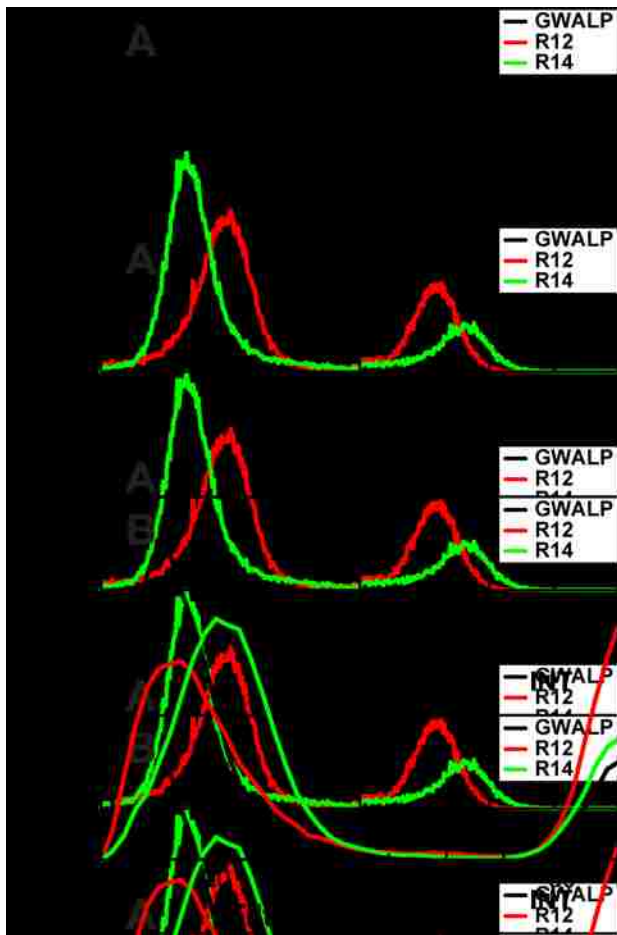


Figure 9. Snapshots taken from atomistic simulations of (A) GWALP23 and (B) GWALP23-R12. Water and phosphate groups are in spacefill representations (red/white, and brown), the peptide backbone is shown with tryptophan and arginine residue side chains in stick representation. Bilayer deformation and water penetration can be clearly seen in the GWALP23-R12 simulation but not in the GWALP23 simulation, reflecting the effect of incorporating a charged arginine residue in the bilayer core.

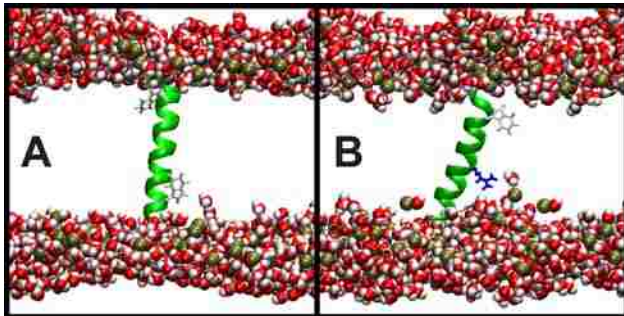
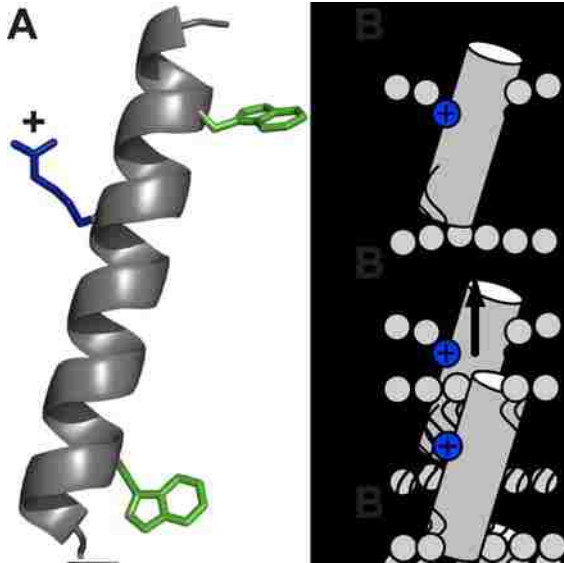


Figure 10. (A) Model to illustrate the orientation of GWALP23-R14 tilted at $\sim 17^\circ$ with respect to the bilayer normal of DOPC. Side chains were constructed using a rotamer library and do not represent experimental data. (B) Schematic “cork” model for vertical displacement of GWALP23-R14 toward its C-terminal in a lipid bilayer membrane, as observed in the CG-MD simulations. Together the displacement and snorkeling, along with membrane thinning, allow the charged guanidinium side chain to reach the bilayer-water interface.



4.10 Supporting Information

Figure S1. Circular dichroism spectra for GWALP23 (A), GWALP23-R12 (B) and GWALP23-R14 (C) in DOPC. Note that the far-UV (<203 nm) region is not accessible due to strong absorption by the DOPC double bond.



Figure S2. Selected deuterium NMR spectra ($\beta = 0^\circ$ sample orientation) for singly labeled alanines in GWALP23-R12 in DOPC. Isotope labels were introduced in position 7 (top) or 15 (bottom). Note that even a single alanine gives rise to multiple pairs of peaks in each spectrum.



Figure S3. Natural abundance ^2H NMR spectrum of DOPC, $\beta=90^\circ$ orientation.



Figure S4. Tilt-rotation RMSD contour plots for GWALP23 (A) and GWALP23-R14 (B) in DOPC, fit with different values for the principal order parameter S_{zz} : 0.7 (red), 0.8 (green), 0.88 (blue). The contour lines are plotted at RMSD of 3 kHz. The value of $\varepsilon_{//}$ for the alanine side chains was fixed at 59.4° .

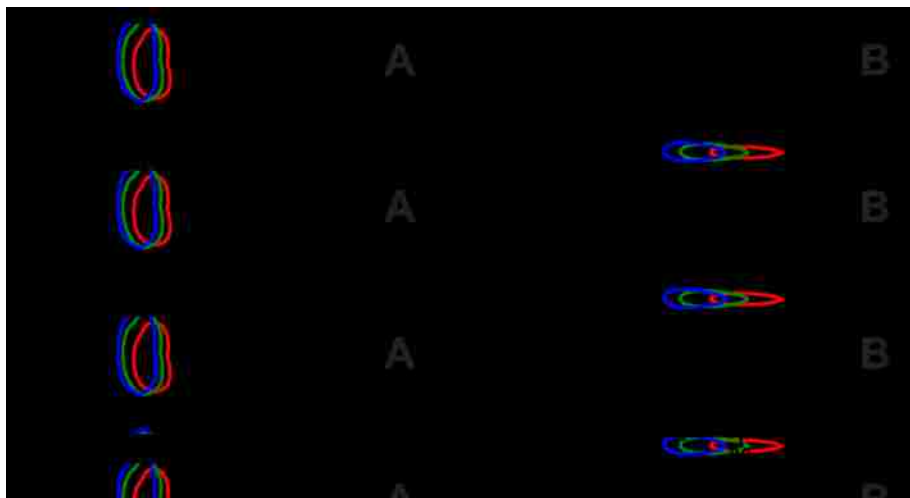


Figure S5. Tilt-rotation contour plots for GWALP23 (A) and GWALP23-R14 (B) from CG simulations in DPPC.

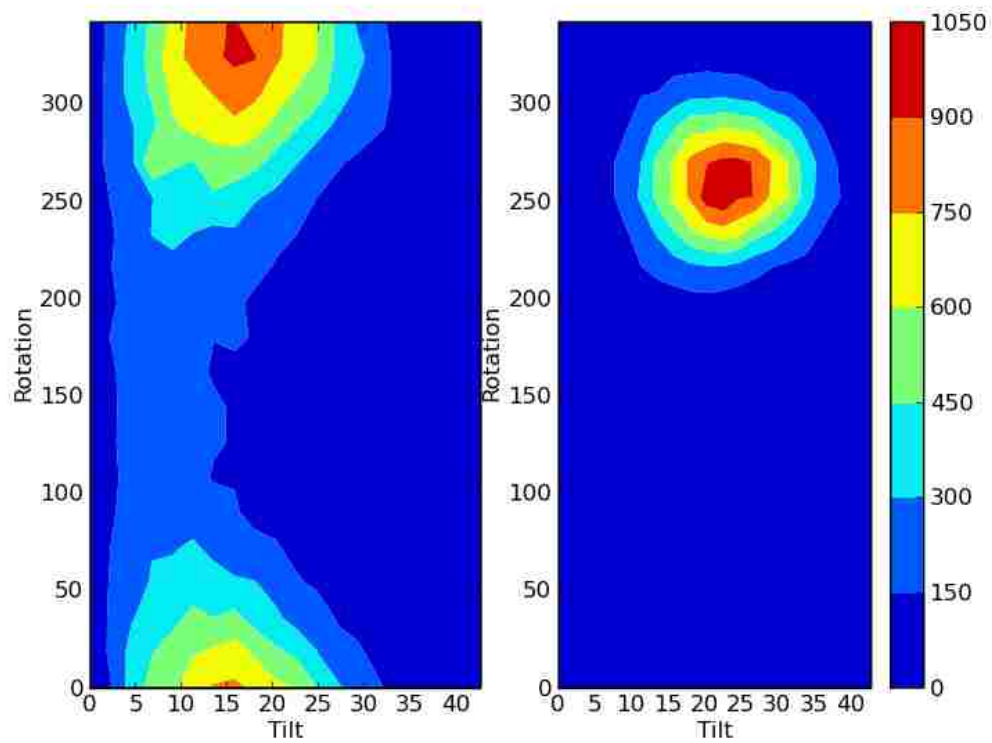


Figure S6. Physical data for GWALP23-R12, including HPLC chromatogram (A) and mass spectrum (B). Predicted monoisotopic mass of the non-deuterated peptide is 2302.4 a.m.u. The isotopic distribution pattern is seen for the $[MH^+ + 4D]$ and $[MH^+ + 8D]$ peptides.



4.11 Copyright Clearance Form

AMERICAN CHEMICAL SOCIETY LICENSE TERMS AND CONDITIONS

Mar 17, 2011

This is a License Agreement between Vitaly V Vostrikov ("You") and American Chemical Society ("American Chemical Society") provided by Copyright Clearance Center ("CCC"). The license consists of your order details, the terms and conditions provided by American Chemical Society, and the payment terms and conditions.

All payments must be made in full to CCC. For payment instructions, please see information listed at the bottom of this form.

License Number: 2630881403707

License Date: Mar 16, 2011

Licensed content publisher: American Chemical Society

Licensed content publication: Journal of the American Chemical Society

Licensed content title: Changes in Transmembrane Helix Alignment by Arginine Residues Revealed by Solid-State NMR Experiments and Coarse-Grained MD Simulations

Licensed content author: Vitaly V. Vostrikov et al.

Licensed content date: Apr 1, 2010

Volume number: 132

Issue number: 16

Type of Use: Thesis/Dissertation

Requestor type: Not specified

Format: Print

Portion: Full article

Author of this ACS article: Yes

Order reference number

Title of the thesis / dissertation: Protein-Lipid Interactions: Influence of Anchoring Groups and Buried Arginine on the Properties of Membrane-Spanning Peptides

Expected completion date: May 2011

Estimated size(pages): 150

Billing Type: Invoice

Billing Address: University of Arkansas, CHEM-201, Fayetteville, AR 72701, United States

Customer reference info

Total: 0.00 USD

Terms and Conditions

Thesis/Dissertation

ACS / RIGHTSLINK TERMS & CONDITIONS THESIS/DISSERTATION

INTRODUCTION

The publisher for this copyrighted material is the American Chemical Society. By clicking "accept" in connection with completing this licensing transaction, you agree that the following terms and conditions apply to this transaction (along with the Billing and Payment terms and conditions established by Copyright Clearance Center, Inc. ("CCC"), at the time that you opened your Rightslink account and that are available at any time at <<http://myaccount.copyright.com>>).

LIMITED LICENSE

Publisher hereby grants to you a non-exclusive license to use this material. Licenses are for one-time use only with a maximum distribution equal to the number that you identified in the licensing process.

GEOGRAPHIC RIGHTS: SCOPE

Licenses may be exercised anywhere in the world.

RESERVATION OF RIGHTS

Publisher reserves all rights not specifically granted in the combination of (i) the license details provided by you and accepted in the course of this licensing transaction, (ii) these terms and conditions and (iii) CCC's Billing and Payment terms and conditions.

PORTION RIGHTS STATEMENT: DISCLAIMER

If you seek to reuse a portion from an ACS publication, it is your responsibility to examine each portion as published to determine whether a credit to, or copyright notice of, a third party owner was published adjacent to the item. You may only obtain permission via Rightslink to use material owned by ACS. Permission to use any material published in an ACS publication, journal, or article which is reprinted with permission of a third party must be obtained from the third party owner. ACS disclaims any responsibility for any use you make of items owned by third parties without their permission.

REVOCATION

The American Chemical Society reserves the right to revoke a license for any reason, including but not limited to advertising and promotional uses of ACS content, third party usage, and incorrect figure source attribution.

LICENSE CONTINGENT ON PAYMENT

While you may exercise the rights licensed immediately upon issuance of the license at the end of the licensing process for the transaction, provided that you have disclosed complete and accurate details of your proposed use, no license is finally effective unless

and until full payment is received from you (by CCC) as provided in CCC's Billing and Payment terms and conditions. If full payment is not received on a timely basis, then any license preliminarily granted shall be deemed automatically revoked and shall be void as if never granted. Further, in the event that you breach any of these terms and conditions or any of CCC's Billing and Payment terms and conditions, the license is automatically revoked and shall be void as if never granted. Use of materials as described in a revoked license, as well as any use of the materials beyond the scope of an unrevoked license, may constitute copyright infringement and publisher reserves the right to take any and all action to protect its copyright in the materials.

COPYRIGHT NOTICE: DISCLAIMER

You must include the following copyright and permission notice in connection with any reproduction of the licensed material: "Reprinted ("Adapted" or "in part") with permission from REFERENCE CITATION. Copyright YEAR American Chemical Society."

WARRANTIES: NONE

Publisher makes no representations or warranties with respect to the licensed material.

INDEMNITY

You hereby indemnify and agree to hold harmless publisher and CCC, and their respective officers, directors, employees and agents, from and against any and all claims arising out of your use of the licensed material other than as specifically authorized pursuant to this license.

NO TRANSFER OF LICENSE

This license is personal to you or your publisher and may not be sublicensed, assigned, or transferred by you to any other person without publisher's written permission.

NO AMENDMENT EXCEPT IN WRITING

This license may not be amended except in a writing signed by both parties (or, in the case of publisher, by CCC on publisher's behalf).

OBJECTION TO CONTRARY TERMS

Publisher hereby objects to any terms contained in any purchase order, acknowledgment, check endorsement or other writing prepared by you, which terms are inconsistent with these terms and conditions or CCC's Billing and Payment terms and conditions. These terms and conditions, together with CCC's Billing and Payment terms and conditions (which are incorporated herein), comprise the entire agreement between you and publisher (and CCC) concerning this licensing transaction. In the event of any conflict between your obligations established by these terms and conditions and those established by CCC's Billing and Payment terms and conditions, these terms and conditions shall control.

JURISDICTION

This license transaction shall be governed by and construed in accordance with the laws of the District of Columbia. You hereby agree to submit to the jurisdiction of the courts located in the District of Columbia for purposes of resolving any disputes that may arise in connection with this licensing transaction.

THESES/DISSERTATION TERMS

Regarding your request for permission to include **your** paper(s) or portions of text from **your** paper(s) in your thesis/dissertation, permission is now automatically granted; please pay special attention to the **implications** paragraph below. The Copyright Subcommittee of the Joint Board/Council Committees on Publications approved the following:

Copyright permission for published and submitted material from theses and dissertations ACS extends blanket permission to students to include in their theses and dissertations their own articles, or portions thereof, that have been published in ACS journals or submitted to ACS journals for publication, provided that the ACS copyright credit line is noted on the appropriate page(s).

Publishing implications of electronic publication of theses and dissertation material

Students and their mentors should be aware that posting of theses and dissertation material on the Web prior to submission of material from that thesis or dissertation to an ACS journal may affect publication in that journal. Whether Web posting is considered prior publication may be evaluated on a case-by-case basis by the journal's editor. If an ACS journal editor considers Web posting to be "prior publication", the paper will not be accepted for publication in that journal. If you intend to submit your unpublished paper to ACS for publication, check with the appropriate editor prior to posting your manuscript electronically.

Reuse/Republication of the Entire Work in Theses or Collections: Authors may reuse all or part of the Submitted, Accepted or Published Work in a thesis or dissertation that the author writes and is required to submit to satisfy the criteria of degree-granting institutions. Such reuse is permitted subject to the ACS' "Ethical Guidelines to Publication of Chemical Research"

(<http://pubs.acs.org/page/policy/ethics/index.html>); the author should secure written confirmation (via letter or email) from the respective ACS journal editor(s) to avoid potential conflicts with journal prior publication*/embargo policies. Appropriate citation of the Published Work must be made. If the thesis or dissertation to be published is in electronic format, a direct link to the Published Work must also be included using the ACS Articles on Request author-directed link - see <http://pubs.acs.org/page/policy/articlesonrequest/index.html>

* Prior publication policies of ACS journals are posted on the ACS website at <http://pubs.acs.org/page/policy/prior/index.html>

If your paper has not yet been published by ACS, please print the following credit line on the first page of your article: "Reproduced (or 'Reproduced in part') with permission from [JOURNAL NAME], in press (or 'submitted for publication'). Unpublished work copyright [CURRENT YEAR] American Chemical Society." Include appropriate information.

If your paper has already been published by ACS and you want to include the text or portions of the text in your thesis/dissertation in **print or microfilm formats**, please print the ACS copyright credit line on the first page of your article: "Reproduced (or 'Reproduced in part') with permission from [FULL REFERENCE CITATION.] Copyright [YEAR] American Chemical Society." Include appropriate information.

Submission to a Dissertation Distributor: If you plan to submit your thesis to UMI or to another dissertation distributor, you should not include the unpublished ACS paper in your thesis if the thesis will be disseminated electronically, until ACS has published your paper. After publication of the paper by ACS, you may release the entire thesis (not the individual ACS article by itself) for electronic dissemination through the distributor; ACS's copyright credit line should be printed on the first page of the ACS paper.

Gratis licenses (referencing \$0 in the Total field) are free. Please retain this printable license for your reference. No payment is required.

If you would like to pay for this license now, please remit this license along with your payment made payable to "COPYRIGHT CLEARANCE CENTER" otherwise you will be invoiced within 48 hours of the license date. Payment should be in the form of a check or money order referencing your account number and this invoice number RLNK10950178.

Once you receive your invoice for this order, you may pay your invoice by credit card. Please follow instructions provided at that time.

**Make Payment To:
Copyright Clearance Center
Dept 001
P.O. Box 843006
Boston, MA 02284-3006**

For suggestions or comments regarding this order, contact Rightslink Customer Support: customercare@copyright.com or +1-877-622-5543 (toll free in the US) or +1-978-646-2777.

CHAPTER 5

“Rescue” of a Central Arginine in a Transmembrane Peptide by Changing the Placement of Anchor Residues

5.1 Abstract

Both Trp and Arg in transmembrane protein domains make important interactions with lipids at the membrane/water interface, but at different depths. Derivatives of the designed peptide GWALP23, acetyl-GGALW⁵LALALALALALW¹⁹LAGA-amide, with single Trp anchors, have proven to be useful for characterizing such interactions. Indeed previous work has revealed quite different effects emanating from Arg substitutions at positions 12 and 14 within GWALP23, with the R12 peptide exhibiting multiple positions and orientations with respect to DOPC bilayer membranes. To seek further understanding of the multi-state behavior, we have moved the Trp “anchor” residues to more outer positions 3 and 21 in GWALP23 itself, and in the R12 and R14 derivatives. Selected alanines were deuterated during chemical synthesis of these peptides. The locations and orientations of the peptides with respect to lipid bilayer membranes of differing thickness were then investigated by means of solid-state ²H NMR spectroscopy and coarse-grained molecular dynamics simulations. Interestingly, in these experiments, we were able to use ²H quadrupolar splittings not only from the Ala side chains but also from selected backbone C_α deuterons. With the Trp anchors now relatively far from the peptide and bilayer center, the results indicate significantly large apparent tilt angles, for example close to 30° for the new R12 and R14 peptides with respect to the bilayer normal of DLPC membranes. The R12 side chain indeed is “rescued” to a stable position when the Trp anchors are moved farther out and to another

face of the helix. At the same time, the R14 side chain of GW^{3,21}ALP23 also retains a stable favored position.

5.2 Introduction

Ionizable amino acid residues usually are poorly tolerated in non-polar surroundings, whether the hydrophobic core of a protein or the acyl-chain interior of a lipid bilayer. In cases where charged residues are present in such environments, the residues often are highly conserved and essential for protein function. The “buried” charged side chains also may be stabilized by formidable networks of protein-protein interactions (Bartlett et al., 2002; Doyle et al., 1998). In other cases the presence of polar or charged residues in unfavorable, hydrophobic regions can have detrimental consequences for protein stability and/or function (Loladze et al., 2001; Sine et al., 2002). Furthermore, many of the permissible mutations which place an ionizable residue in the hydrophobic core of a protein are accompanied by pK_a shifts which render side chain non-charged (Karp et al., 2010; Takayama et al., 2008). In similar fashion, burying a polar amino acid in the hydrophobic interior of a lipid bilayer is a challenging task. Selected examples do exist, such as for example the voltage-sensing S4 domains that regulate selected cation channels by means of multiple Arg residues; yet their accommodation in the membrane could involve extensive charge compensation (Swartz, 2008).

Numerous investigations have addressed the question: How difficult is it to incorporate an uncompensated charged residue in a lipid bilayer membrane? While an ultimate goal is discovery of principles or “rules” that govern the behavior of transmembrane proteins, many intermediate goals call for the testing of specific hypotheses. For example, a

profound effect of the charge state on the membrane insertion has been demonstrated for the case of an isolated α -helix with four histidine residues. At high pH a model peptide was capable of spanning the membrane, but His protonation under acid conditions caused an alteration of peptide topography and resulted in its exclusion from the lipid bilayer (Aisenbrey et al., 2006; Bechinger, 1996). Such pH-dependent behavior is manifest both for acidic and basic ionizable residues, for example by a sequence derived from bacteriorhodopsin, termed pH low insertion peptide (pHLip). Such peptides contain aspartic acid residues within a hydrophobic stretch which, when protonated at low pH, allow the peptides to incorporate into lipid bilayer membranes (Andreev et al., 2007; Hunt et al., 1997).

Another important factor will be the sequence position of a charged residue. A comprehensive study of translocon-mediated insertion of α -helices coupled with a glycosylation assay produced Gaussian-shaped free energy profiles for the charged residues, with maxima close to the bilayer center (Hessa et al., 2007). Hydrophilic amino acids with flexible side chains nevertheless are capable of “snorkeling” toward the more polar membrane-water interfaces, thus allowing such residues to “bridge” nonpolar and polar environments. Additionally, an entire peptide or domain may be “lifted” toward the interface of one leaflet to satisfy some of the polarity preferences (Krishnakumar and London, 2007; Vostrikov et al.).

Previously, we examined a single arginine incorporated near the center of GWALP23 (GGALW⁵[LA]₆LW¹⁹LAGA) – a designed transmembrane peptide, derived from the “WALP” sequences (Killian et al., 1996; Vostrikov et al., 2008), but importantly having

only one Trp residue flanking each end of a hydrophobic [LA]_{6.5} core helix. Two peptides having identical amino acid composition and a single Arg at either position 12 or position 14 within GWALP23 (Table 1) displayed markedly different behavior. While GWALP23-R14 adopted a transmembrane orientation, the R12 sequence isomer populated both transmembrane and interfacial states in DOPC (Vostrikov et al., 2010b). The position of Arg, relative to the two tryptophans, is different on a helical wheel projection of these peptides (Figure 1A), such that R12 is between the Trp indole rings, while R14 is on a different face of the projection. Several factors could contribute to the variable membrane topography of GWALP23-R12. The proximity of R12 to the bilayer center is likely to impose an energetic penalty for membrane insertion, and it also is plausible that the positions of the Trp side chains could play a significant role, for example by blocking water access to the R12 guanidinium group (Vostrikov et al., 2010b).

To better understand the control of the topography of membrane-associated peptides, and to gain additional insights concerning Arg, Trp and lipid bilayer interactions, we have tested the influence of changing the GWALP23 Trp residue locations, both with and without R14 or R12 being present. By moving each of the anchoring Trp residues a distance corresponding to one Leu-Ala dipeptide segment toward the respective peptide terminals, an isomer of GWALP23 with an effectively longer hydrophobic helical core was constructed, namely GGW³(LA)₈LW²¹GA, designated GW^{3,21}ALP23 (Table 1). The rationale for the sequence modification can be seen in the idealized helical wheel projection of the sequence (Figure 1B). Switching Trp⁵ to position 3 alters its radial

projection by -200° , while moving Trp¹⁹ to position 21 alters its radial projection by $+200^\circ$. As a result, the two Trp residues in GW^{3,21}ALP23 again project from one side of the helix (in similar fashion to GW^{5,19}ALP23)—but now the tryptophans are located on the helix face close to R14 instead of R12 (compare Figure 1A and 1B). Substitutions of L12→R12 or L14→R14 in this new sequence context reverse the respective Arg positions relative to the Trp residues. Residue 12, which was between the two Trp rings in GW^{5,19}ALP23 (Vostrikov et al.), is no longer “sandwiched” in the modified sequence. In contrast, residue 14, which was far from Trp⁵ and Trp¹⁹, now becomes placed radially near Trp³ and Trp²¹.

It is of further interest to note that the Trp-Arg separation distances are 7 residues between R12 and either W5 or W19, as well as between R14 and W21. Residue R12 retains the truly central location, both in terms of the overall sequence and its position relative to the two tryptophans within each sequence. Consequently, the new and expanded peptide design will enable incisive investigations into the root causes of the multistate behavior. Together these new sequences will provide significant insights into the adaptation of peptide orientation with respect to lipid bilayer membranes.

5.3 Materials and Methods

Lipids were purchased from Avanti Polar Lipids (Alabaster, AL). Peptides were synthesized on a model 433A peptide synthesizer (Applied Biosystems by Life Technologies, Foster City, CA) and cleaved from Rink resin as described previously (Vostrikov et al.). Protected amino acids were obtained from NovaBiochem (San Diego, CA). Deuterium-enriched alanines (Ala-d₄ or Fmoc-Ala-d₃) were purchased from

Cambridge Isotope Laboratories (Andover, MA). The Ala-d₄ was manually derivatized with an Fmoc group as reported earlier (ten Kortenaar et al., 1986). Typically, two ²H-labeled alanines were incorporated per peptide at a different isotope abundance levels. If necessary to resolve ambiguities among spectral assignments, selected peptides were prepared with only one Ala-d₄ label. Peptides were purified on an octyl silica column (Zorbax Rx-C8, 9.4 × 250 mm, 5 μm particle size; Agilent Technologies, Santa Clara, CA) in a 92-96% methanol gradient (with 0.1% trifluoroacetic acid) over 24 min, with detection based on absorbance at 280 nm. Analytical HPLC and mass spectral data are shown in Figures S1 and S2 of the Supporting Information.

Samples (1/60, peptide/lipid ratio) for solid-state NMR spectroscopy were prepared by mechanical alignment utilizing previously reported procedures (van der Wel et al., 2002). The peptide/lipid mixture was deposited on glass slides (Marienfeld; Lauda-Königshofen, Germany) from methanol:water (95:5), dried extensively and hydrated with ²H-depleted water (Cambridge) to achieve 45% hydration (w/w). Deuterium NMR spectra were obtained with a quadrupolar echo pulse sequence (Davis et al., 1976) at β=0° and β=90° macroscopic sample orientations using two Bruker Avance 300 spectrometers (Billerica, MA) operated at 46.1 MHz, for detection of ²H resonances. The pulse time was 3.2 μs or 4.5 μs; echo delay was 110 μs or 125 μs; and the recycle delay was 90 ms. Typically 700,000 transients were acquired, with the exception that 1,500,000 transients were acquired for GW^{3,21}ALP23-R12 in DMPC and DOPC. Data were collected in a 32,768 point time domain, zero filled to 5,120 points and left shifted to the echo maximum. Fourier transformation was accomplished using exponential apodization with 100 Hz line

broadening. Resonances were assigned based upon the relative peak intensities in relation to the respective isotope enrichment levels used for different alanines in the sequence. Difference spectra between double- and single-labeled peptides were sometimes employed to complete the assignments (see Figure S3 of the Supporting Information).

Deuterium NMR spectra were analyzed according to the “GALA” formalism, using the peptide rotation ρ , tilt τ and principal order parameter S_{zz} as variables (Strandberg et al., 2009; van der Wel et al., 2002). Angle $\varepsilon_{//}$, defining the Ala side chain geometry in the α -helix (van der Wel et al.), was fixed at 59.4° . The quadrupolar coupling constant (QCC) was set to 168 kHz (backbone $C_\alpha D$ signals) or 56 kHz (side chain $C_\beta D_3$ signals). Dynamics were estimated using a variable S_{zz} parameter (Strandberg et al.), which provides a suitable treatment for GWALP23 and many membrane-associated peptides (Vostrikov et al.), particularly when a single arginine is present (Vostrikov et al.). Due to variations in the preferred order parameter to fit backbone as opposed to side chain signals (see Results), a two-step procedure was implemented: (i) S_{zz} , τ and ρ were first varied to fit $C_\beta D_3$ data; (ii) τ and ρ were then fixed to the best-fit values for the side chains, and a separate backbone S_{zz} was varied to fit $C_\alpha D$ data.

In the case of $GW^{3,21}ALP23-R12$ in DLPC lipid bilayers, a more explicit treatment of dynamics, based upon “Model 6” of Strandberg *et al.* (Strandberg et al., 2009), was considered. In this case, rigid body motion of the peptide is modeled as Gaussian distributions of the τ and ρ angles, centered at the average values τ_0 and ρ_0 with standard deviations of σ_τ and σ_ρ respectively. A fixed order parameter S_{zz} value of 0.88 was used

to account for the internal motion (the resulting product $QCC \times S_{zz}$ therefore being fixed to 49.3 kHz). A grid search was performed by varying σ_τ in the 0-30° range, σ_ρ in the 0-200° range, τ_0 from 0° to 90° and ρ_0 from 0° to 359°. Due to a larger solution field, τ_0 , ρ_0 , σ_τ and σ_ρ were incremented at 1° intervals during the grid search.

Samples for CD spectroscopy were prepared using small unilamellar vesicles (1/60, peptide/lipid) obtained by ultrasonic treatment. The peptide concentrations were in the 100 μ M range and were determined by UV spectroscopy, using $\epsilon_{280}=5600 \text{ M}^{-1}\text{cm}^{-1}\text{Trp}^{-1}$. Five scans were acquired and averaged, utilizing a Jasco J710 spectropolarimeter (Easton, MD) using 1.0 mm path length, 1.0 nm band width and 20 nm/min scan rate.

Steady state fluorescence spectra were recorded on a Perkin Elmer LS-55 fluorescence spectrometer. Samples were prepared by 50-fold dilution of the samples that were used for CD spectroscopy. The excitation wavelength was set to 284 nm, and the emission range was 300-500 nm. Excitation and emission pathlengths were 10 mm and 1 mm, respectively (Ladokhin et al., 2000); slit widths were 7.5 nm. Ten scans were acquired at 200 nm/min and averaged.

Coarse-grained molecular dynamics simulations (CG MD) were performed using the Sidekick high throughput software (Vostrikov et al., 2010a). Coarse grained simulations are run with the MARTINI forcefield (Monticelli et al., 2008). In this representation, a 4:1 mapping of non hydrogen atoms to CG particles is used, with Lennard Jones interactions between particles based on 4 classes (polar, apolar, mixed polar and apolar, and charged, with subtypes describing polarity and hydrogen bonding capabilities) and a

lookup table. Lennard Jones interactions shifted to zero between 9 and 12 Å and electrostatic interactions were shifted to zero between 0 and 12 Å. Simulations were performed with Gromacs 3.3 (www.gromacs.org). Temperature was coupled using a Berendsen thermostat at 323 K ($\tau_T = 1$ ps), and pressure was coupled anisotropically at 1 bar (compressibility = 3×10^{-5} bar⁻¹, $\tau_P = 10$ ps). 100×200 ns were performed for each peptide.

5.4 Results

To investigate changes in peptide/lipid interactions caused by shifting the positions of the Trp “anchor” residues in the GW^{5,19}ALP23 framework, we have employed solid-state NMR spectroscopy using peptides specifically labeled with ²H-alanine residues. Due to the fast rotational averaging of methyl deuterons in the alanine side chain, the primary axis of the quadrupolar interaction is directed along the C_α-C_β bond, which can be further related to the orientation of the peptide itself (Strandberg et al., 2004; van der Wel et al., 2002). The technique known as “GALA” (Geometric Analysis of Labeled Alanines) provides a way of deducing an apparent magnitude (τ) and direction (ρ) of the peptide tilt with respect to the lipid bilayer normal, as well as a measure of dynamic behavior in the form of a principal order parameter (S_{zz}), which does not assume a particular motion model, or more detailed molecular motions (Strandberg et al.).

Here we employ the previously introduced approach of labeling two sequential Ala residues (separated by one leucine, or about 200° around a helical wheel projection) at different isotope abundance levels, which gives rise to two pairs of signals that usually

are distinguishable and often can be assigned based upon their relative intensities. Compared to the original GW^{5,19}ALP23 sequence, GW^{3,21}ALP23 has an extended central core region, which provides two additional alanine residues for labeling and analysis (Figure 1). To verify that the peptides retain their α -helical character upon the arginine incorporation, CD spectra were recorded (Figure S4 of the Supporting Information). In similar manner to GW^{5,19}ALP23, GW^{3,21}ALP23 and also its derivatives incorporating single arginines remained substantially helical. Each Leu-to-Arg substitution leads to a small increase of the $\epsilon_{222}/\epsilon_{208}$ ratio from ~ 0.80 to ~ 0.84 , while the overall mean residue ellipticity is either the same (R14) or somewhat diminished (R12).

To further enhance understanding of the complex balance among the peptide tilt, displacement and arginine position, we have investigated the properties of the R12 and R14 peptides in lipids of varied hydrophobic length, namely bilayers composed of DLPC, DMPC and DOPC lipids. Remarkably, both of the GW^{3,21}ALP23-Arg peptides in all three lipids exhibit strong unique pairs of ^2H resonances for each of the A17 and A19 side chains (Figure 2), characteristic of one conformation and one dominant average orientation of the peptide. Indeed the results for GW^{3,21}ALP23-R12 contrast sharply with those for GW^{5,19}ALP23-R12, which produced multiple low intensity signals in DOPC (Vostrikov et al.). A similarity with other GWALP peptides is that the spectra in Figure 2 also are consistent with fast rotational averaging around the bilayer normal (peptide “precession”), as can be seen by the two-fold reduction in the ^2H $\Delta\nu_q$ value for each alanine side chain when the macroscopic sample orientation is changed from $\beta=0^\circ$ to

$\beta=90^\circ$ (Figure 2). Such averaging is usually observed for monomeric transmembrane peptides and is possible also for some interfacial orientations (see (Vostrikov et al.)).

Also evident in Figure 2D is one additional pair of ^2H resonances for $\text{GW}^{3,21}\text{ALP23-R14}$ in DLPC and DMPC. These resonances, which have a large $|\Delta\nu_q|$ magnitude and likely arise from a backbone C_\square deuteron, were later assigned to A17 (see below). These particular $\text{C}_\square\text{-D}$ resonances are much less intense in DOPC or when the sample orientation is $\beta=90^\circ$ (Figure 2); we do not yet understand the reasons for the dependence upon lipid identity and macroscopic alignment with respect to H_0 . While the three-site jump motion of Ala side-chain methyl group deuterons results in a three-fold reduction of the effective QCC, such averaging is absent for the aliphatic $\text{C}_\alpha\text{-D}$ groups, making possible a wider range of $\Delta\nu_q$ values. In the case of a low mobility peptide (having $S_{zz} \sim 0.9$, for example), the backbone signals therefore could span a range of ~ 220 kHz, compared to only ~ 75 kHz for the methyl group signals. The larger $\Delta\nu_q$ span and the absence of local bond rotational averaging are also associated with increased line broadening and decreased intensity of the backbone signals (see also (Killian et al.)). To verify that the “new” resonances with large $|\Delta\nu_q|$ values indeed arise from backbone deuterons, we synthesized $\text{GW}^{3,21}\text{ALP23-R12}$ with either Ala- d_3 or Ala- d_4 present in residues A13 and A15 (Ala- d_3 labels only C_β and not C_α). Deuterium NMR spectra of these peptides (Figure 3) show that the signals having $|\Delta\nu_q|$ of 110 kHz are present only with Ala- d_4 and not with Ala- d_3 labeling. The signals which are absent for the case of Ala- d_3 labeling therefore indeed arise from a C_α -deuteron.

The ^2H quadrupolar splitting magnitudes were measured for the side-chain methyl groups of all eight core alanine residues in $\text{GW}^{3,21}\text{ALP23-R12}$ and $\text{GW}^{3,21}\text{ALP23-R14}$; each in DLPC, DMPC and DOPC bilayer membranes. The corresponding NMR spectra are included as Supplementary Material (Figures S5-S7). Many of the alanines also produced readily detectable backbone C_α deuterium signals (Figures S5-S7). The measured ^2H quadrupolar splitting magnitudes for Ala C_βD_3 and C_αD groups in $\text{GW}^{3,21}\text{ALP23-R12}$ and $\text{GW}^{3,21}\text{ALP23-R14}$ in each lipid bilayer system are summarized in Table 2. Previously (Vostrikov et al.), we reported the ^2H NMR data for labeled alanines in $\text{GW}^{5,19}\text{ALP23-R14}$ in DOPC; now in Table 2 we include also the measured $\Delta\nu_q$ values in DLPC and DMPC. Data for $\text{GW}^{5,19}\text{ALP23-R12}$ are not included in Table 2 because the peptide was found previously to exhibit multi-state behavior in DOPC (Vostrikov et al.), and we find similar behavior in shorter DMPC and DLPC lipid bilayers.

An increase of the number of observed backbone ^2H signals makes it possible for the first time to incorporate this additional information for the determination of the peptide apparent orientations in the lipid membranes. The ensemble of both the $\text{C}_\alpha\text{-D}$ and $\text{C}_\alpha\text{-C}_\beta$ bond vectors from the alanines is expected to provide high sensitivity concerning the tilt of a particular peptide's helix axis with respect to a given bilayer normal.

To begin a combined analysis, we sought to examine the apparent orientation of $\text{GW}^{3,21}\text{ALP23-R12}$ in DLPC, since the backbone signals in this system are observed for five alanine positions (Table 2). The joint analysis of eight methyl and five backbone ^2H $|\Delta\nu_q|$ values initially gave a poor fit for the backbone signals, due primarily to the remarkably large $|\Delta\nu_q|$ values associated with the Ala¹¹ and Ala⁵ backbone signals. The

combined fit nevertheless improves if the principal order parameter for the backbone deuterons is increased (arbitrarily) to a value ~ 0.1 higher than that of the methyl groups (Figure 4B).

Due to a decreased signal-to-noise ratio, only two backbone deuterons can be assigned unambiguously for $\text{GW}^{3,21}\text{ALP23-R12}$ in DMPC or DOPC. Since these signals for A9 and A13 are furthermore observed in the plateau region of the backbone quadrupolar wave plot, they prove not to contribute useful information for the GALA fits. Nevertheless, three useful backbone signals are observed for $\text{GW}^{3,21}\text{ALP23-R14}$ and four or five for $\text{GW}^{5,19}\text{ALP23-R14}$ in all three lipids, making it possible to employ these data within the analysis. Once again, the best fits for each of the $-R14$ peptides in each lipid are obtained when the backbone apparent S_{zz} value is somewhat higher than the side-chain methyl value (Table 3; Figures 4-5).

From the magnitudes of quadrupolar splittings, it is apparent that the peptides are significantly tilted with respect to the lipid bilayer normal. Indeed, the GALA analysis of quadrupolar splittings returns tilt angles as large as 30° (Table 3). Visual inspection of the best-fit quadrupolar curves for $\text{GW}^{3,21}\text{ALP23-R14}$ and $\text{GW}^{3,21}\text{ALP23-R12}$ reveals that the R12 peptide has higher apparent tilt (larger $\Delta\nu_q$ values) and somewhat different tilt direction, as the curves for R12 and R14 are some $20\text{-}40^\circ$ out of phase. Conversely, the best-fit curves for both $-R14$ peptides nearly overlap, indicating highly similar peptide orientations. Due to the shallow RMSD minimum as a function of S_{zz} , the apparent τ and ρ angles for $\text{GW}^{5,19}\text{ALP23-R14}$ in DOPC differ marginally from a previous report (Vostrikov et al., 2010b).

Several general trends can be observed when examining the GALA curves for the arginine-containing peptides. As the lipid bilayer thickness increases, there is a rise in the best-fit value of S_{zz} , suggesting, lower amplitude motions for the peptides in DOPC. Furthermore, for the –R14 peptides in DOPC, the RMSD function does not reach a minimum over the whole range of S_{zz} but rather would fit best at S_{zz} values close to unity. The tilt direction does not change significantly with lipid identity for either the –R14 or –R12 series; and both –R14 peptides exhibit similar apparent tilt angles in corresponding lipids.

As the hydrophobic length of the membrane increases, there is a marked decrease in the spectral quality for $\text{GW}^{3,21}\text{ALP23-R12}$. Nevertheless, the positions of peaks in the spectra for $\text{GW}^{3,21}\text{ALP23-R12}$ in DMPC and DOPC for both sample orientations can be nearly superimposed over those in DLPC, suggesting that the peptide's apparent orientation does not change significantly with lipid bilayer thickness. On the other hand, the –R14 analogue retains good signal-to-noise ratio in each of the lipids regardless of thickness, and significant changes in the $|\Delta v_q|$ magnitudes are evident (Table 2; Figures S5-S7). GALA analysis reveals that in DMPC and DOPC a transmembrane topography is retained for both $\text{GW}^{3,21}\text{ALP23-R14}$ and $\text{GW}^{3,21}\text{ALP23-R12}$ (Figure 5). The tilted transmembrane orientations furthermore are fitted with excellent RMSD values that are below 1.5 kHz, attesting to highly helical structures (Table 3).

The differences in orientation among the single-Arg $\text{GW}^{5,19}\text{ALP23-R14}$ and $\text{GW}^{3,21}\text{ALP23-R14}$ and –R12 peptides are apparent in RMSD contour plots, graphed as a function of the apparent τ and ρ angles for each peptide in DLPC, DMPC and DOPC

lipid bilayer membranes (Figure 6). One notes that GW^{3,21}ALP23-R12 has the most centrally located arginine and exhibits very similar tilt angles in all three lipids, as can be seen by the contour levels clustered in a narrow range. Conversely, GW^{3,21}ALP23-R14 and GW^{5,19}ALP23-R14 are sensitive to the membrane hydrophobic thickness, with both of the R14 peptides adopting apparent tilt angles that span a range of 10° or more. When the host lipid is changed, the direction of the tilt does not change much for any of the peptides, as the tilt is most likely dictated by the radial position of the single Arg residue. Indeed, the tilt direction of both –R14 variants is essentially identical for each of the lipids tested. The tilt direction for GW^{3,21}ALP23-R12 also does not change with the lipid thickness. Visualization of the tilted peptides yields models where Arg¹² seems to snorkel toward the N-terminal leaflet, while the Arg¹⁴ side chain may adopt a conformation which favors C-terminal snorkeling (Figure 7).

The NMR methods are sensitive to peptide orientation but not to translocation. To probe this possibility for GW^{3,21}ALP23-Arg peptides we performed CG MD simulations in DLPC bilayer membranes. Both the –R12 and –R14 substituted GW^{3,21}ALP23 peptides adopted transmembrane orientations in 80-85% of the runs. The trends for GW^{3,21}ALP23-R14 are similar to those observed with G^{5,19}WALP23-R14 (Vostrikov et al., 2010b). Both R14 peptides undergo vertical displacement toward the C-terminal leaflet (Figure 8) by 2-4 Å, which may be explained if side-chain snorkeling alone is not sufficient for the positively-charged Arg guanidinium group to reach the aqueous interface, causing also the peptide to alter its center of mass. The rotation angle for GW^{3,21}ALP23-R14 is well defined with a sharp maximum (Figure 8D), and indeed is very close to that of

GW^{5,19}ALP23-R14 obtained by CG MD (Vostrikov et al., 2010b). The CG-MD simulations show a single orientation of GW^{3,21}ALP23-R14 in the membrane, with a tilt of $\sim 36^\circ$ in DLPC and $\sim 25^\circ$ in DPPC, in agreement with the experimentally observed sensitivity of the peptide to membrane thickness.

On the other hand, GW^{3,21}ALP23-R12 adopts a bimodal distribution in DLPC (Figure 8), with C- and N-terminal peptide center-of-mass shifts and Arg snorkeling orientations displaying similar populations. The behavior resembles that of GW^{5,19}ALP23-R12 in DOPC or DPPC, although the distributions are now narrower and better defined when the tryptophans are farther removed from the arginine. While CG MD reports two orientations of GW^{3,21}ALP23-R12, it can be seen from the intensities of the rotation plot (Figure 8C) that one of the rotation angles is more prevalent. This particular population, corresponding to arginine snorkeling toward the N-terminal, is the one observed by ²H NMR (see Discussion). Considering that this CG model does not reproduce the known preference of arginine residues to snorkel N terminally (Vostrikov et al., 2010b), we would expect increased preference for N terminal snorkeling. The tilt of GW^{3,21}ALP23-R12 is measured from the simulations to be $\sim 35^\circ$ in DLPC and $\sim 28^\circ$ in DPPC. Both of the W^{3,21} peptides induce deformations in the bilayer through the arginine snorkeling, and allow limited water access, as previously observed in GW^{5,19}ALP23-R12 and -R14 (Vostrikov et al., 2010b).

In order to probe experimentally the peptide asymmetric position in lipid bilayers, we have measured intrinsic Trp fluorescence (Figure 9), a notably sensitive indicator of the environment polarity (Lakowicz, 2006). The interpretation of fluorescence data is

complicated by the presence of two tryptophans in GWALP23 peptides. Qualitative comparisons indicate that the emission maximum (344 nm) is similar for GW^{3,21}ALP23 itself and the -R12 analog in DLPC, but some 3 nm higher for the -R14 analog, suggesting that the latter peptide adjusts its transverse position for R14 to reach toward an aqueous phase, similar to CG MD observations (Figure 9B). The bimodal distribution, observed by CG MD for GW^{3,21}ALP23-R12, would suggest little net peptide displacement, on average, in agreement with the fluorescence results. In thicker DOPC membranes GW^{3,21}ALP23 yields λ_{\max} of 340 nm, while both the -R12 and -R14 derivatives exhibit much higher values (347 and 349 nm, respectively), which approach λ_{\max} of Trp in water (Figure 9A).

The full width at half maximum (FWHM) for the fluorescence emission provides additional insight into the peptide behavior, as peptide “lifting” with respect to the lipid bilayer center would essentially move one Trp deeper into the bilayer, while transferring the other one to more polar media. The net result would be an expected broadening of the spectra. Indeed the FWHM values (Figure 9C) suggest heterogeneous environments for the Trp residues in GW^{3,21}ALP23-R^(12 or 14) peptides, in comparison with the native sequence when no Arg is present. Such behavior is particularly manifest in DOPC, where the FWHM for both Arg-containing peptides is ~5 nm larger than for the parent GW^{3,21}ALP23. For comparison, a CG MD simulation of GW^{3,21}ALP23-R14 in DLPC shows an asymmetric distribution of the Trp residues, suggesting “lifting” of the peptide, along with bilayer deformation to accommodate water access to the R14 residue in the tilted peptide (Figure 9D).

5.5 Discussion

Previously reported substitutions of Leu to Arg at position 12 or 14 in the model GW^{5,19}ALP23 sequence had dramatic consequences for the peptide orientation: the R14 variant remained transmembrane with a larger tilt angle in a different direction, while the R12 analogue populated multiple states with respect to a DOPC bilayer membrane. Here we have examined structurally isomeric GW^{3,21}ALP23-R12 and -R14 peptides, with the aim of elucidating the reasons for such behavior. Remarkably, both of the new sequences adopt well-defined transmembrane orientations, contrasting sharply with multiple populations that were observed for GW^{5,19}ALP23-R12. The transmembrane topography of GW^{3,21}ALP23-R12 indicates that a single arginine residue indeed *can* be tolerated in the central position of the peptide sequence, under certain conditions, although not within GW^{5,19}ALP23-R12. A notable structural feature of GW^{5,19}ALP23-R12 is the spatial arrangement of the Trp and Arg side chains. With the large W5, R12 and W19 side chains all projecting from the same face of an α -helix, the R12 guanidinium group is effectively sandwiched between the two bulky aromatic groups of tryptophan. Removal of this motif by shifting the Trp residues from W^{5,19} to W^{3,21} is sufficient to “rescue” the arginine from a tryptophan “cage.” Furthermore, with GW^{3,21}ALP23-R14, the Trp and Arg side chains again project from the same side of a helix; but now the increased spacing between the Trp residues effectively enlarges the cage, apparently allowing sufficient access of Arg to a polar environment, such that the peptide once again can adopt a major transmembrane orientation.

Both approaches—opening or enlarging the “cage”—seem to work fine in lipid bilayers of different thickness, a noteworthy feature here because the decrease of lipid acyl chain length alone did not promote formation of a dominant state for GW^{5,19}ALP23-R12. Indeed, the analysis of the GW^{3,21}ALP23-Arg orientations suggests that in these sequences the R12 or R14 guanidinium group can reach the aqueous phase by preferentially adjusting the magnitude and direction of the helix tilt. Due to an arginine residue being close to the peptide center, Arg side-chain snorkeling to the surface requires large tilt angles, which indeed were deduced from the solid-state NMR spectra (Figure 6, Table 3). The tilt angles are largest for GW^{3,21}ALP23-R12, presumably due to the truly central location of the arginine. Notably, for this peptide the tilt magnitudes do not differ significantly among the different lipid bilayer membranes, suggesting that alternative mechanisms of adaptation take place. It is important to note that although the major driving force defining the tilt of GW^{x,y}ALP23-Arg peptides arises from the Arg residue, the anchoring Trp residues also contribute. Tryptophans have preferences for the membrane-water interface, and their displacement away from this region imposes a penalty on the system. It is possible that the maximum observed tilt value of 30° may approach an upper limit for a 23-residue peptide with single Trp anchors near each end, and that further adaptation is therefore achieved by translating the peptide along the bilayer normal (Krishnakumar and London, 2007; Vostrikov et al., 2010b).

The situation is somewhat different for the GW^{5,19}ALP23-R14 and GW^{3,21}ALP23-R14 peptides, which exhibit large tilt angles only for the thinner lipid bilayer membranes. Unlike GW^{3,21}ALP23-R12, the R14 peptide tilt magnitudes do scale with the lipid bilayer

thickness, displaying values of 15-25°. R14 is located closer to the peptide C-terminus; however, due to the helix geometry dictating that all of the C_{α} - C_{β} bond vectors point toward the N-terminus, the R14 side chain has to reorient to enable its snorkeling toward the C-terminus. It follows from the identical tilt directions of both –R14 peptides that the responses are similar, irrespective of which helix face is occupied by the Trp residues. The strikingly identical rotation angles also imply that oscillating motion around the peptide helix axis would be highly restricted, and therefore does not average the NMR observables for these particular peptides.

It is intriguing that the Arg-containing analogues of $GW^{x,y}ALP23$ display prominent backbone $C_{\alpha}D$ signals at selected alanine positions. Although Ala- d_4 labels have been used routinely for many experiments, backbone C_{α} -D resonances nevertheless have generally not been observed for WALP-like peptides, except when Pro or Arg is present in the sequence (Thomas et al.; Vostrikov et al.). Here we have employed the orientational constraints from these additional signals together with the Ala $C_{\beta}D_3$ constraints to deduce the orientations of the peptides. Interestingly, we deduced somewhat different dynamic descriptions of these two groups, namely a somewhat higher S_{zz} value for fitting the backbone $C_{\alpha}D$ signals. As noted earlier, little variation from the average orientation is expected for $GW^{x,y}ALP23$ -Arg peptides. The high S_{zz} values (Table 3) further attest to this display of minimal peptide dynamics. The apparent variations in order parameter between the Ala methyl and backbone groups may suggest that more motion is allowed for the β -carbons. Additionally, a higher apparent S_{zz} value may reflect actual differences in the quadrupolar coupling constant for aliphatic C_{α} -D

groups. While the value of 167 ± 1 kHz has been reported for methyl groups in proteins (Mittermaier and Kay, 1999), a somewhat larger value of 171 ± 3 kHz has been observed for deuterated C_α sites (Sheppard et al., 2010).

The high values for the S_{zz} order parameter indicate that the motion of the $GW^{x,y}ALP23$ -Arg peptides in lipid bilayer membranes is restricted. To provide further estimates of the individual components of this motion, we have completed an explicit dynamics analysis of $GW^{3,21}ALP23$ -R12 in DLPC. The calculations were performed in two ways: first, using only the side-chain $C_\beta D_3$ Δv_q values; and second, using a full combination of eight side-chain and five backbone $C_\alpha D$ backbone signals, using the same $S_{zz} = 0.88$ for both.

In the latter case RMSD was calculated according to:

$$RMSD = \sqrt{\frac{\sum_{N_{CD_3}} (\Delta \Delta v_q)^2 + \sum_{N_{CD}} (0.3 \cdot \Delta \Delta v_q)^2}{N_{CD_3} + N_{CD}}}$$

In the above equation, $\Delta \Delta v_q$ is the difference between the observed and calculated values, and N is the number of data points. We scaled the error associated with the backbone signals by the factor of 0.3 to account for uncertainty due to the C_α - 2H peak broadening.

The results of the explicit dynamics analysis (Figure 10) show widespread agreement with the GALA analysis. Irrespective of whether or not the backbone signals are included in the calculations, the overall orientation and dynamics are nearly identical. Small oscillations about the average τ_0 and ρ_0 values give the best fits (Figure 10), consistent with an order parameter not much below 0.88. Importantly, considering explicit dynamics

does not lower RMSD or change the deduced values of τ_0 and ρ_0 when the C_α -D data are included. Furthermore, the semi-static GALA analysis of either backbone or side-chain signals is sufficient to determine the τ_0 and ρ_0 values for the peptides considered here.

While the reasons for “unmasking” of selected backbone resonances are incompletely understood, we note that a major enhancement of the C_α -D signal intensity at $\beta=0^\circ$, accompanied by line narrowing, occurs over a fairly small frequency range of $\Delta\nu_q$ between 95 and 115 kHz, corresponding to angle θ of $38.5^\circ \pm 1.5^\circ$. Outside of this range, the backbone signals are either not detectable or are observed only as broad, low-intensity peaks for samples oriented with $\beta=90^\circ$ and not $\beta=0^\circ$.

The CG MD simulations offer an opportunity for detailed views of the systems under examination. Of major importance is the observation that the simulations closely reproduce the peptide orientations deduced from solid-state NMR. Furthermore, CG MD offers valuable insights into significant other aspects, such as peptide lifting from the center of the lipid bilayer, membrane deformations and water defects. For both arginine containing peptides, a thinning of $\sim 3 \text{ \AA}$ was observed in simulations (relative to unmodified $\text{GW}^{3,21}\text{ALP23}$), increasing the number of contacts between the peptide and phosphate and water particles. In the case of $\text{GW}^{3,21}\text{ALP23-R12}$, CG MD predicts a multi-state response of the system, which was not detected by solid-state NMR. Detailed yet unknown features of the system dynamics, spectral overlap or equilibrium between the states all could contribute to one population not being detected. Nevertheless, the reduced signal/noise ratio for $\text{GW}^{3,21}\text{ALP23-R12}$ could suggest the presence of minor population(s), possibly in fast exchange with the major state.

While the solid-state NMR experiments do not provide direct information on peptide transverse shifts in the membrane, such data can be obtained by alternative techniques. Nevertheless, the design of GWALP23 peptides means that the overall fluorescence spectra will result from superposition of contributions from the individual tryptophans. For this reason, the spectral comparisons among the different peptides may be more informative than any one individual spectrum. In this context, the Arg-containing peptides exhibit a red shift in the Trp emission λ_{max} , indicating a more polar environment for at least one of the two Trp residues. The increase in the spectral width further indicates heterogeneous environments of the two tryptophans, as expected for a peptide positioned asymmetrically in the membrane. In addition to the red shift, the more polar exposed Trp may also have a higher quantum yield, which could then cause a shifting of the “average” λ_{max} , in addition to broadening the spectra.

The single, central, Arg residue in GWALP23-R12, acetyl-GGALW⁵LALALAR¹²ALALALW¹⁹LAGA-amide displayed multi-state behavior and induced the peptide to exit from a bilayer membrane of DOPC (Vostrikov et al., 2010b). In the present article, we report that the Arg can be “rescued,” with restoration of a stable, tilted transmembrane orientation for the peptide when the Trp anchors are moved from residues (5, 19) to residues (3, 21). The results reinforce the concept of multiple mechanisms by which Arg can “escape” or exit from the bilayer center. Coarse-grained molecular dynamics simulations and solid-state NMR experiments show substantial agreement on these principles—although a difference remains to be resolved (with future work) concerning whether only one or possibly two peptide rotation and Arg snorkeling

states remain dominant for GW^{3,21}ALP23-R12. The corresponding R14 analogues, regardless of having Trp anchors at (5, 19) or (3, 21), display single-state transmembrane behavior in DLPC, DMPC and DOPC; as deduced by both NMR experiment and CG MD simulation, with a tilt magnitude that scales with the bilayer thickness. The relative positions of the Trp and Arg residues are therefore crucial for the detailed protein/lipid interactions, as reflected by the properties of the transmembrane helices.

5.6 Acknowledgments

This work was supported in part by grants from the US National Science Foundation (MCB-0841227), the Oxford Center for Integrative Systems Biology, the BBSRC and MRC, the Oxford Supercomputing Center, and the Arkansas Biosciences Institute. The NMR facility was supported by NIH grant RR31154.

5.7 References

- Aisenbrey, C., R. Kinder, E. Goormaghtigh, J.M. Ruyschaert, and B. Bechinger, 2006. Interactions involved in the realignment of membrane-associated helices. An investigation using oriented solid-state NMR and attenuated total reflection Fourier transform infrared spectroscopies. *J Biol Chem* 281: 7708-7716.
- Andreev, O.A., A.D. Dupuy, M. Segala, S. Sandugu, D.A. Serra, C.O. Chichester, D.M. Engelman, and Y.K. Reshetnyak, 2007. Mechanism and uses of a membrane peptide that targets tumors and other acidic tissues in vivo. *Proc Natl Acad Sci U S A* 104: 7893-7898.
- Bartlett, G.J., C.T. Porter, N. Borkakoti, and J.M. Thornton, 2002. Analysis of catalytic residues in enzyme active sites. *J Mol Biol* 324: 105-121.
- Bechinger, B., 1996. Towards membrane protein design: pH-sensitive topology of histidine-containing polypeptides. *J Mol Biol* 263: 768-775.
- Davis, J.H., K.R. Jeffrey, M. Bloom, M.I. Valic, and T.P. Higgs, 1976. Quadrupolar echo deuteron magnetic resonance spectroscopy in ordered hydrocarbon chains. *Chem Phys Lett* 42: 390-394.
- Doyle, D.A., J. Morais Cabral, R.A. Pfuetzner, A. Kuo, J.M. Gulbis, S.L. Cohen, B.T. Chait, and R. MacKinnon, 1998. The structure of the potassium channel: molecular basis of K⁺ conduction and selectivity. *Science* 280: 69-77.
- Hessa, T., N.M. Meindl-Beinker, A. Bernsel, H. Kim, Y. Sato, M. Lerch-Bader, I. Nilsson, S.H. White, and G. von Heijne, 2007. Molecular code for transmembrane-helix recognition by the Sec61 translocon. *Nature* 450: 1026-1030.
- Hunt, J.F., P. Rath, K.J. Rothschild, and D.M. Engelman, 1997. Spontaneous, pH-dependent membrane insertion of a transbilayer α -helix. *Biochemistry* 36: 15177-15192.
- Karp, D.A., M.R. Stahley, and B. Garcia-Moreno, 2010. Conformational consequences of ionization of Lys, Asp, and Glu buried at position 66 in staphylococcal nuclease. *Biochemistry* 49: 4138-4146.
- Killian, J.A., M.J. Taylor, and R.E. Koeppe II, 1992. Orientation of the valine-1 side chain of the gramicidin transmembrane channel and implications for channel functioning. A ²H NMR study. *Biochemistry* 31: 11283-90.
- Killian, J.A., I. Salemink, M.R. de Planque, G. Lindblom, R.E. Koeppe 2nd, and D.V. Greathouse, 1996. Induction of nonbilayer structures in diacylphosphatidylcholine model membranes by transmembrane α -helical peptides: importance of

- hydrophobic mismatch and proposed role of tryptophans. *Biochemistry* 35: 1037-1045.
- Krishnakumar, S.S., and E. London, 2007. The control of transmembrane helix transverse position in membranes by hydrophilic residues. *J Mol Biol* 374: 1251-1269.
- Ladokhin, A.S., S. Jayasinghe, and S.H. White, 2000. How to measure and analyze tryptophan fluorescence in membranes properly, and why bother? *Analytical Biochemistry* 285: 235-245.
- Lakowicz, J.R., 2006. *Principles of Fluorescence Spectroscopy*. 3 ed. Springer.
- Loladze, V.V., D.N. Ermolenko, and G.I. Makhatadze, 2001. Heat capacity changes upon burial of polar and nonpolar groups in proteins. *Protein Sci* 10: 1343-1352.
- Mittermaier, A., and L.E. Kay, 1999. Measurement of methyl ^2H quadrupolar couplings in oriented proteins. How uniform is the quadrupolar coupling constant? *J Am Chem Soc* 121: 10608-10613.
- Monticelli, L., S.K. Kandasamy, X. Periole, R.G. Larson, D.P. Tieleman, and S.J. Marrink, 2008. The MARTINI Coarse-Grained Force Field: Extension to Proteins. *J Chem Theory Comput* 4: 819-834.
- Sheppard, D., D.W. Li, R. Godoy-Ruiz, R. Bruschweiler, and V. Tugarinov, 2010. Variation in quadrupole couplings of alpha deuterons in ubiquitin suggests the presence of $\text{C}^\alpha\text{-H}^\alpha\cdots\text{O}=\text{C}$ hydrogen bonds. *J Am Chem Soc* 132: 7709-7719.
- Sine, S.M., H.L. Wang, and N. Bren, 2002. Lysine scanning mutagenesis delineates structural model of the nicotinic receptor ligand binding domain. *J Biol Chem* 277: 29210-29223.
- Strandberg, E., S. Esteban-Martin, J. Salgado, and A.S. Ulrich, 2009. Orientation and dynamics of peptides in membranes calculated from ^2H -NMR data. *Biophys J* 96: 3223-3232.
- Strandberg, E., S. Ozdirekcan, D.T. Rijkers, P.C. van der Wel, R.E. Koeppe 2nd, R.M. Liskamp, and J.A. Killian, 2004. Tilt angles of transmembrane model peptides in oriented and non-oriented lipid bilayers as determined by ^2H solid-state NMR. *Biophys J* 86: 3709-3721.
- Swartz, K.J., 2008. Sensing voltage across lipid membranes. *Nature* 456: 891-897.
- Takayama, Y., C.A. Castaneda, M. Chimenti, B. Garcia-Moreno, and J. Iwahara, 2008. Direct evidence for deprotonation of a lysine side chain buried in the hydrophobic core of a protein. *J Am Chem Soc* 130: 6714-6715.

- ten Kortenaar, P.B.W., B.G. Van Dijk, J.M. Peeters, B.J. Raaben, P.J.H.M. Adams, and G.I. Tesser, 1986. Rapid and efficient method for the preparation of Fmoc-amino acids starting from 9-fluorenylmethanol. *Int J Pept Protein Res* 27: 398-400.
- Thomas, R., V.V. Vostrikov, D.V. Greathouse, and R.E. Koeppe 2nd, 2009. Influence of proline upon the folding and geometry of the WALP19 transmembrane peptide. *Biochemistry* 48: 11883-11891.
- van der Wel, P.C., E. Strandberg, J.A. Killian, and R.E. Koeppe 2nd, 2002. Geometry and intrinsic tilt of a tryptophan-anchored transmembrane α -helix determined by ^2H NMR. *Biophys J* 83: 1479-1488.
- Vostrikov, V.V., A.E. Daily, D.V. Greathouse, and R.E. Koeppe 2nd, 2010a. Charged or aromatic anchor residue dependence of transmembrane peptide tilt. *J Biol Chem* 285: 31723-31730.
- Vostrikov, V.V., C.V. Grant, A.E. Daily, S.J. Opella, and R.E. Koeppe 2nd, 2008. Comparison of "Polarization Inversion with Spin Exchange at Magic Angle" and "Geometric Analysis of Labeled Alanines" methods for transmembrane helix alignment. *J Am Chem Soc* 130: 12584-12585.
- Vostrikov, V.V., B.A. Hall, D.V. Greathouse, R.E. Koeppe 2nd, and M.S.P. Sansom, 2010b. Changes in transmembrane helix alignment by arginine residues revealed by solid-state NMR experiments and coarse-grained MD simulations. *J Am Chem Soc* 132: 5803-5811.

5.8 Tables

Table 1. Peptide sequences for GWALP23 and derivatives.*

Peptide	Sequence
GW ^{5,19} ALP23	GGAL W LALALAL <u>AL</u> <u>AL</u> AL W LAGA
GW ^{5,19} ALP23-R12	GGAL W LALALAR <u>AL</u> <u>AL</u> AL W LAGA
GW ^{5,19} ALP23-R14	GGAL W LALALAL <u>AR</u> <u>AL</u> AL W LAGA
GW ^{3,21} ALP23	GG W LALALALAL <u>AL</u> <u>AL</u> ALAL W GA
GW ^{3,21} ALP23-R12	GG W LALALALAR <u>AL</u> <u>AL</u> ALAL W GA
GW ^{3,21} ALP23-R14	GG W LALALALAL <u>AR</u> <u>AL</u> ALAL W GA

*Sequence positions 12 and 14 are underlined, for emphasis. The parent GWALP23 sequence included tryptophans (**W**) at positions 5 and 19.

Table 2. Alanine C β D $_3$ and C α D quadrupolar splitting (kHz) for selected GW^{x,y}ALP23-R^z peptides incorporated in DLPC, DMPC or DOPC.

Peptide	Lipid	C β D $_3$ position							
		5	7	9	11	13	15	17	19
GW ^{3,21} ALP23-R12	DLPC	30.4	29.3	6.8	7.9	29.8	27.6	35.1	43.0
	DMPC	29.1	28.1	6.4	6.4	30.3	30.3	35.1	41.8
	DOPC	26.8	26.8	7.2	6.4	29.6	26.6	35.8	38.2
GW ^{3,21} ALP23-R14	DLPC	37.7	33.1	22.2	24.7	7.6	7.6	28.9	24.2
	DMPC	26.8	28.1	13.2	20.7	12.2	0.7	27.5	21.0
	DOPC	17.9	26.6	9.9	18.4	10.6	1.2	25.4	17.1
GW ^{5,19} ALP23-R14	DLPC	–	33.0	21.1	25.7	9.3	6.8	30.8	–
	DMPC	–	30.6	14.1	21.3	10.3	3.7	29.1	–
	DOPC ^a	–	26.6	5.5	16.0	13.1	1.3	28.0	–
		C α D position							
		5	7	9	11	13	15	17	19
GW ^{3,21} ALP23-R12	DLPC	106		110	169	110		89	
	DMPC			114		113			
	DOPC			117		112			
GW ^{3,21} ALP23-R14	DLPC			103			114	103	
	DMPC			106			94	102	
	DOPC			100			84	97	
GW ^{5,19} ALP23-R14	DLPC	–		107	106	115	148	106	–
	DMPC	–		100	94	111	130	104	–
	DOPC	–		92	82	105		96	–

a. Data from (Vostrikov et al., 2010b).

b. Entries left blank were not observed in the ²H NMR spectra.

Table 3. GALA fit results *

Peptide	GALA fit results					
	S_{zz}		τ , deg	ρ , deg	RMSD, kHz	
	$C_{\beta}D_3$	$C_{\alpha}D$			$C_{\beta}D_3$	$C_{\alpha}D$
DLPC						
GW ^{3,21} ALP23-R12	0.84	0.94	29.7	225	1.1	8.8
GW ^{3,21} ALP23-R14	0.82	0.94	26.0	262	1.2	8.3
GW ^{5,19} ALP23-R14	0.83	0.97	26.7	260	1.6	6.4
DMPC						
GW ^{3,21} ALP23-R12	0.84	–	29.3	223	1.4	–
GW ^{3,21} ALP23-R14	0.83	0.99	20.3	253	1.1	11.0
GW ^{5,19} ALP23-R14	0.78	0.91	25.3	252	1.3	6.6
DOPC						
GW ^{3,21} ALP23-R12	0.87	–	26.3	223	1.4	–
GW ^{3,21} ALP23-R14	0.89	1.0	15.3	253	1.2	15.5 ^{**}
GW ^{5,19} ALP23-R14	0.93	1.0	15.0	247	0.9	12.9 ^{**}

* Alanine methyl group ²H quadrupolar splittings were used to obtain the apparent tilt and rotation angles as well as S_{zz} . Backbone quadrupolar waves were calculated using τ and ρ obtained from the methyl group fits, and using backbone S_{zz} as the only free parameter. Angles $\epsilon_{//}$ and ϵ_{\perp} (van der Wel et al., 2002) were fixed at 59.4° and –43° respectively for $C_{\beta}D_3$; the corresponding values for $C_{\alpha}D$ were 122.0° and 55°.

** RMSD falls if the “apparent” S_{zz} for backbone groups is allowed to rise above 1.0.

5.9 Figures

Figure 1. Helical wheel projections of $\text{GW}^{x,y}\text{ALP23-R}^z$: **A.** $X = 5, Y = 19$; **B.** $X = 3, Y = 21$. ($Z = 12$ or 14 both in **A** and **B**). Trp residues are shown in green, and ^2H -labeled alanines are grey. The possible locations for a single Arg are blue, with only one Arg being present in each peptide. When residues 12 and 14 are not Arg, they are Leu; see also Table 1.

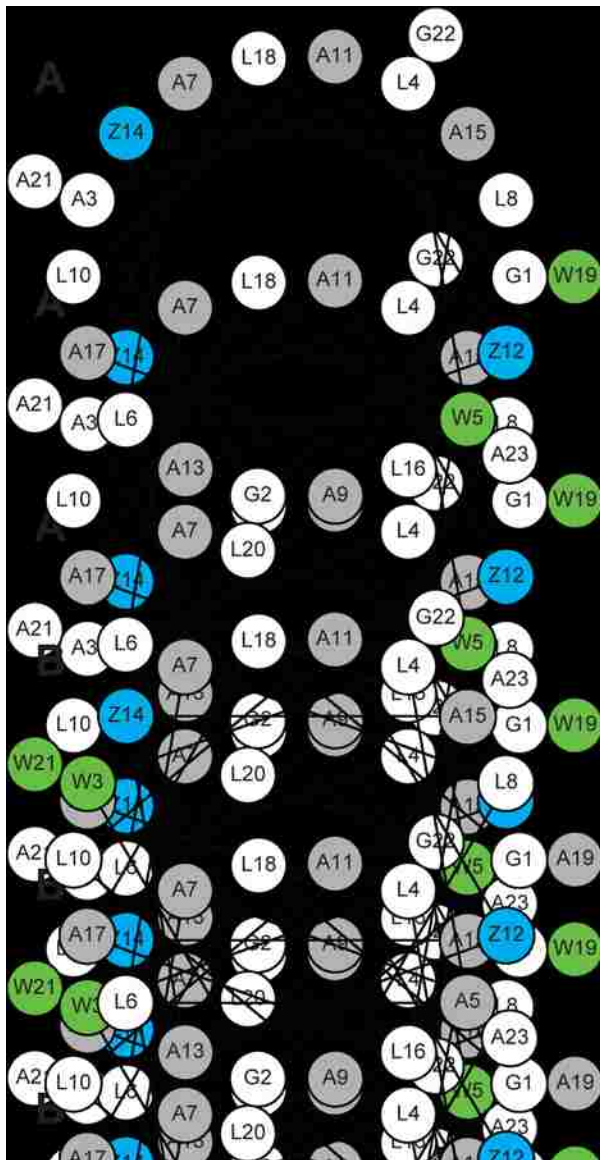


Figure 2. Deuterium NMR spectra of $\text{GW}^{3,21}\text{ALP23-R}^Z$ peptides labeled at alanines 17 (full deuteration) and 19 (partial), incorporated in: **A.** DLPC ($Z = 12$); **B.** DLPC ($Z = 14$). **C.** DLPC, DMPC and DOPC (top to bottom; $Z = 12$); or **D.** DLPC, DMPC and DOPC (top to bottom; $Z = 14$). Sample orientation is $\beta=90^\circ$ (A and B) or $\beta=0^\circ$ (C and D). Note that the kHz scale is expanded by a factor of two in A and B.

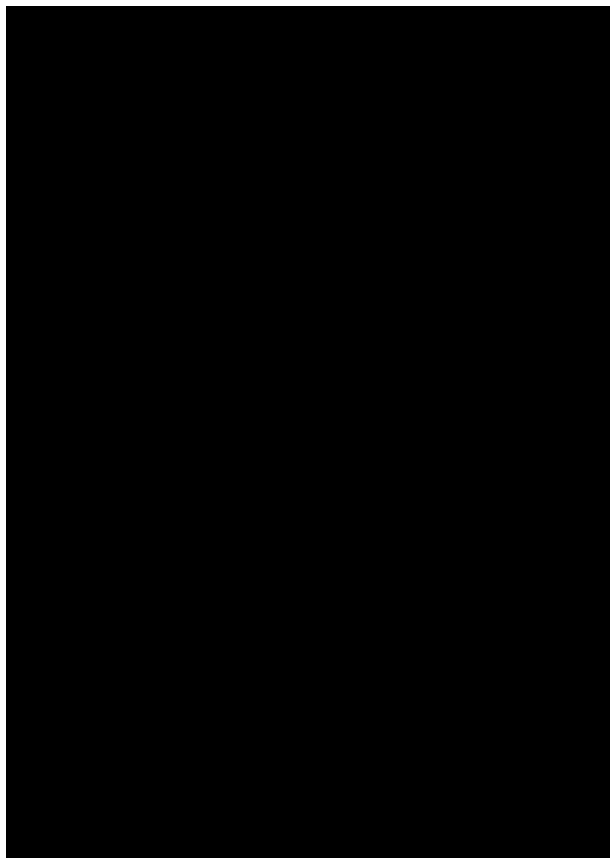


Figure 3. Deuterium NMR spectra of GW^{3,21}ALP23-R¹² labeled at positions 13 (full deuteration) and 15 (partial deuteration) in DLPC. **A.** Ala-d₄ label; **B.** Ala-d₃ label. Note that two methyl signals at ~28 kHz are not resolved.

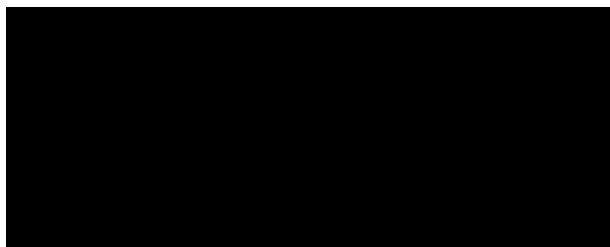


Figure 4. GALA quadrupolar wave plots for methyl and backbone groups of $\text{GW}^{3,21}\text{ALP23-R}^z$ and $\text{GW}^{5,19}\text{ALP23-R14}$ in DLPC. **A.** Methyl signals for $Z = 12$ (red), $Z = 14$ (blue) and $\text{GW}^{5,19}\text{ALP23-R14}$ (green). **B.** Backbone signals for $Z = 12$ (red), $Z = 14$ (blue) and $\text{GW}^{5,19}\text{ALP23-R14}$ (green). Alanine positions are indicated. Order parameter was 0.82-0.84 for methyl groups and 0.94-0.97 for backbone groups (Table 3).

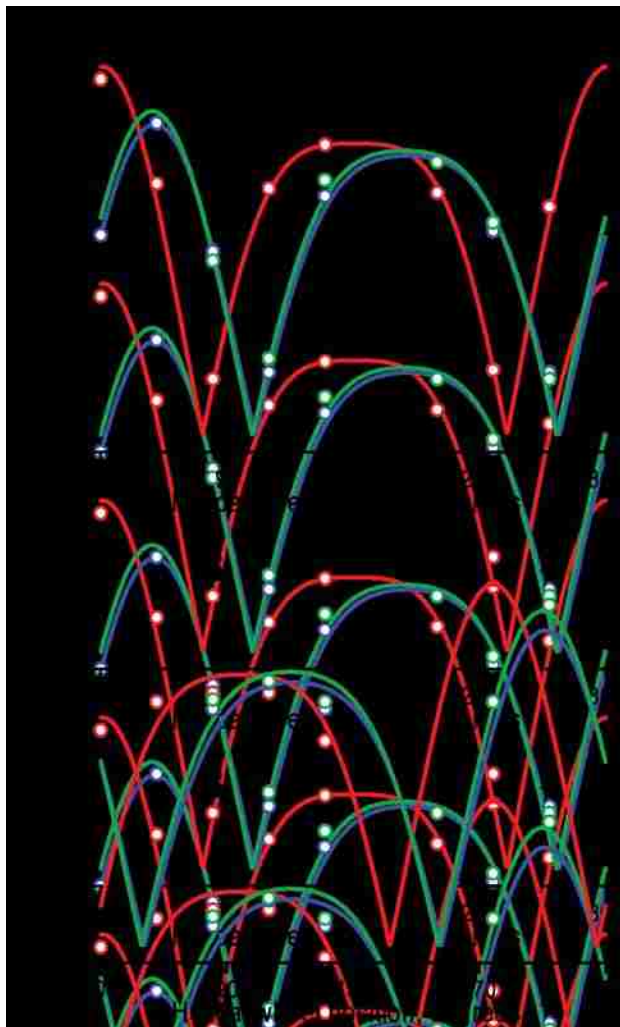


Figure 5. GALA quadrupolar wave plots for methyl groups of $\text{GW}^{3,21}\text{ALP23-R}^z$ and $\text{GW}^{5,19}\text{ALP23-R14}$ in: **A.** DMPC; **B.** DOPC. $Z = 12$ (red), $Z = 14$ (blue) and $\text{GW}^{5,19}\text{ALP23-R14}$ (green).

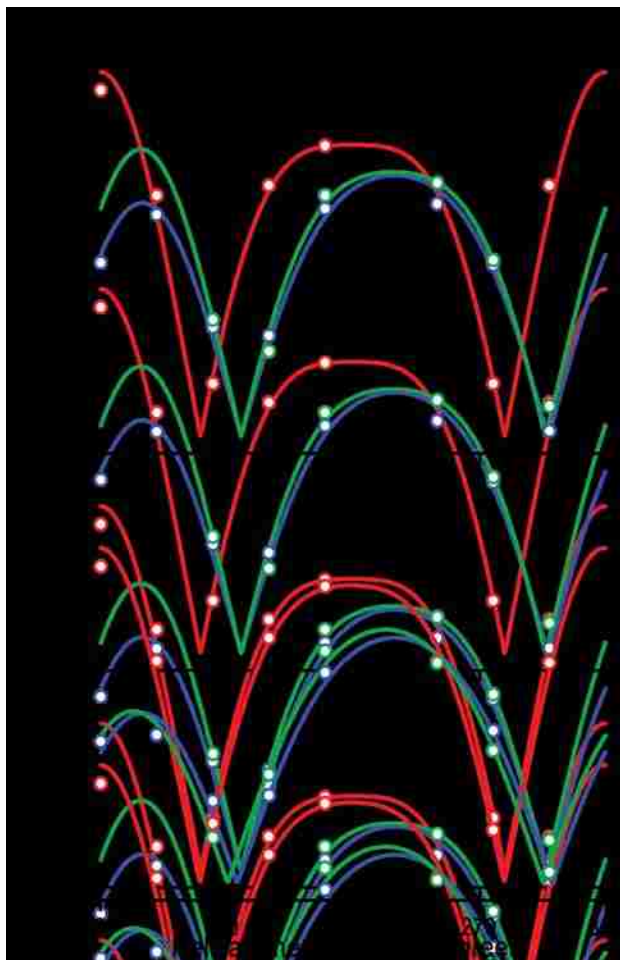


Figure 6. RMSD contour plots for $GW^{x,y}ALP23-R^z$ in DLPC (red), DMPC (green) and DOPC (blue). **A.** $X = 3, Y = 21, Z = 12$; **B.** $X = 3, Y = 21, Z = 14$; **C.** $X = 5, Y = 19, Z = 14$. Contours are plotted at 1, 2 and 3 kHz.

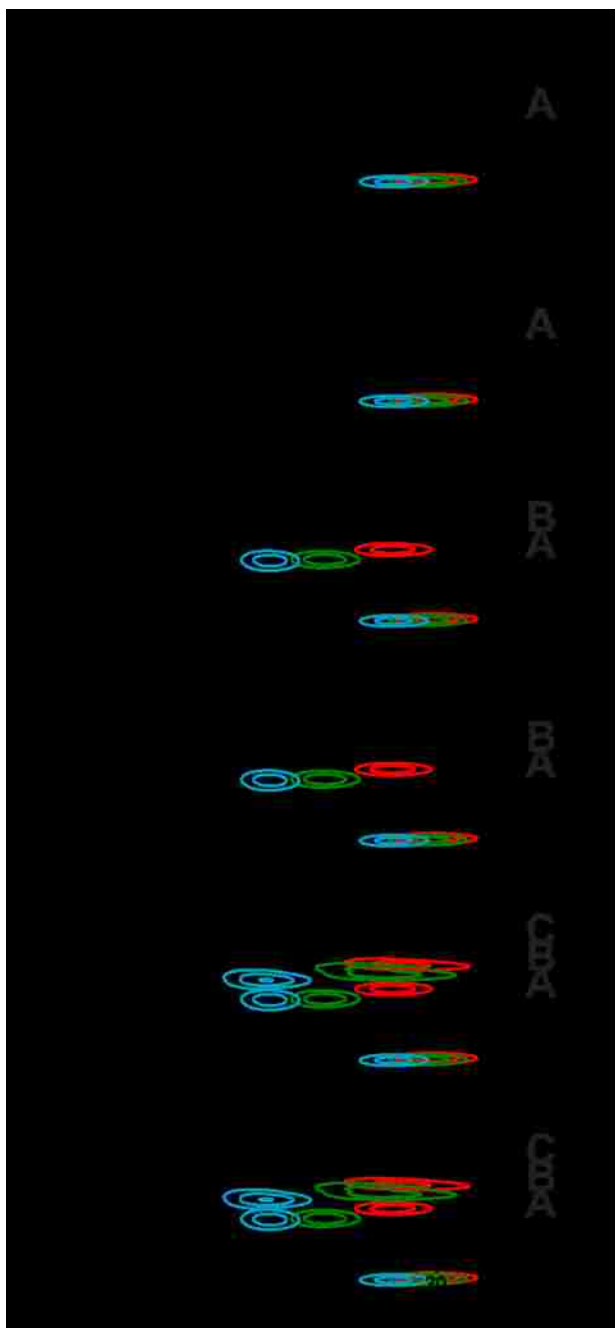


Figure 7. Molecular models of tilted $GW^{x,y}ALP23-R^z$ in DLPC.

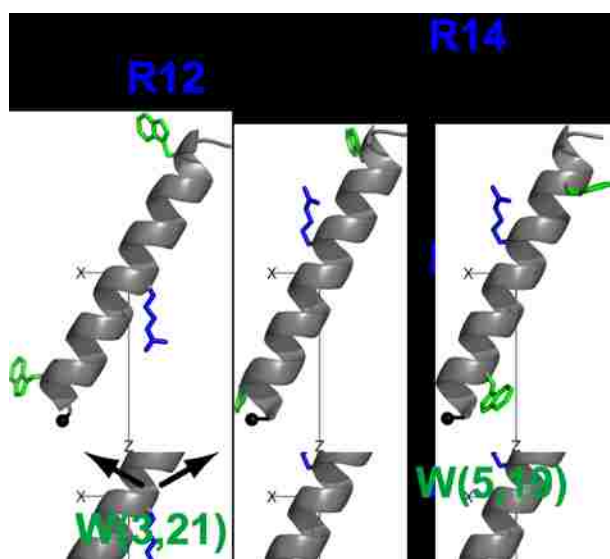


Figure 8. CG MD simulations. **A.** Displacement of GW^{3,21}ALP23-R12 relative to DLPC bilayer center. **B.** Same as A, but for GW^{3,21}ALP23-R14. **C.** Distribution of rotation angles of GW^{3,21}ALP23-R12 in DLPC. **D.** Same as C, but for GW^{3,21}ALP23-R14.

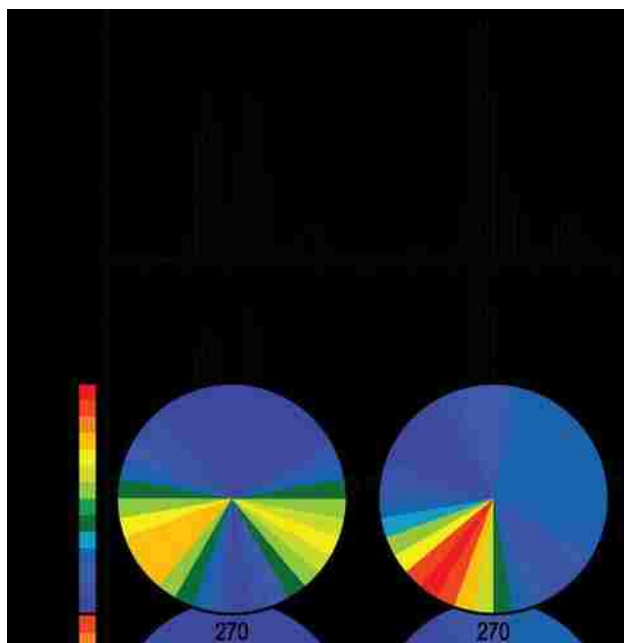


Figure 9. Steady state fluorescence. **A.** Fluorescence spectra of $\text{GW}^{3,21}\text{ALP23-R}^z$ in DLPC; **B.** Emission maxima; **C.** Full width at half maximum values. Grey line in A is tryptophan in water. Other colors are consistent through panels A-C. WT refers to the host $\text{GW}^{3,21}\text{ALP23}$ peptide without arginine substitutions. Panel D illustrates a CG MD simulation result for $\text{GW}^{3,21}\text{ALP23-R14}$ in DLPC, suggesting not only that W3 is more buried than W21 but also that membrane deformation allows water access to R14 in the tilted peptide.

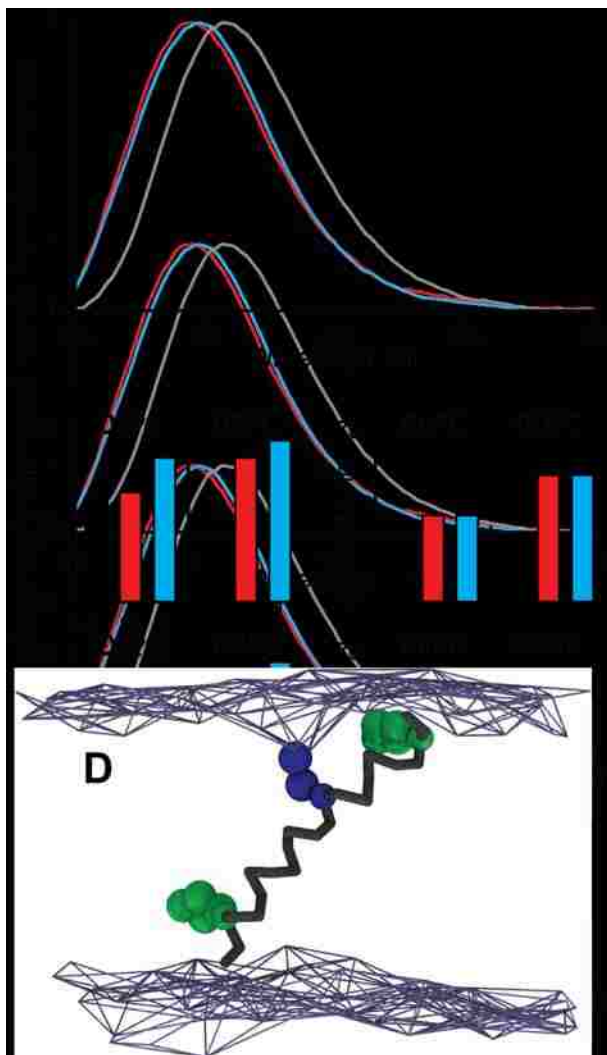
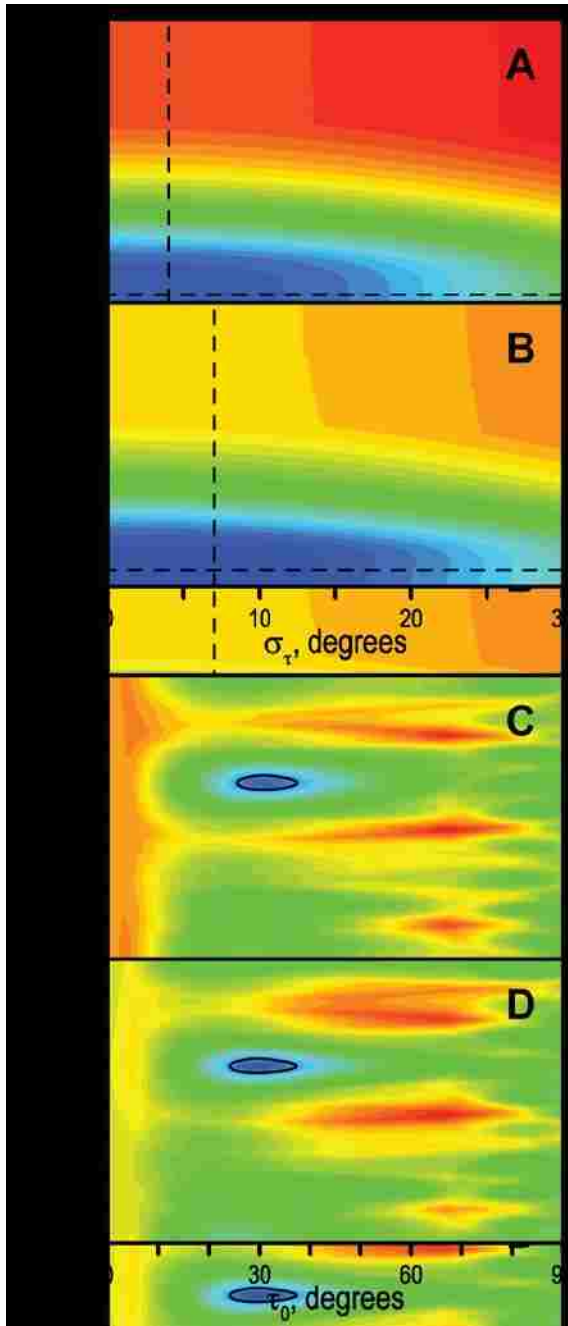


Figure 10. Explicit dynamics analysis of GW^{3,21}ALP23-R12 in DLPC, showing the standard deviations of Gaussian distributions (A, B) and their centers (C, D). Analyzed data included either both C_βD₃ and C_αD signals (A, C) or C_βD₃ signals alone (B, D). Dashed lines in A and B indicate the best fit σ_τ and σ_ρ , which were used for generating the plots in C and D respectively. Color scale is identical between A and B (0 to 28 kHz) and between C and D (0 to 31 kHz). Color increments are at 1 kHz; solid line in C, D is drawn at 5 kHz level. Best fits (τ_0 , σ_τ , ρ_0 , σ_ρ) are (31, 4, 224, 6) for combined C_βD₃ + C_αD set and (30, 7, 224, 11) for C_βD₃ set alone.



5.10 Supporting Information

Figure S1. Analytical HPLC of GW^{3,21}ALP23-R^z.

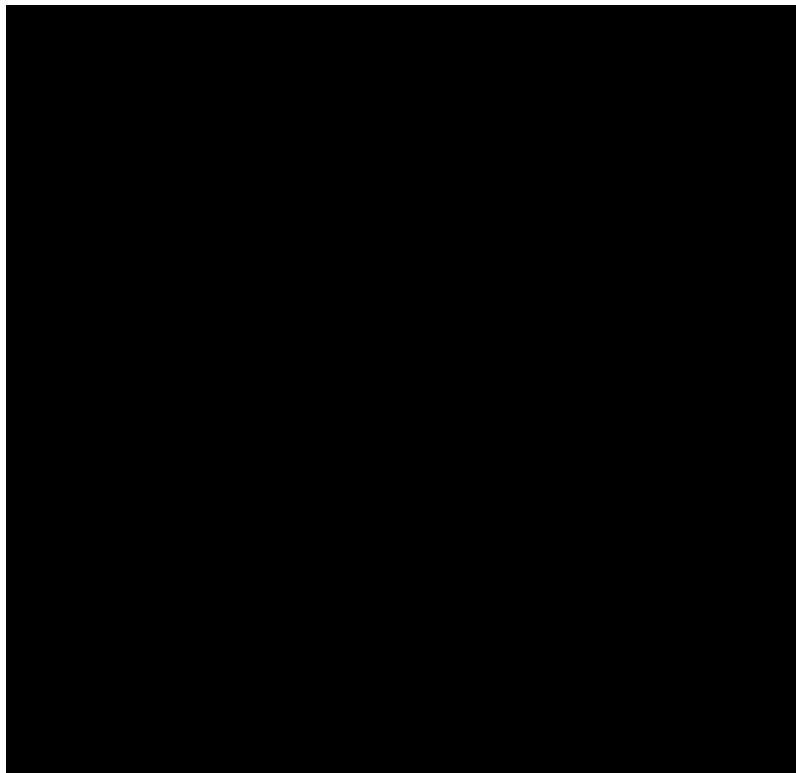


Figure S2. MALDI mass spectra of GW^{3,21}ALP23-R^z, containing two ²H-labeled alanine residues.

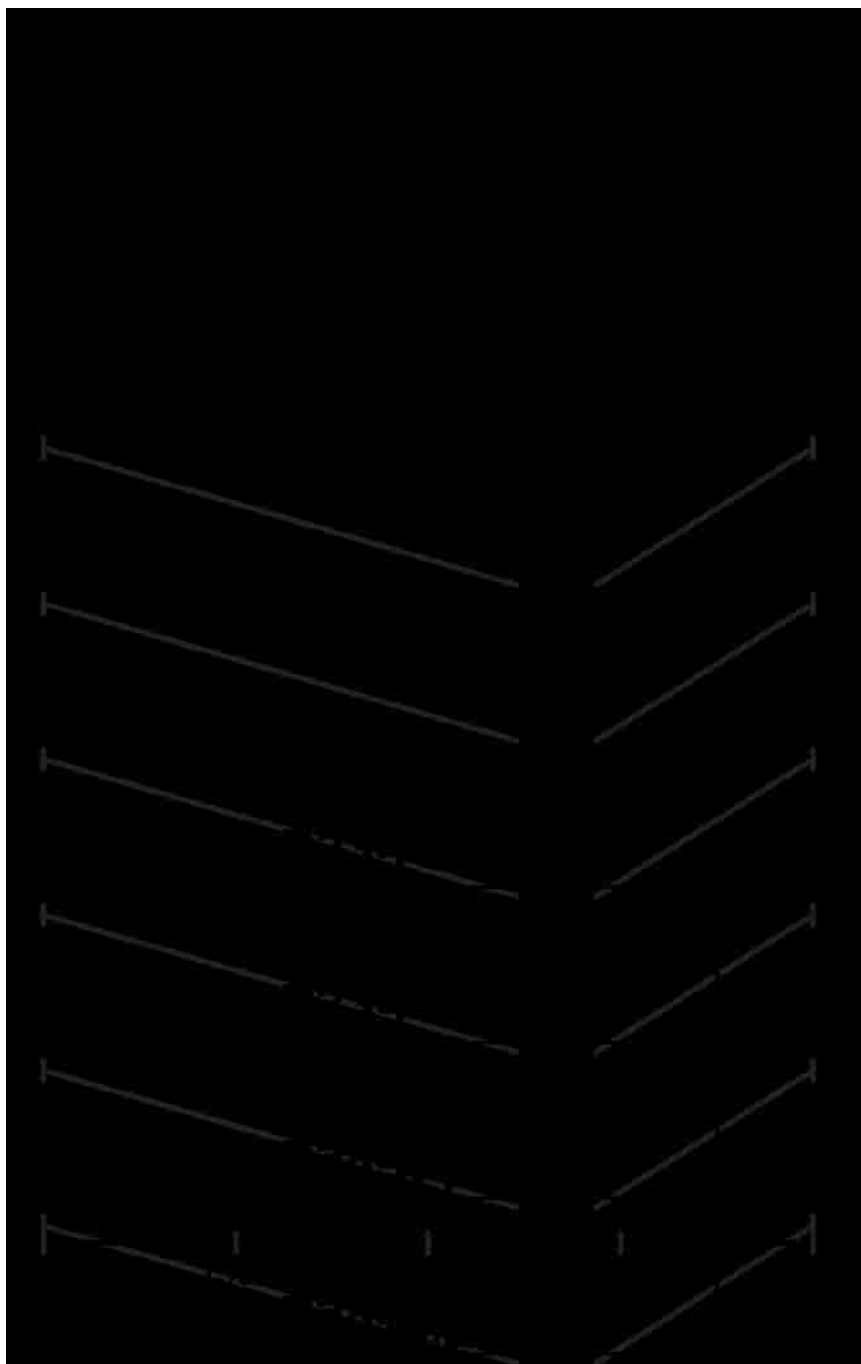


Figure S3. Difference spectra between double and single labeled peptides were used to assign the overlapping peaks. Sample is GW^{3,21}ALP23-R12 in DLPC, $\beta=90^\circ$.

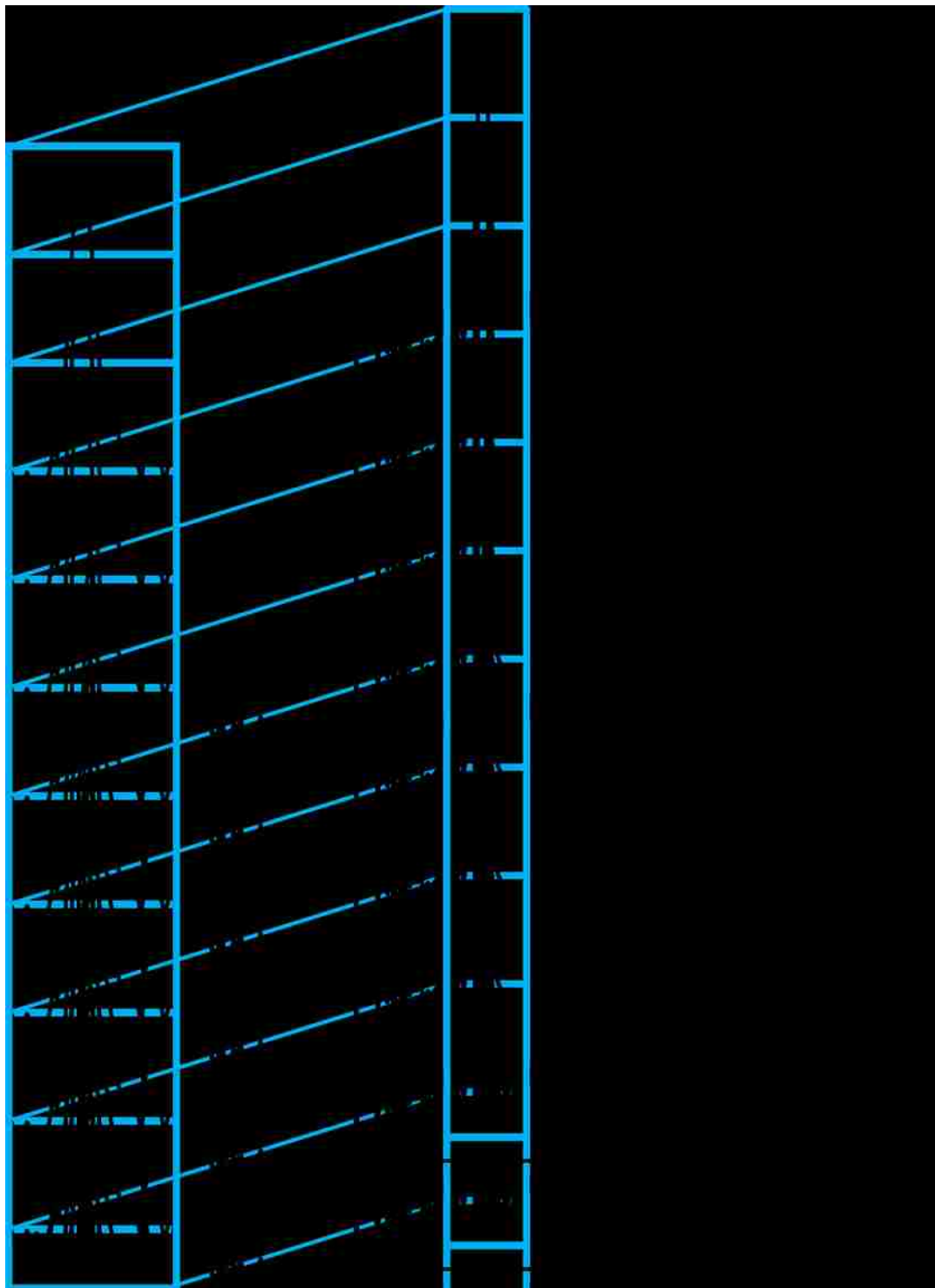


Figure S4. Circular dichroism of GW^{3,21}ALP23 and -Arg^Z peptides in DLPC. Black: native sequence; Red: Z = 12; Blue: Z = 14.

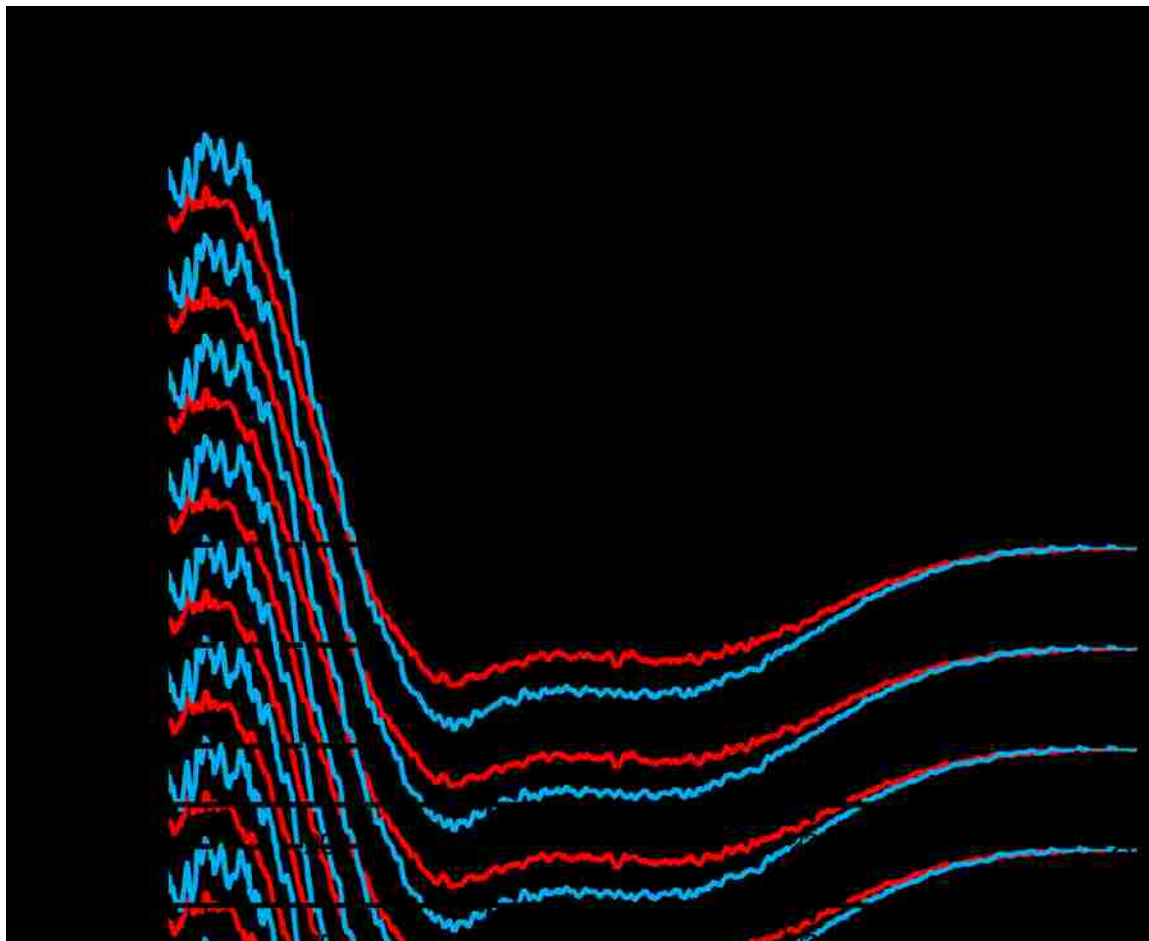


Figure S5. Deuterium NMR spectra of GW^{3,21}ALP23-R12 in DLPC, DMPC, DOPC.
Sample orientation is $\beta=0^\circ$.

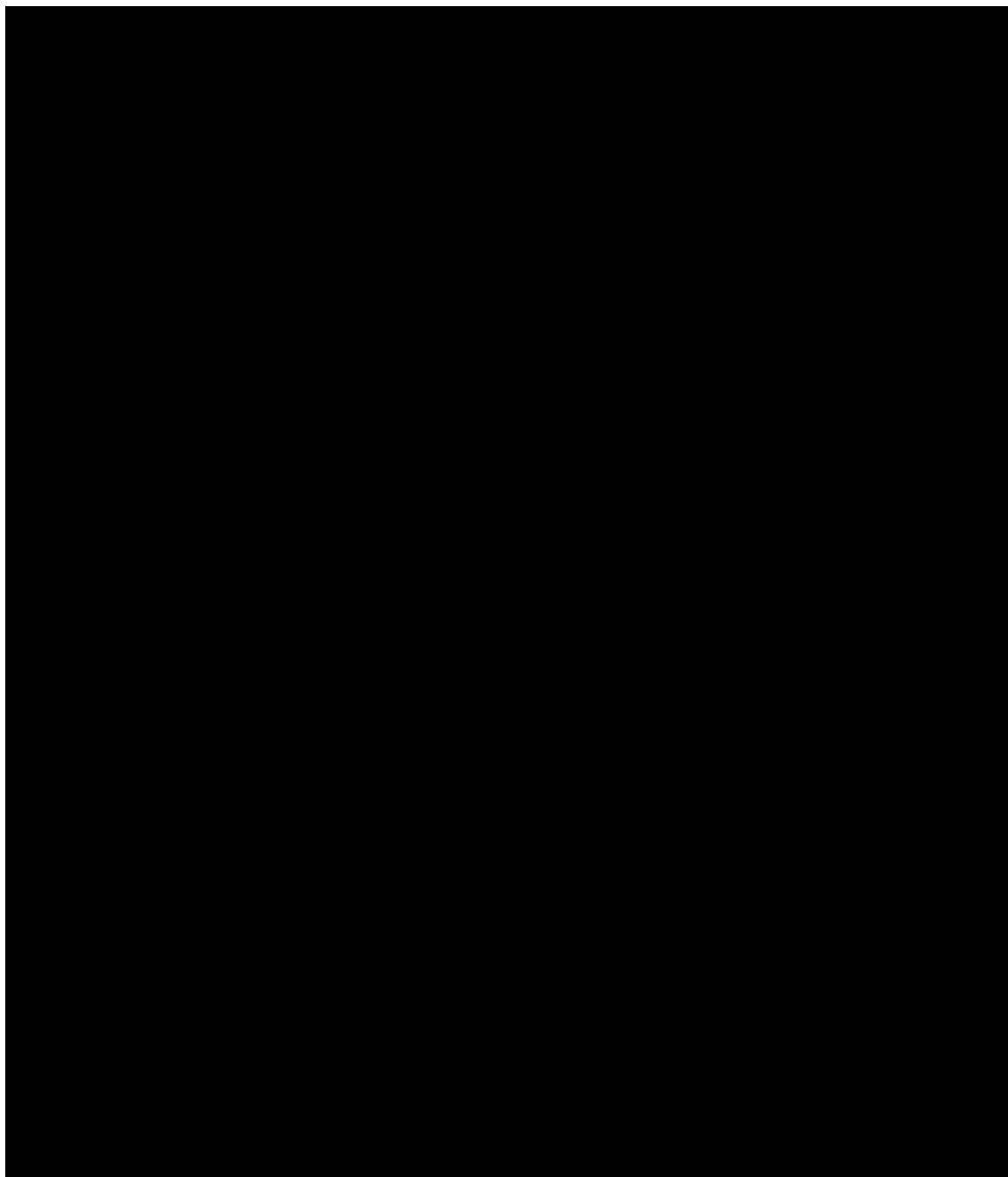


Figure S6. Deuterium NMR spectra of GW^{3,21}ALP23-R14 in DLPC, DMPC, DOPC. Sample orientation is $\beta=0^\circ$.

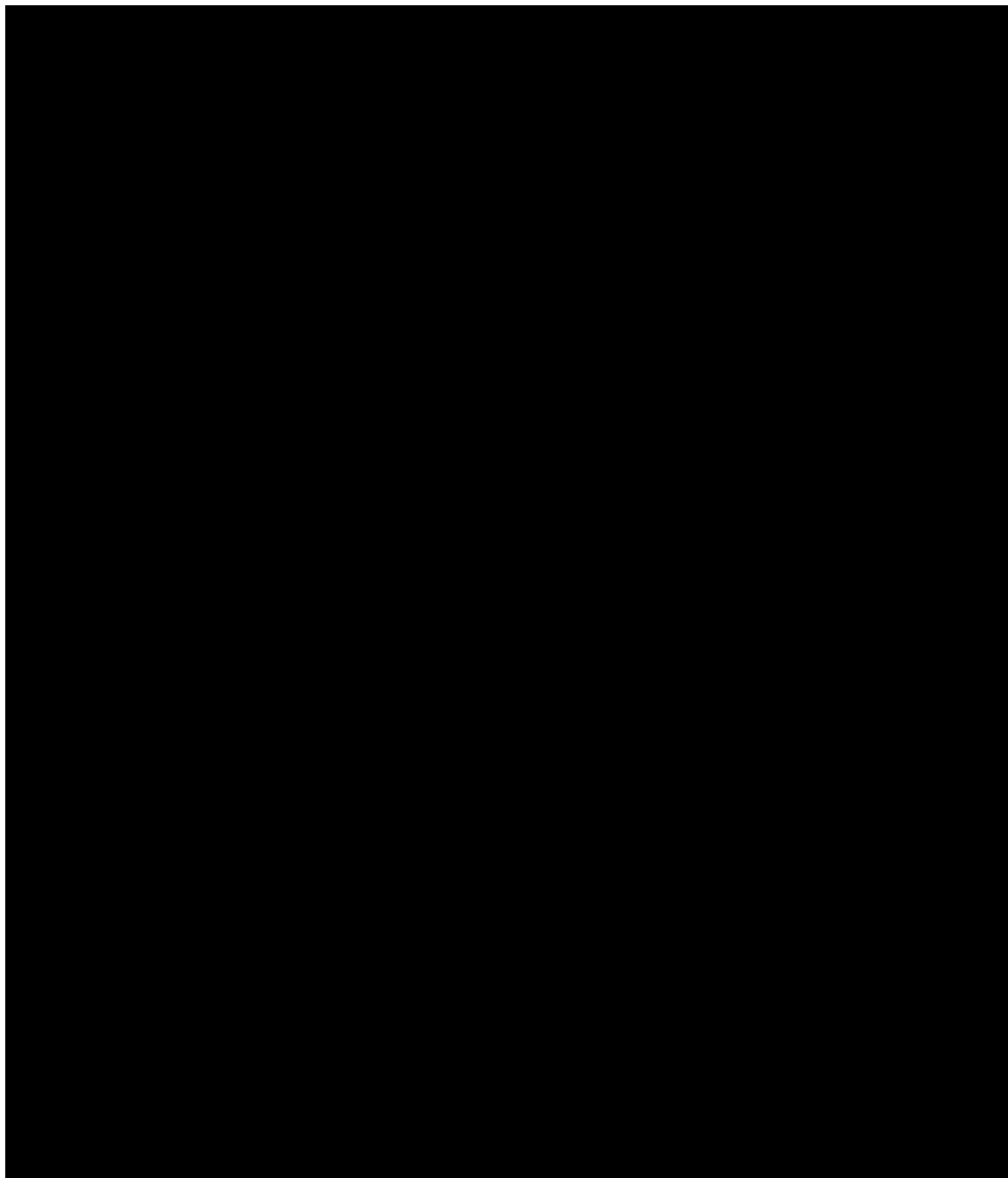
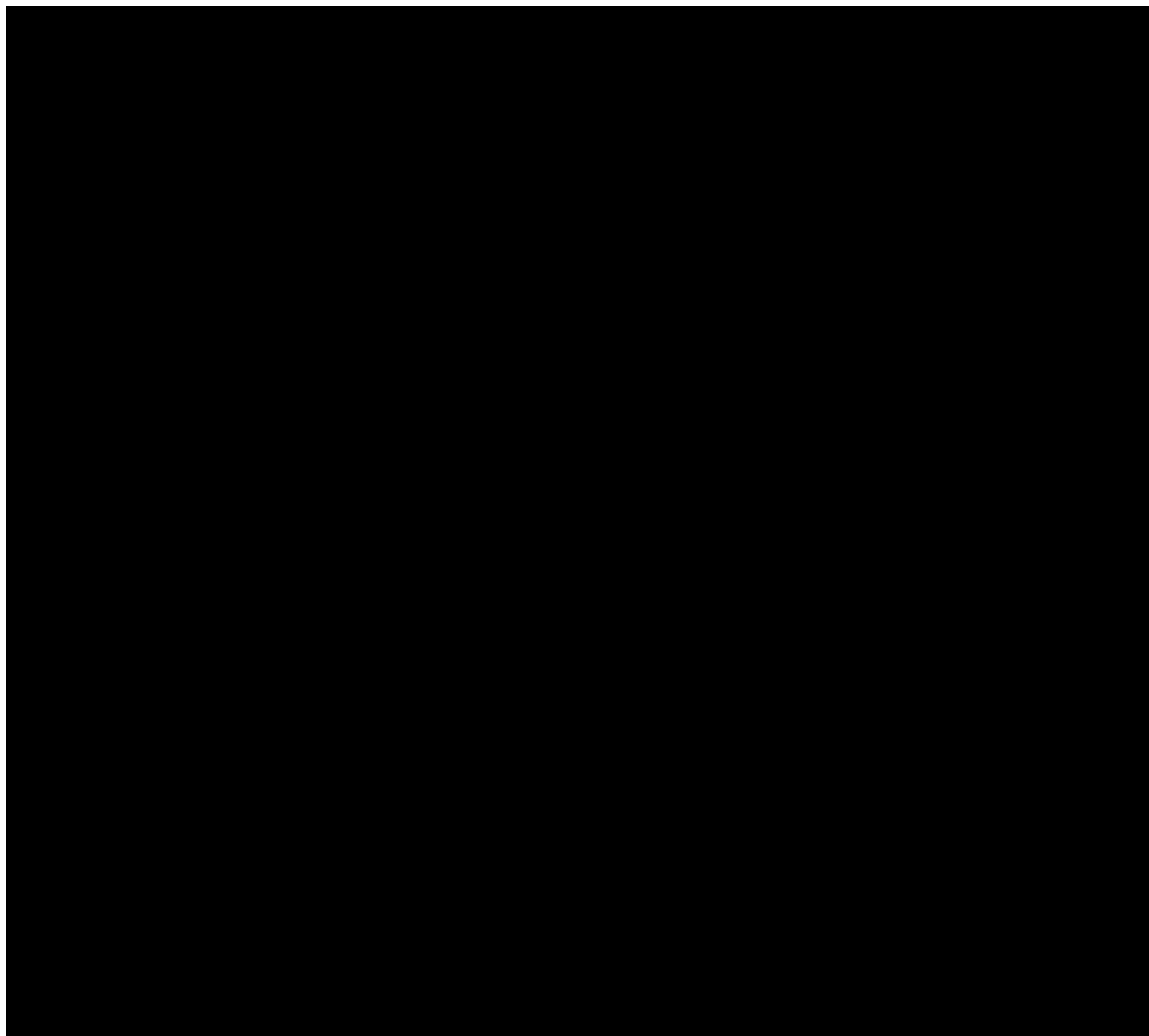


Figure S7. Deuterium NMR spectra of GW^{5,19}ALP23-R14 in DLPC, DMPC, DOPC. Sample orientation is $\beta=0^\circ$.



CONCLUSIONS

Membrane proteins and lipids are major players in a multitude of vital processes for the living cell, such as signal transduction, cell metabolism and transport. Despite their importance, relatively little is known about their fundamental interactions between protein domains and the lipid bilayer membrane. In this context, model systems may provide a relatively convenient means for the testing of specific hypotheses.

Nevertheless, some model systems may suffer particular limitations, an example being the extensive dynamics and nonsystematic behavior of peptides in the original WALP series. Even seemingly “simple” peptide sequences may exhibit complex behavior, highlighting the importance of model systems for fundamental understanding (Chapter 1). The novel design of the GWALP23 sequence, with a single tryptophan residue near each terminus, proved to be highly advantageous for the investigations of diverse phenomena, such as anchoring amino acids (Chapter 2), hydrophobic matching (Chapter 4) and the interaction of a lone charged residue with a lipid bilayer (Chapters 3-5). In this way, model systems prove to be powerful tools for probing important aspects of the complex interplay between lipids and proteins. Future applications of lessons learned from designed sequences for the understanding of biological systems is the ultimate goal.

